N° 41517

UNIVERSITÉ DES SCIENCES ET TECHNOLOGIE DE LILLE 1

Ecole Doctorale
Science de la Matière du Rayonnement et de l'Environnement

THÈSE

Présentée et soutenue en vue de l'obtention du grade de

Docteur
Spécialité Molécules et Matière Condensée

Par **Franck Estimé NGOHANG**

Combination of mass loss cone, Fourier transform infrared spectroscopy and electrical low pressure impactor to extend fire behaviour characterization of materials

---

Soutenue le 17 Octobre 2014 devant la Commission d'Examen composée de :

Prof. Sophie DUQUESNE	Ecole Nationale Supérieure de Chimie de Lille	Presidente
Prof. Giovanni CAMINO	University of Torino, Italy	Rapporteur
Prof. Anna. A STEC	University of Central Lancashire, U.K	Rapporteur
Dr. Laurent GAY	Electricité De France, Chatou	Examinateur
Dr. Gaëlle FONTAINE	Ecole Nationale Supérieure de Chimie de Lille	Co- directrice
Prof. Serge BOURBIGOT	Ecole Nationale Supérieure de Chimie de Lille	Directeur

ACKNOWLEDGMENTS

I am deeply grateful to my supervisors, Prof. Serge Bourbigot and Dr. Gaëlle Fontaine, for their understanding, encouragement and guidance throughout. They have always been available and ready to lend me a helping hand. I also offer sincere thanks to Dr. Laurent Gay for his constant follow-up and for his dedication to this thesis project in which, moreover, he played an initiating role.

I wish to express my sincere thanks to Prof. Giovanni Camino and Prof. Anna. A Stec for having accepted to be external examiners of my Ph.D; and also to Prof. Sophie Duquesne for chairing the jury.

My acknowledgments also go to the department of Fluid Mechanics Power and Environment at Electricité de France Recherche et Développement (EDF R&D) and, in particular, to the successive leaders of group I81,notably Dr. Isabelle Flour who managed this experimental project in its initial stages and Ing. Cecile Clarenc Mace who later took over its management.

During these years, I have worked with great people for whom I have a very high regard. I take this opportunity to extend my further thanks to Mr. Robert Gracia, Sylvere Mongruel and Maxime Lemesle from EDF R&D and to Mr. Pierre Bachelet, Andreas Messina and the entire PhD students and research team at UMET-ISP (ENSCL).

Finally, my thanks go to my family and friends whose combined support has been invaluable, especially my mother and father who instilled the motivation for me to broaden my horizons.

ABSTRACT

A bench-scale test combining mass loss cone, Fourier transform Infrared Spectroscopy and Electrical Low Pressure Impactor (MLC/FTIR/ELPI) was developed to enable simultaneous evaluation of the flammability parameters, the gases evolved (qualitative and quantitative evaluation) and the smoke particles (size distribution and concentration) generated by the combustion of the studied materials. This bench test is designed specifically to investigate the fire behaviour of manufactured products such as electric cables, as it is difficult to fully examine the latter with bench tests of the type thermogravimetry or pyrolysis - gas chromatography/mass spectrometry, which can only hold small quantities of sample (from µg to a few mg). After setting up the MLC/FTIR/ELPI coupling, methodologies were established for qualitative and quantitative analysis of evolved gases and smoke particles. Experimental trials conducted on ethylene vinyl acetate (EVA) and ethylene vinyl acetate/aluminium trihydroxide (EVA/ATH) as reference materials demonstrated that the bench test provides accurate, meaningful and repeatable results.

In the fire tests on neat EVA, acetic acid, from the de-acetylation of the vinyl acetate group, was detected as the highest concentrate gas in the smoke release prior to ignition. The concentration peak of the acetic acid is shown to increase in line with the applied external heat flux level. With regard to the yield of acetic acid released, it is demonstrated to be proportional to the external heat flux (25, 35, 50 and 75 kW/m²). Concerning the carbon dioxide, carbon monoxide and water content in the smoke emission of ethylene vinyl acetate, it was clearly apparent that, on the contrary, variations in the applied external heat flux had no significant effect on the peaks of concentration and persistence of these gases. The latter were mostly released during the flaming phase of ethylene vinyl acetate combustion.

In relation to the fire behaviour test of the ethylene vinyl acetate material filled with aluminium trihydroxide, it is noteworthy that high concentrations of water were detected not only during the burning phase but also before ignition, from the early stages of thermal decomposition. This is due to the dehydration of the aluminium trihydroxide. In this case, the peaks of concentration of water, carbon dioxide and carbon monoxide in the smoke emission increased with the applied heat flux level. Moreover, a noticeable change occurred in the initial decomposition pathway (EVA vs EVA/ATH) with a shift from acetic acid evolution to acetone production. This is ascribed to the Lewis acid/base interactions between the CH_3COOH released from the EVA decomposition and the Al_2O_3 from the dehydration of

ATH, leading to the transformation of CH_3COOH into CH_3COCH_3. In addition, EVA/ATH gave higher CO yields than those of the neat EVA.

In relation to the evaluation of the flammability parameters, it was determined that piloted ignition can occur if EVA is subjected to a constant heat flux of above 15 kW/m², whereas piloted ignition of EVA/ATH can only occur under constant heat flux of above 20 kW/m². Moreover, the measured total heat release and the average effective heat of combustion of the flame retardant EVA/ATH (19 ± 1 MJ/kg) is lower than that of neat EVA (27 ± 3 MJ/kg). Regarding the soot particles analyses, it was confirmed in both cases (EVA and EVA/ATH) that the size distribution of particles emitted in the smoke falls predominantly within the range of ultrafine (≤ 0,1µm) and fine (≤ 1µm) particles. In addition, heat flux variation does not modify the general size range of particles, which is dominated by particles of ≤ 1µm. Although particles above 1 µm are also measured, they are in very low concentrations (beyond 70% below) as compared to the ultrafine and fine particles. Furthermore, the smallest measured particles (6 nm) were detected in the smoke emission of EVA/ATH.

The MLC/FTIR/ELPI coupling was then applied to a real case of halogen free flame retardant electric cable. The results proved to be consistent, highlighting the effectiveness and reliability of MLC/FTIR/ELMPI as an appropriate experimental approach for investigating the fire behaviour of manufacturing products such as electric cables. The conclusion is therefore drawn that the MLC/FTIR/ELPI combination appears to be a complete analytical system that enables to extend the understanding of the fire behaviour of materials. It should be an effective and useful tool in the field of fire risk assessment, as it permits to evaluate, from a single fire test, flammability parameters and also fire effluents (gas species and particles) during a fire scenario.

Keywords: Mass Loss Cone, Fourier Transform Infrared Spectroscopy, Electrical Low Pressure, Ethylene Vinyl Acetate/Aluminium Trihydroxide, smoke, gas and particles.

RÉSUMÉ

L'incendie reste un des sujets redoutés par les industries, les services et autres moyens de production. Ce phénomène par définition incontrôlé dans le temps et dans l'espace est souvent responsable de perte de vies et de biens. Deux types d'agression peuvent être répertoriés en cas d'incendie l'agression thermique par suite de génération de chaleur engendrant la destruction des matériaux et l'agression liée aux fumées toxiques et/ou corrosives, capables de se répandre au-delà du foyer incendie. Pour approfondir les connaissances sur le comportement au feu de matériaux tel que les câbles électriques, cette étude consiste à mettre au point un banc expérimental par couplage Mass Loss Cone, Spectromètrie Infrarouge à Transformée de Fourier et Impacteur Basse Pression (MLC/FTIR/ELPI). Dans l'optique de caractériser simultanément les paramètres physiques de dégradation (taux de dégagement de chaleur, flux critique, chaleur effective de combustion), les gaz et suies (qualitativement et quantitativement) dans les fumée d'incendie. Après la conception du couplage MLC/FTIR/ELPI, le développement des méthodologies compatibles avec l'analyse qualitative et quantitative des gaz et des suies : la justesse, la fiabilité et la répétabilité du banc ont été démontrées avec l'éthylène vinyle acétate/Aluminium tri-hydroxyde comme matériaux de références. Le couplage MLC/FTIR/ELPI a été ensuite appliqué sur un cas réel de câble électrique non halogéné. Il est apparu comme une proposition complète pour la caractérisation du comportement au feu des matériaux et répondre à des questions de sûreté incendie et de recherche et développement.

Mots clefs: Mass Loss Cone, Spectromètrie Infrarouge à Transformée de Fourier, Impacteur Basse Pression, Éthylène vinyle acétate/Aluminium tri-hydroxyde, fumes, gaz et suies.

TABLE OF CONTENTS

LIST OF ABBREVIATIONS

ATH	*Aluminium trihydroxide*
C_2H_2	*Ethyne*
C_2H_4	*Ethylene*
C_2H_6	*Ethane*
C_3H_8	*Propane*
CH_3COCH_3	*Acetone*
CH_3COOH	*Acetic acid*
CH_4	*Methane*
CNC	*Condensation Nucleus Counter*
CNT	*Carbone nanotubes*
CO	*Carbon monoxide*
CO_2	*Carbon dioxide*
DMA	*Differential Mobility Analyzer*
DSC	*Differential Scanning Calorimetry*
EHC	*Effective heat of combustion*
EVA	*Ethylen vinyl acetate copolymer (M :VA content varying from 40 to 80 wt%)*
FR	*Fire retardant (compound)*
H_2O	*Water vapour*
HBr	*Hydrobromic acid*
HCl	*Hydrochloric acid*
HCN	*Hydrogen cyanide*
HF	*Hydrofluoric acid*
HFFR	*Halogen free flame retardant*
HRR	*Heat release rate*
MCT	*Mercury cadmium telluride*
MDH	*Magnesium dihydroxide*
M_i	*molar mass of the species*
m_i	*mass flow rate of species i*
MLC	*Mass loss cone*
MLR	*Mass loss rate*
NH_3	*Ammonia*
NO	*Nitrogen monoxide*
NO_2	*Nitrogen dioxide*
NPP	*Nuclear power plant*
O_2	*Oxygen*
PAHs	*Polycyclic aromatic hydrocarbons*

PCFC	*Pyrolysis Combustion Flow Calorimeter*
PSAs	*Probabilistic Safety Assessments*
PTFE	*Polytetrafluoroethylene*
PVC	*Polyvinyl chloride*
Py-GC/MS	*Pyrolysis - Gas Chromatography coupled with Mass Spectroscopy*
R	*universal constant of ideal gas*
Sb_2O_3	*Antinomy oxide*
SMLR	*Specific mass loss rate*
SMPS	*Scanning Mobility Particle Sizer*
SO_2	*Sulfur dioxide*
SPR	*Smoke production rate*
STA/FTIR	*Simultaneous Thermal Analysis coupled with to Fourier Transform Infrared spectroscopy*
TEOM	*Tapered Element Oscillating Microbalance*
TGA/FTIR	*Thermogravimetry Analysis coupled to Fourier Transform Infrared spectroscopy*
THR	*Total heat release*
t_{ig}	*time of ignition*
V_e	*volumetric flow rate of the gas phase in the exhaust line*
V_m	*molar volume*
X_i	*concentration of species i*
ΔHc	*Gross heat of combustion*
μm	*micrometer*

LIST OF FIGURES

LIST OF TABLES

INTRODUCTION

Fire has an important place in the classification of risks in industrial, public transport and building facilities, principally because it can lead to loss of lives and damage to materials. Given the number and extent of potentially flammable materials encountered in everyday life, fire safety concerns remain a current and ever present issue. In particular, two types of aggression are commonly reported as a result of fires: thermal aggression, namely a rapid rise in heat generated by the fire development and growth stage, which can in turn trigger the combustion of nearby materials, and toxic aggression from the toxic and/or corrosive elements in the smoke, which can be transported a considerable distance away from the fire origin. Smoke inhalation has been recognized as the primary cause of injury or death in indoor fires because of the asphyxiate and/or irritant gases it contains.[1]

Furthermore, the risks posed by corrosive gas species and particles in the case of smoke propagation in the vicinity of electric or electronic devices, including loss of metallic or mechanical contact, corrosion and accelerated ageing of parts in the mid to longer term have also raised some concerns regarding the safe use of this type of device. The studies conducted at Sandia National Laboratory[2,3,4,] by Mangs[5] or Newman[6] highlight the potential effects of smoke impact on digital instrumentation, notably an increased risk of instrument malfunction. Where it serves to ensure the safety of production processes, a malfunction in digital equipment could provoke shutdown, resulting in potentially important economic consequences for the facility concerned.

Detailed knowledge of the flammability parameters of specific materials and of the evolution of gases and soot particles in the smoke generated by the combustion of these materials is therefore critical in the evaluation of fire risks and/or for improving fire safety policies and regulations in industrial facilities. When information on the thermal decomposition parameters and evolved gases of specific materials is required, small bench scale tests such as Pyrolysis - Gas Chromatography coupled with Mass spectroscopy (Py-GC/MS), Thermogravimetry coupled to Fourier Transform Infrared spectroscopy (TGA/FTIR)or a Simultaneous Thermal Analysis coupling with Fourier Transform Infrared spectroscopy (STA/FTIR) have been often used.[7,8] However, in addition to the limited nature of the study itself, only a small amount of sample (from µg to few mg) are analysed, which means the study results are hardly applicable to a full “real” fire scenario. Moreover, this type of analysis (except STA/FTIR) does not generally take into account the aspects of quantitative gas evaluation nor does it include an investigation of the characteristics of soot particles present in the smoke. These aspects are crucial because airborne gases and particles can lead to health and environmental issues.[9,10]

As part of its expertise, Electricité De France Research & Development (EDF R&D) encourages the department of Fluid Dynamics, Power Generation and Environment (MFEE) to acquire in-depth knowledge of the flammability parameters of some materials that are widely present in nuclear power plants (NPPs), and also of the gases and particles contained in the smoke produced by a fire involving these materials, such as electrical cables. In addition, Probabilistic Risk Assessments studies (PRA) have classified fire as the major risk in NPPs[11] because of the potential consequences of this type of event, including complete shutdown of facilities and the economic consequences arising from materials damage and production loss.

Several examples of fires at nuclear power plants can be cited: the first modern fire at Browns Ferry NPP (USA, 1975) caused by an electrical cable failure,[12] to the recent outbreaks of fire at the Penly and Fessenheim NPPs (2013), although rapidly brought under control, serve as a reminder that zero risk has not been yet achieved as far as fire is concerned.

It is in this context that the present study was initiated, as part of the Fire Safety Project at EDF R&D and in collaboration with the Materials and Transformation Unit (UMET) of Ecole Nationale Supérieure de Chimie de Lille (ENSCL). It consists of the development and validation of an experimental bench test allowing the simultaneous determination of the: (i) flammability parameters (heat release rate, critical heat flux, and effective heat of combustion), (ii) evolved gases (qualitative and quantitative evaluation) and (iii) soot particles (size distribution and concentration) present in the smoke of a fire of specific materials. Ethylene vinyl acetate/aluminium trihydroxide were chosen as reference materials, because of the widespread use of this copolymer formulation as a coating or covering material for halogen-free electrical cables. The fire behaviour of ethylene vinyl acetate both filled with aluminium trihydroxide and unfilled will be revisited in order to validate the experimental bench test proposed herein. In addition to the collection of additional data, the validation should demonstrate the efficiency of this “simultaneous” technique for investigating in real time not only the flammability parameters of materials but also the gas phase and soot particles present in the smoke.

In order to describe the development and validation of the simultaneous bench test, intended for application over an entire range of manufactured products, this study is divided in five chapters, outlined as follows:

The first chapter is consecrated to a background statement explaining the conditions under which a fire can occur and the related parameters that may be used to describe the fire behaviour of materials. The focus is subsequently on the thermal decomposition of polymers and also flame retardancy mechanisms and compounds. Subsequently, a state of the art screening of current analytical techniques to examine the fire behaviour of materials is presented.

The second chapter is dedicated to the design development of the coupled Mass Loss Cone, Fourier Transform Infrared Spectroscopy and Electrical Low Pressure Impactor (MLC/FTIR/ELPI) as a simultaneous experimental bench test. The choice of MLC, FTIR and ELPI as analysis techniques, in accordance with the objectives of this project will be detailed and discussed.

The third chapter deals with validation of the MLC/FTIR/ELPI coupling as an effective and reliable experimental bench test. It consists of revisiting the fire behaviour of ethylene vinyl acetate both unfilled and filled with aluminium trihydroxide.

The fourth chapter describes the impact of various fire scenarios, more specifically, the effect of external heat flux variations on flammability parameters evaluation, quantitative gas analyses and the evaluation of smoke particles. In consequence, the fire related parameters of ethylene vinyl acetate unfilled and filled with aluminium trihydroxide are investigated under different thermal aggression scenarios.

Finally, the fifth chapter reports on the application of the MLC/FTIR/ELPI coupling to the case of real halogen free flame retardant low voltage electrical cable intended for use in EDF’s NPPs.

CHAPTER 1: BACKGROUND STATEMENT

Fire is generally defined as an uncontrolled combustion, meaning a self-sustaining and exothermic process of oxidation of fuel along with the evolution of heat and light; or smouldering combustion in its condensed phase.[13] This uncontrolled phenomenon involves numerous and complex physical and chemical reactions in solid, liquid and gas phase. It is often associated with the release of smoke, which may contain irritant gases and or corrosive species. The fire behaviour of materials is also specific to the thermal decomposition and the chemical nature of the material. Its characterization requires different equipment some of which may be scale-dependent should the parameters and the materials studied require this functionality. A short discussion on fire and related parameters, the thermal decomposition of polymeric material and flame retardants, as well as on the equipment used to investigate the fire process of materials is necessary as a preliminary background to the final equipment selection, the conducted analysis and an interpretation of the experimental results.

The first section of this chapter outlines the basic principles of fire as a process and the elements that are essential to trigger its outbreak. The following section introduces the related parameters that enable characterization of fire phenomenon, namely flammability parameters, gas species and also soot particles. In the third section, the focus is on general aspects of thermal decomposition of both polymers and flame retardant systems. The last section, prior to the conclusion, consists of a state of the art screening of the analytical techniques widely used to investigate flammability parameters, as well as gas and particle emissions, in order to select the techniques most appropriate to the purpose of this project.

1 Fire conditions and related parameters

Three elements are essential for a fire to occur, fuel, an oxidizing agent and energy (heat). The interaction between these elements is, in fact, indispensable in fire ignition and for maintaining the fire, as summarized by the fire triangle (Fig.1) first reported by Emmons.[14]

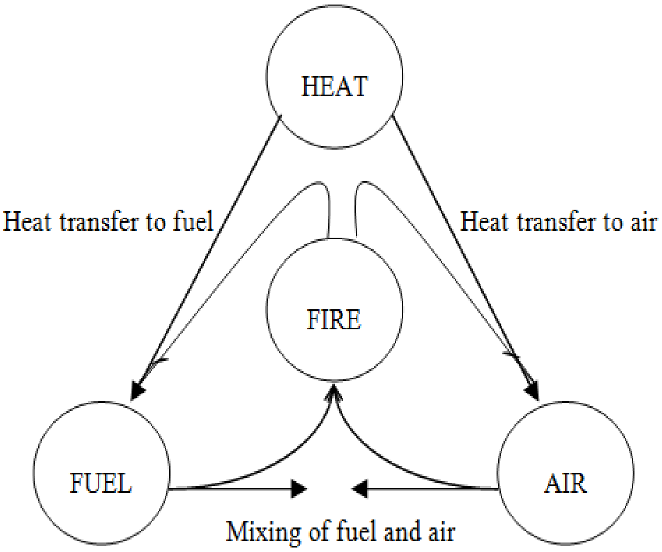

Figure 1. Fire triangle

The fuel can be any of a large number of materials in solid, liquid or gas state, which is not in its highly oxidized state. Heat is the energy source required for fuel pyrolysis and it can be provided by convection, conduction and/or radiation from a source such as radiant panels, flames, etc. The oxidizing agent, in most cases oxygen (O_2) is indispensable to sustaining the combustion process. Many physical and chemical parameters can therefore be used to describe how a material behaves in a fire situation. Some of these are introduced and discussed below.

1.1 Flammability parameters

Some of the physical parameters used to describe how a material behaves in a fire situation are the heat release rate (HRR), which is directly related to the power of fire; the time of ignition (t_{ig}), i.e. when the sample starts burning with a sustained flame; the Mass Loss Rate (MLR) describing phenomenon taking place in the condensed phase; the total heat release (THR); the critical heat flux (CHF) and the effective heat of combustion (EHC). Concurrently with the physical parameters mentioned above, fire can also generate smoke, which is considered as a non-thermal fire parameter. This smoke consists of a mixture of gases in which small solid particles of soot are dispersed, absorbing and scattering light and thus reducing visibility.[15] The next sections introduce these non-thermal fire related parameters (gases and particles).

1.2 Gases in fire smoke

Numerous irritant, asphyxiating and/or corrosive gases can be found in fire smoke. Carbon dioxide (CO_2) and carbon monoxide (CO) are always found in the fire smoke produced by combustion of any organic compound. Furthermore, depending on the ventilation conditions and the chemical composition of the material undergoing thermal decomposition, other gases can also be found. A list (non-exhaustive) of the main gases associated to the combustion of polymeric materials and the potential risks related to these are summarized in Table1.

Table 1. Gases potentially found in fire smoke and principal risks [14,16,17]

	Type of gas	**Example of sources**	**Principal risks to human beings and/or materials**
1	Carbon dioxide (CO_2)	All combustion	Asphyxia at high concentration
2	Carbon monoxide (CO)	All combustion	Asphyxia
3	Hydrochloric acid (HCl)	Chlorine contents (PVC, polyesters, etc.)	Asphyxia, burns, corrosion,
4	Hydrobromic acid (HBr)	Bromide contents (Br flame retarded)	
5	Hydrogen cyanide (HCN)	Nitrogen contents (polyamides, nylon)	
6	Hydrofluoric acid (HF)	Fluorine contents (PTFE, PVDF)	
7	Acetic acid (CH_3COOH)	Ethylene vinyl acetate copolymers	May cause damage to the skin, eyes, etc.
8	Acetone (CH_3COCH_3)	Epoxy resin composites	May cause drowsiness and dizziness
9	Nitrogen monoxide (NO)	Polyacrylonitriles and polyamides	Poisonous, corrosive, oxidizer (accelerate the combustion)
10	Nitrogen dioxide (NO_2)		
11	Ammonia (NH_3)	Polyurethane, nylon	Irritant, corrosive to the skin, eyes etc.
12	Sulfur dioxide (SO_2)	Sulfur contents (polymers, polysulfides)	Burns, irritation to the eyes, skin and respiratory tract
13	Methane (CH_4),	Hydrocarbon materials	May cause an oxygen deficient environmental high concentrations
14	Ethane (C_2H_6)		
15	Propane (C_3H_8)		
16	Ethylene (C_2H_4)		
17	Ethyne (C_2H_2)		
18	Water (H_2O)	All combustion	May reduce visibility at a short distance

1.3 Particles in fire smoke

Soot particles result from incomplete combustion or from the pyrolysis of hydrocarbon fuels. They are released into the atmosphere by a number of combustion processes, such as those occurring in wood burning, diesel engines, power plants, air craft emissions and with plastics.[18,19,20] In the case of a flaming process, particles are produced in the more reactive flame zone (appearance of a bright yellow plume) and then dispersed in the smoke layer. Suspended in the atmosphere, these soot particles are known to be harmful to human health, responsible for climate change effects [21] and also for the malfunctioning of electric or electronic devices;[2-6] hence, the interest of investigating particles contained in the smoke of a materials fire.

The mechanism by which particles are formed is a complex multi-stage process. One of the difficulties with the explanation of particles generation is the transition from a hydrocarbon molecular system with a hydrogen-carbon ratio H/C≈2, into systems having 10^5 carbon atoms with a ratio H/C≈0.1.[22] Nonetheless, the formation mechanism of particles is currently summarized by the following steps: nucleation, coagulation, surface growth, aggregation and oxidation.[21, 23, 24, 25] At the nucleation stage (Fig 2), condensed materials form from the pyrolysis or oxidation of fuel molecules such as acetylene (C_2H_2) and polycyclic aromatic hydrocarbons (PAHs), which are the key intermediate compounds in soot particle formation. This nucleation leads to very small particles called nuclei with diameters of up to 2 nm. Once nuclei are formed, the quantity of soot particles is determined by the competing processes of surface growth and destruction through oxidation. The surface growth corresponds to the magnification of nuclei by heterogeneous reactions through interactions with the gaseous phase. During the surface growth phenomenon, the number of particles remains constant but their diameters and volume fractions increase until the particles attain a substantially spherical shape, designated as spherule, with a diameter of between 10 to 30 nm. The oxidation is caused by the presence of oxygen (O_2) and hydroxyl radicals (OH•); O_2 induces internal oxidation resulting in fracture and break-up of particles, whereas OH• oxidation diffuses over the surface of particles tending to break down the aggregates and reduce their mass. Collisions between small particles of about 10 nm can promote coalescence (two particles merge to form one). Particles above 10 nm agglomerate, i.e. they come into contact and bond without merging. The process of soot particle formation discussed above is summarized in Fig. 2.

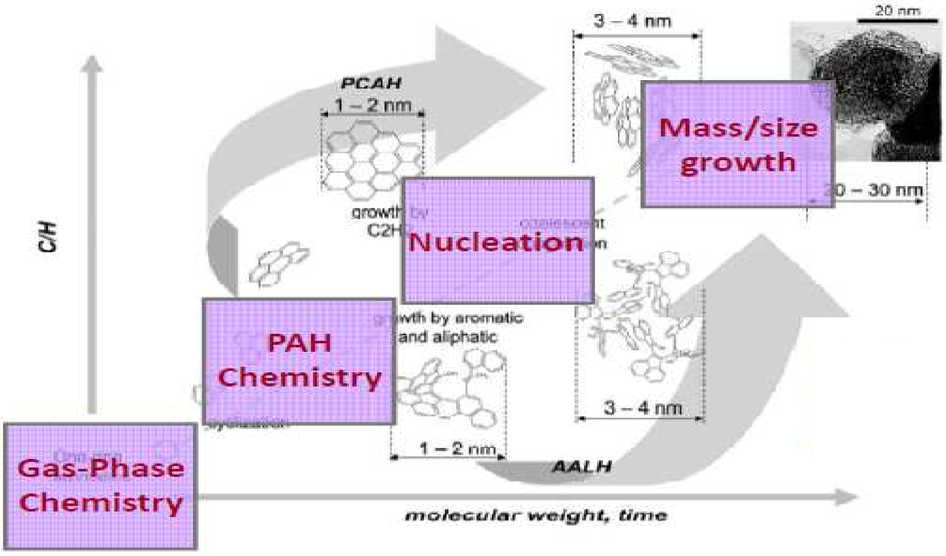

Figure 2. Schematic diagram of the formation of soot particles[17]

2 Thermal decomposition of polymers

Due to their chemical and mechanical properties, polymeric materials are incorporated in many manufactured products used in everyday life, including furniture, building materials, transports, textiles, etc. However, they are high flammable as they are mainly composed of carbon and hydrogen atoms.[26] Thermal decomposition is the main aspect governing the fire behaviour of polymers and it is therefore discussed in this section with specific emphasis on the ethylene vinyl acetate copolymer. A survey of flame retardant systems is also presented.

2.1 General aspects of the thermal decomposition of polymers

The thermal decomposition of polymers is characterized by physical and chemical changes that occur as a result of overheating.[27] When a polymer is exposed to a heat source, its temperature increases by heat transfer from the surface to the bulk. During this step, thermoplastic polymers soften. This is not the case for hard and rigid thermoset polymers. In both cases, at a critical temperature, the chemical bonds of the polymeric chains break (chain scission), producing volatile species of low molecular weight. Some of these volatile compounds mix with the oxygen in air by their diffusion into the layer close to the polymer surface .This creates free radicals capable of igniting spontaneously (self-ignition) or in the presence of an external spark (piloted ignition). The combustion of these gases that results from the formation of hydrogen radical (H•) and OH• radicals increases the production of new combustible gases which sustain the fire process as schematically shown in Fig. 3. Certain steps, such as charring and thermal oxidation in the condensed phase (smouldering), do not always take place, these being dependent on the polymer concerned and thermal decomposition conditions (ventilation, heat flux, etc.)

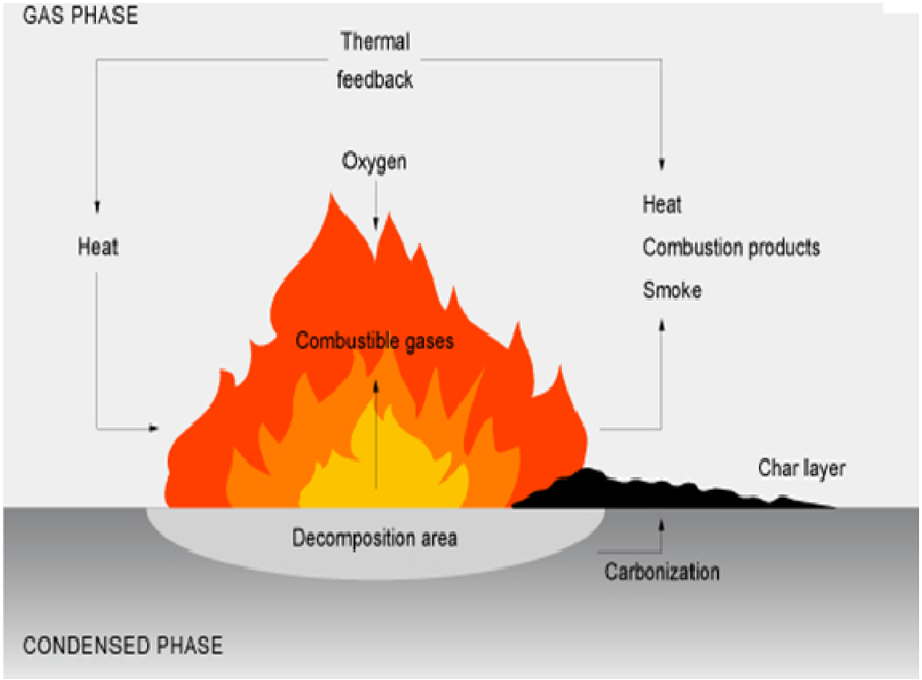

Figure 3. Schematic of polymer thermal decomposition and combustion

The thermal decomposition case of ethylene vinyl acetate, which will be used as a reference polymer in this study, is developed below.

2.2 Case of ethylene vinyl acetate copolymers (EVA)

2.2.1 Polymerization and properties

Ethylene-vinyl acetate is produced from the copolymerization of ethylene and vinyl acetate monomers as shown in Fig. 4. It represents the largest share of the ethylene copolymer market and more than 150 grades are available, with applications in the automotive industry and electrical cables insulation and coating.[28]

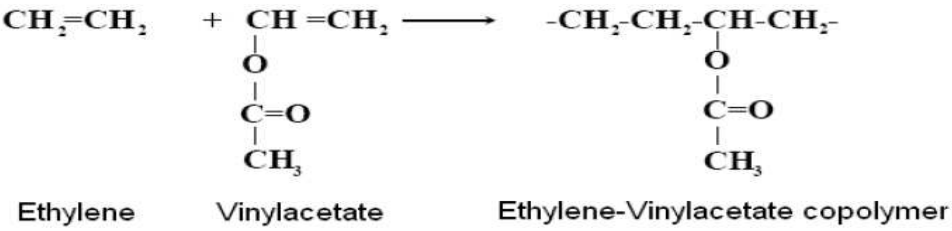

$$CH_2{=}CH_2 + \underset{\substack{| \\ O \\ | \\ C{=}O \\ | \\ CH_3}}{CH}{=}CH_2 \longrightarrow -CH_2\text{-}CH_2\text{-}\underset{\substack{| \\ O \\ | \\ C{=}O \\ | \\ CH_3}}{CH}\text{-}CH_2\text{-}$$

Figure 4. Schematic of the polymerization of ethylene-vinyl acetate

Polymerization of ethylene-vinyl acetate can be carried out for every ratio of the co-monomers and the behaviour of the resulting copolymer is determined by its vinyl acetate content.[29] If vinyl acetate (VA) is added in proportions of up to 33 wt.% or above 80 wt.%, the copolymers are thermoplastic; at ratios between 40 and 80 wt.% of VA, the material denoted EVM (Fig. 5) exhibits an elastomeric behaviour.

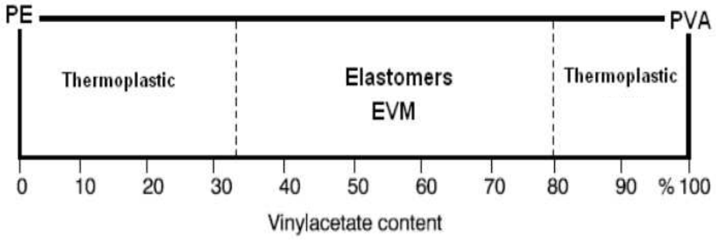

Figure 5. Schematic of ethylene vinyl acetate according to vinyl acetate content

This copolymer has attracted the attention of manufacturers because it can incorporate high filler loading levels while retaining good mechanical properties.[30] Its thermal decomposition process is also well known and reported below.

2.2.2 Thermal decomposition of EVA

The thermal decomposition of ethylene-vinyl acetate under air, assessed in small scale tests like TGA/FTIR or STA/FTIR, has been widely reported in literature as being a two-step process.[31,32,33,34,35,36,37,38] The first step occurring at temperatures between 250 and 350 °C corresponds to the decomposition of the vinyl acetate group generating the release of acetic acid (CH_3COOH) and the formation of an unsaturated linear polyene structure. The higher the vinyl acetate content, the greater is the release of acetic acid. It is also reported that a secondary reaction occurs (between 250 and 350 °C), leading to the release of CO, CO_2 and CH_4. The second decomposition step, occurring at around 350 to 450°C, involves random chain scission of the linear polyene with the release of CO_2, CO, H_2O and saturated and/or unsaturated hydrocarbons such as methane, ethylene, butadiene[31, 34] and indene, eicosane and dodecane.[38] The nature of the hydrocarbons released from thermal decomposition can be influenced by experimental conditions. In an oxidative environment and depending on VA content, the polymer surface can rapidly cross link leading to the formation of a carbonaceous layer, also known as char. In addition, as they are mainly composed of a hydrocarbon structure, ethylene-vinyl acetate copolymers are highly flammable, with a relatively high exothermic effect. Fig. 6 shows the influence of vinyl acetate content on the heat of combustion of EVA, which varies from 25 to 45 MJ/Kg.[39]

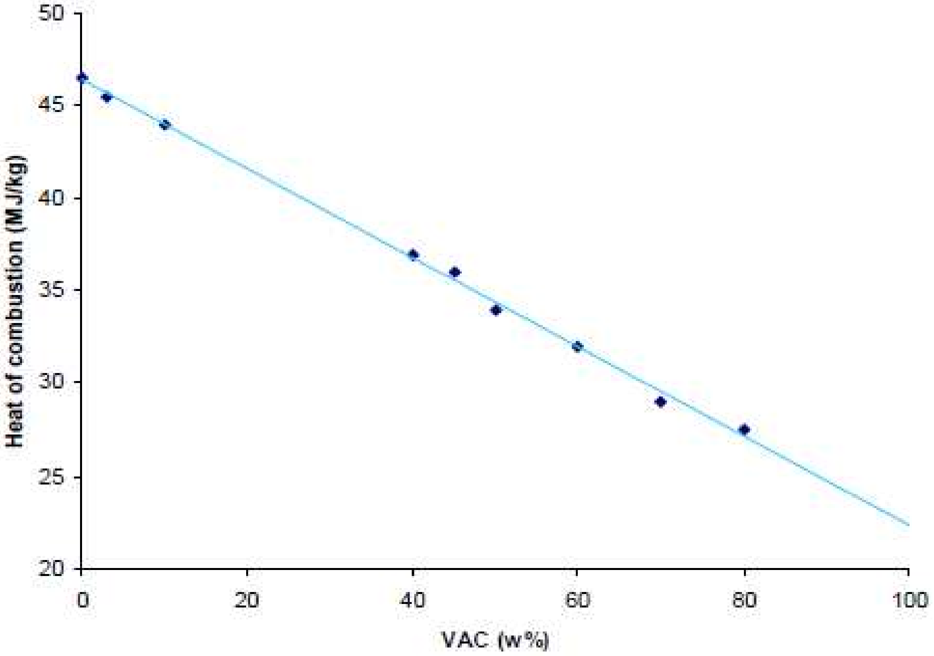

Figure 6. Heat of combustion of ethylene-vinyl acetate according to vinyl acetate content [39]

As a result, when ethylene-vinyl acetate copolymers or other polymers are used in the manufacture of elaborated products such as wire insulation or electrical cables coatings, they must be flame retarded to meet legal requirements in the case of fire (reduced ignitability, reduced flame spread, reduction of hazardous species in the smoke, etc.).

There are many means of imparting flame retardancy to polymers, including graft polymerization of flame retarding monomers, incorporation of an additives combination in the host polymer or surface treatments.[40] The recognized flame retardant approaches are surveyed below with special emphasis on ethylene-vinyl acetate and electric cable coating.

3 Flame retardants and their modes of action

Flame retardants (FRs) act to inhibit and/or stop the combustion reactions of polymers. A distinction is made between reactive FRs and additive FRs[41]: reactive FRs are chemically grafted onto polymeric chains during the polymer synthesis, whereas additive FRs are incorporated into the polymer as filler. Depending on their nature, the elements in FRs can react chemically and/or physically with fire in their solid, liquid or gas phases.[41] Although the use of reactive FRs is not excluded, additive FRs appear to be more convenient and currently represent the best compromise between process, cost and performance. FRs are traditionally divided into 4 classes: halogenated, metal hydroxides, phosphorus and nitrogen-based FRs. Their modes of action, in both the condensed and the gas phase, are discussed in the following sections.

3.1 Halogenated flame retardants

Halogenated compounds have historically been used as flame retardants and have proved very efficient at moderate concentration.[42] In the class of halogenated FRs, brominated and chlorinated derivatives are used in preference to fluorine and iodine compounds, because the former is too thermally stable and the latter too thermally unstable to provide good flame retardancy action.[43]

To interrupt or reduce fire combustion, halogenated FRs interact chemically in their gaseous phase with radicals formed in the fire process. These consist of H• and OH• radicals, with H• the active agent in free-radical cross-linking reactions and OH• causing the oxidation reactions, both of which known to be highly exothermic reactions. The inhibition mechanism of halogen in gaseous phase is described in Fig. 7: the active H• and OH• radicals are replaced by less active halogens atoms (X•). This prevents the exothermic chain reactions from occurring, resulting in a cooling down and a decrease of mass fluxes in the polymeric material undergoing thermal decomposition.[44, 45]

Decomposition reactions:
$\text{R-X} \rightarrow \text{R}\bullet + \text{X}\bullet$
$\text{P-H} + \text{X}\bullet \rightarrow \text{H-X} + \text{P}\bullet$

With R-X the halogenated flame retardant and P-H the polymer

Flame retardation mechanisn
$\text{H–X} + \text{H}\bullet \rightarrow \text{H}_2 + \text{X}\bullet$
$\text{H–X} + \text{OH}\bullet \rightarrow \text{H}_2\text{O} + \text{X}\bullet$

Figure 7. Mechanism of action of halogenated flame retardants in gaseous phase

The radical trap mechanism described above is not the only mode of action of halogenated flame retardants. It has been demonstrated that halogenated FRs also have a physical effect on the combustion process: by virtue of their heat capacity and endothermic bond dissociation properties they can act as a heat sink.[46, 47] Furthermore, to attain high levels of flame retardancy and enhance the features of the finished product, halogenated FRs are often combined with synergists. One of the most effective synergists is antimony trioxide (Sb_2O_3).

Although not a flame retardant per se, it enhances the efficiency of halogenated additives via the formation of volatile antimony halides that have higher flame inhibition properties than those of hydrogen halides.[48] Zinc borates,[49] zinc sulphide,[50] zinc stagnates[51] and N-alkoxy hindered amines [52] have been also reported as synergistic agents in halogenated FR formulations. These promote dehydro-halogenation resulting in an increase of cross-linking reactions, the formation of char and reduced smoke production.

Concerning ethylene-vinyl acetate, the first attempts at increasing its flame retardancy have consisted in the use of halogenated FRs grafted onto the copolymer chain. As far as ascertained, the only references in scientific literature are those of Atwell [53] and Yang.[54] In the field of electric cable insulators and coatings, the most celebrated examples of flame retardant compounds are polyvinyl chloride (PVC), which is intrinsically fire retardant, and ethylene propylene rubber (EPR), in which brominated additives are likely to also be present, both of which are used in electric cable jacketing.

Despite their considerable efficacy, halogenated FRs may have negative consequences for health and the environment[55,56] and their use is contested on these grounds by both the European community and Greenpeace. In particular, a ban on the use of polybrominated diphenylethers has been in place since 2006, under the European Risk of Hazardous Substance directive. Furthermore, the degradation products of halogenated compounds are also known to produce corrosive, toxic and obscuring smoke.[57] This is the reason for the increasing focus in research and development on zero halogenated additives (or halogen-free) FRs and their commercial application. This focus is also prompted by the growing demand, led by the industrial sector, for an alternative enabling to circumvent the problems that arise with halogenated FRs. One such alternative is the use of metal hydroxides FRs.

3.2 Metal hydroxides

Over the past two decades, extensive use has been made of metal hydroxides as a viable alternative to halogenated FRs, this being due to their low cost and high level of flame retardancy. The three main types of metal hydroxides reported in the literature are: aluminium trihydroxide (ATH), magnesium dihydroxide (MDH) and, less frequently, hydromagnesite ($(Mg_5(CO_3)_4(OH)_2.4H_2O$.[58,59,60] It is worth noting that a number of other alternatives have been evaluated, however no record was found of their use on a larger scale and it is assumed that their commercialisation, if at all, remains subject to confidentiality clause.

The fire retardant action of metal hydroxides is based on endothermic release of water in the gas phase and formation of an oxide residue in the condensed phase. For example, ATH decomposes endothermically at relatively low temperatures (180 - 220 °C) releasing non-combustible water as shown in equation 1.

$$2Al(OH)_3 \rightarrow Al_2O_3 + 3H_2O \qquad (1)$$

The endothermic water elimination (dehydration associated with a high energy density of 1050 J/g) slows down polymer decomposition, helps maintain the polymer below ignition temperature and dilutes the concentration of flammable gases. The aluminium oxide (Al_2O_3) formed in the condensed phase acts as a physical protective layer.[61] In a similar manner, MDH decomposes endothermically but at higher temperature (300 – 350 °C) associated with a higher dehydration energy density (1300 J/g) than that of ATH. Its decomposition also generates an oxide residue (MgO) as shown in equation 2.

$$Mg(OH)_2 \rightarrow MgO + H_2O \qquad (2)$$

ATH is today the best-selling of the metal hydroxides and the most used FR in ethylene-vinyl acetate copolymers. It is very popular in a wide range of applications, including as an alternative electric cable coatings to that of halogenated flame retardants. The main reasons for its commercial success are its low cost, process ability, efficiency and its reputations for being “environmentally friendly”. Nevertheless, ATH has its disadvantages, principally the need for high loadings (up to 60 wt. %) in order to pass the FR-standards tests. Such high loading levels have a negative impact on the mechanical properties of materials.[62] In the manufacture of electric cables covering, the viscosity of the formulations is increasing in line with the increased amounts of ATH being used. It is hoped, however, that synergistic compounds, such as zinc borates, metal nitrates, silicon-based (silicones, silicas, organosilanes, silsesquioxanes, Montmorillonite), carbon nanotubes (CNT), will enable to decrease the amount of ATH required to achieve high fire performance.[63, 64, 65, 66] In addition to synergistic effects, the physical characteristics of inorganic hydroxides, notably particle size, particle size distribution and particle shape are also important to achieving the highest levels of performance. Combinations of red phosphorus (3 to 5 wt.%) with ATH or MDH enable obtaining good fire performance at loadings of about 30 - 40 %.[67]

3.3 Phosphorus compounds

The use of phosphorous-based compounds as FRs in polymers is currently increasing as the latter represent available alternative to halogenated compounds and metal hydroxides. Phosphorus-based additives can be classified according to their phosphorus oxidation states. Red phosphorus (elementary phosphorus), phosphates and polyphosphates, phosphonates and phosphinates (Fig. 8) are widely used FR additives.

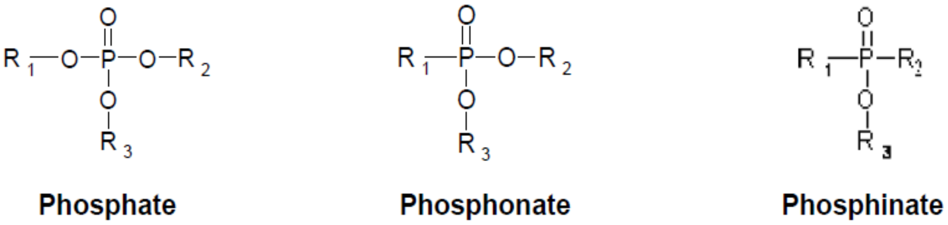

Figure 8.Chemical structures of widely used phosphorous FR additives

Phosphorous-based flame retardant additives can act both in the condensed and gas phases. In the condensed phase they promote polymer charring, or a protective carbonaceous mantle, thereby reducing heat and mass transfer which in turn inhibits fire development. In gaseous phase, their mode of action is similar to that of halogenated compounds.[68]

In the case of ethylene-vinyl acetate copolymers, there has been reported use of ammonium polyphosphate (APP) as a FR. Unfortunately; APP and EVA exhibit low compatibility, meaning they cannot be used for industrial applications.[69] In general, quite small amounts (<10%) of phosphorus additives are required to effectively inhibit ignition and reduce smoke production.[70] However, some additives can be water-sensitive which may lead to eventual ageing problems. Phosphorous-based compounds would not therefore be used as principal FRs in cable material formulations but could be considered as synergistic agents in combination with other FR additives.

3.4 Nitrogen based compounds

Nitrogen flame retardants are melamine based compounds. Numerous melamine-based additives, such as pure melamine, organic or inorganic melamine salts (melamine cyanurate, melamine phosphates) and also melamine degradation products (Fig. 9) melam, melon and melem, are used in thermoplastics and elastomers.

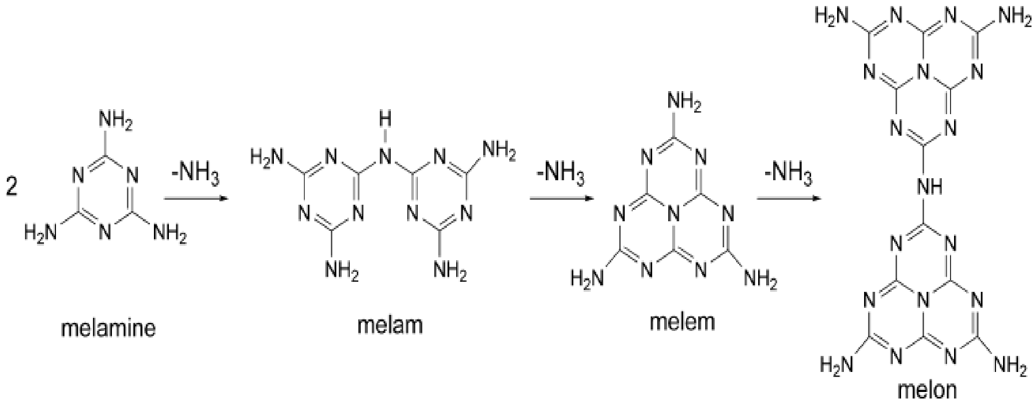

Figure 9. Thermal decomposition of melamine and related products

Their flame retardant modes of action vary according to the type of additive. Pure melamine combines gas phase and condensed phase action as its degradation implies two processes: endothermic sublimation and both condensation and decomposition in the condensed phase to form melam, melem and finally melon, all of which are thermally stable compounds.[71] Melamine salts mainly exhibit a condensed phase action. Some oxynitride-type structures are formed at temperatures higher than 600 °C and the high thermal stability of these compounds explains the melamine retention in the condensed phase.[72]

The influence of melamine on the fire retardancy of EVA with 26 wt.% VA content was investigated by Zilbermann.[73] Incorporating melamine in the EVA copolymer led to a drastic increase in the HRR peak under cone calorimeter test conditions, suggesting that melamine actually diminishes the flame retardant properties of neat EVA. This result is contradicted however by the gas analysis results which indicate, on the contrary that the addition of melamine to EVA does impart flame retardant properties to the polymeric matrix. Regarding insulator or cable formulation, no reports of nitrogen additive FRs were discovered in our review of the literature.

To summarize, the principal strategies for enhancing EVA flame retardancy, as reviewed above, involve the use of FR additives including halogenated compounds, metal hydroxides, phosphorous compounds, melamine and its derivatives, which act respectively in the gaseous and/or the condensed phase. One of the most widely used FRs for improving EVA fire retardancy is ATH.

The next section describes the techniques currently implemented in comparative investigations of the thermal decomposition behaviour of materials and notably of flame retarded polymeric materials.

4 Experimental techniques

The study and/or comparative study of the thermal decomposition and stability of materials is an important element in the research and development of formulations for new high performance materials and also in safety assessments of manufactured products for use in private or public facilities. It is essential therefore that the experimental techniques employed are capable of producing accurate, complete and realistic results. There are numerous tests that yield information about the behaviour of materials during thermal decomposition, each of which focuses on particular parameters and thermal decomposition conditions according to the scale of the study.

This section is dedicated to a review of the experimental techniques used to evaluate the flammability parameters, identify evolved gas species and analyze soot particles present in the smoke generated by the thermal decomposition or combustion of materials. The purpose of this review is to assess the relative merits of these techniques and ultimately to select those most appropriate for the purpose of simultaneously characterizing the physical parameters and effluents (gases and soot particles) of materials in a fire.

4.1 Thermal analyses

Analysis of the thermal decomposition behaviour of materials can be conducted on three scales: (i) micro scale testing, (ii) bench or intermediate scale tests and (iii) full scale tests.

Micro scale test analysis involves small sample sizes, in the range of microgram (µg) to milligram (mg), with minimized heat transfer in the sample, such that the temperature in the sample is considered to be homogeneous (thermally thin material). This experimental scale has the advantage of strict control of both the heating temperature and the ambient working atmosphere so that experiments can be performed under oxidative or inert ambient conditions. One of the micro scale testing techniques whose use is widely reported in the literature is the Thermo Gravimetric Analysis (TGA) technique. With TGA, the sample is heated according to a defined temperature ramp or isothermal temperature. The weight change of the sample is monitored versus time or temperature. TGA enables determining the thermal stability of materials[74] and there are reports in the literature of its use in the investigation of the thermal decomposition of a small amount (mg) of neat EVA and of an EVA blend with FRs additives.[75,76] However, the TGA sample holder cannot be used for an entire portion of an electric cable and the tested sample is often reduced to powder form to avoid the "shape factor" effect.

In addition to TGA, the Differential Scanning Calorimetry (DSC) and the Differential Thermal Analysis (DTA) techniques allow determination of the glass transition temperature of materials. With DTA, the sample and an inert reference, usually an empty crucible, are continuously heated and the temperature difference is recorded as a function of the evolution of heating temperature. When endothermic or exothermic phenomena occur, the temperature of the sample pan becomes respectively lower or higher than that of the empty crucible. Regarding DSC, both sample and reference are heated at a constant rate and the difference in energy required to maintain identical temperatures is recorded. Similarly to DTA, changes in the recorded parameter can indicate glass transition, endothermic or exothermic processes of the thermal decomposition of tested materials.[76] Use of the DSC and DTA techniques in investigations of the thermal decomposition phases of polymeric materials such as polyethylene or ethylene vinyl-acetate copolymer are also widely reported in literature.[77,78] A combination of DTA or of DSC with TGA gives the Simultaneous Thermal Analysis (STA) technique.

Another example of this type of technique is the Pyrolysis Combustion Flow Calorimeter (PCFC) developed by Lyon and Walters [79] and standardized as test ASTM D 7309.[80] The PCFC measures the rate at which the heat of combustion of fuel gases is released by a sample during controlled pyrolysis in an inert gas stream. The fuel gases are mixed with an excess of oxygen and combusted in a separate chamber where the instantaneous heat of combustion of the flowing gas stream is measured by oxygen consumption calorimetry.[78] This technique has already been used to investigate the flammability parameters of electric cable coverings [81,82,83] (insulators and jacketing), however each part of the cable was studied separately due to the PCFC sample holder limitation, which is only a few µg.

To summarize, despite the strict control of heating temperature and working atmosphere, the sample size limitation of micro scale techniques means they are not suitable for the purpose of this project, which is to investigate entire electric cable.

Bench or intermediate bench tests allow the analysis of materials in sample quantities ranging from grams (g) to kilograms (kg). These may therefore be appropriate for investigating the fire behaviour of an entire section of electric cable or other finished product. The experimental approach at this scale often involves measurement of heat release rate and/or flame spread of material subjected to a constant heat source. Among the techniques widely used the this scale, it is worth mentioning the classic example of the Cone Calorimeter referenced in ISO 5660-1,[84] or its derivative Mass Loss Cone referenced in ISO 13927.[85] This equipment enables the study of the fire reaction of materials using a sample size in the range 100 x 100 mm and up to 50 mm thick under a constant heat flux of 10 to 100 kW/m².[84, 85] These calorimeters are widely used in research and development for evaluating the flammability parameters, such as time to ignition and the heat release rate, of high performance fire-resistant polymeric materials[86, 87] Nonetheless, a drawback of cone calorimetry testing worth noting is its failure to take account of the dripping effect and flame spread.

Other intermediate scale tests, of the type single burning item (SBI), Steiner tunnel and those reported in standard IEC/EN 60332, are more suited to evaluating parameters such as flame spread and HRR. For instance, SBI is one of the key tests employed, according to EN 13823, in the Euroclass system for linings and most construction materials.[88] It investigates the fire response of a product in a corner configuration (Fig. 10) using two test samples of 0.5 x 1.5 m² and 1.0 x 1.5 m² placed in the same configuration and exposed to a 30 kW gas flame ignition. Measurements of fire growth, HRR, light obscuration and smoke production rate (SPR) are the principal results obtained with SBI.

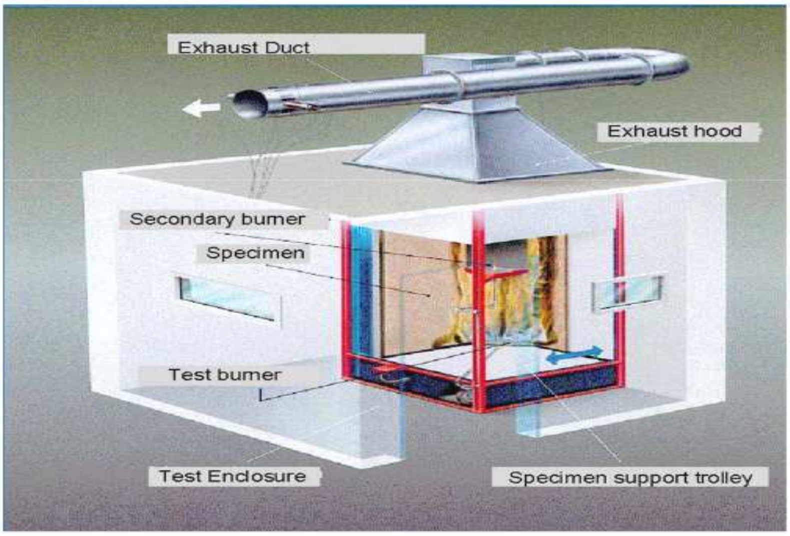

Figure 10. Single Burning Item test set-up

The Steiner tunnel is also widely used to test finished building products for their potential to sustain or propagate fire and their role in smoke production. Developed by Al Steiner of Underwriters Laboratories, the Steiner tunnel test has been incorporated into the North American Standards for Materials Testing as ASTME84.[89] The tunnel section is 7.3 meters long, 0.56 meters wide and 0.305 meters high (Fig. 11). The apparatus is equipped with two gas burners providing a flame intensity of 89 kW with air and combustion products being propagated through the tunnel by a ventilation system at a controlled velocity of 73 metres per minute.

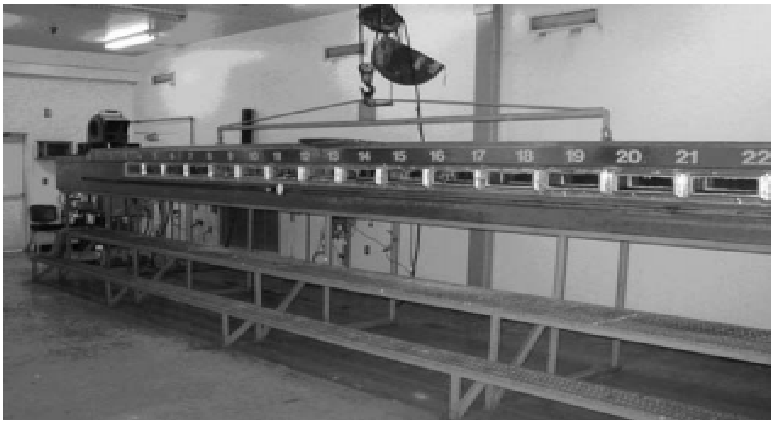

Figure 11. The Steiner tunnel test

The progress of the front of the flame across the test material is measured by visual observation and the smoke emitted estimated using optical density criteria. A flame spread index and a smoke-developed index are then calculated for the product from these results. However, the Steiner tunnel test does not measure the ignitability of the materials, the heat release rate or dripping. In addition to the SBI and Steiner tunnel, standard methods referenced according to IEC/EN 60332 [90] are also noted. These are based on a flame spread assessment for a 3.5 m length of vertically bunched wires or cables. Basically, a calibrated flame is applied to the sample using a 45 ° tilted burner (Fig. 12) and the damaged length measured at the end of the test. Based on this measurement, the cable or wire is declared to either pass or fail the prescribed standards.

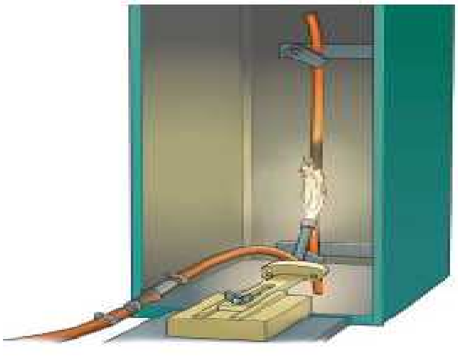

Figure 12. IEC/EN 60332 -1-3 flame test of resistance to vertical flame distribution

IEC/EN 60332 methods are not limited to a measure of the physical damage to the length of wire or electric cable; parameters such as Heat Release Rate (HRR) and Smoke Production Rate (SPR) are also tested. IEC/EN 60332 standard tests have already been used in cable testing.[91, 92]

Although the equipment mentioned above is suited to the characterization of the flammability parameters of materials under controlled conditions, depending on the finished product, these investigations may not be sufficient to describe their behaviour in a realistic fire scenario. For this reason, it is also necessary to perform full fire tests on the finished materials but the latter are both time consuming and very expensive.

The aim of this project is to develop a bench test enabling simultaneous analysis of flammability parameters, gas evolution and smoke particles of finished materials during a fire event. As a result of this review, particular attention is now focused on a cone calorimeter as a fire model, more specifically a mass loss cone, as the latter allows investigating samples in the size range of 100 x 100 x 50 mm^3 and is therefore suitable to test an entire section of electric cable. The secondary considerations which prompted the choice of a mass loss cone calorimeter as the fire model will be discussed in chapter 2.

In addition to the evaluation of flammability parameters, an exhaustive investigation of the fire behaviour of materials must necessarily include analysis of the evolved gases and particles in the smoke. The analytical techniques usually employed in particles and gas phase investigations are presented in the following section.

4.2 Gas phase analysis

Due to the large number of chemical species potentially released in the smoke and to the dynamics of fire itself, analysis of evolved gases in the smoke generated by a materials fire is a complex process. Nonetheless, with appropriate sampling and chemical analysis instruments, investigation of the gas phase during thermal decomposition of materials should be possible.[93] A review of analysis techniques commonly used for identification of chemical species in the gas phase is presented hereafter.

One of the techniques widely reported in relation to investigations of gas emissions in the smoke produced by thermal decomposition of material is Fourier Transform Infrared Spectroscopy (FTIR). This technique is based on the interaction of matter and IR radiation. It enables not only qualitative but also quantitative “real time” analysis of many chemical species (organic and inorganic). FTIR has already been used in combination with TGA or STA in the qualitative analysis of gases evolved from the thermal decomposition of unfilled EVA and of EVA filled with additive FRs.[31, 38]

Apart from the FTIR technique, another gas analysis technique is Gas Chromatography Coupled to the Mass Spectrometry (GC/MS), combining one technique for separating the vaporized compounds (GC) and another for elucidating the structure of these molecules by measuring their mass to charge ratio (MS).[94] The GC/MS combination enables investigation of complex mixtures in trace amounts. GC/MS is currently equipped with a pyrolyzer, forming an analytical system known as Pyrolysis/Gas Chromatography/Mass spectroscopy (Py-GC/MS) (Fig. 13). The latter has been used in polymer research for various purposes, including structure identification, qualitative determination, thermal degradation kinetics and additives analysis.[95, 96]

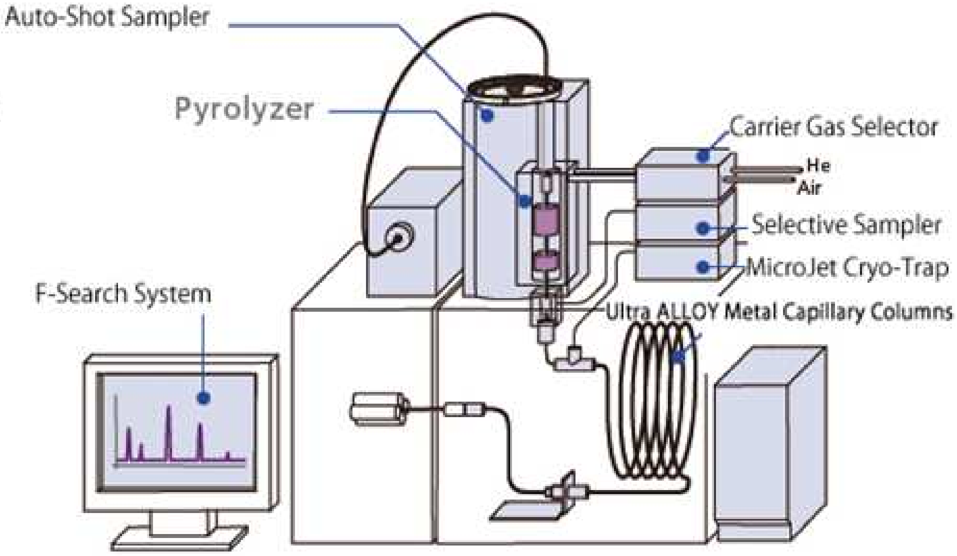

Figure 13. Schematic representation of Pyrolysis/Gas Chromatography/Mass spectroscopy

However, a notable drawback of GC/MS is that it cannot follow the gas species released during the thermal decomposition process in real time, because the detection of volatiles compounds by MS detector only occurs as the separated substances start leaving the GC column. Apart from FTIR and GC/MS, several other specific gas analysis techniques are also described in literature;[96] for example, the Electron Paramagnetic Resonance (EPR) suiting the analysis of paramagnetic molecules such as O_2, NO and NO_2.

In view of the GC/MS cannot be used to study evolved gases in real time, FTIR appears the most appropriate technique for monitoring, in real time, the gas phase of the smoke emitted during cone calorimetry. Knowledge of soot particles dispersed in smoke is also of interest in this project and therefore techniques specifically dedicated to the analysis of particles released out of the flame are presented in the next section.

4.3 Particle analysis

Analysis of the particles released as a result of thermal decomposition or the fire processes of materials often consists of determining their size distribution, number or mass concentration and their structure and/or morphology. Regarding the analysis of particles in a fire event, one of two reported approaches can be taken: (i) an «in situ» approach involving the direct study of particles inside the flame and (ii) an «ex situ» approach in which the particles suspended in the smoke are analyzed. In this project, only the second approach is of interest.

Particle size analyzer equipment is generally based on the principles of electric mobility and/or aerodynamic diameter of particles. Among the «ex situ» devices currently used to analyze particles in the smoke or airborne, we can mention the Scanning Mobility Particle Sizer (SMPS). SMPS is mainly made of an ionization system or charger, a Differential Mobility Analyzer (DMA) or electrostatic classifier and particles counter or Condensation Nucleus Counter (CNC, Fig. 14).

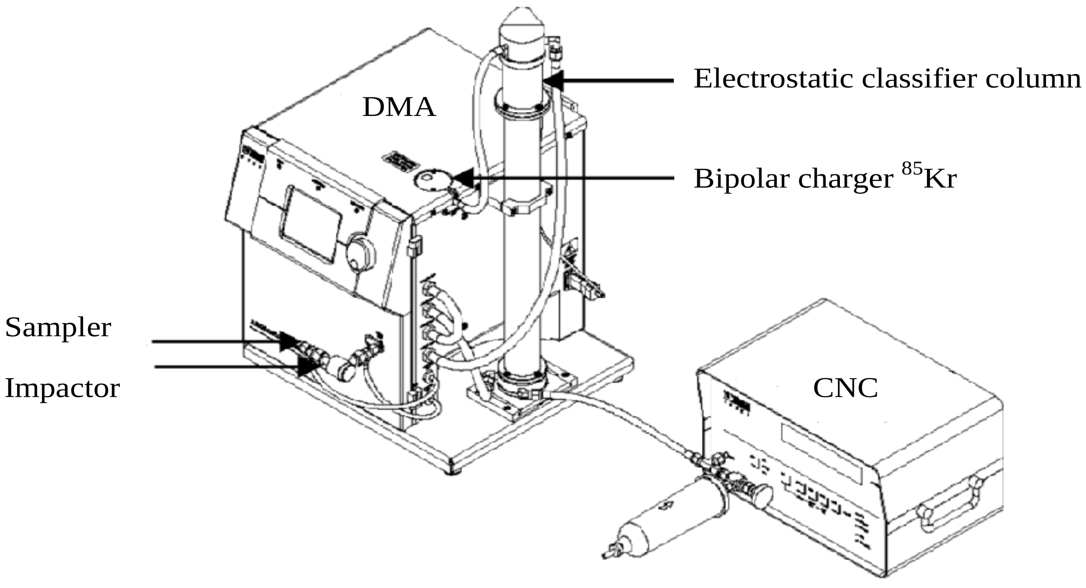

Figure 14. Schematic diagram of Scanning Mobility Particle Sizer

The principle of SMPS consists of imposing a charge to the particles sample through the ionization system, after which particles are classified in the DMA according to their electrostatic mobility and then counted in the CNC.[97] The use of SMPS has been reported in the investigation of particles emitted during the thermal decomposition of wood pellets used for domestic heatin[98] and in the investigation of motor vehicle particules emission.[99] However, it is important to note that SMPS has the disadvantage of limiting determination of particle-size distributions to within the sole range of submicron or nanometric particles (< 1µm) and does not take account of certain parameters such as the mass concentration. The empirical technique, using high efficiency filter weighing before and after the collection of particles, is still used to evaluate the mass of emitted particles. This technique is used to investigate the mass of motor vehicle particles emissions, however it does not allow for a real time analysis of this parameter.

In this regard, the Tapered Element Oscillating Microbalance (TEOM) (Fig. 15) is worth mentioning. This instrument is based on a quasi-instantaneous measurement of the mass of particles collected on an exchangeable filter cartridge. The technique consists of monitoring the corresponding frequency changes on a tapered element: the more mass is accumulated on the exchangeable filter, the more the tube's natural frequency of oscillation decreases. There is a direct relationship between the change in the tube’s frequency and the corresponding mass on the filter.[100] The vibration frequency is converted to mass concentrations every 13 s. To eliminate the effect of water associated with hygroscopic salts, temperatures at the sampler inlet and at the TEOM filter are usually maintained at 50°C.

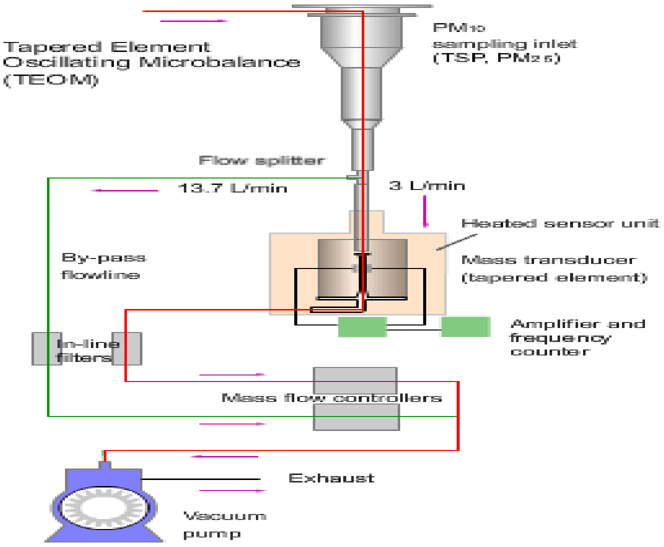

Figure 15. Schematic diagram of the Tapered Element Oscillating Microbalance

Apart from the SMPS, filter weight and TEOM techniques described above, use of a cascade impactor as an ex situ particles analyzer is also reported in the literature. With this technique, the mass of the particles is expressed in terms of their size distribution. The function of the cascade impactor can be directly deduced from its design (Fig. 16), which consists of a powered flow chamber containing a number of discs, each disc within the flow chamber representing a stage of the impactor. These stages are assembled in order of decreasing size allowing separation of particles according to their size fractions: from large (20 µm) to small (0.5 µm). Inside the cascade impactor, particles are drawn from stage to stage, each stage providing progressively smaller jets: the lighter the particle, the further it travels into the impactor. Once the entire sample has passed through the impactor, the particle quantities captured on each of the discs are individually collected allowing the user to then determine the dispersion rate of particles emitted from the material under study.

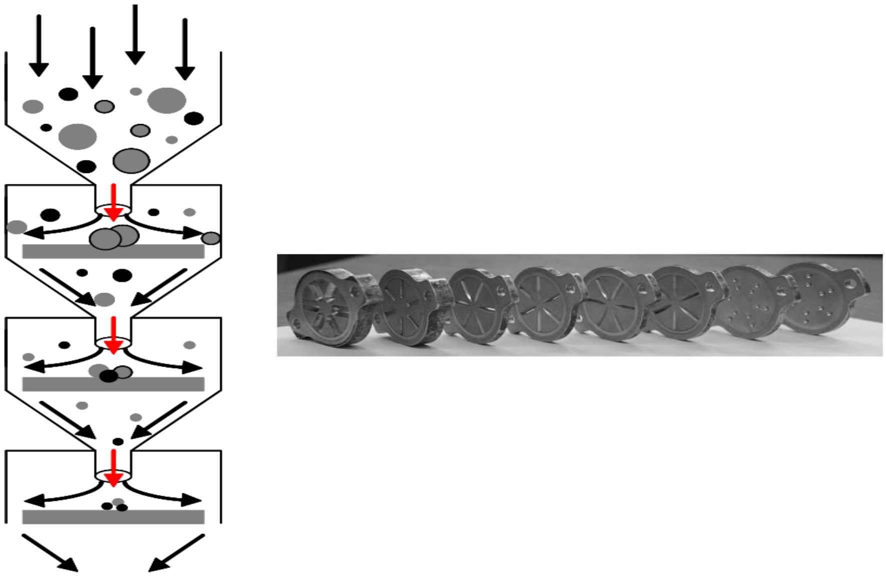

Figure 16. Schematic diagram of the cascade impactor with photographed discs [101]

As reported in literature, a cascade impactor was used for characterization of the smoke particles released during a fire test of polymers containing nanocomposite additives (materials found in buildings), as part of an investigation into their toxicological impact.[101] However, in spite of its ability to provide particle-size distributions, the cascade impactor does not allow for evaluation of concentration in number of particles.

On the other hand, a relatively new instrument, developed by Keskinen et al.[102] is being increasingly used as an ex situ particles analysis technique. This is the Electrical Low Pressure Impactor (ELPI) which combines a variety of functionalities including particle charging, size classification according to aerodynamic diameter (da) and electrical detection. This enables investigating, in real-time, not only the size distribution but also the concentration of particles in the size range of 6 nm to 10 µm. In addition, ELPI can be used for sampling particles with the use of filters, for further chemical or morphological analysis with scanning electron microscopy, etc. In contrast to SMPS, TEOM, and the cascade impactor, all of which are limited to the measure of one or two parameters only, ELPI finally assembles in the one instrument multifunctional capacity, especially for real time analysis of the size distribution and concentration in number and mass of particles over a wide size range. ELPI appears to be the suitable instrument for the study of particles in fire smoke and therefore to meet the requirements of this project. It has already shown its capacity as a particles analyzer in numerous applications including airborne, automotive diesel and indoor air, as well as for pharmaceutical processes.[103] However, the literature review found no published data to confirm its previous use in the investigation of soot particles present in the smoke generated by thermal decomposition of polymers.

5 Conclusion

This first chapter was dedicated to a discussion of the specific problems addressed by this project, namely fire and related parameters; polymer decomposition and flame retardancy, as well as a state of the art on experimental techniques for the characterization of flammability, evolved gases and soot particles. Fire prevention and/or mitigation remains a current issue due to the loss of life, property damage and economic consequences engendered by fire; in particular the associated heat release and toxic and/or corrosive gases and particles emissions carried in (often travelling) smoke. Some fire-related risks, such as heat release rate, evolved gases and particles, may vary in function of the fire conditions and the chemical compositions of burning materials. A common risk mitigating measure is the use of fire retardant materials and/or additives. However, some halogenated compounds, previously used as flame retardants, are now banned in Europe. As a consequence, research laboratories and industrial manufacturers alike are now focusing their efforts on zero-halogenated additives such as aluminium trihydroxide, etc.

Numerous experimental techniques currently employed in the study of the thermal decomposition characteristics of materials (TGA, DSC, DTA, MLC...), gas phase evolution (FTIR, GC/M, FID...) and particles (SMPS, TEOM, ELPI…) have been reviewed and compared as to their efficacy and drawbacks. In line with the aim of this project, which is to extend fire behaviour characterization of electric cable materials under fire simulation conditions to an entire section of cable, the following have been selected as the most appropriate techniques: a Mass loss cone fire model, Fourier transform infrared spectroscopy gas analysis technique and Electrical low pressure impactor for particles analysis.

Each of these techniques is presented and discussed in the next chapter. The design concept of coupling the Mass Loss Cone/Fourier Transform Infrared spectroscopy/Electrical Low Pressure Impactor as a simultaneous experimental bench test will then be fully commented.

CHAPTER 2: CONCEPTION OF COUPLING MASS LOSS CONE, FOURIER TRANSFORM INFRARED SPECTROSCOPY AND ELECTRICAL LOW PRESSURE IMPACTOR

Synthetic and man-made polymers are the prevailing materials of choice for manufacturers of finished materials and end-users alike. The study of the fire behaviour of these materials in terms of decomposition parameters as well as the analysis of their fire effluents are an essential prerequisite for assessing their potential health, safety and environmental impacts. This chapter is dedicated to the design concept of an experimental bench test allowing to simultaneously assess (i) flammability parameters, (ii) evolved gases (qualitatively and quantitatively) and (iii) soot particles (size distribution and concentration) present in smoke. This experimental bench test will focus on the fire characterization of specific materials such as electric cables, which are difficult to fully examine with small scale tests like TGA/FTIR or Py-GC/MS. The instruments selected for the purpose of this work are the Mass Loss Cone (MLC) as fire model, Fourier Transform Infrared Spectroscopy (FTIR) as gas analysis technique and Electrical Low Pressure Impactor (ELPI) for particles analysis.

The first section of this chapter contains a detailed presentation of the equipment (MLC, FTIR, ELPI) used. In the second section, the design concept of coupling MLC/FTIR/ELPI as a simultaneous bench to investigate the evolving gases and particles during MLC test is explained. This is extended to include a description of the setup of FTIR gas acquisition parameters and the development of the gas quantitative analysis method. This is followed by a similar report on the ELPI setup for studying particles released out of the flame.

1 Experimental equipment

1.1 Mass loss cone

Mass loss cone is widely recognized as a fire model for the evaluation of calorimetric parameters. Similarly to the standard cone calorimeter, a mass loss cone consists of a conical heater that generates controlled heat fluxes from 10 - 100 kW/m² to simulate fire dynamics. The mass loss cone is equipped with a thermopile which is constituted of four thermocouples located at the top of a chimney, directly connected to the conical heater. This chimney collects all the smoke released during the fire test and the thermopile, previously calibrated with methane, evaluates HRR. Here, the temperature change of the air mass flow is measured using the sensible enthalpy rise approach[104, 105] rather than the oxygen consumption method of standard cone calorimeter.[85] The simplicity of use of MLC, its collection of smoke in the chimney and the acceptable sample size range (up to a maximum 100 x 100 x 50 mm^3) have confirmed the choice of this instrument as the most suitable fire model for this project. A schematic representation of the MLC manufactured by Fire Testing Technology (FTT), which is used in this study, is provided in Fig. 17.

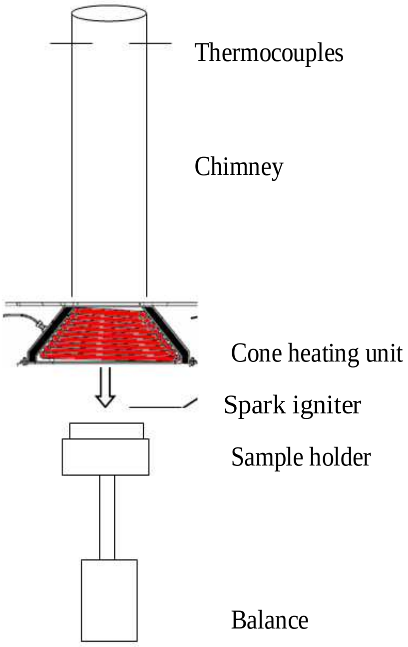

Figure 17. Schematic presentation of mass loss cone

In addition to the heating unit and thermopile, the MLC incorporates a mass balance to follow sample mass evolution during a fire test, a sample holder and an intermittent spark igniter 13 mm above the sample to trigger piloted ignition (Fig. 17). The parameters measured with MLC are: heat release rate (HHR), time to ignition (t_{ig}), mass loss rate (MLR), as well as derivative parameters such as the Total Heat release (THR), Critical Heat Flux (CHF) and Effective Heat of Combustion (EHC) of materials. A detailed description of Mass Loss Cone and the calibration of its thermopile are reported in ISO 13927.[85] Despite the simplicity of measuring the flammability parameters of materials in fire conditions with MLC, a limitation of this instrument is the lack of analysis of evolved gases and soot smoke particles.

Detailed knowledge of these fire phenomena (gas and particles) is of vital interest not only because of the potential risks they pose to health and the environment but also because of growing concerns about their impact on the safety of electronic/digital systems and devices.

For this reason, it is proposed to couple MLC with online gas and particles analysis techniques, namely FTIR and ELPI, as an alternative experimental bench test.

1.2 Infrared spectroscopy and Fourier Transform Infrared Spectroscopy

Infrared (IR) spectroscopy is a well-known chemical analysis technique whose operating principal is based on the interaction of IR radiation with matter: It is commonly known that molecules can absorb infrared radiation, inducing vibrational and/or rotational transitions within the chemical bonds as a normal consequence of thermal (IR) activity.[106] Three types of IR analysis spectrometer have been developed: classical Infrared spectroscopy, Non Dispersive Infrared Spectroscopy (NDIR) and Fourier Transform Infrared spectroscopy (FTIR). The last mentioned is one of the most powerful and widely used techniques for monitoring species in solid, liquid or gas phase state.[107,108] FTIR outclasses traditional Infrared spectroscopy owing to its use of the Michelson Interferometer and application of the Fourier transform mathematic operation, which enables simultaneous analysis of numerous components over a relatively short time span (few seconds).[109] The evident advantages of FTIR as a multi component and real time analysis technique motivated the decision to use this technique to study the gas species present in the fire smoke of material under study. The basic concepts of infrared spectroscopy are next briefly reiterated and a presentation of the iS10 FTIR spectrometer, which will be used in this study, follows.

As mentioned above, infrared spectroscopy exploits the fact that molecules can absorb IR radiations at specific frequencies inducing vibration and/or rotation of their chemicals bonds. If the frequency of IR radiation matches the natural vibration frequency of molecular bonds, the radiation is absorbed causing changes in the amplitude of the molecule energy which passes from its ground electronic state to an excited state. More precisely, the electric field of the incident electromagnetic radiation interacts with the dipole moment of chemical bonds.[104] This means that only molecules possessing a dipole moment, or positive and negative charge regions between their atoms, can interact with IR light and therefore be active in infrared spectroscopy. Many chemicals species, whether organic or inorganic, in solid, liquid or gas state possess this FTIR basic requirement. However, homo-nuclear diatomic molecules such as oxygen (O_2) and nitrogen (N_2) are transparent in IR owing to their lack of polarized bonds. In the same way, noble gases like helium (He) and argon (Ar) cannot absorb infrared radiation and so do not have infrared activity. In addition, since each molecule is a unique combination of atoms, two compounds will not have the same infrared activity. In consequence, IR spectroscopy will be used as an explicit approach to identifying chemical species. However, as with all chemical techniques based on the interaction of matter with electromagnetic radiation, an overlapping phenomenon that occurs between species having similar properties (for example same functional group) may represent a limitation and should be taken into account during exploitation and interpretation of infrared spectra. Further explanations regarding the fundamental theory of infrared spectroscopy can be found elsewhere.[106-109]

For this project, a Thermo Nicolet iS10 FTIR spectrometer equipped with an Ever-glo TM GLOBAR infrared source capable of producing IR radiation over a wide range (from 50 to 7400 cm^{-1}), an optical path length of 2 m, a 0.2 L volume gas cell and a nitrogen MCT (Mercury Cadmium Telluride) detector will be applied to the online analysis of the gas phase in fire smoke. Note that an FTIR background spectrum, which gives information about the energy of the IR source, the detector, the gas cell components, mirrors, windows, etc. (Fig. 18), must be run prior to any analysis, in order to limit any influence by the work environment; for instance, ambient water and carbon dioxide interacting widely with IR light.

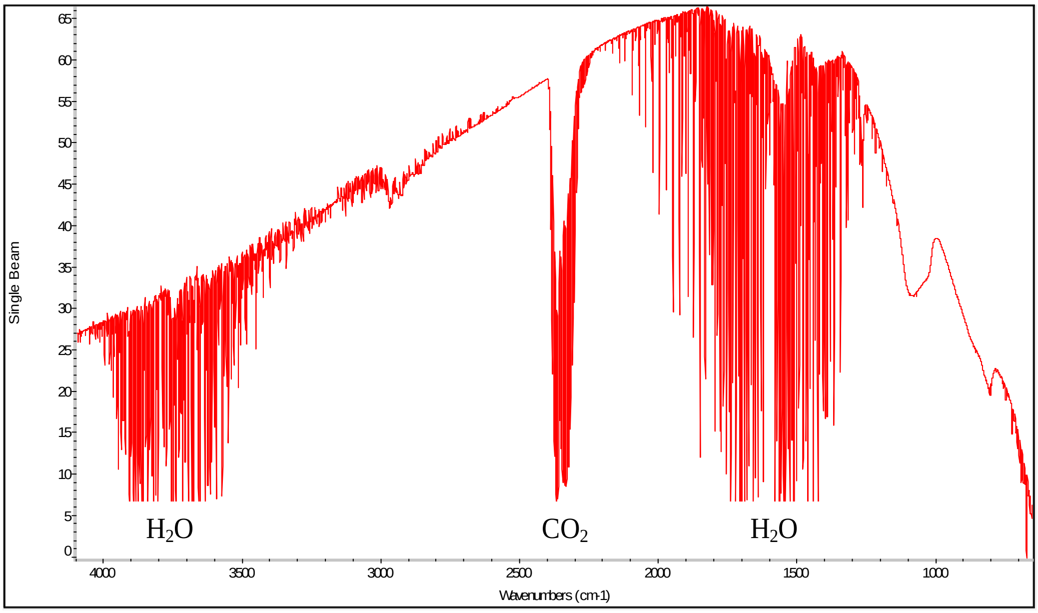

Figure 18. iS10 FTIR background spectrum from ambient atmospheric

Furthermore, FTIR spectrum is originally plotted as transmittance (Fig. 19) according to Equation 3. However, to facilitate usage of IR spectra for quantitative analysis of species, the transmittance spectrum is converted to absorbance or optical density (Fig. 20) according to equation 4.

$$\%T = 100 \times I/I_o \qquad (3)$$

Where I_0 is the intensity of incident beam, I the transmitted intensity after passing through the measuring cell and T the transmittance in percent

$$A = -\log T \qquad (4)$$

Where A is the absorbance

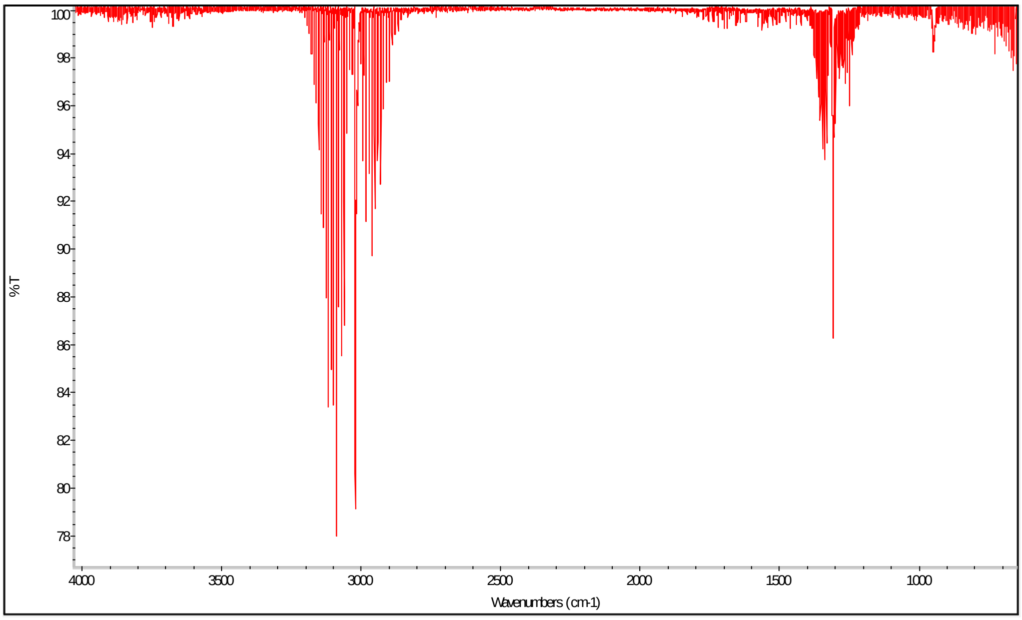

Figure 19. FTIR spectrum in transmission with methane as standard gas

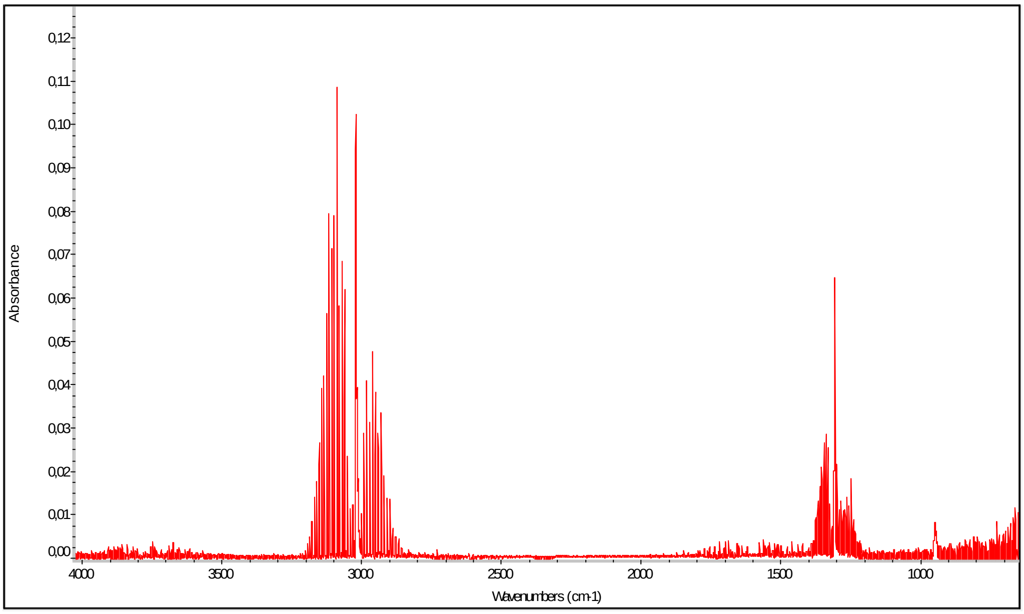

Figure 20. FTIR spectrum in absorbance with methane as standard gas

Beside the requirement for characterization of gas species present in fire smoke, particles dispersed in the gas phase are also of interest to this study. The latter will be measured using the Electrical low pressure impactor.

1.3 Electrical Low Pressure Impactor

The Electrical Low Pressure Impactor is a particles analyzer that combines particle charge, particle size (according to aerodynamic diameter) and electrical signal.[110] For this reason, ELPI is of major interest in the context of this project to characterize soot particles present in the smoke of the fire simulation. It can also be used for filter collection of particles, for morphological or elementary analysis with analytical techniques. The Dekati ELPI^{+TM} used in this project, principally composed of a sample inlet, charger, impactor and electrometers, is shown at Fig. 21. Its operating principle and factors that may have an influence on measurements and the interpretation of ELPI data will be discussed hereafter.

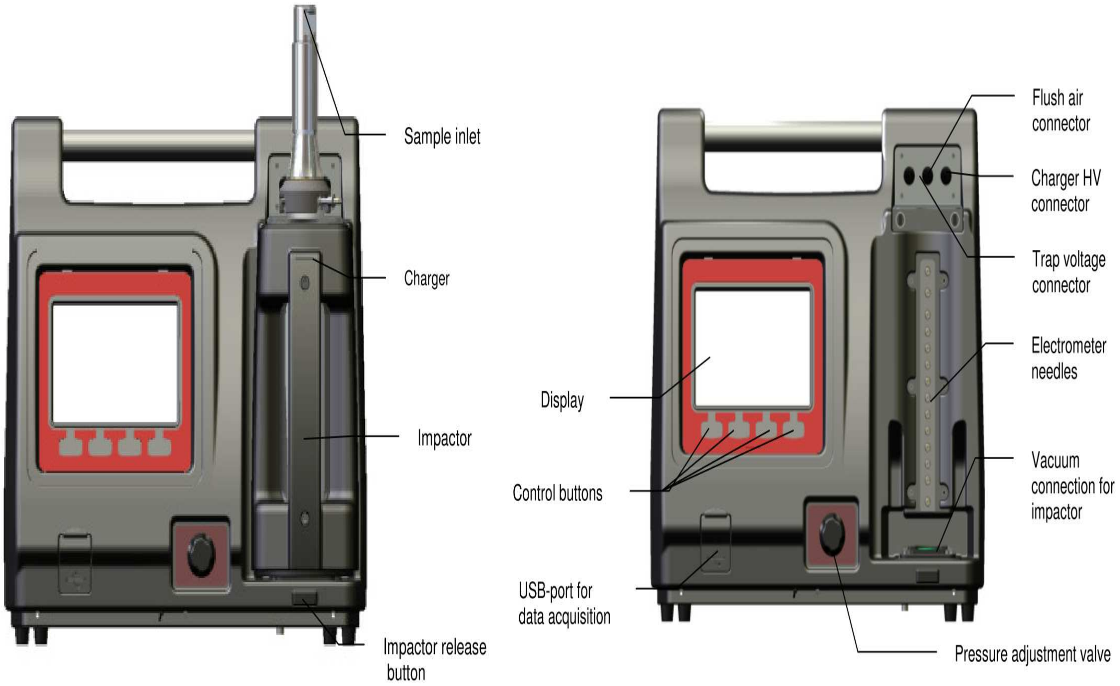

Figure 21. Electrical Low Pressure Impactor, housing and connectors

Given that the analytical instruments selected above (FTIR, ELPI) are capable of gas phase characterization, the interest of integrating this equipment with MLC fire model is evident.

2 Combination of mass loss cone, Fourier transform infrared spectroscopy and electrical low pressure impactor

To realize the MLC/FTIR/ELPI coupling (Fig. 22), it was necessary to incorporate some modifications with respect to the mass loss cone. These modifications were made in order to extract smoke from the chimney for analysis with the FTIR and ELPI instruments. A stainless steel extension of 250 mm was first added to the MLC chimney so that two smoke retrieval probes could be installed just above the thermopile (50 mm). It is assumed that the smoke stream flow at this location can be considered homogeneous and laminar (Reynolds number estimated to be less than 2000 considering that the fluid in this case is mainly air in the chimney). To monitor gas phase release during the MLC test, a sampling system between one of the probes in the chimney and the FTIR gas cell was next set up. It consists of a first ceramic filter cylinder (10 µm) installed close to the probe, which is linked to a 6 m length of polytetrafluoroethylene (PTFE) transport line, and of a second filter (2 µm) connected to the FTIR gas cell by a PTFE line of 1 m. This section of the gas sampling system (shown on the right side of Fig. 22) as well as the FTIR gas cell are equipped with a controlled heater blanket and, for the FTIR cell, heater housing. In addition, a pump system with an integrated flow meter and valve to provide controlled and constant sample flow was placed on the bench at the far side of the FTIR. A pressure gauge equipped with a regulator valve to maintain constant pressure in the gas cell was also installed. The two filters are designed to protect the FTIR gas cell, in particular the beam and the mirror, from smoke particles by filtering these out of the sample before it enters the cell.

To enable simultaneous analysis of particles with the ELPI, a second sampling system (shown on the left side of Fig. 22) is also set up. This consists in connecting the second retrieval probe to a heated antistatic PTFE line to prevent static electricity build up during transfer of the particles sample from the chimney to the ELPI analyzer. A vacuum pump located at the far side of the ELPI is set by the manufacturer to regulate isokinetic flow to a rate of 10 L/min. Similarly to the FTIR line, the antistatic PTFE line is equipped with a controlled heater blanket to prevent humidity effects on particle measurements.

Finally, to enable quantitative determination of the gases evolved from the MLC fire test, an FTIR gas calibration system was also developed. Shown at the top right side of Fig. 22, it consists of multiple compressed gas cylinders at a given concentration. These cylinders are linked to a platinum (divider/diluter) gas mixing device comprising mass flow meters specific to each gas of interest. The latter are controlled via an automated computer system to allow delivery of a precise amount of mixed gases, with nitrogen as the dilution gas, to obtain calibration points. All of the details mentioned above are schematically illustrated in Fig. 22.

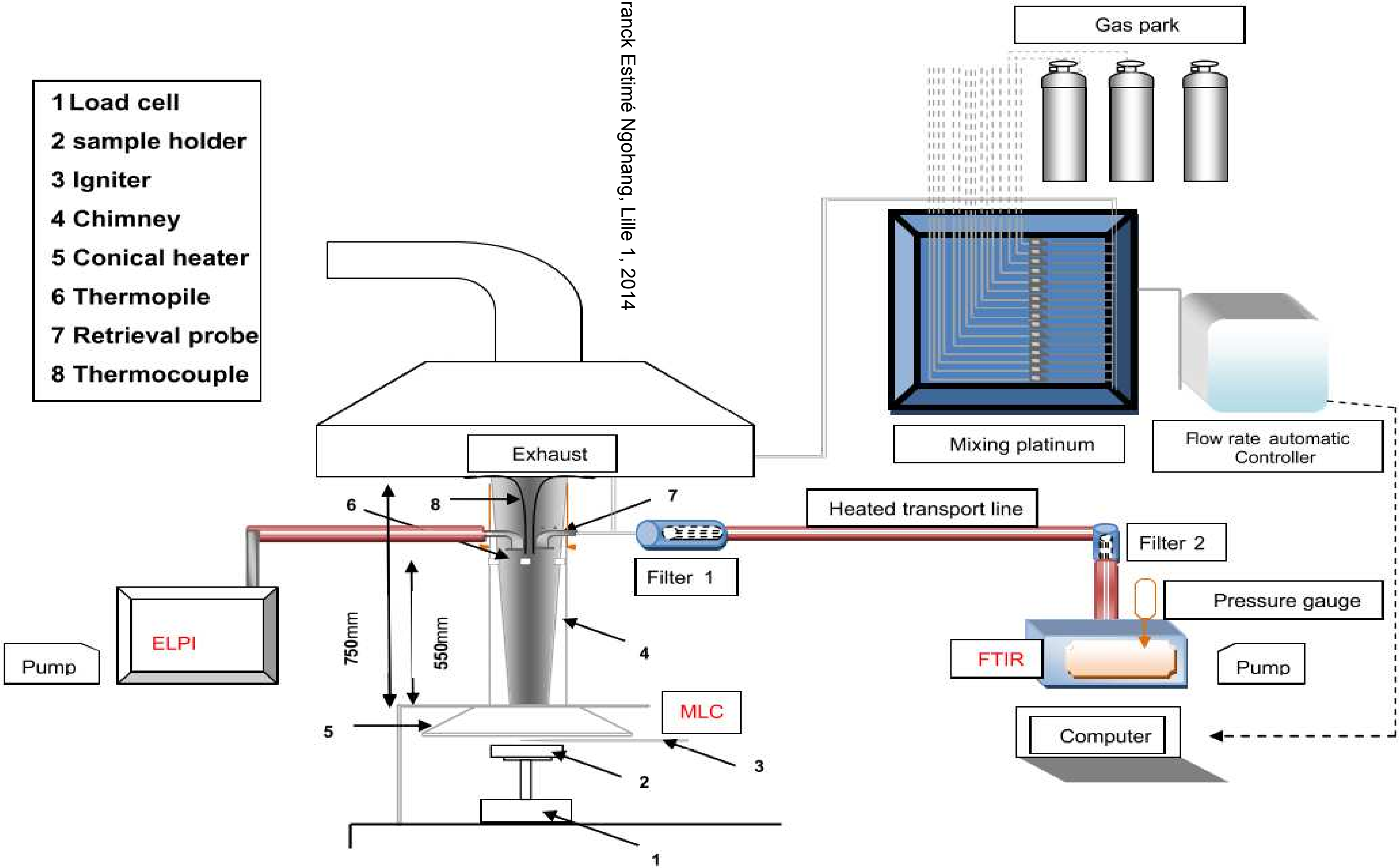

Figure 22. Design layout of the mass loss cone, Fourier transform infrared spectroscopy and electrical low pressure impactor coupling

2.1 FTIR gas analysis method

Investigation of gas species in the smoke from the MLC fire test will be carried out in two stages, the first of which consists in identifying the nature of the gases generated during the combustion process of the material. The second step comprises the quantitative analysis over time of the evolving gases. Because fire is a dynamic phenomenon, the FTIR spectrometer must be set up (configuration of acquisition parameters) to follow the gas - phase chemistry changes throughout the fire process. Spectral resolution and number of scans are the main FTIR internal parameters and these have to be carefully established owing to their effect on the acquisition time and the form of the infrared spectrum.[111] Other parameters, including the apodization function or experimental conditions such as temperature and pressure in the FTIR gas cell, must also be taken into account to ensure that the gas phase analysis yields accurate and repeatable results.

2.1.1 Configuration of acquisition parameters

The IR light spectrum can be divided into three regions, near, mid and far-infrared. The region of interest in this study is mid-infrared, more precisely from 4100 to 650 cm^{-1}, this being because the absorption spectra of most organic and inorganic compounds lie within this region. Other acquisition parameters (spectral resolution, number of scan(s), etc.) are configured as follows:

a) Spectral resolution

Spectral resolution (SR) is the ability to resolve two neighbouring bands in a spectrum into their separate components. Expressed in inverse centimetres (cm^{-1}), spectral resolution has a major impact on gas analysis results: the higher the spectral resolution (lower numerical value), the more the significant becomes the spacing between adjacent spectral features.[110] An analyst will naturally select the SR according to the application involved and also depending on the physical state of the sample. A sample with many chemical environments, for example one that is in liquid or condensed state, will inherently have wide bands and therefore require low SR. On the other hand, samples with few chemical environments such as vapours and gases will characteristically show narrow absorption bands. Consequently, a high SR shows more spectral features than a low SR in the case of gas phase analysis.[110] Fig. 23 contains the plotted results of nitrogen monoxide (NO) and methane (CH_4) spectra acquired with the iS10FTIR spectrometer with SR set at 2 and then 0.5 cm^{-1}. As can be seen, the spectra acquired at 0.5 cm^{-1} show more features (absorption bands) than those acquired at 2 cm^{-1}. In consequence, the higher spectral resolution (0.5 cm^{-1}) is selected for gas phase analysis in the context of the present study.

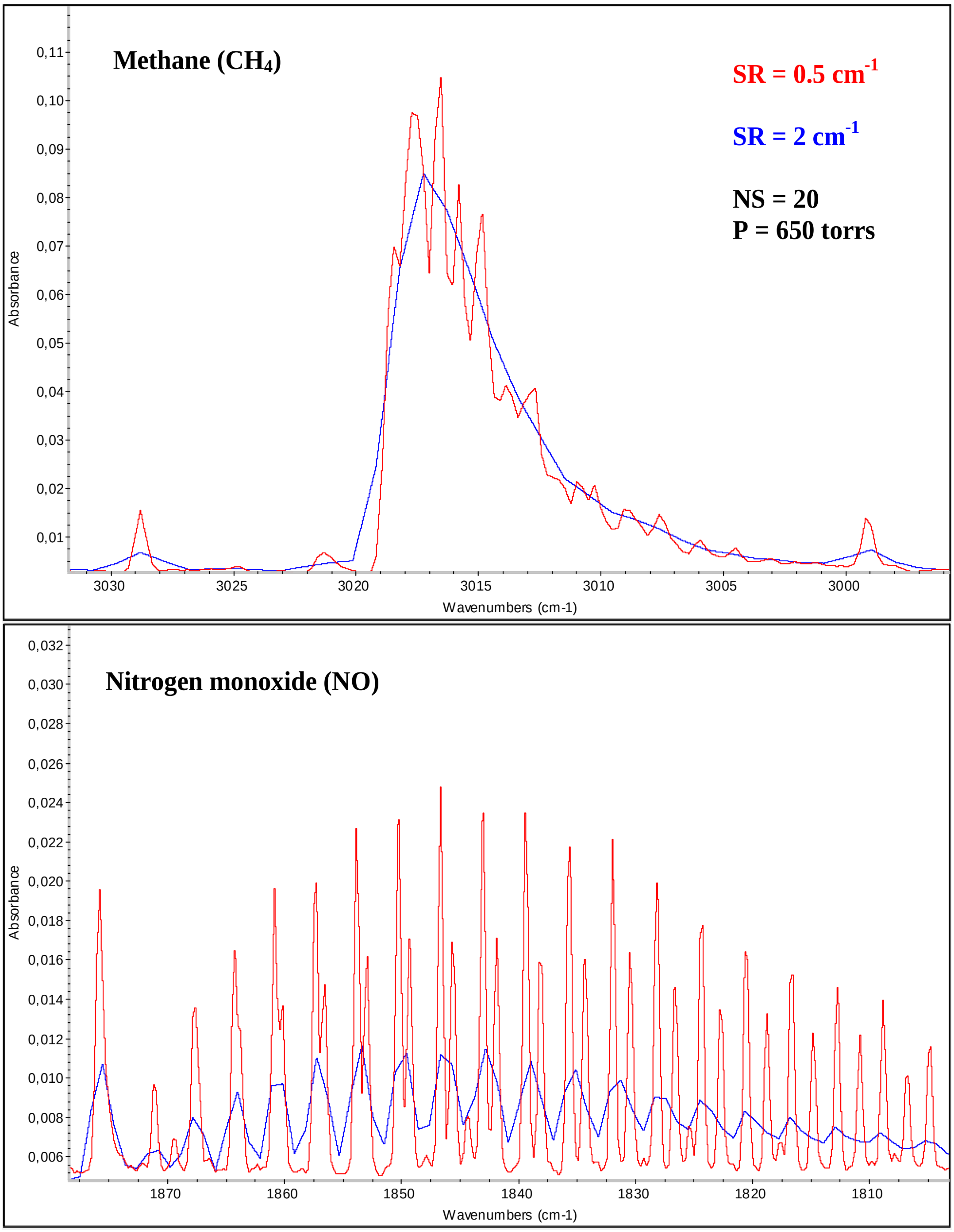

Figure 23. Comparison of spectra acquired for CH_4 and NO illustrating separation of close lying peaks in high resolution mode as against the merged peaks at low resolution

b) Number of scans

The number of scans (NS) determines the number of required paths for the movable mirror in the interferometer. Increasing the NS increases the signal-to-noise ratio and thus the sensitivity of the FTIR apparatus. On the other hand, it also increases the total time required to obtain FTIR spectra.[110] The effect of NS on the signal: noise ratio of the iS10 FTIR spectrometer during acquisition of nitrogen (inactive gas in IR) absorption spectrum, with NS = 1 and NS = 20 is shown at Fig. 24. It can clearly be seen that the spectral noise response of the iS10 FTIR spectrometer, in the spectral range from 4100 to 650 cm^{-1}, is higher for NS = 1 (0.004 A.U) than for NS = 20 (0.001 A.U), with A.U being arbitrary units. For real time monitoring of evolved gases, a number of scans equal to one (NS = 1) is the preferable choice to prevent information being lost because of the longer acquisition time required for multiple scanning.

However, with regard to the FTIR gas quantitative method, a number of scans equivalent to one may affect calibration point accuracy (especially for lower concentrations) as the noise ratio is relatively high. Thereupon, a number of scan equal to twenty (NS = 20) has been selected, as a compromise, to avoid high noise ratio when acquiring the absorbance spectrum of a standard gas with known concentration during FTIR gas cell calibration.

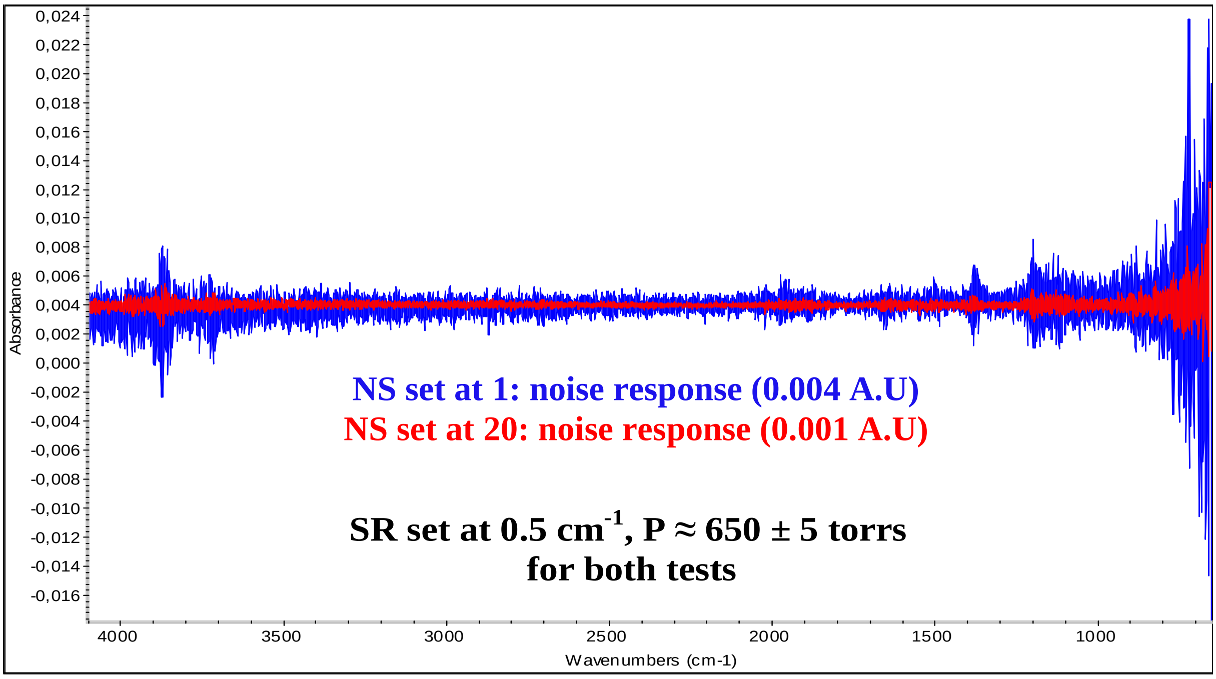

Figure 24. Noise ratio of iS10 FTIR spectrometer with IR-inactive nitrogen as a function of NS, for NS =1 and NS=20

c) Apodization function

Numerous steps are involved in the acquisition of an infrared spectrum, potentially inducing instrumental imperfections or limits in the basic digitization. These electronic or optical imperfections may introduce erroneous features (side lobes) from the interferogram to the FTIR spectrum.[112] An apodization function, applied on the interferogram prior to the Fourier transform operation, is used to correct the artificial creation of spectral features. Several apodization functions are available with the iS10 FTIR spectrometer, among which are the Triangular apodization, allowing to reduce side lobes but which may result in poorly resolved peaks; the Boxcar apodization which allows maximum resolution but can result in ringing effects, and the Happ-Genzel apodization, which is preferred because it minimizes band side lobes with minimal loss of resolution. The Boxcar and Happ-Genzel apodizations are the more appropriate for gas phase analysis.[113] However, as Boxcar can result in ringing effects, the Happ-Genzel is the preferred choice for this study.

d) Temperature and pressure

The temperature and pressure parameters that are not directly integrated in the internal configuration of the iS10 FTIR spectrometer. However, they must be taken into account in order to obtain accurate and repeatable results. In fact, the energy level of the molecule is governed by the Boltzmann distribution, which is temperature dependent.[114] As a result, variations in the temperature can in turn induce variations in peak intensity and hence in species concentration. For reproducible quantitative results, it is therefore essential to work at constant temperature: the same temperature for the standard gas and the fire smoke sample within the gas analyzer system. Likewise, pressure changes in the gas cell will result in a broadening of spectral bands and changes to their intensity. This is ascribed to collisions between molecules which are associated with energy in addition to that associated with the absorption of infrared radiation. Hence, it is important to maintain constant pressure in the FTIR gas cell. Numerous studies report the influence of temperature and pressure on infrared absorption spectra. With these as a reference, it was decided to set the temperature of the gas analysis system, from the transport line to the FTIR gas cell at 180 °C and the pressure in the FTIR gas cell below the atmospheric pressure at 650 ± 5 torrs.[115, 116]

With the configuration of the FTIR gas cell acquisition parameters and the appropriate experimental conditions to obtain gas phase spectra determined, value may now be added to the FTIR spectrometer through the development of gas quantitative analysis methods. In this regard, it is worth remarking that of the exploitation of the FTIR instrument's capacity for gas quantitative analysis is associated by some with high initial start-up costs (infrastructure, knowledge, time consuming) and therefore often overlooked. The next section of this study focuses on the development of an FTIR quantitative analysis method for gases.

2.1.2 Quantitative analysis method

FTIR will only be considered a valuable quantitative analysis instrument providing the area under the peaks of absorbance bands is related to the concentration of chemical species within the sample. All infrared quantitative analysis is based on Beer's law which states the linear relationship between the absorbance of an IR-absorbing substance and its concentration (equation 5).

$$A = \varepsilon l c \qquad (5)$$

Where A is the measured absorbance, ε the molar absorptivity, l the path length and c the concentration.

However, over a wide range of concentrations the linearity of Beer' law is limited, notably due to the nonlinearity caused by electrostatic interactions between molecules in close proximity.[117] Beer's law also has its limits concerning the quantification of complex mixtures. Absorbance being additive, when two or more substances absorb at the same wavelength, Beer' law does not allow their differentiation. Owing to the necessity of assessing species concentrations in numerous applications, computational models have been developed to help overcome these limitations, i.e. nonlinearity and overlapping of absorption bands. Among the mathematical and chemometric models, it is worth mentioning, by decreasing order of complexity: Principal Components Regression (PCR), Implicit Non-linear Latent Variable regression (INLR), Partial Least Square (PLS) and Classical Least Square (CLS). The process of these mathematical models is basically a multi-dimensional interpolation of the calibration spectra to best fit measured spectrum. These models can also provide higher precision and detection limits than peak height or areas methods, as they use all the information contained within spectral region. Classical Least Square (CLS) has been used for the quantification of gas species in a complex matrix such as smoke.[118] This algorithm will be used in this study; hence, the next paragraph explains the procedure of shaping gas quantitative curves.

a) Classical Least Square algorithm

The CLS algorithm is commonly used for analyzing data, especially those used in multivariate calibration to resolve overlapping phenomenon between species.[119] To explain the CLS model, the example can be given of a complex mixture with five compounds all absorbing in the spectral region between 1800 and 1700 cm^{-1}. The CLS application consists in creating a K- matrix representing absorbance at each wave-number of the spectral region of interest. In this example (between 1800 and 1700 cm^{-1}) there are 101 points, the first at 1800 cm^{-1}, the second at 1799 cm^{-1}and so on to the last at 1700 cm^{-1}. If S(i) corresponds to a vector represented by the matrix, R(*i*,*j*) represents, similarly, the spectrum of each standard *j* at wave-number *i*. This vector is normalized so that the concentration of standards must be 1 ppm (unit used for the quantification). Hence, the vector S(i) is regarded as a linear combination of these five compounds according to the relation shown in equation 6.

$$\sum_{j=1}^{5}[cjR(i,j)] = S(i) \qquad (6)$$

Where cj is the concentration of compound j in the sample.

The next step of the CLS model consists of finding the linear combination giving the minimum residual Δi (equation 7).

$$\Delta i = S(i) - \sum_{j=1}^{5}[cjR(i,j)] \qquad (7)$$

This calculation makes use of 101 available equations to eliminate background noise and then finds the linear combination that is most representative of the real spectrum. For the purpose of the present study, the CLS model, using FTIR TQAnalyst computational software, was applied to develop calibration curves following the steps outlined below:

1) Standard spectra are acquired for each gas of interest at a minimum of five different concentrations. The calibration curves are determined by measurement of numerous peak heights or areas.
2) Selection of specific absorption bands for the CLS computation is made avoiding, if possible, any overlapping phenomenon.

3) Overlapping specie(s) in bands or regions selected for a specific gas of interest (if any) must be specified in the CLS computational model.
4) Selection of relatively low absorption bands, depending on the quantification range, is recommended, in order to avoid any saturated phenomenon and to obtain linear calibration over a large concentration range.
5) The CLS model can then be applied to compute calibration curves following which the latter are examined for their linearity.

b) Standard gases

Eighteen reference gases were selected based on the chemical composition of smoke (e.g. CO_2, CO), the toxicity or corrosion impact (e.g. HF, HCl, HBr) and the potential to obscure other species in infrared spectroscopy (e.g. H_2O, very strong absorber over a wide range of mid infrared). The spectra of these eighteen gases acquired with the iS10 FTIR are assembled at Fig. 25. The respective absorbance bands of each gas can be seen as can most of the overlapping phenomenon between these gas species.

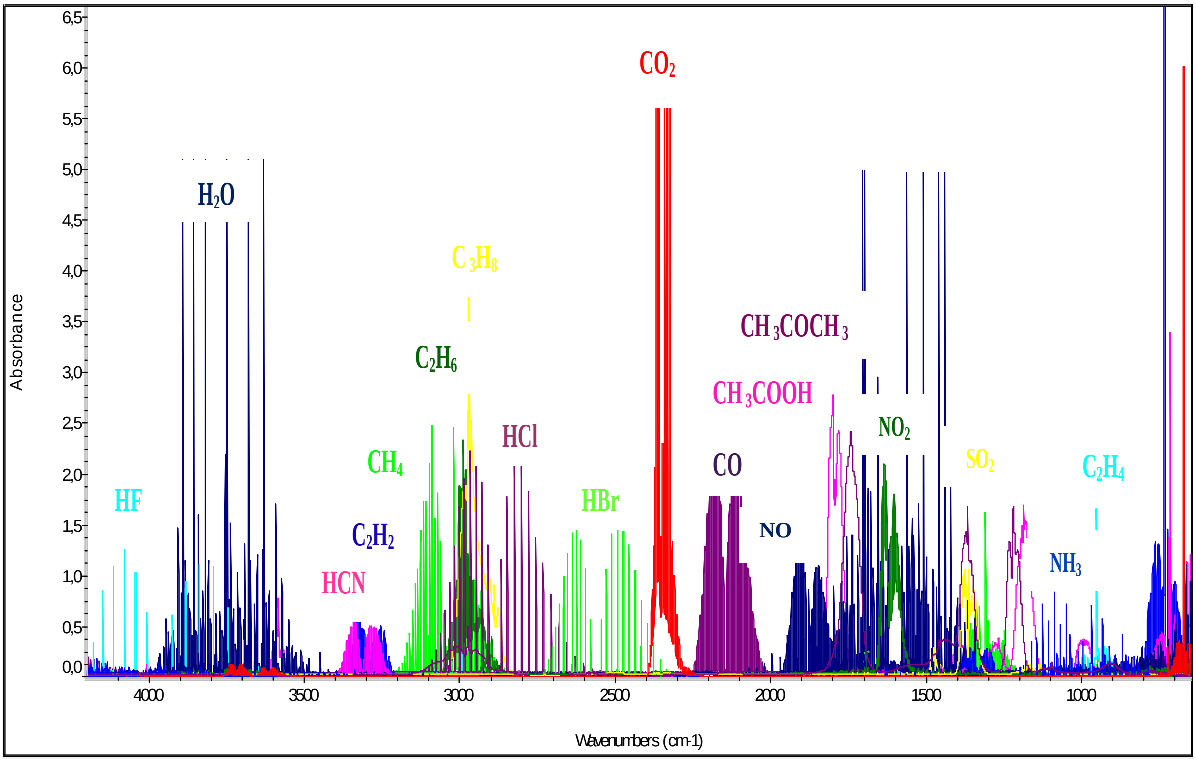

Figure 25. FTIR spectra of reference gases illustrating potential overlapping of species in the fire smoke

With the exception of the initial concentrations of reference gases, certified by the supplier, the calibration points are constructed by mixing the reference gas with pure nitrogen as diluting gas. Using mass flow meters (cf. Fig 22), a precise amount of the calibrated gas and nitrogen (IR-inactive) can be delivered to obtain diluted concentrations. For each calibration point, at least three spectra are acquired to ensure the dilution accuracy of the resultant concentration. Fig. 25 contains a database (library) of gases designed to aid qualitative analysis of unknown spectrum and in the selection of appropriate bands or regions during application of the CLS FTIR quantitative mode

c) Selection of quantitative analysis area and calibration curves

The precision and accuracy of the CLS computational model for FTIR gas quantitative analysis also depend on an appropriate selection of absorption peak(s) or of calibration region in the spectrum of each standard gas. Therefore, it is important to select peak(s) or regions in which, ideally, no interference would disrupt calibration. In practice, overlapping phenomena often occurs between gas species in IR, as previously shown in Fig. 25. If the selected peaks or regions of the gases of interest interfere with other component(s) or are suspected to contribute to the absorption peaks’ height or area, they must be signalled as overlap in the CLS computational model. An example of the selection of peaks and/or regions for the calibration of CO_2, CO, CH_4, C_2H_4, CH_3COOH and CH_3COCH_3 is illustrated at Fig. 26. The resultant calibration curves obtained for these gases using the CLS model are assembled at Fig. 27, revealing good fit between actual and calculated concentrations according to a correlation coefficient (R^2) close to 1.

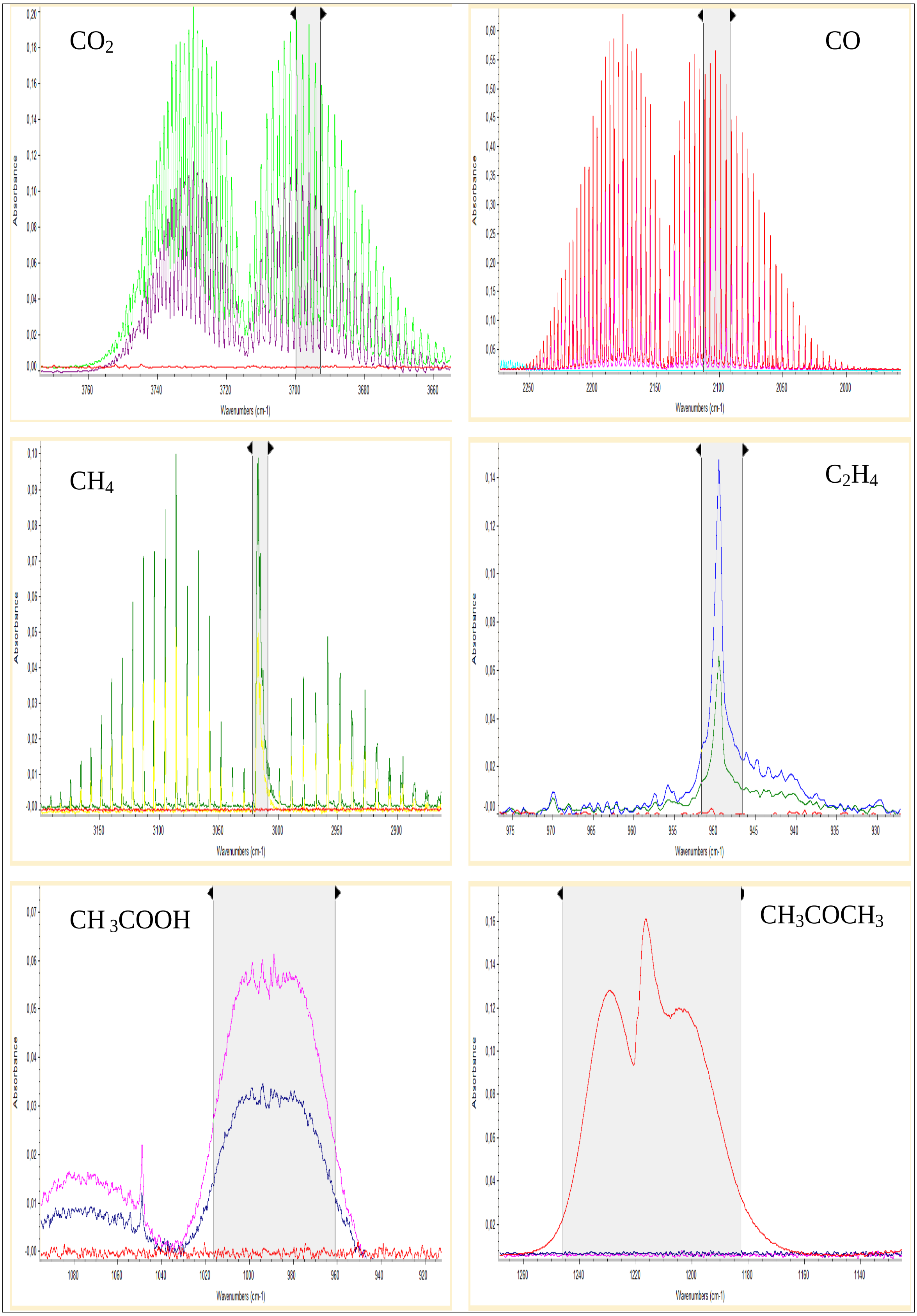

Figure 26. Selection of absorption bands for the CLS quantitative model

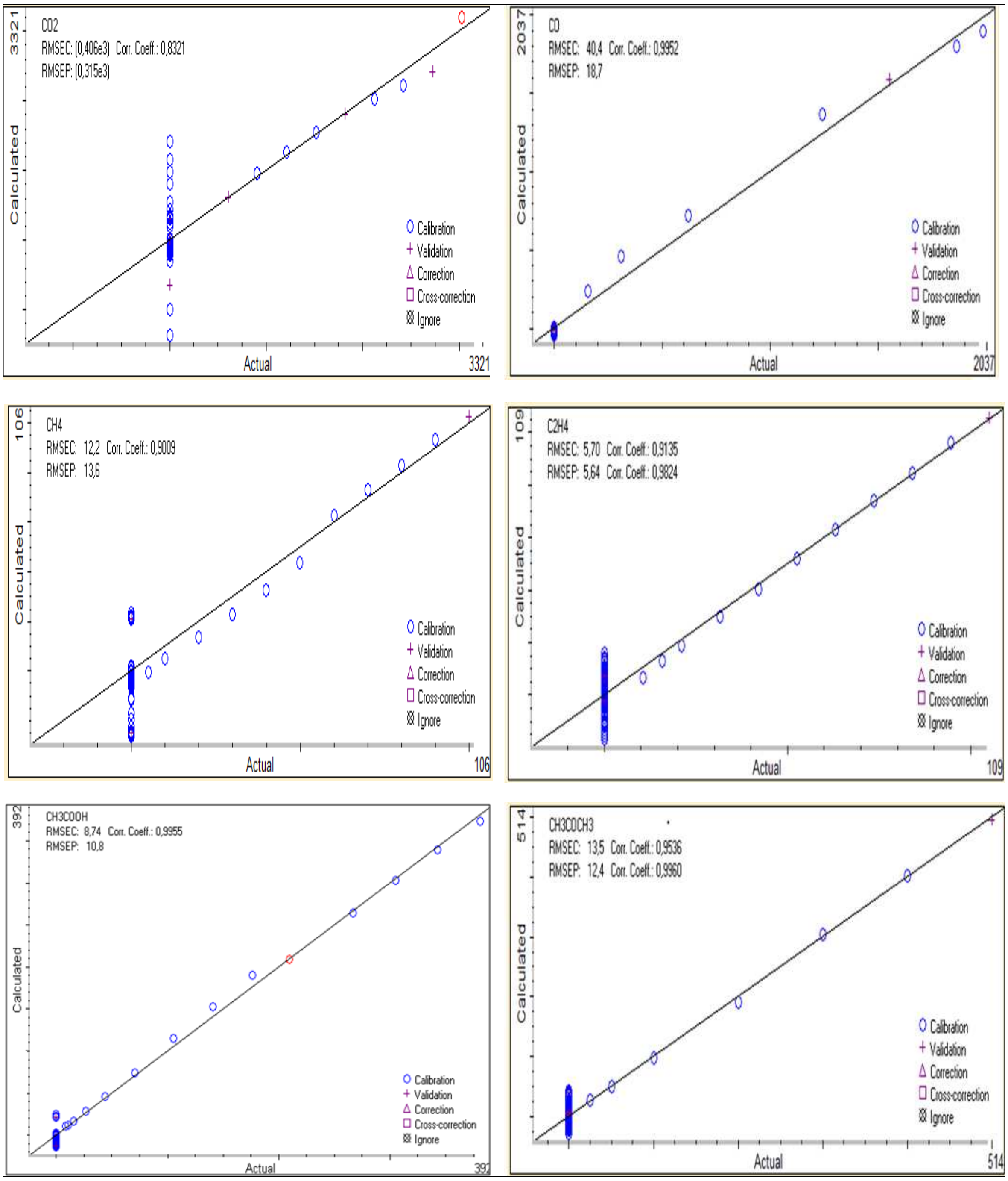

Figure 27. Calibration curves of CO_2, CO, CH_4, C_2H_4, CH_3COOH and CH_3COCH_3

The results for all gases calibrated in this study are summarized in table 2. For each gas, the selected calibration region, the correlation coefficients (R^2) of the calibration curves and interference gases are reported. All gases calibrated with the CLS computational model show a correlation coefficient close to 1 (between 0.83 and 0.99), thereby confirming the linearity of quantitative curves (see appendix 1 for the other gas calibration curves). Note that the calibration of hydrofluoric acid (HF) was not done, to avoid the risk of potentially damaging or disturbing the FTIR gas cell. Moreover, because HF is highly corrosive, only one spectrum at 100 ppm was recorded for use in the CLS model in the context of potential overlapping, as well as in the qualitative analysis database, in case it is released during thermal decomposition of materials under study.

Table 2. Summary of gas calibration results

Gas	**Wave numbers regions (cm^{-1})**	**Correlation coefficient (R²)**	**Interferences**
CO_2	3702 - 3692	0.83	H_2O, NO_2, SO_2, NH_3, C_2H_4
CO	2049 – 2140	0.99	H_2O, CO_2, NO_2
CH_4	3020 - 3010	0.90	H_2O, CO_2,HCl, C_2H_4, C_3H_8
C_2H_4	951 - 946	0.91	H_2O, CO_2,NO_2, SO_2
CH_3COOH	1022- 968	0.99	H_2O, CH_3COCH_3
CH_3COCH_3	1249-1210	0.95	H_2O, CH_3COOH
H_2O	3951-3914	0.98	NH_3
HCl	2823-2848	0.98	H_2O, CO_2, HBr, C_2H_4, C_3H_8, NO_2
HBr	2527-2431	0.99	HCl
HCN	715-710	0.99	C_2H_2
NO	1876-1870	0.96	H_2O, CO_2, CO
NO_2	1634-1628	0.99	H_2O, CO_2, CO, HCl, CH_4, C_2H_4, C_3H_8
NH_3	935-924	0.99	H_2O, CO_2,NO_2, SO_2
SO_2	1362-1358	0.99	H_2O, CO_2, CH_4,C_3H_8, NO_2
C_2H_6	2957-2949	0.97	HCl, CH_4, C_2H_4, C_3H_8
C_3H_8	2971-2964	0.98	HCl, CH_4, C_2H_4, C_3H_8
C_2H_2	3315-3307	0.96	HCN
HF	-	-	-

In addition to the quantitative analysis of evolved gases, analysis of the size distribution and concentration of smoke particles he will be performed using the ELPI interface with the MLC fire model.

2.2 ELPI for particles analyses

ELPI was developed relatively recently[102] and has become increasingly utilized for the investigation of airborne, automotive diesel and combustion particles in general, as reported in literature.[103]

2.2.1 Principle

ELPI is mainly constituted of a corona charger, cascade impactor, a series of electrometers connected to each impactor stage and a vacuum pump as shown at Fig. 28. The operating principle of the ELPI is quite simple and can be summarized in three consecutive steps. Firstly, particles from the sample are exposed to a unipolar positive ion environment in the corona charger, where they are electrically charged to a known charge level.

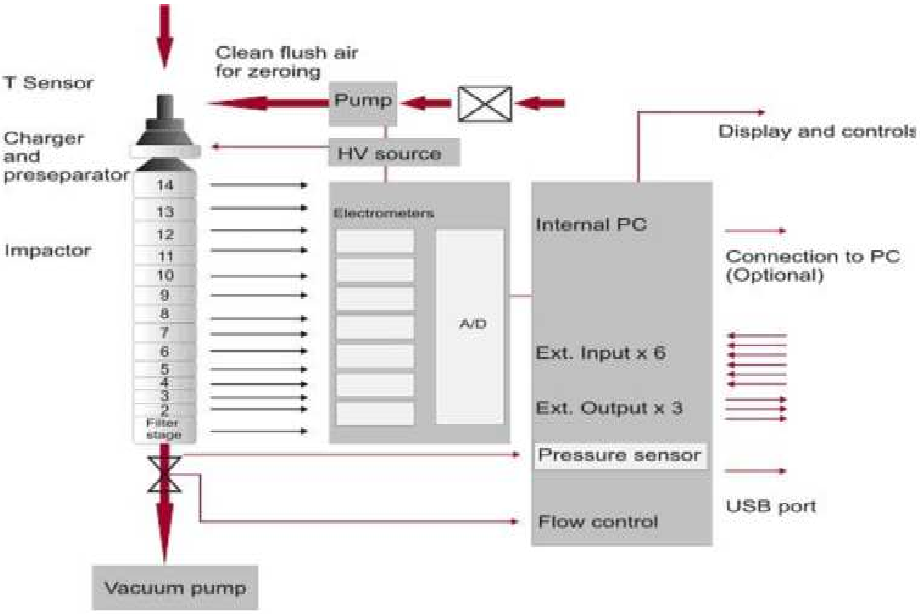

Figure 28. Schematic presentation of ELPI features

The corona charger[120] (Fig. 29) is composed of a thin electrode (a) in needle shape with a width of 5 mm positioned relative to a second outer cylindrical electrode (b). The potential difference between these two electrodes is 5 kV thereby generating a corona discharge from the tip of the inner electrode.

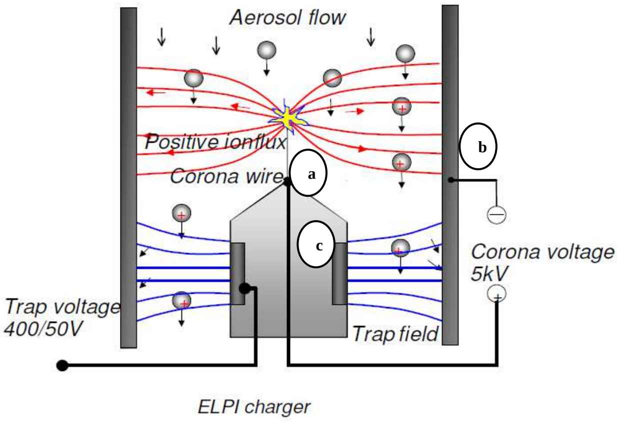

Figure 29. Corona charger

This discharge produces positive ions which move toward the external electrode because of the potential difference. Particles passing through the gap between the two electrodes are charged through collisions with the ions. Moreover, a third short cylindrical electrode (c) getting a potential difference of 400 V with respect to the external high cylindrical electrode serves to retain very small particles below the ELPI impactor cut-off range, determined by their electrical mobility. Consequently, the charge of particles below the cut-off range of the device will not be measured by the ELPI electrometers.

In the second step, the charged particles enter the low pressure cascade impactor where they are classified into size fractions of 6 nm to 10 µm according to their aerodynamic diameter (da), the latter determining their deposition at a particular ELPI stage. When their da is inferior to the cut-off diameter of the ELPI stage, the particles continue their course to the next stage; otherwise, they impact against the collection plate as illustrated at Fig. 30, where the blue particle is larger than green, in turn larger than the red particle.

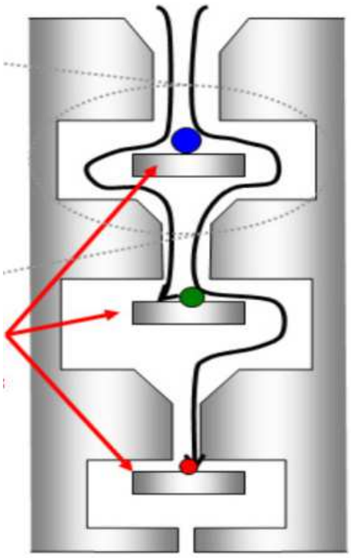

Figure 30. Particle impaction principle in the ELPI

In the final step, the charges carried by particles are continuously measured, at each impactor stage, by sensitive electrometers located inside the ELPI (Fig 28) with the measured currents being proportional to the number of particles. The concentration of particles per cm^3 is then determined for each size range according to Equation 8 and using transfer functions provided by the manufacturer.[104,121]

$$C = \frac{I}{PNeQ} \qquad (8)$$

Where C is the number concentration (# / cm^3), I the measured current (A), P the penetration through the charger, N the average number of charge per particles, e the electron charge (1.602×10^{-19} C) and Q the flow rate (10 L/min = 1.6×10^{-4} m^3/s).

2.2.2 Factors influencing ELPI measurements

Despite the theoretical simplicity of its operating principle, some experimental issues concerning the ELPI may have an influence on measurement data. One of these is the rebound phenomenon; in other words, particles bouncing off and possibly fragmenting on impact with the collection plate. This phenomenon may result in fragmented particles passing towards the lower stages of the impactor where the cut-off diameter is smaller. The consequences are the artificial displacement of “real particles” and the charge transfer between their fragmented counterparts and the lower plates, thereby biasing both the size distribution measurement and the evaluation of particles concentration. This phenomenon is reduced by greasing the ELPI collection substrates, which favours the entrapment of particles by capillary forces and thus prevents the rebound phenomenon occurring.[121]

Furthermore, in order to process the ELPI measurements, one parameter only must be entered by the user, namely the density of the particles. This parameter is involved in the conversion of the aerodynamic diameter. Inaccurate density values can give rise to overestimations or underestimations in the measurements. In the framework of the present study, the density of particles will be assumed as 1000 kg/m^3. Note that if the actual density of the particles in the measured sample is 8 times this density, then the concentration of ultrafine particles will be calculated to be 10 times smaller than their actual concentration; however, this effect is less noticeable for micrometric particles.[122]

Moreover, not all particles that enter the corona charger actually reach the impactor stage. Indeed, some particles, subjected to radial acceleration towards the walls of the charger due to the electric field, actually remain there. The factor of penetration P of the particles was therefore defined as a given fraction of particles crossing through the charger with respect to the total in the sample.[123]

3 Conclusion

This chapter has highlighted the motivating factors that led to the selection of the Mass Loss Cone, Fourier transform infrared spectroscopy and electrical low pressure impactor as preferred techniques in the construction of a bench test for investigation of flammability parameters, as well as the gases and particles contained in fire smoke. The design concept of coupling MLC/FTIR/ELPI was presented and its appropriateness with reference to the requirement of characterizing smoke gases and particles during fire scenario testing discussed in detail. Qualitative and quantitative analysis methods for the determination of gas-phase species in the smoke with FTIR were developed. Gas quantitative curves were also developed using the implementation shown at Fig. 22 and the CLS computational model as provided by TQAnalyst software and have revealed good linearity or correlation between actual calibration standard gases' concentrations and those calculated with the computational model.

Finally, the operating principles of the ELPI were also discussed. Despite its apparent simplicity, there are some valid concerns linked to the accuracy and integrity of experimental data; specifically, the bounce phenomenon which can bias measurement of particle-size distributions. Steps taken to correct this bias by greasing the ELPI substrate and setting the density of particles in the ELPI analyzer were presented.

An essential element of this project is to evaluate the effectiveness, reliability and repeatability of results obtained with the proposed bench test. These topics are covered in the next chapter, with ethylene vinyl acetate unfilled and filled with aluminium trihydroxide being used as reference materials.

CHAPTER 3: VALIDATION OF MLC/FTIR/ELPI WITH ETHYLENE VINYL ACETATE UNFILLED ANDFILLED WITH ALUMINIUM TRIHYDROXIDE

Ethylene vinyl acetate and aluminium trihydroxide are increasingly used as raw materials in the formulation of zero halogen electrical cable coatings.[124] The fire behaviour of ethylene vinyl acetate unfilled and filled with aluminium trihydroxide is revisited in this chapter in order to evaluate and to validate the accuracy, precision and added value of coupling MLC/FTIR/ELPI for the characterization of fire behaviour of polymeric materials. After presenting the reference materials evaluated in this study, validation the MLC/FTIR/ELPI coupling will be conducted as follows:

As a first step, the effect of the sampling probes installed close to the thermopile in the chimney on the measurement of MLC data (HRR and t_{ig}) is examined. Results of the qualitative analysis of gases in the smoke generated by ethylene vinyl acetate combustion using MLC/FTIR will then be compared to published data from TGA/FTIR and/or Py - GC/MS micro scale tests. The accuracy and precision of the FTIR method developed for the quantitative determination of changes in the chemistry of gas species during the MLC test will be subsequently discussed as will the accuracy and precision of coupling MLC/ELPI to determine the size distribution and concentration of particles in the smoke.

Secondly, validation of MLC/FTIR/ELPI is extended to the study of flame retarded ethylene vinyl acetate filled with aluminium trihydroxide as reference material. In fact, this experimental setup is originally proposed for use in fire behaviour characterizations of flame retarded materials, such as electrical cables and combustible materials in general.

The benefit of coupling MLC/FTIR/ELPI to expand the knowledge of the characteristic parameters of the fire of materials under study is subsequently highlighted. In this regard, a comparative and synthetic study of the fire effluents of ethylene vinyl acetate unfilled and filled with aluminium trihydroxide is performed in the third step, using MLC/FTIR/ELPI.

In summary, this chapter presents the results of evaluations of the proposed MLC/FTIR/ELPI combination demonstrating that this technique is an efficient and valid experimental bench test for simultaneously analysing evolved gases (qualitatively and quantitatively), particles (size distribution and concentration) and flammability parameters (HRR, tig...) during a fire scenario simulated by MLC experiment.

1 Reference materials

Ethylene-vinyl acetate copolymer containing 28% of vinyl acetate (hereafter called EVA) supplied by Arkema and aluminium trihydroxide (ATH) supplied by Martinswerk (Bergheim, Germany) are used as raw materials to make plates of virgin EVA and EVA/ATH. Sample plates are prepared using a Brabender mixer 350/EH with a shear rate of 50 rpm at 180 °C. EVA is initially heated to molten state for 5 min; thereafter, in the case of the fire retarded EVA/ATH material formulation, raw ATH is incorporated and mixed for a further 15 min (total elapsed duration: 20 min). The EVA/ATH formulation contains 35 wt.% polymer and 65 wt.% ATH respectively. Finally, neat EVA and EVA/ATH are pressed in appropriately sized molds (100 x 100 x 4 mm^3) at 200 °C under pressure of 20 kN for 3 min, followed by 5 min under 40 kN, then cooled to room temperature before demolding.

2 Set-up validation with Ethylene Vinyl Acetate (EVA) as reference material

2.1 Influence of smoke sampling probes on mass loss cone measurements

The original operating principle of MLC is based on evaluating parameters, such as HRR, by measuring the temperature change of mass air flow via a thermopile located in the MLC chimney. The question addressed is “Does the location of two smoke retrieval probes in close proximity to the thermopile disrupt measurement of MLC data?”

A comparison of HRR and t_{ig} values obtained from fire tests conducted with MLC in its basic configuration and equipped with two smoke retrieval probes for gas and particles analysis is presented at Fig. 31 and table 3. The curves at Fig 31 represent an average of the results obtained over three tests, in each case for EVA and at 35 kW/m². It also includes the temperature evolution of smoke at the sampling point in the chimney. The thermocouples used to measure temperature are located below the heated sample lines going out to the FTIR and ELPI analyzers. In both cases, it can be seen that the use of two smoke retrieval probes in close proximity to the thermopile does not influence instrument measurements. There is good agreement between the HRR and t_{ig} measurements (values in the range of 10% error), as well as the smoke temperature measurements taken before and after the installation of the two retrieval probes. The Standard deviation for the profiles is estimated at 4% for t_{ig} and 9% for HRR.

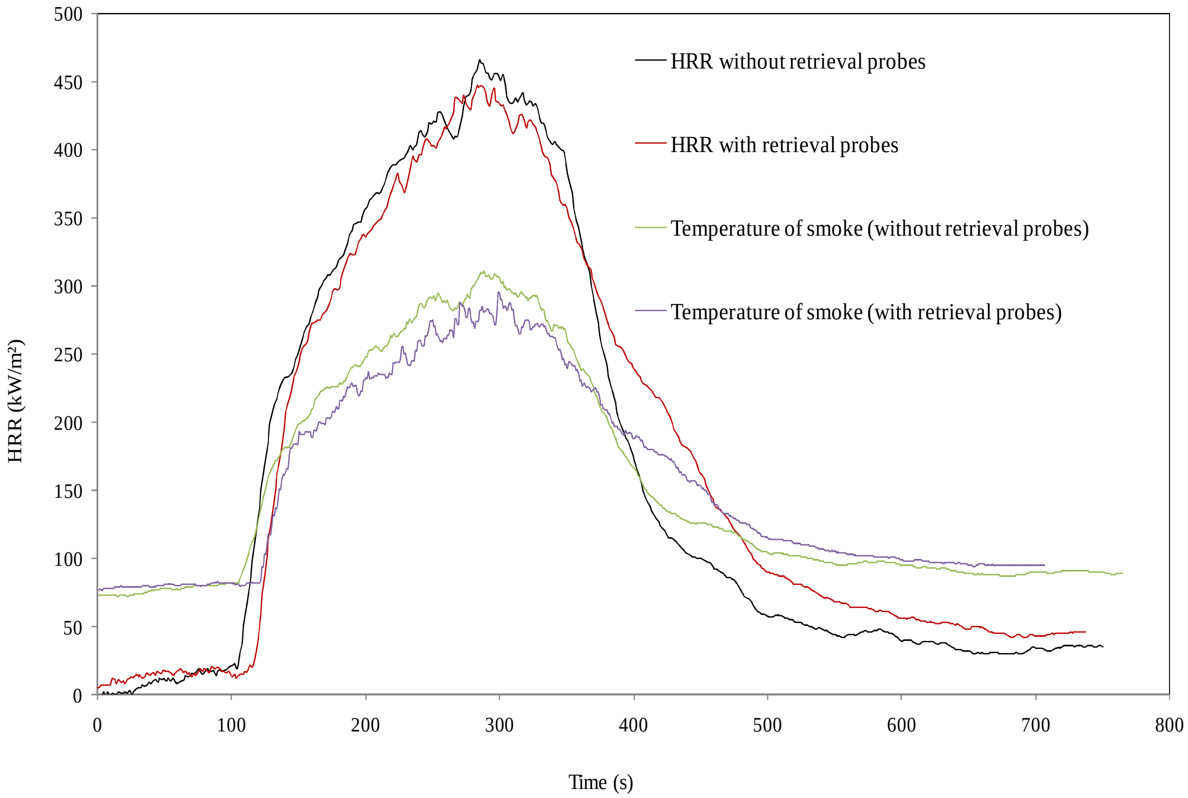

Figure 31. HRR of EVA with and without retrieval probes at the top of the chimney (35 kW/m²)

It is reasonable to assume therefore that the experimental bench test configuration allows measuring usual cone data with simultaneous analysis of gases and particles during an MLC test.

Table 3. Mass loss cone data with and without smoke retrieval probes

	MLC device in its original configuration			**MLC device with two smoke retrieval probes above the thermopile**		
	t_{ig} (s)	pHRR (kW/m²)	flame out (s)	t_{ig} (s)	pHRR (kW/m²)	flame out (s)
Test 1	96	460	495	105	450	497
Test 2	103	465	510	110	447	512
Test 3	106	455	500	109	446	531

The next step is to validate the capacity of the MLC/FTIR/ELPI coupling to provide accurate and repeatable results when used in the real-time analysis of evolved gases and particles released during combustion of EVA.

2.2 Gas phase analysis

Validation of this bench for monitoring evolved gases in fire smoke is conducted in two steps. The first of these consists of a qualitative analysis of gases from EVA using MLC/FTIR. The data obtained are then compared data from small scale tests (TGA/FTIR, Py-GC/MS) available in the literature. The second is focused on validation of the accuracy and precision of the quantitative analysis of gases detected over time using the FTIR gas quantitative method previously developed.

2.2.1 Qualitative analysis of gases

In order to evaluate the evolution of gases during combustion of EVA at 35 kW/m², FTIR spectra are recorded at specific times. These times are: before ignition, during flaming and close to flame out. These spectra are compared to those of reference gases from the database library (Fig. 32 - 34). Thereafter, only the characteristic peak permitting the identification of the gases are given. Before ignition (107 s) Fig. 32 shows the C=O stretching in the region around 1810 - 1790 cm^{-1} and -O-H bending around 998 cm^{-1} attributable to CH_3COOH; CO_2 corresponding to the absorption bands around 2357 - 2310 cm^{-1}; CO with absorption bands around 2187 - 2115 cm^{-1} and CH_4 with its characteristic peak around 3030 - 2990 cm^{-1}.

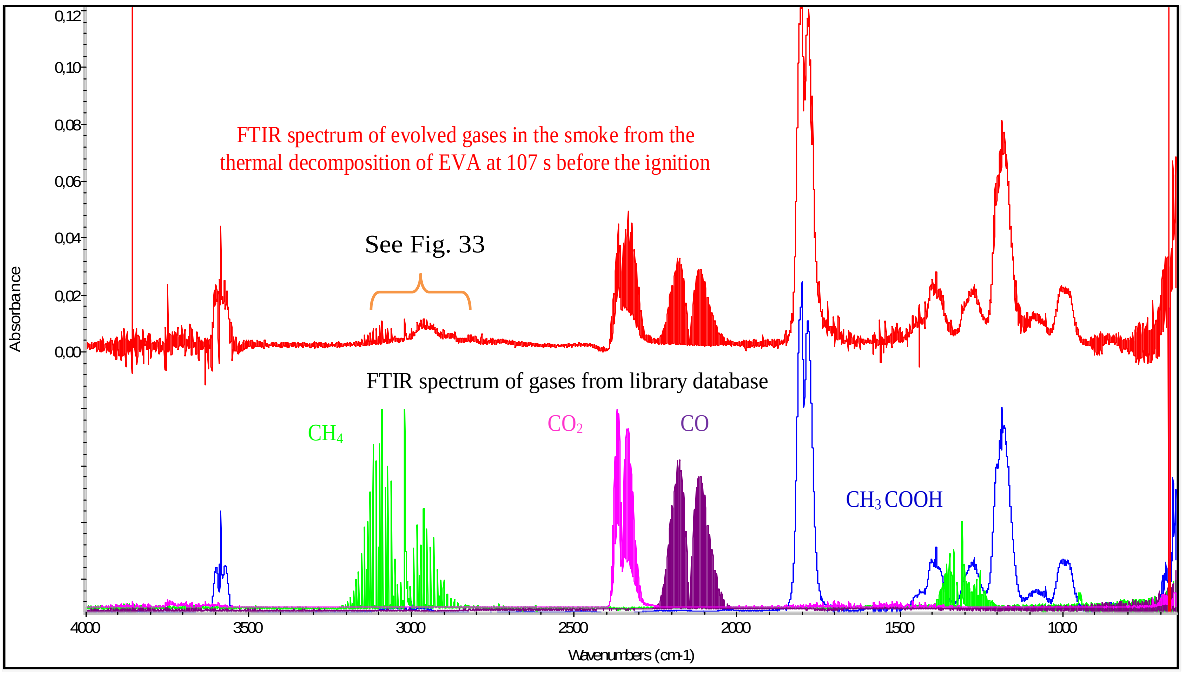

Figure 32. Qualitative analysis of the gas in EVA smoke before ignition

(MLC/FTIR - 35 kW/m²)

Furthermore, an overlapping phenomenon at around 3000 - 2800 cm^{-1}, ascribed to the C-H asymmetrical stretching, is observed as illustrated at Fig. 33. The release of CH_4 (absorption around 3200 - 2990 cm^{-1}), CH_3COOH (with C-H stretching peak at 2995 cm^{-1}) and also of C_2H_4 (peak at 2985 cm^{-1}) exhibiting low-intensity absorbance are identified.

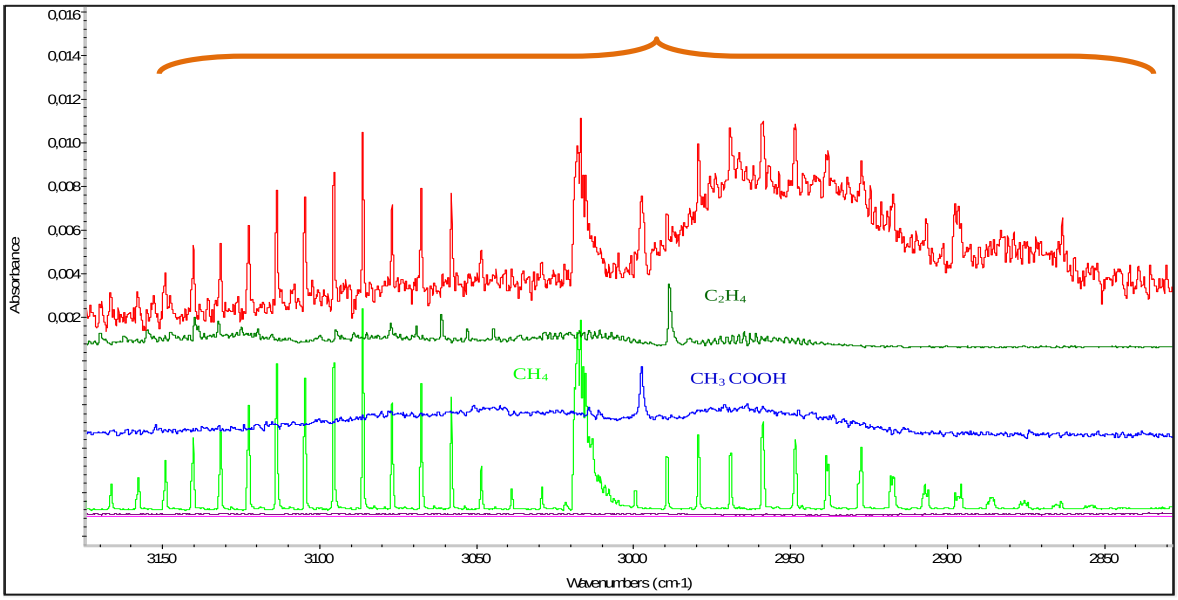

Figure 33. Identification of hydrocarbon gases in EVA smoke before ignition

(MLC/FTIR - 35 kW/m²)

During the flaming phase at 286 s, broad bands are observed (Fig. 34) at around 3900 - 3500 cm^{-1} and 1900 - 1250 cm^{-1} attributable to H_2O high-intensity absorbance. The signals observed around 2357 - 2310 cm^{-1} (high intensity) and 2187 - 2115 cm^{-1} (low intensity) are ascribed to CO_2 and CO respectively. These results are consistent with the degradation gases (CO_2, CO and H_2O), usually detected during combustion of polymeric materials.[125]

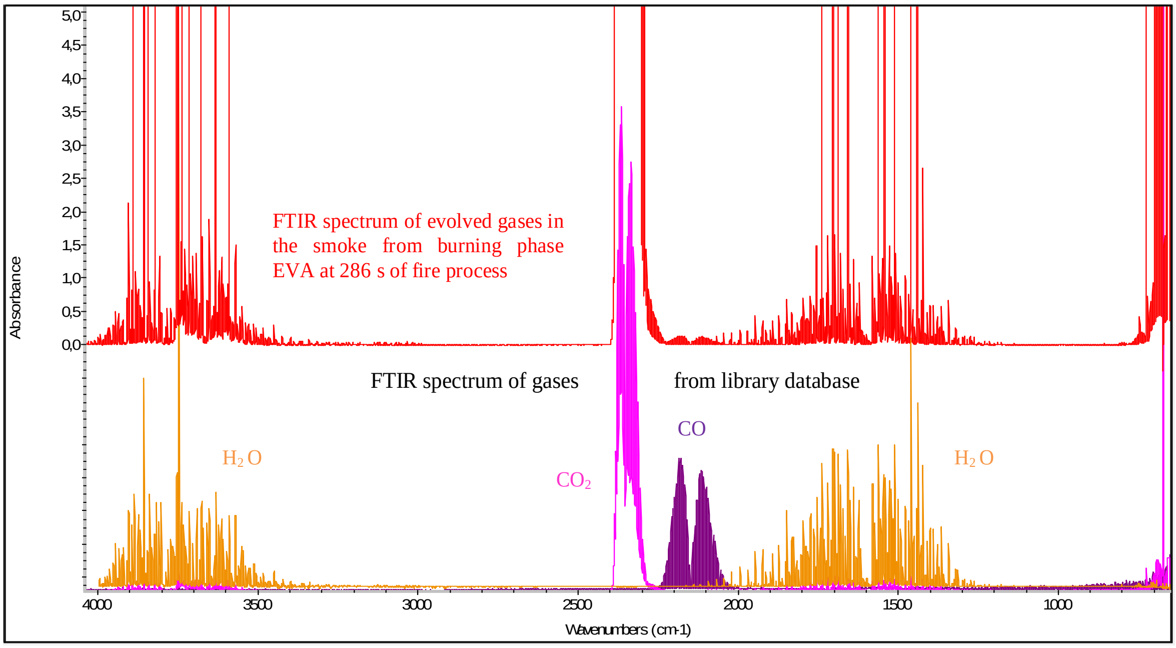

Figure 34. Qualitative analysis of the gas in EVA smoke during flaming phase

(MLC/FTIR - 35 kW/m²)

Close to flame out at 413 s, the signal intensities attributed to the evolved gases CO_2, CO and H_2O decrease (Fig. 35). This is due to the lack of fuel resulting from the complete combustion of EVA during the MLC test.

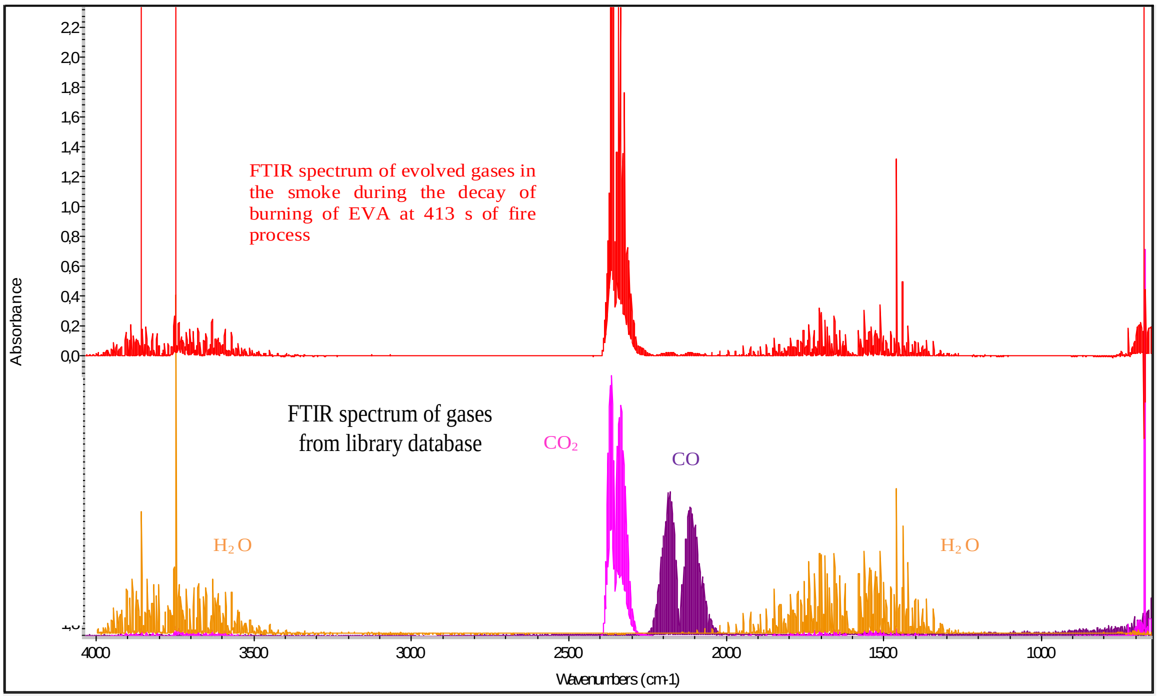

Figure 35. Qualitative analysis of the gas in EVA smoke during fire decay phase

(MLC/FTIR - 35 kW/m²)

These results, namely the detection of CH_3COOH, CH_4, C_2H_4, CO_2, CO, H_2O, [31 - 38] demonstrate that the MLC/FTIR coupling configuration enable identification of evolved gases in fire smoke.

2.2.2 Quantitative analysis of EVA fire smoke

In order to quantify the evolving gases during combustion of EVA, MLC/FTIR experiments at 35 kW/m² were performed. The concentrations of evolving CH_3COOH, CO_2, CO, H_2O, CH_4, and C_2H_4 are followed as function of time (Fig. 36). To evaluate repeatability, all experiments were performed three times. Acceptable repeatability is observed.

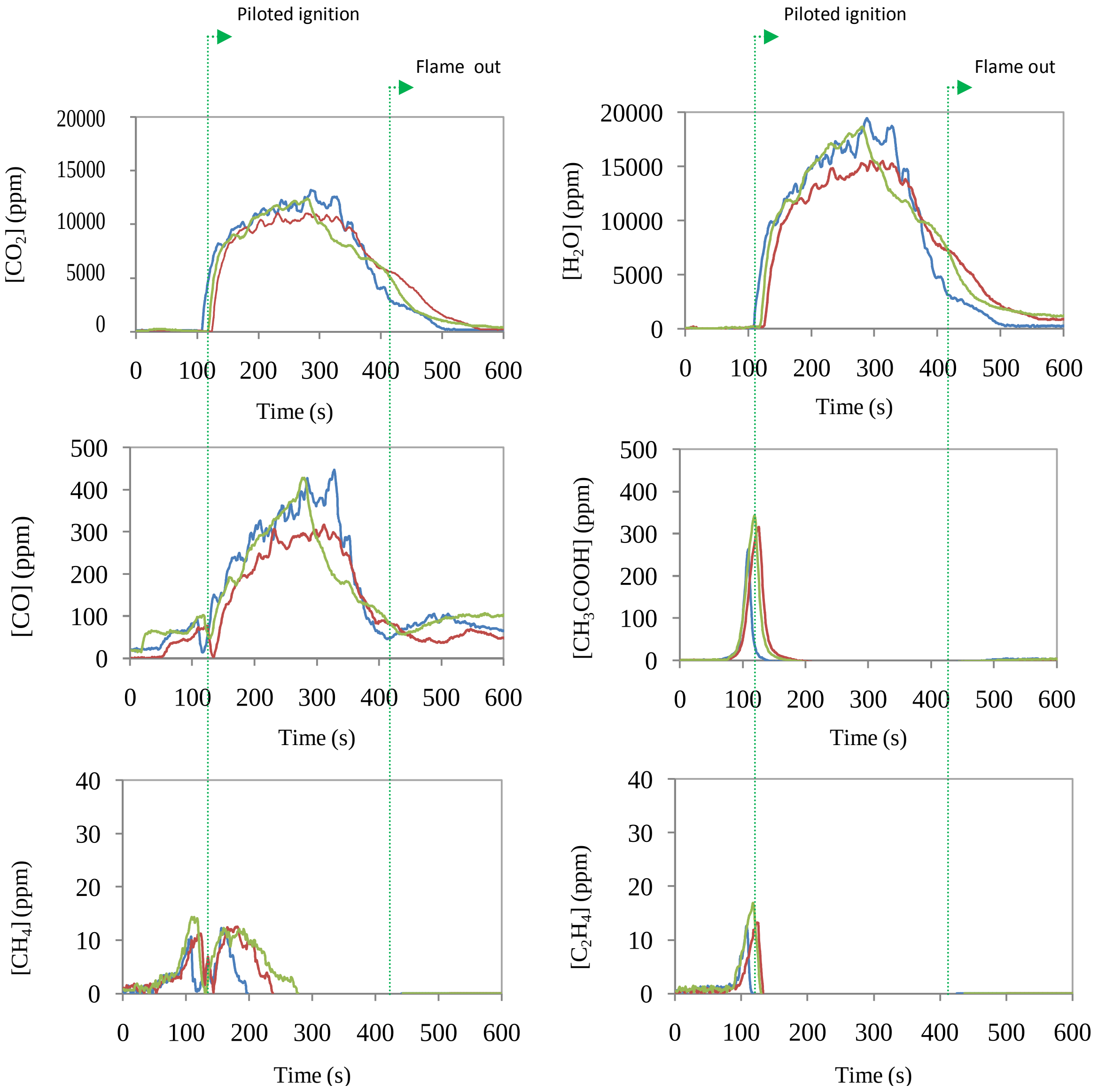

Figure 36. Repeatability evaluation of quantitative analyses of evolved gases during EVA combustion (MLC/FTIR - 35 kW/m²)

Moreover, the standard deviations (∂) are calculated for all of the gas released (Fig. 37) resulting in: 3% for CO_2, 4% for H_2O, 8% for CO and 9% for CH_3COOH. For CH_4 and C_2H_4, the standard deviations were estimated at 11% and 13% respectively. The increase in standard deviation, which is higher for low gas concentrations (CH_4 and C_2H_4), may be attributed to the signal-to-noise ratio of the FTIR configuration with NS = 1, since the influence of this ratio is globally higher as the measured concentration decreases.

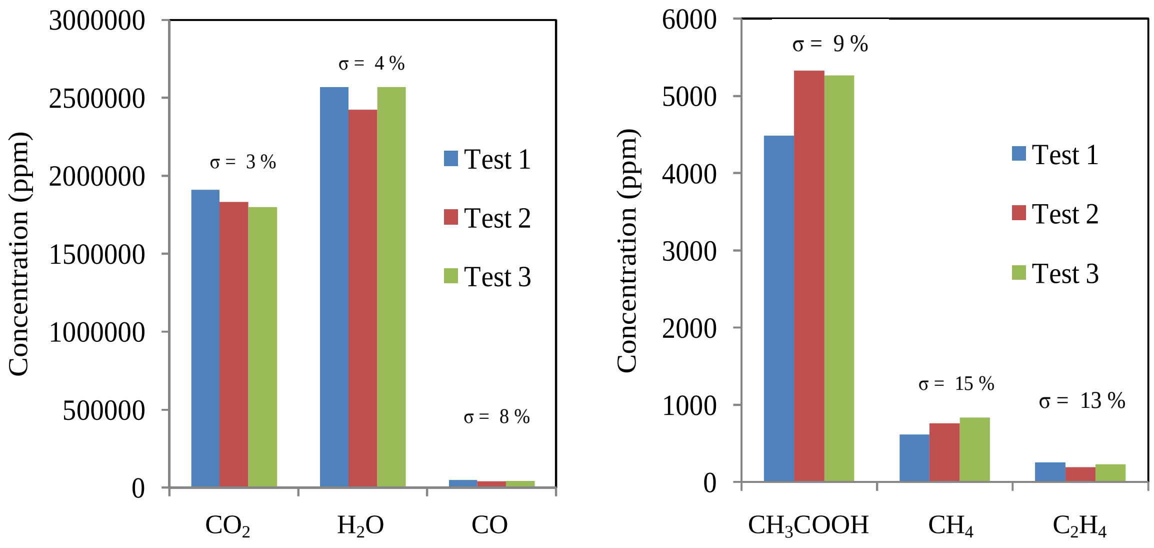

Figure 37. Total gas release during degradation of EVA (MLC/FTIR at 35 kW/m²)

These results demonstrate the accuracy of this bench for quantitative monitoring of gases in the smoke during an MLC test. To obtain accurate and repeatable results, some experimental conditions that require particular attention should be noted: prevention of cold points in the gas transfer line; maintaining constant pressure in the FTIR gas cell (identical for calibration and for the unknown gas in the smoke) and preheating all experimental equipment related to the gas-phase analysis (filters, transfer line and FTIR gas cell).

Furthermore, the concentration of evolved gases as a function of time are consistent with the combustion mechanism of EVA described in the literature.[31 - 39]

(i) The first stage, from the beginning of the experiment to ignition, is characterized by the release of CH_3COOH and CO. CH_3COOH reaches a peak of almost 262 ppm at 108 s, and CO a peak of 76 ppm at 108 s. Although CH_4 and C_2H_4 are also released, their concentrations are lower: peaks of 10 and 12 ppm respectively are observed. H_2O is also detected during this stage, but in very low concentrations compared to those measured during combustion. This quantitative analysis confirms that acetic acid resulting from the deacetylation of vinyl acetate (Fig. 38) has the highest concentration of all gases released during the first stage of EVA thermal decomposition.

(ii) The second stage (from ignition to flame out) is characterized by a spontaneous increase of CO_2 and H_2O (reaching concentrations, respectively, of 13119 and 19419 ppm at 286 s) while the concentration of CH_3COOH, C_2H_4 and CH_4 drops to zero soon after ignition. A local decrease in CO occurs at ignition, followed by an increase during the flaming phase, with a peak of 431 ppm at 327 s. This release of CO during the flaming process of EVA is consistent with the incomplete combustion of hydrocarbons. It is also noteworthy that the EVA plate becomes liquid (molten EVA) during the flaming phase, leading to a pool fire (visual observation) in the sample holder.

These results are in agreement with previous studies reported in the literature.[31 - 38] The thermal degradation of EVA takes place in two stages, the first (between 250 and 350 °C) corresponds to decomposition of the vinyl acetate group, with release of CH_3COOH and CO, as well as CO_2, CH_4, H_2O (the latter gases being related to the secondary pyrolysis reaction of vinyl acetate). [34, 126] According to Barrall, in GC analysis,[127] the release of CH_4 results from the degradation of saturated bonds at the end of carbon chains. The second stage (around 350 to 450 °C) corresponds to the degradation of polyene characterized by the release of CO_2, CO, H_2O and saturated or unsaturated hydrocarbons composed of 1 to 6 atoms.[31, 128]

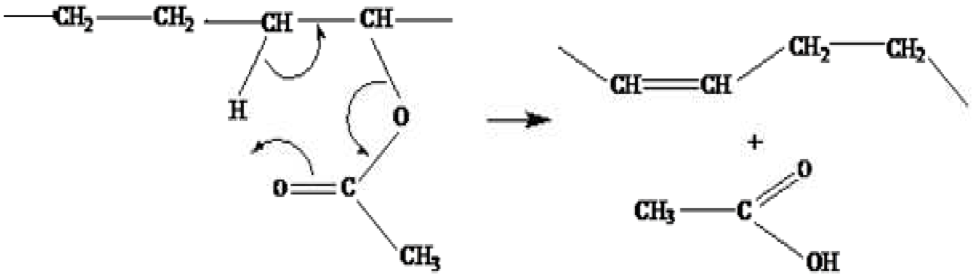

Figure 38. Mechanism of deacetylation of ethylene vinyl acetate

2.3 Particle analysis from EVA fire smoke: size distribution and concentration

Investigation of particles emitted by diesel engines has been reported in numerous studies,[129] but little data is available on the characterization of particles from the flame during a fire. This is due to the difficulty of sampling particles of soot present in the smoke.[130] Nevertheless, there is a general consensus that the particle size in the case of particles emitted from a material undergoing combustion has a widely submicron distribution (<1µm) and that this is dependent on the nature of fuel, ventilation conditions and temperature.[131] Establishing a methodology for the investigation of the size distribution and concentration of particles in fire smoke will consequently create added value in the context of characterizing the fire behaviour of materials. This section focuses on evaluating the performance of the experimental bench in the characterization of the size distribution and concentration of particles in the smoke of a fire of materials.

In relation to the gas phase analysis discussed above, measurements of the size distribution and concentration of particles per cm^3 in the EVA fire smoke were made at the same time, using ELPI and MLC. Fig 39 indicates that the particles emitted in the smoke during combustion of EVA are principally ultrafine (< 0.1 µm), followed by fine or submicron particles (< 1µm). Two characteristic peaks are detected, the first of which for particles of 16 nm, with an average of 3.10^7 ± 27 % particles per cm^3 and the second for 93 nm particles with an average of 2.10^7 ± 15 % particles per cm^3. This observation of the release of mainly ultrafine and fine particles in smoke during EVA combustion is consistent with previous studies in which it has been reported that the size range of particles in fire smoke of polymeric materials lies mainly below 1 µm.[131] In addition, MLC/ELPI is more precise about the size distribution of these submicron particles, as it reveals two characteristic peaks at 16 and 93 nm, highlighting the precision of the bench in characterizing submicron particles emitted in the smoke from combustion of material (here, EVA). Although particles above 1 µm, or more precisely in the size range of 1.5 to 6.67 µm, were also detected, these were found in smaller concentrations as compared to ultrafine particles (in the order of 10^5 particles per cm^3). This information about the size distribution of particles is important, as the potential effect of smoke particles emission on human health, for instance, is directly related to their size distribution.

Acceptable repeatability is observed in the results of the particle-size distribution evaluation (x-axis, Fig. 39). However, for the number of particles per cm^3 (y-axis), some standard deviations are evaluated (between 10 and 30%) as having a random variation.

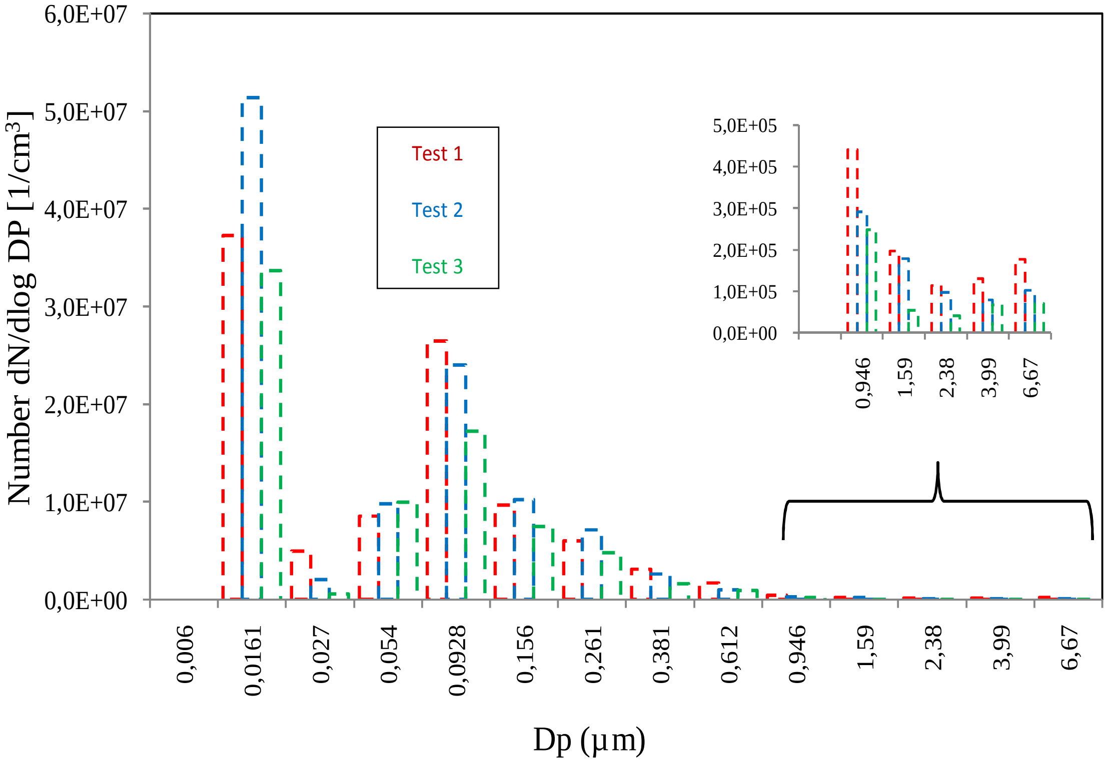

Figure 39. Repeatability evaluation of soot size distribution and number in the EVA fire smoke (MLC/ELPI -35 kW/m²)

These random standard deviations limit the repeatability of the determination of particles concentration in the smoke. This can be attributed to:

- The dynamics of the fire itself, which represents a challenge to monitoring concentrations of evolving particles in smoke.[132]
- An abrupt variation in the amount of particles passing through the ELPI impactor stages, which may induce a faulty reading in the current measurements by the electrometers.[133]
- The rebound phenomenon, charging efficiency and particles penetration through the ELPI charger may also be factors that impact on the repeatability of results from the experimental determination of particles concentration in the smoke.

In consequence, when the current implementation of the MLC/ELPI coupling is used to determine particles concentration in the smoke of a fire of material, it is imperative that standard deviations be taken into account when results are being reported.

These results demonstrate the accuracy and precision of the MLC/ELPI coupling in the investigation of size distributions of particles in the smoke produced during a fire of materials. With respect to the determination of the concentration of these particles in the smoke, relatively high standard deviations are reported and this must be taken into account when analyzing the results. After evaluating virgin EVA, the validation test of the MLC/FTIR/ELPI coupling is extended to flame retarded ethylene vinyl acetate filled with aluminium trihydroxide.

3 Set-up validation with ethylene vinyl acetate/aluminium trihydroxide (EVA/ATH)

As the proposed MLC/FTIR/ELPI coupling was designed for the purpose of characterizing the fire behaviour of flame retarded materials, a second validation test was conducted with fire retardant EVA (EVA/ATH). There bibliography contains extensive published documentation on the flame retardancy of EVA/ATH, [38, 134, 135, 136] which makes it an excellent reference material for the present study. As for the previous validation (see paragraph 2), heat release rate, gas phase qualitative and quantitative analysis as well as particle-size distribution and concentration have been examined and compared to available published data.

3.1 Heat release rate of fire of EVA/ATH

The EVA/ATH formulation was evaluated at 35 kW/m² (Fig. 40). The HRR curve presents a pHRR of 92 kW/m², with time to ignition being 183 s and flame out at 315 s. During measurement of HRR, evolved gases and particles in the smoke were also recorded. The results obtained are presented below. The data has been selected from a series of three tests that yielded similar results with standard deviations of 3% for t_{ig}, and 7% for HRR. After the fire test, a residue remains as shown at Fig. 41, which corresponds principally to the formation of Al_2O_3 from the dehydration of ATH [137] (cf. Eq. 1, chapter 1, page 30).

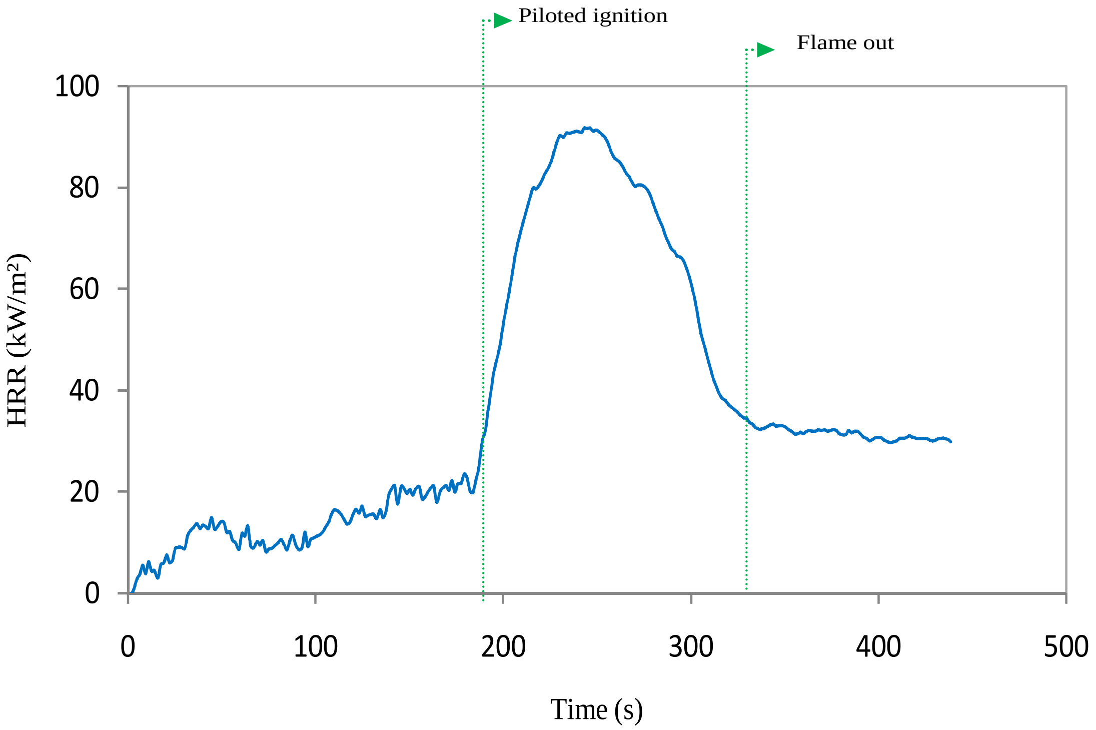

Figure 40. Heat release rate of EVA/ATH as a function of time (MLC-35 kW/m²)

Figure 41. Residue of EVA/ATH (MLC-35kW/m²)

3.2 Gas phase analysis of EVA/ATH fire smoke

3.2.1 Qualitative analysis of EVA/ATH fire smoke

Results of the gas qualitative analysis for the main gases released at specific times during the combustion of EVA/ATH material are reproduced in Fig.42 - 45. The specific times taken from the HRR curve are: before ignition (180 s), at pHRR (286 s) and after flame out (315 s).

Before ignition of EVA/ATH (Fig. 42), H_2O (broad bands around 3900 - 3500 cm^{-1} and (1900 - 1250 cm^{-1}), CO_2 (absorption around 2357 - 2310 cm^{-1}), CO (absorption around 2187 - 2115 cm^{-1}), CH_4 (low absorbance peak around 3030 - 2990 cm^{-1}) and C_2H_4 (low absorbance peak at 2985 cm^{-1}) are detected. In addition, an intense absorption around 1750 cm^{-1} (C=O stretching), characteristic of the overlap of the carbonyl group with water, is also identified.

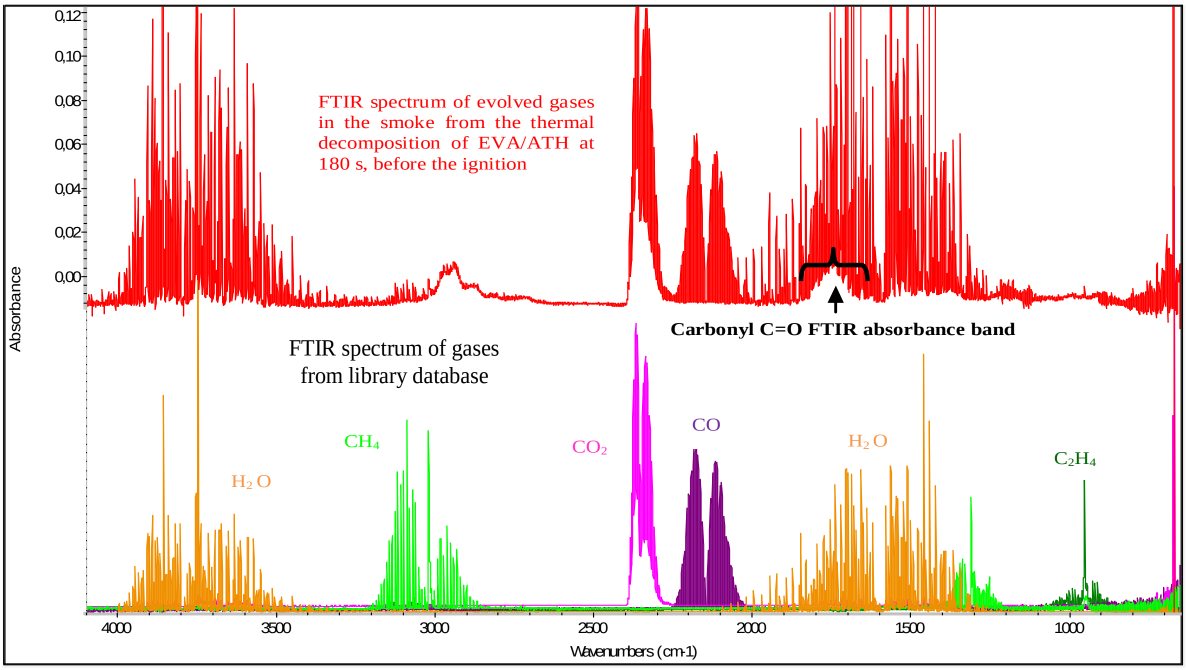

Figure 42. Qualitative analysis of the gas in the smoke of EVA/ATH before ignition (MLC/FTIR - 35 kW/m²)

This carbonyl signal is attributed to possibly acetone rather than to acetic acid, as there is a better fit with CH_3COCH_3 (absorption band between 1775 and 1700 cm^{-1}) than with CH_3COOH shifted to the left (absorption between 1850 and 1750 cm^{-1}) as shown at Fig. 43. This release of acetone rather than acetic acid can be ascribed to the catalytic effect of Al_2O_3, which promotes transformation of CH_3COOH to CH_3COCH_3.[38]

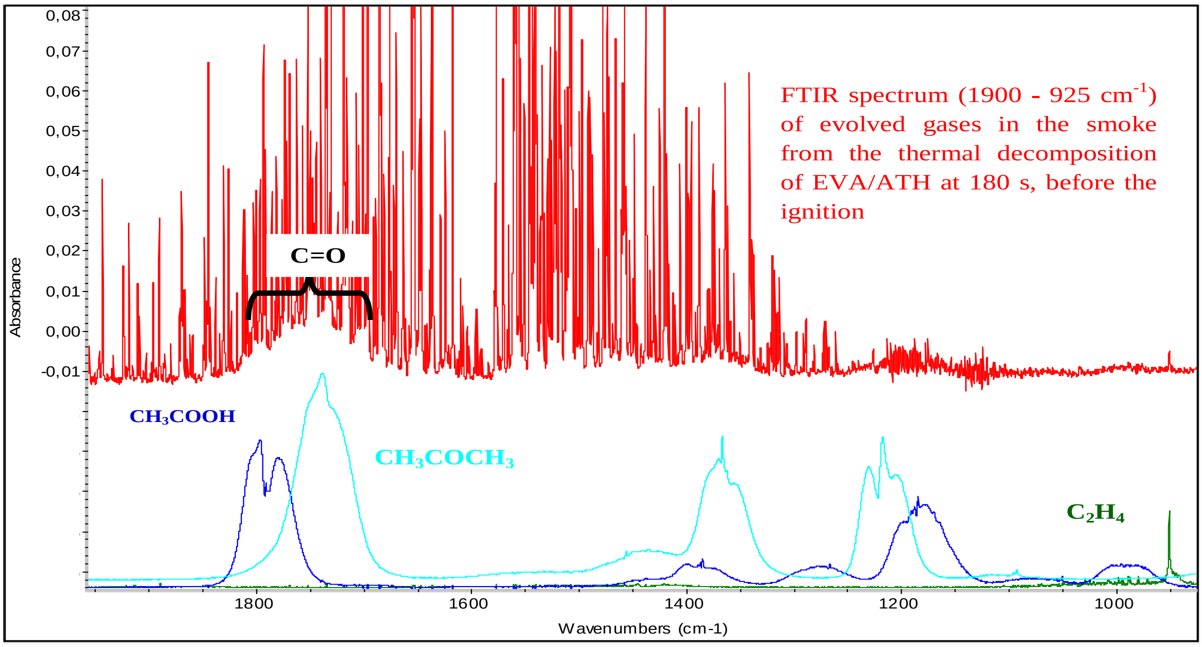

Figure 43. Comparison of FTIR spectrum of evolved gases with acetone and acid acetic spectrum

During the flaming phase (286 s), intense absorbance bands of CO_2 (absorption around 2357 - 2310 cm^{-1}), H_2O (broad bands around 3900 - 3500 cm^{-1} and 1900 - 1250 cm^{-1}) and low absorbance of CO (absorption around 2187 - 2115 cm^{-1}) are observed (Fig. 44). The low absorbance of CO is due to the combustion reaction; moreover, there is a noteworthy disappearance of CH_4 and C_2H_4 signals (at 3030 - 2990 cm^{-1} and 2985 cm^{-1} respectively).

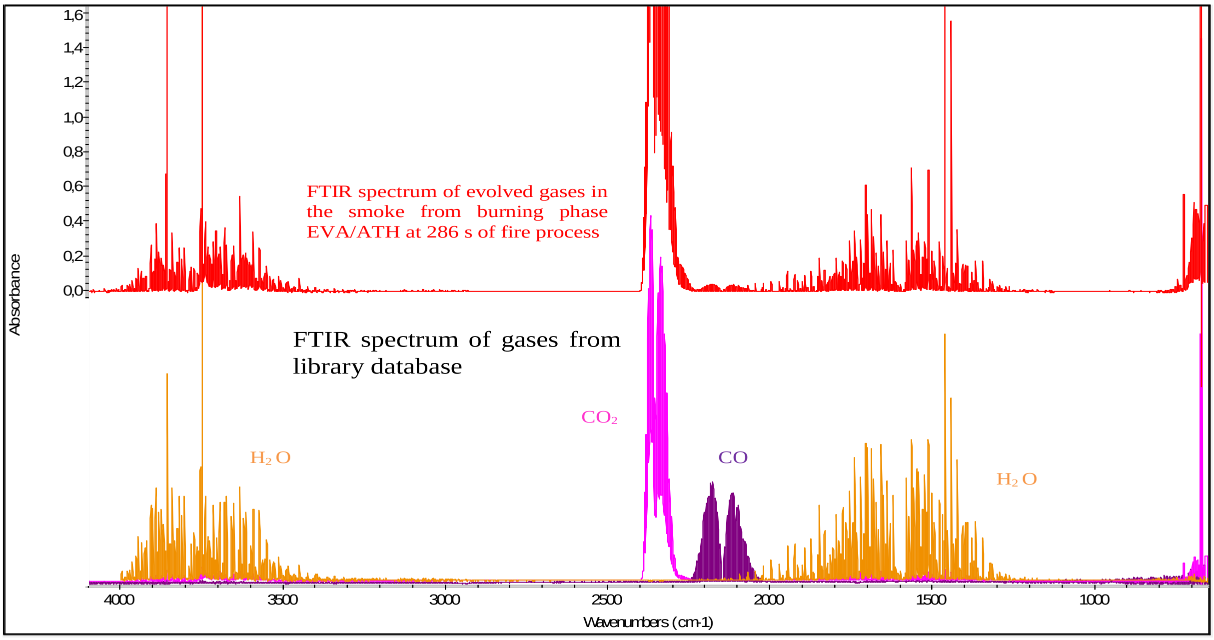

Figure 44. Qualitative analysis of the gas in the EVA/ATH smoke during flaming (MLC/FTIR-35 kW/m²)

Lastly, after flame out (413 s), the absorbance bands of CO (absorption 2187 - 2115 cm^{-1}) and hydrocarbons (C-H stretching between 3100 to 2800 cm^{-1}) increase because of the smoldering of the EVA/ATH residue (visual observation), whereas H_2O and CO_2 absorbance intensities decrease (Fig. 45).

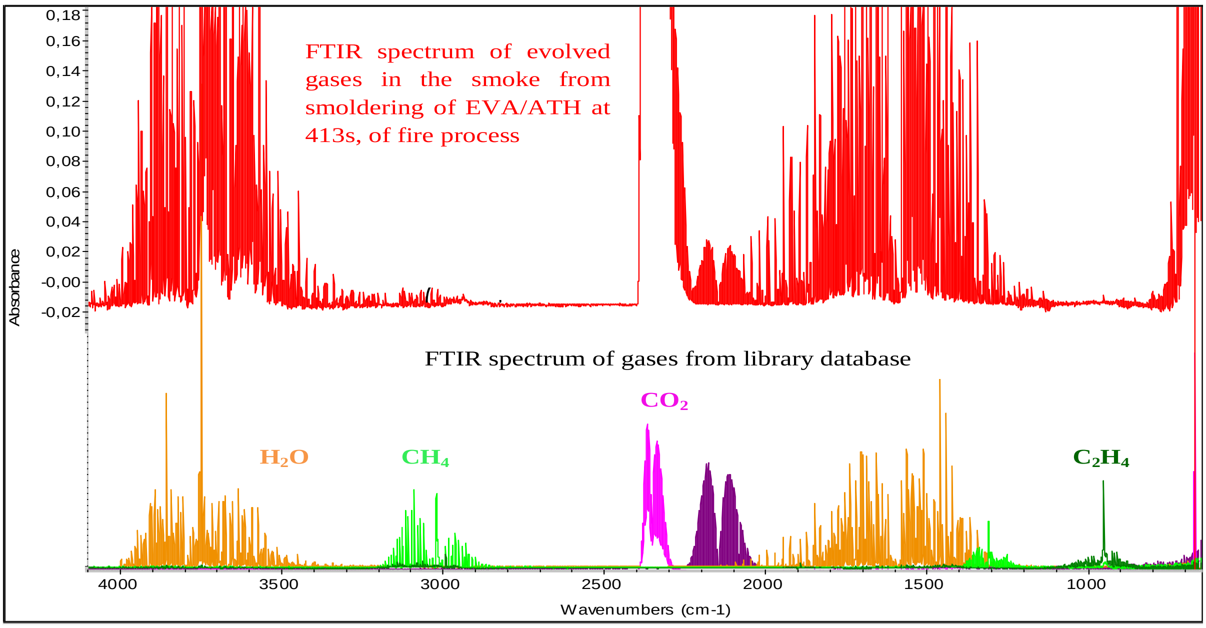

Figure 45. Qualitative analysis of the gas in the EVA/ATH smoke during smouldering (MLC/FTIR - 35 kW/m²)

This qualitative analysis of gas release during combustion of EVA/ATH (H_2O, CO, CO_2, CH_4, C_2H_4 and CH_3COCH_3) is consistent with the literature.[31 - 38] It highlights the accuracy and the interest of this bench test for qualitative determination of gases in fire smoke.

3.2.3 Quantitative analysis of EVA/ATH fire smoke

In addition to the identification of evolved gases in the EVA/ATH fire smoke, these gases have been quantified over time (Fig. 46). The combustion process of EVA/ATH can be divided into three stages. The first, from the outset of the test to ignition (180 s), is characterized by the release of H_2O, CO (200474 and 16278 ppm respectively) and CO_2 (66087 ppm) with low concentrations of C_2H_4 and CH_4 (352 and 730 ppm respectively). Furthermore, this quantitative analysis gives clear indication of a competitive release of CH_3COCH_3 as against CH_3COOH, with concentration of 427 ppm for acetone and only 206 ppm for acetic acid. It appears that the deacetylation of the vinyl acetate group in the EVA copolymer loses its autocatalytic character in the presence of ATH. This can be explained by Lewis acid/base interactions between CH_3COOH released by EVA and Al_2O_3 resulting from ATH dehydration, leading to the transformation of CH_3COOH into CH_3COCH_3.[38]

The second stage consists in ignition to flame out (315s); the concentrations of H_2O, CO_2 and CH_3COCH_3 reach their maximum (588057, 311553 and 1623 ppm respectively). At the same time, the release of CO decreases (8953 ppm) and CH_4, C_2H_4 and CH_3COOH are close to 0 ppm throughout the flaming phase (Fig 46). The third and final stage is from flame out to the end of the experiment. After flame out, smoldering of EVA/ATH residue was observed, resulting in additional release of CH_4, C_2H_4, CO, CO_2, H_2O, CH_3COCH_3 and CH_3COOH.

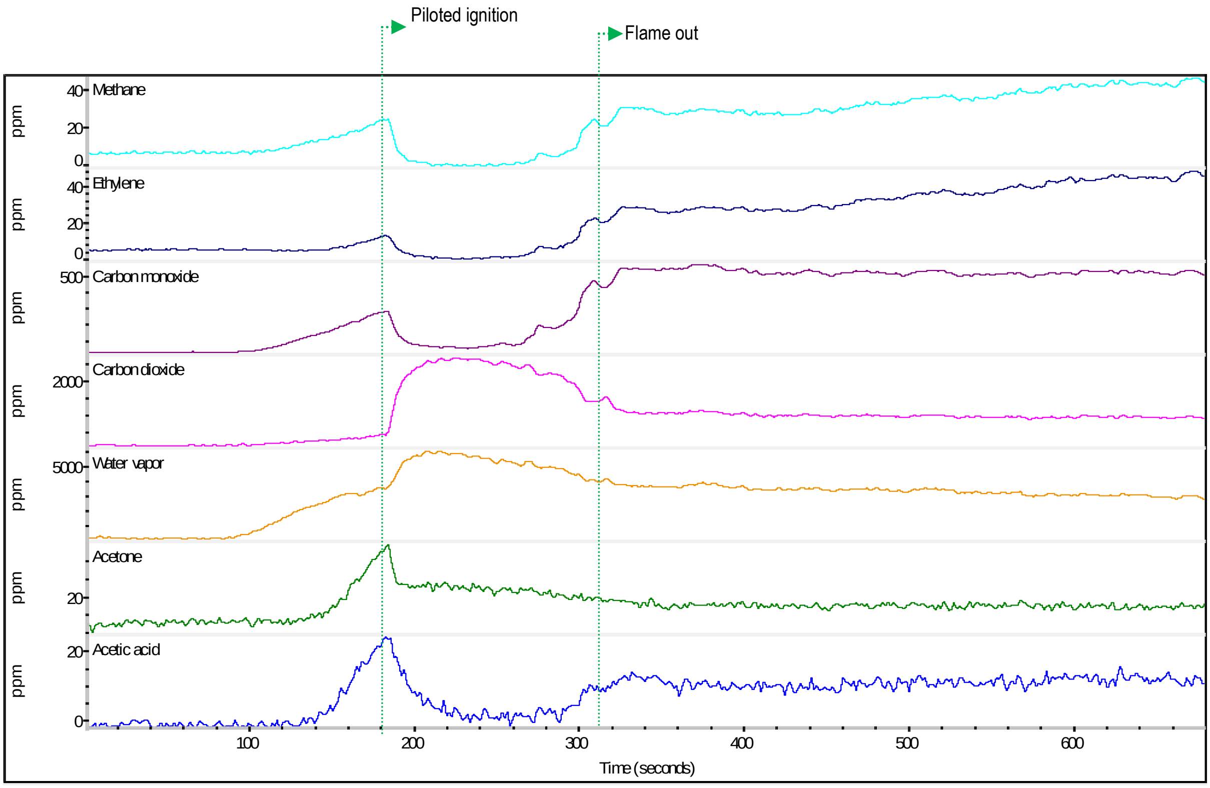

Figure 46. Gas concentration of EVA/ATH as a function of time (MLC/FTIR - 35 kW/m²)

3.3 Particle analysis in EVA/ATH fire smoke

The size distribution and number of particles emitted (per cm^3) during the combustion of EVA/ATH, measured with the ELPI during the MLC test are presented at Fig. 47. Particles emission consists mainly of ultrafine particles (< 0.1 µm) followed by fine particles (< 1 µm). The highest concentration by number of particles in the smoke is observed for particles of 54 nm with 3.10^7 ± 20 % particles per cm^3. Particles larger than 1 µm are also observed, although in concentrations lower by a factor of 10^3 than those of the ultrafine particles. This result confirms the preponderant release of submicron particles with a specific peak of 54 nm particles, highlighting the precision of the ELPI interface with MLC in determining particle-size distribution in the smoke of the EVA/ATH fire.

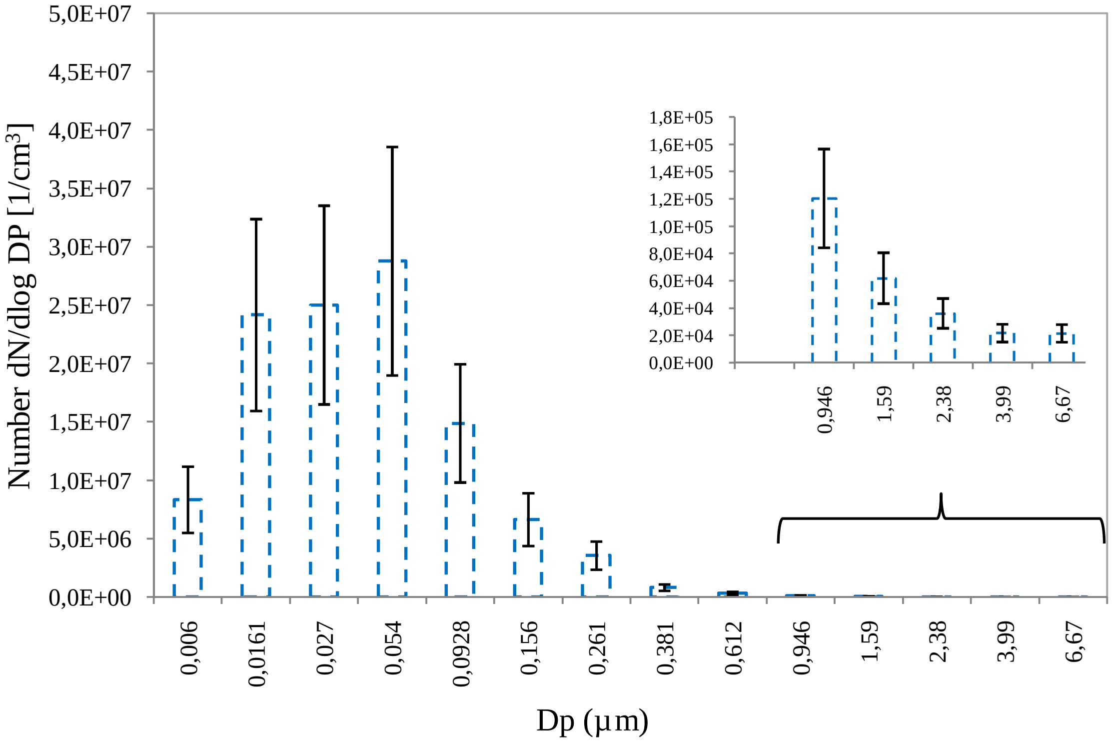

Figure 47. Particle-size distribution and number per cm^3 in the EVA/ATH smoke

(MLC/ELPI - 35 kW/m²)

Promising results emerge from these analyses of gas phase and particles in the EVA and EVA/ATH fire smoke using the MLC/FTIR/ELPI coupling. This bench test can now be used to compare the fire behaviour of EVA with and without ATH.

4 EVA vs EVA/ATH: what is the added value of using MLC/FTR/ELPI?

An overview of the results provided by MLC/FTIR/ELPI appears at Fig. 48 a-d. It brings together HRR and quantitative analysis of gases (Fig. 48 a and b) as well as mass per m^3 of particles (Fig. 48 c and d) emitted in the smoke during combustion of EVA and of EVA/ATH. When comparing the effect of ATH on EVA fire behaviour, three main differences are highlighted: (i) increase in ignition time, (ii) reduction of HRR peak, (iii) dilution of evolved gases (Table 4). Furthermore, a significant amount of H_2O is released for EVA/ATH, reaching a local maximum of 2520 ppm at 180 s (before ignition), while for pure EVA, the concentration of H_2O is undetectable (Fig. 48.a). H_2O release at an early stage for EVA/ATH is due to dehydration of ATH and formation of Al_2O_3 in the condensed phase (cf. Eq. 1, chapter 1, page 30). The delay in ignition time and the lower HRR of EVA/ATH compared to EVA is explained by the extent of endothermic dehydration of ATH into alumina and also to the dilution of the gas phase by the release of water. The evolution of the mass of soot particles (mg/m^3) in the smoke during the fire was also evaluated, extending the knowledge of the impact of ATH on EVA fire behaviour. The comparative evaluation indicates: (iv) the large amount of soot particles before ignition of the EVA/ATH material (almost 7.10^3 mg/m^3 at 175 s) whereas, for neat EVA, no particles were detected before ignition; (v) the global dilution, by a factor of 10, of soot mass during combustion of EVA/ATH in comparison to EVA (Fig. 48.c and d) because of the greater quantity of hydrocarbons in EVA compared to EVA/ATH.

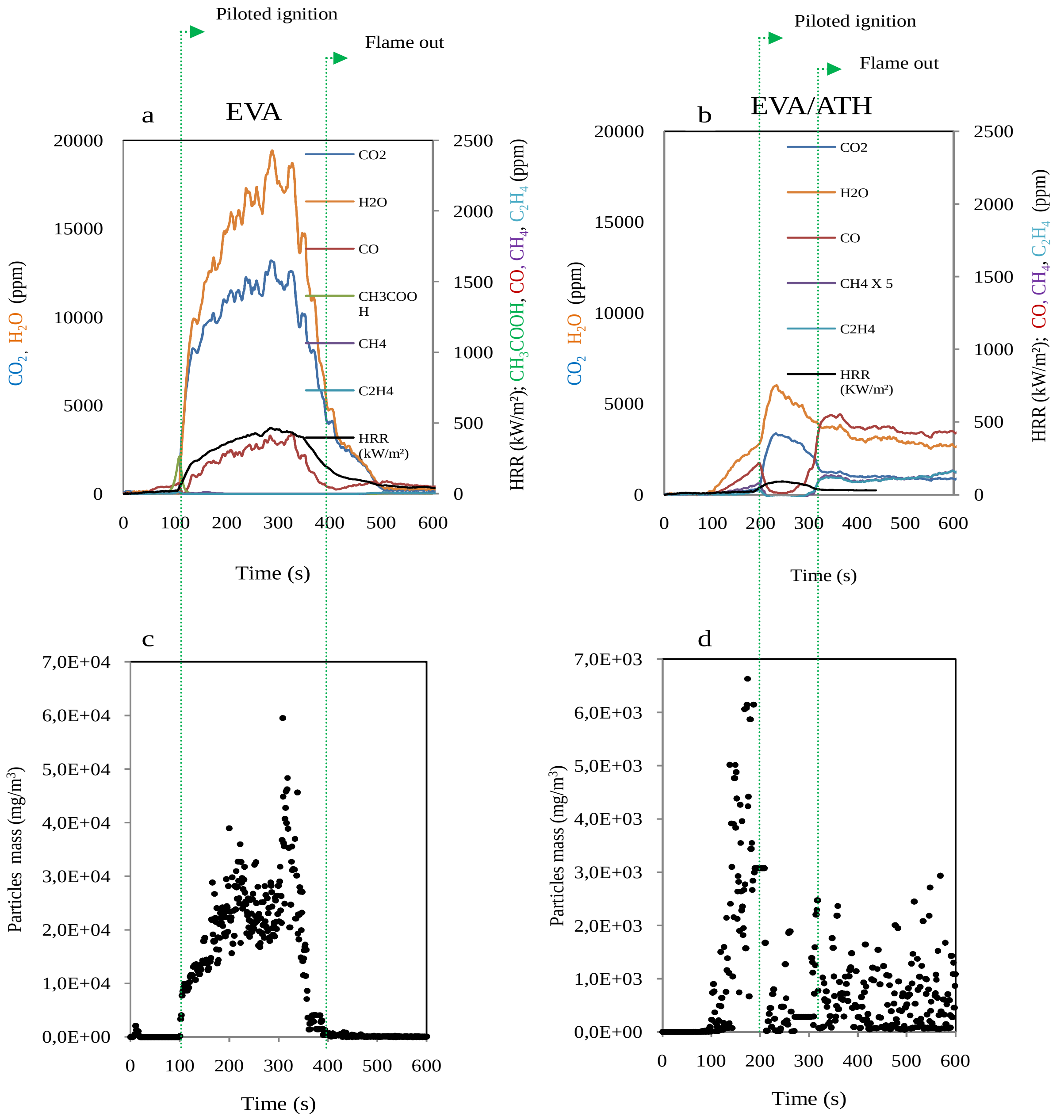

Figure 48. Heat release rate, gas quantification and mass of evolved particles in the smoke of EVA and EVA/ATH (MLC/FTIR/ELPI 35 kW/m²)

Table 4. Main physical parameters and concentration of gases for EVA and EVA/ATH (MLC/FTIR/ELPI 35 kW/m²)

	t_{ig} (s)	pHRR (kW/m²)	Total gas release (ppm) from test start to flame out						
			H_2O	CO_2	CO	CH_3COOH	CH_3COCH_3	CH_4	C_2H_4
EVA	103	456	4101654	3010474	75905	4073	-	694	230
EVA/ATH	183	97	1336493	472050	81390	401	3005	3475	2072

A comparison of size distributions and concentrations in number of particles per cm^3 in the fire smoke of EVA unfilled and filled with ATH is provided at Fig. 49. This reveals that, in both cases, particles emitted in the smoke have quite similar size distributions, i.e. mainly in the range of ultrafine and fine particles.

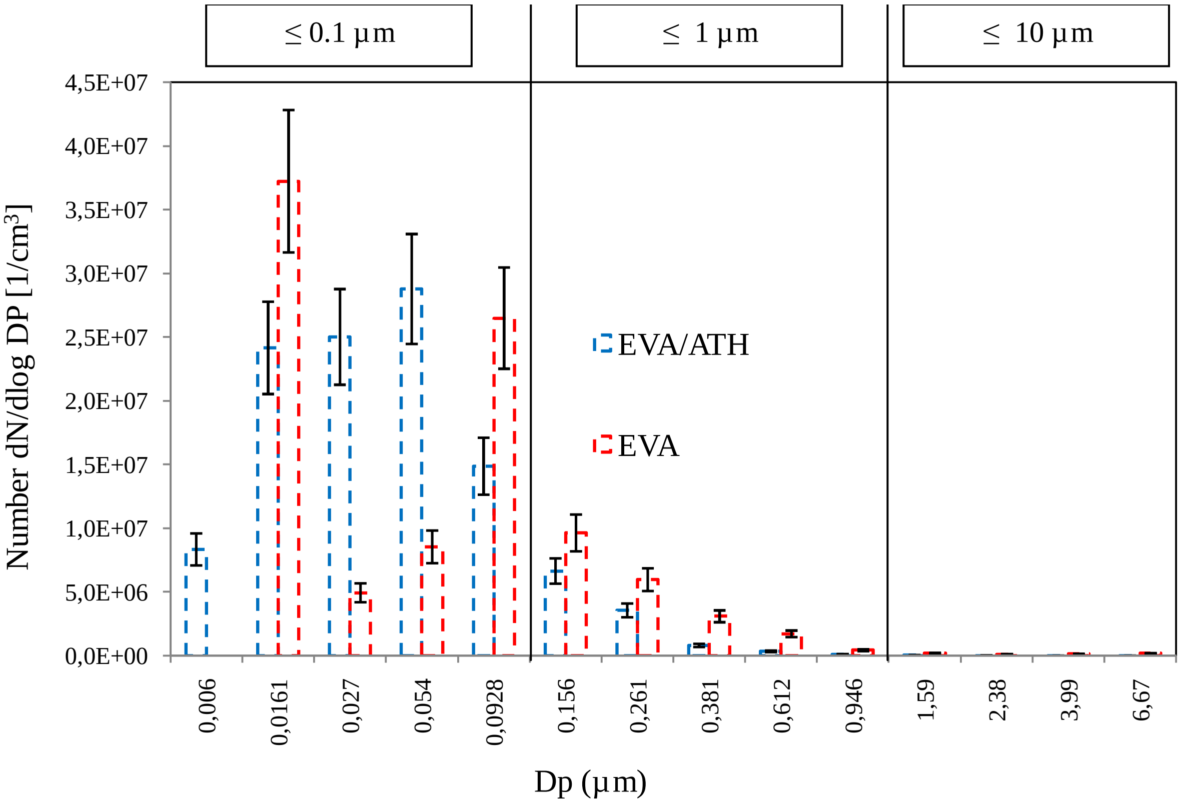

Figure 49. Comparison of particle size distribution and number in EVA and EVA/ATH smoke EVA/ATH (MLC/ELPI - 35 kW/m²)

Nonetheless, the precision of the ELPI determination of particle-size distributions of particles enables observation of particles of 6 nm being released during the combustion of EVA/ATH but not during combustion of EVA, which suggest that ATH in combination with EVA favours the release of more ultrafine particles. This result can be explained by the fact that the flame retarded material (EVA/ATH) tends to reduce the oxidation of a highly combustible material (EVA) thereby promoting the formation of ultrafine particles in the smoke, as reported by Hertzberg.[138] This result also corresponds with the observation of J. Rhodes,[101] who mentioned in his report that the presence of additive flame retardants may increase the formation of smaller-sized particles as compared to pure polymers.

5 Conclusion

This chapter has focused on the validation of the MLC/FTIR/ELPI coupling as an applicable and reliable experimental bench for quantitative and simultaneous characterization of heat release rate and of the concentration of gases and particles in the smoke produced during a fire test. Using ethylene vinyl acetate as the reference material, the experimental bench was found to exhibit high repeatability and to provide accurate results in chemical analyses of the gases and particles associated with regular cone data. It is nonetheless noteworthy, that account must be taken of the relative standard deviations relating to the concentration per cm^3 of particles detected in fire smoke with the current implementation of MLC/FTIR if the results are to be correctly presented and interpreted. It is worth noting that it may be possible to reduce these standard deviations by implementing a dilution system for the ELPI analyzer. On the other hand, application of MLC/FTIR/ELPI to the fire behaviour characterization of EVA/ATH confirms that ATH improves ignition time, reduces the heat release rate and, in the main, dilutes combustion gases. The transformation of acetic acid to acetone according to the Lewis acid/base interactions between the Al_2O_3 resulting from ATH dehydration and CH_3COOH from EVA deacetylation was also observed with the MLC/FTIR coupling. Moreover, particles emitted in the smoke during combustion of EVA and EVA/ATH have been shown to be predominantly in the ultrafine particles (<0.1 µm) followed by fine particles (<1 µm) size range. It is also worth noting that ATH appears to promote the formation of ultrafine particles (specifically, 6 nm), which is not the case of neat EVA. In addition, during combustion of neat EVA, two main peaks in the number of particles emitted per cm^3 were reported, the first for particles of 16 nm (almost $3.70.10^7$ per cm^3) and the second for 93 nm particles (average of $2.70.10^7$ particles per cm^3), whereas for EVA/ATH, concentration peaks occurred for particles of 16 nm, 27 nm and 54 nm (almost $2.4.10^7$, $2.6.10^7$ and $3.0.10^7$ particles per cm^3 respectively). To summarize, these results confirm the efficiency and the added value of the MLC/FTIR/ELPI coupling. Considering the advantages of the bench, the fire behaviour of EVA and EVA/ATH will now be tested in different fire scenarios. The next chapter is consecrated to providing a description of these tests as well as a presentation and discussion of the results.

CHAPTER 4: INVESTIGATION OF HEAT FLUX EFFECT ON EVA AND EVA/ATH FIRE BEHAVIOUR USING THE MLC/FTIR/ELPI COUPLING

Investigations into the fire behaviour of polymeric materials are often conducted at 35 and/or at 50 kW/m² [139, 140] because these heat fluxes best reproduce the thermal aggression and heat stresses generated respectively by a mild fire and/or a flashover fire situation and enable realistic laboratory simulation. When it comes to determining thermal stability or degradation of materials during flaming combustion, tests at different thermal stresses can lead to a better understanding of fire performance as well as improve knowledge of the transient evolution of gases in terms of decomposition kinetics and the type of particles emitted in the smoke. The focus of this chapter is to study the effect of heat flux on the characteristic fire behaviour of materials using the MLC/FTIR/ELPI combination. As for the two last chapters, EVA and EVA/ATH are used as reference materials. Four external heat fluxes have been selected to simulate different fire scenarios: 25 kW/m² to simulate a situation of low thermal aggression, 35 kW/m² to simulate a mild fire, 50 kW/m² a flashover fire situation, and 75 kW/m² to simulate sudden onset of intense thermal stress.

The first section of this chapter reports on the first stage of the investigation, which lay in the examination of parameters like HRR, t_{ig}, THR, EHC and CHF, thereby enabling comparison of the flammability performances of EVA and EVA/ATH in the above mentioned thermal stress situations. The second section deals with the effects of heat flux on the quantitative analysis of evolved gases as evidenced by the calculation of their respective yields per gram of degraded EVA and EVA/ATH. The third section is focused on the effect of heat flux on the analysis of size distribution and concentration of particles out of the flame of the EVA and EVA/ATH fires. In the fourth section, an attempt will be made to provide a global answer to the question of "How experiments conducted at different heat flux levels with the MLC/FTIR/ELPI combination could facilitate a better understanding of the fire behaviour of materials?"

1 Flammability of EVA and EVA/ATH at different heat fluxes

Numerous thermo-physical or flammability parameters can be evaluated so as to describe and classify the fire behaviour of a material. These parameters depend on the test scale and instrumentation. With MLC as a fire model, it is possible to measure HRR, t_{ig}, MLR and derived parameters like THR, CHF and EHC. These parameters will first be commented on before being examined at different heat fluxes to assess EVA and EVA/ATH behaviour at different thermal stresses.

1.1 Heat release rate and ignition time of EVA vs EVA/ATH

HRR is considered to be the most significant parameter for characterizing the fire hazards of materials, since it controls the growth rate of the fire: heat, mass loss and smoke emission.[141] The t_{ig} or combustion initiation of a material represents the time at which the sample starts to burn. The HRR and t_{ig} values of EVA and EVA/ATH at 25, 35, 50 and 75 kW/m² are plotted at Fig. 50 a-d. As expected, the flame retarded EVA/ATH exhibits lower pHRR values (by around 80% as compared to those of neat EVA (Table 5). As discussed in the previous chapter, the relatively low pHRR of EVA/ATH in contrast to neat EVA can be attributed to the physical and chemical actions of ATH.[38, 135, 136] The physical mode of action leads to the formation of a ceramic layer of Al_2O_3 that acts as a barrier limiting heat and mass transfer, while the chemical action in the condensed and gaseous phases corresponds to the endothermic dehydration of ATH resulting in dilution of the gaseous fuel.

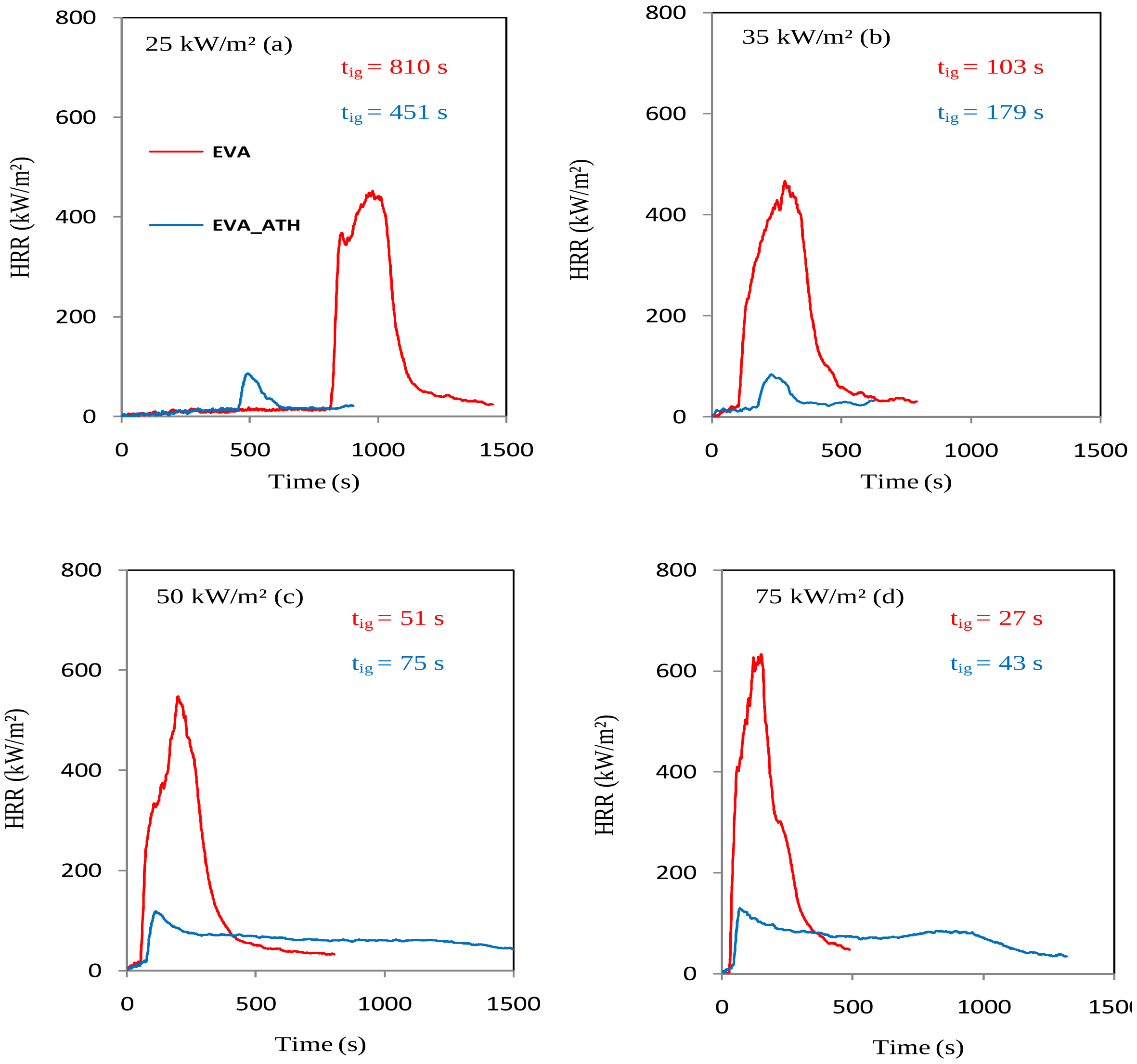

Figure 50. Heat release rate as a function of time for EVA and EVA/ATH formulations

(MLC - 25, 35, 50, 75 kW/m²)

Table 5. Peaks heat release rates and ignition time of EVA and EVA/ATH formulations at 25, 35, 50, 75 kW/m²

Heat flux (kW/m²)	pHRR (kW/m²)		t_{ig} (s)	
	EVA	EVA/ATH	EVA	EVA/ATH
25	452	85	810	451
35	447	91	103	179
50	547	118	51	75
75	633	129	27	43

For heat fluxes of 35, 50 and 75 kW/m², the t_{ig} of EVA/ATH is longer than that of pure EVA. This observation is consistent with the physical and chemical actions of ATH already reported. However, for tests performed at 25 kW/m², a remarkable inversion between EVA and EVA/ATH is observed. The piloted ignition of pure EVA is observed at 810 s, whereas it is at 451 s for the EVA/ATH formulation. To investigate this unexpected result, photographs of the samples at the ignition time are analysed (Fig 51 a-d).

During the experiment performed at 25 kW/m², the thermal decomposition of EVA is observed to result in the formation of a carbonaceous layer (char) before the piloted ignition. This carbonization phenomenon was not observed during the tests conducted at 35, 50, and 75 kW/m². Indeed, prior to ignition, the samples of EVA exhibit a viscous aspect at 35 kW/m², and a liquid (melting and bubbling) aspect at 50 and 75 kW/m². In the case of the flame retarded EVA/ATH at 25, 35, 50 and 75 kW/m², the samples in the MLC holder remain in solid state throughout the duration of the fire tests, which is probably due to high ATH content.

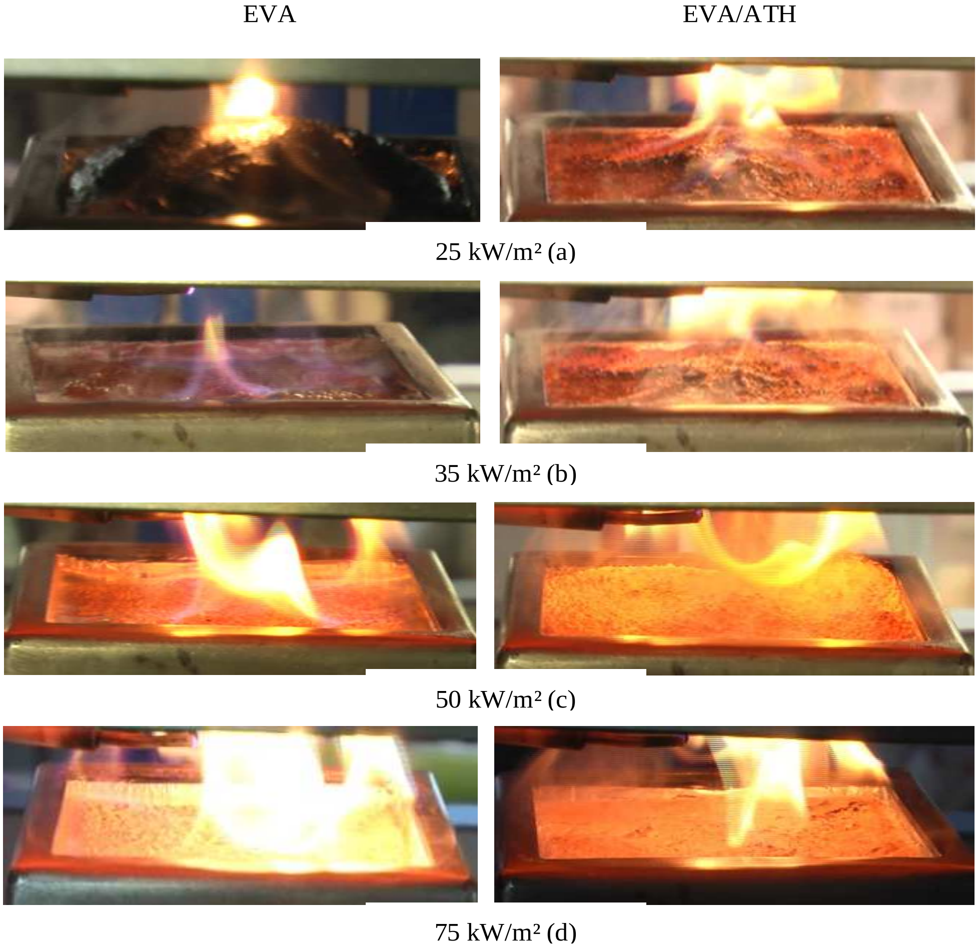

25 kW/m² (a)

35 kW/m² (b)

50 kW/m² (c)

75 kW/m² (d)

Figure 51. Photos of EVA and EVA/ATH at time of ignition (MLC - 25, 35, 50, 75 kW/m²)

Based on visual observations during the tests performed on EVA and EVA/ATH, the major difference between the two materials is the formation of a carbonaceous layer or char during the thermal decomposition of EVA at 25 kW/m² (Fig 51.a). The inversion of the relative magnitudes of the t_{ig} of EVA and that of EVA/ATH at 25 kW/m² might be attributable to the formation of this char which was not observed at 35, 50 and 75 kW/m² (Fig 51.b - d). It can be assumed that the char acts as a protective layer, blocking the release of decomposition gases, including combustion "fuel" gases and consequently delaying the onset of piloted ignition of the EVA sample.

Figure 52 shows the results in the form of Gram Schmidt (describing intensity of all gases released during thermal decomposition) and MLR (decomposition kinetic of the material) profiles, of the neat EVA experiment at 25 kW/m². A stationary phenomenon is observed in both the Gram Schmidt and MLR curves prior to EVA ignition.

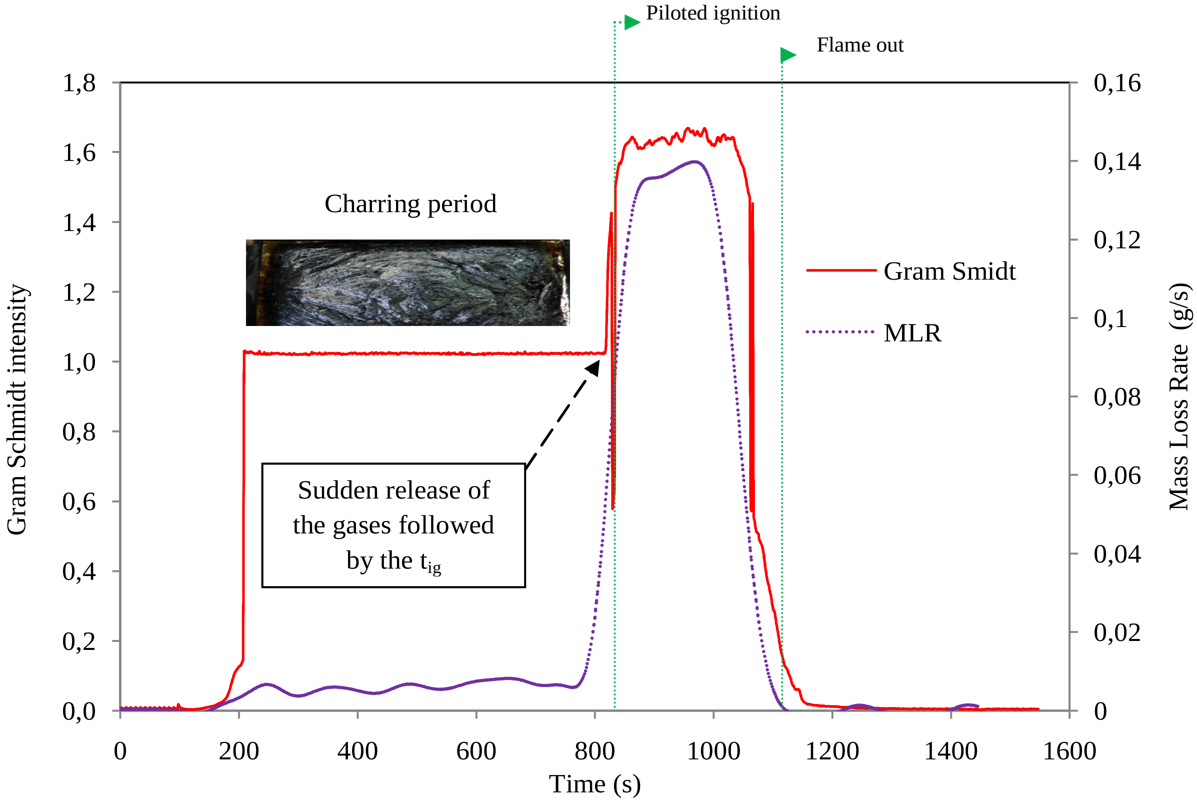

Figure 52. FTIR Gram Schmidt and mass loss rate of EVA (MLC/FTIR-25 kW/m²)

This stationary phenomenon is attributed to cross-linking and charring on the EVA surface, which slows down the flow of fuel in the gas phase and limits oxygen access to the remaining material. [33 - 35] The subsequent rupture of the carbonaceous layer induces a sudden release of gases, as illustrated by the first thin peak on the Gram Schmidt close to 800 s, which is followed by ignition. The formation of the carbonaceous layer is therefore the cause of the delay in ignition of the EVA sample at 25 kW/m².

The Gram Schmidt and MLR profiles for EVA/ATH at 25 kW/m², are plotted at Fig. 53. A continuous increase (from 160 s) is seen in the mass loss rate and the intensity of gases released in the smoke. This relates to the degradation of EVA/ATH, which continues until the gaseous fuels reach the concentration, temperature and pressure necessary to trigger piloted ignition (at 451 s).

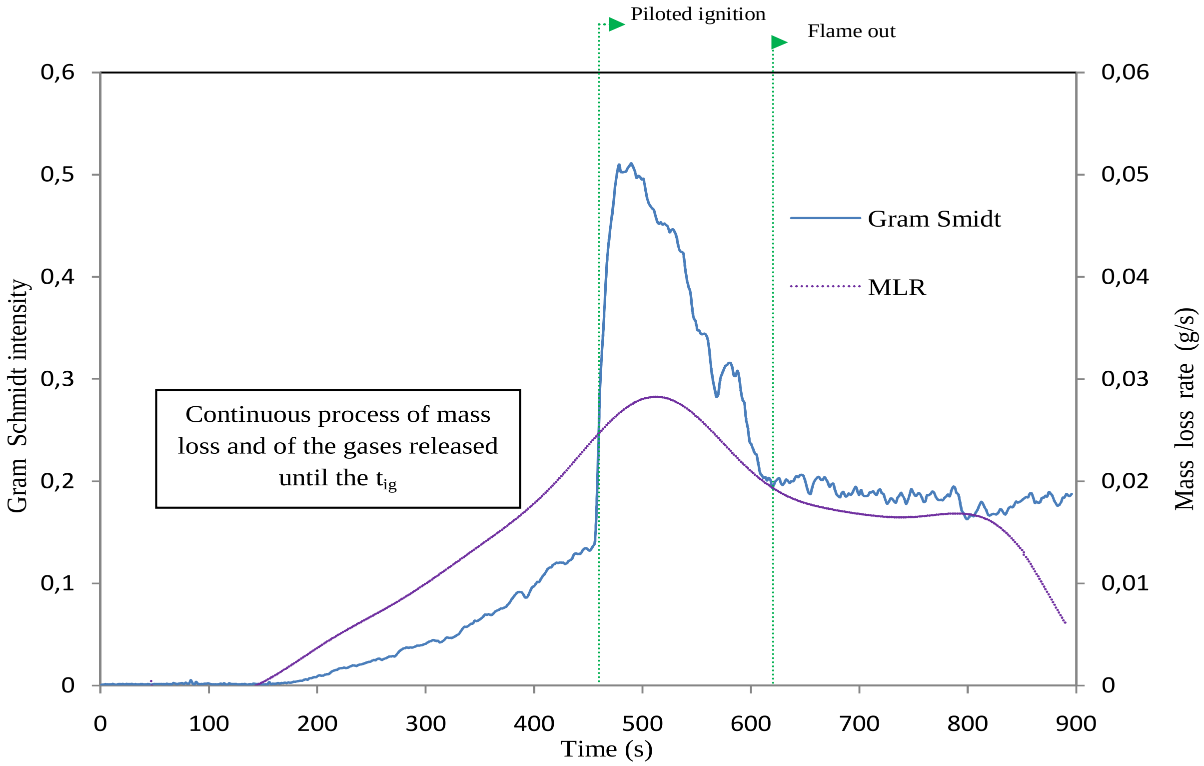

Figure 53. FTIR Gram Schmidt and mass loss rate of EVA/ATH (MLC/FTIR - 25 kW/m²)

These results, obtained with the MLC and FTIR combination, provide empirical evidence that aids in explaining why pure EVA ignition occurs after that of EVA/ATH when these materials are subjected to a heat flux of 25 kW/m². At this heat flux, a char layer is observed to have formed on the EVA material, which has the effect of limiting the evolution of decomposition gases and hence delaying ignition. This demonstration highlights the potential of the proposed simultaneous bench test in comparative investigations of the thermal decomposition pathways and mechanisms of materials. In addition to HRR and t_{ig}, other physical parameters, such as THR, CHF and EHC, can be used to investigate the fire behaviour of materials. These parameters are discussed in the following sections.

1.2 Total heat release of EVA and EVA/ATH at different heat fluxes

Total Heat Release (THR) is a physical parameter that corresponds to the total available energy in a material during a fire. It can be considered as being the area under the HRR curve. The THR of EVA and EVA/ATH at 25, 35, 50 and 75 kW/m² are plotted as a function of time in the graph at Fig. 54. In the EVA case, the THR exhibit at each heat flux a value that lies within the narrow range of 75 ± 2 MJ/m². On the other hand, the measured THR of EVA/ATH (Fig. 54) is proportional to the external heat flux, with measured values at around 15, 17, 56, and 58 MJ/m² for heat fluxes of 25, 35, 50 and 75 kW/m², respectively. A noticeable difference is thus observed between the two cases with the THR values of EVA/ATH lower than those of EVA by 80, 78, 25 and 22 % with respect to the increases in the applied heat flux.

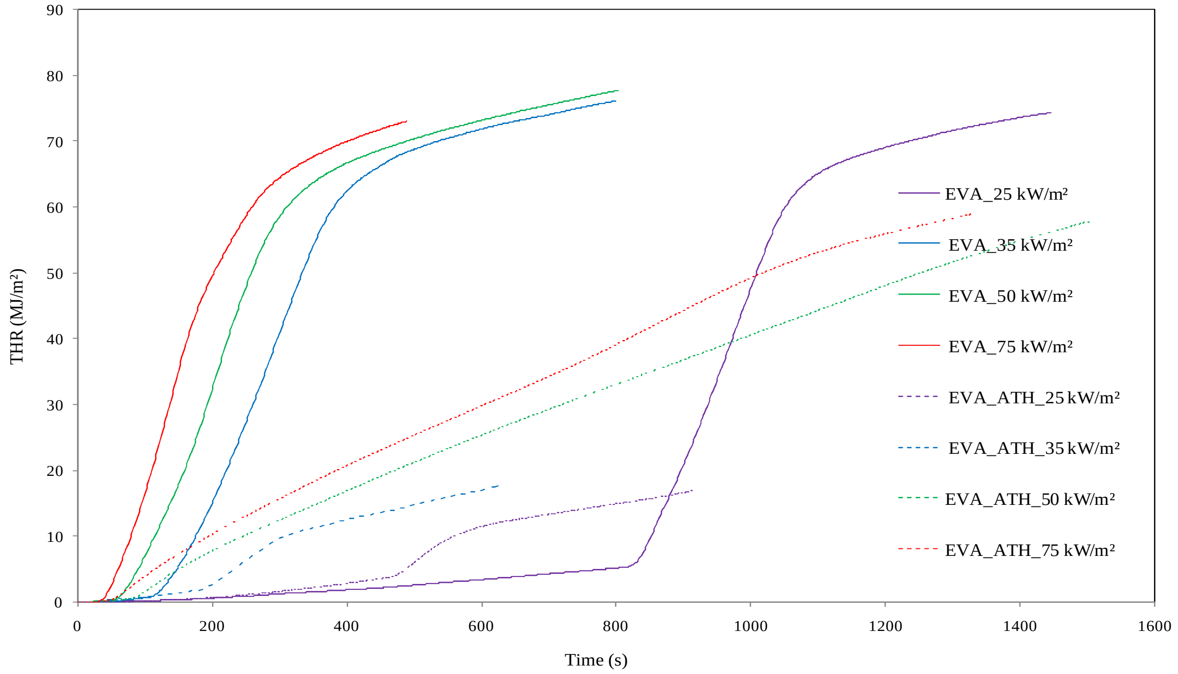

Figure 54. Total heat release as a function of time of EVA and EVA/ATH (MLC - 25, 35, 50, 75 kW/m²)

Moreover, the EVA and EVA/ATH THR curves exhibit a jump in slope shortly after ignition. According to Zanetti et al, [142] the slope of the THR curve can be considered as representative of the flame spread of the material. Given that the jumps in the slopes of the EVA THR curves are steeper than those of EVA/ATH, it can be assumed that the flame spread of EVA during a fire incident will be greater than that of EVA/ATH. The mass losses of EVA and EVA/ATH at 25, 35, 50 and 75 kW/m² are shown at Figures 55 and residues of EVA/ATH at 56. It can be observed from the latter that the EVA samples leave no residue after the fire tests, whatever the heat flux, which explains why all the THR measured for EVA are constant in value. The quantities of degraded EVA/ATH material, on the contrary, increase in line with the heat flux (Fig. 55 and 56) and the corresponding THR also increases concomitantly with the amount of material burned.

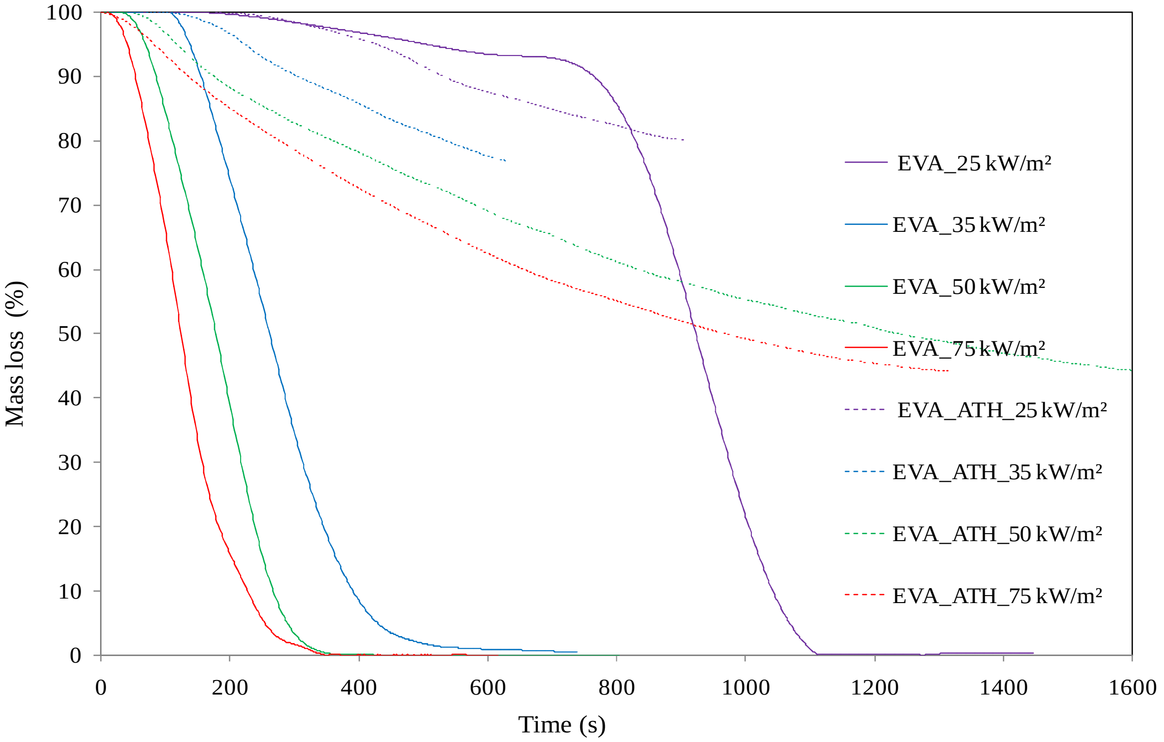

Figure 55. EVA and EVA/ATH mass loss curves (MLC - 25, 35, 50, 75 kW/m²)

25 kW/m²	35 kW/m²	50 kW/m²	75 kW/m²
			

Figure 56. Residues of EVA/ATH (MLC - 25, 35, 50, 75 kW/m²)

1.3 Critical heat flux of EVA and EVA/ATH

Critical heat flux (CHF) represents the maximum heat below which ignition of a material will not be triggered. It can be evaluated by using the linear relationship between t_{ig} and the irradiative heat fluxes, as reported by Mikolla,[143] Kallonen,[144] Jansens,[145] etc. The correlation between t_{ig} and applied heat flux depends on whether a material is considered to be thermally thick, i.e. with a temperature gradient between its surface and interior, or thermally thin, i.e. whose thickness is typically less than 1 - 2 mm.[146] The respective correlations are given below:

- Using the thermally thin approach, the external heat flux is a linear function of the inverse of t_{ig} (equation 9):

$$t_{ig}^{-1} = f(q_{ext}) \qquad (8)$$

- With the thermally thick approach, external heat flux is a linear function of the inverse of the square root of t_{ig} (equation 10):

$$t_{ig}^{-1/2} = f(q_{ext}) \qquad (9)$$

The CHF is then deduced by the absolute value of the intersection of the straight line with the x-axis (heat flux axis). This is also equivalent to the ratio between the intercept of the straight line with the y- axis ($Y_{intercept}$) and the slope (a) of the affine function (Equation 11).

$$CHF = Y_{intercept} / a \qquad (10)$$

The sample plates of EVA and EVA/ATH used for the present study have a thickness of 4 mm and can therefore be considered as being thermally thick. The variations of the inverse of the square root of t_{ig} as a function of the heat flux (thermally thick assumption) for EVA and EVA/ATH at 35, 50 and 75 kW/m² are plotted at Fig. 57.

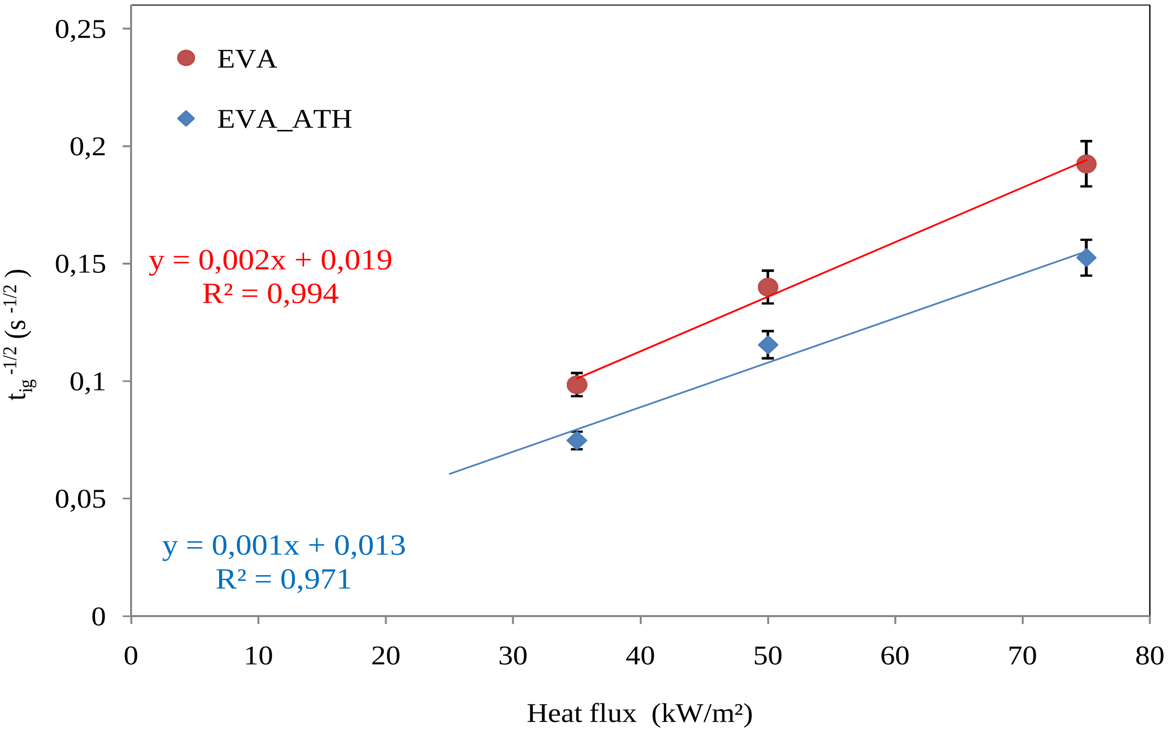

Figure 57. Inverse of the square root of time to ignition versus applied heat flux for thermally thick behaving EVA and EVA/ATH (MLC- 25, 35, 50, 75 kW/m²)

Application of equation 10 gives 9.6 kW/m² for EVA and 13 kW/m² for EVA/ATH. Delichatsios has moreover demonstrated that results from experimental data represent only 64% of the CHF, owing to the loss of irradiance at the sample surface during the fire test.[147] Hence, using the Delichatsios approximation, the CHF of EVA and EVA/ATH are estimated at 15 and 20 kW/m² respectively. This means that under a constant heat flux ≤ 15 kW/m², the EVA plate would not induce a piloted ignition, while EVA/ATH would not induce piloted ignition under a constant heat flux ≤ 20 kW/m². It is worth noting that, according to Spearpoint and Quintere,[148] the experimental intercept data should represent 76% of CHF. Nevertheless, in this study, only the Delichatsios approximation (64%) is considered as it is the more widely applied according to the literature. In addition, the sample plates of EVA and EVA/ATH at 15 and 20 kW/m² respectively have been tested with no piloted ignition reported after 20 min of exposure.

It is worth noting that the t_{ig} data at 25 kW/m², particularly for EVA (and EVA/ATH for homo, was not here taken into account when determining the CHF. In fact, if the t_{ig} of EVA at 25 kW/m² (precisely 816 s or approximately 14 min) is considered, the deduced CHF is 2 kW/m², which is not realistic. Furthermore, according to Tewarson,[149] if a material is not ignited after being exposed to a constant heat flux for 10 min, its t_{ig} may be considered as infinite, which would not tally with any calculation of the CHF from the experimental data.

1.4 Effective heat of combustion of EVA and EVA/ATH

The effective heat of combustion (EHC) is closely associated to the heat of combustion of the gaseous fuel released during thermal decomposition of material. It can be calculated as the ratio between the heat release rate and the mass loss rate per unit of area, as expressed in equation 12.

$$\mathrm{EHC} = \mathrm{HRR}/\mathrm{SMLR} \qquad (11)$$

Where SMLR represents the specific mass loss rate or mass loss rate per unit of area

EHC is generally constant for a material undergoing flaming combustion. It is not expected to be scale-dependent and is of frequent value as an input data for computational fire modelling as it enables simulating mass loss with generated heat of combustion.[150] Nonetheless, it is worth recalling that the EHC derived from mass loss cone data does not correspond to the Gross heat of combustion (ΔHc) from the oxygen-bomb calorimeter. EHC will in fact always be lower than ΔHc because the thermal decomposition of a material in a real fire situation can be associated with incomplete combustion.

Instantaneous EHC values (from ignition to flame out) of EVA at 25, 35, 50 and 75 kW/m² are estimated and the plotted results are found at Fig.58. For all heat fluxes, the ECH drops spontaneously at ignition before oscillating around a globally constant value during the flaming phase and then rising, shortly before flame out, as a result of the decreasing MLR, which leads to a high EHC value. The calculated values for the average effective heat of combustion (AEHC) are 30, 28, 25 and 26 MJ/kg at 25, 35, 50 and 75 kW/m² respectively. This is equivalent to an overall average of 27 ± 3 MJ/kg. At 25 kW/m², a very prominent shoulder of EHC is observed shortly after ignition, reaching a peak of 37 MJ/kg. This shoulder appears to substantiate the sudden release of gaseous fuel trapped in the char, as discussed beforehand. This phenomenon was not however observed at 35, 50 and 75 kW/m² due to the melting of EVA at these heat fluxes leading to a pool fire.

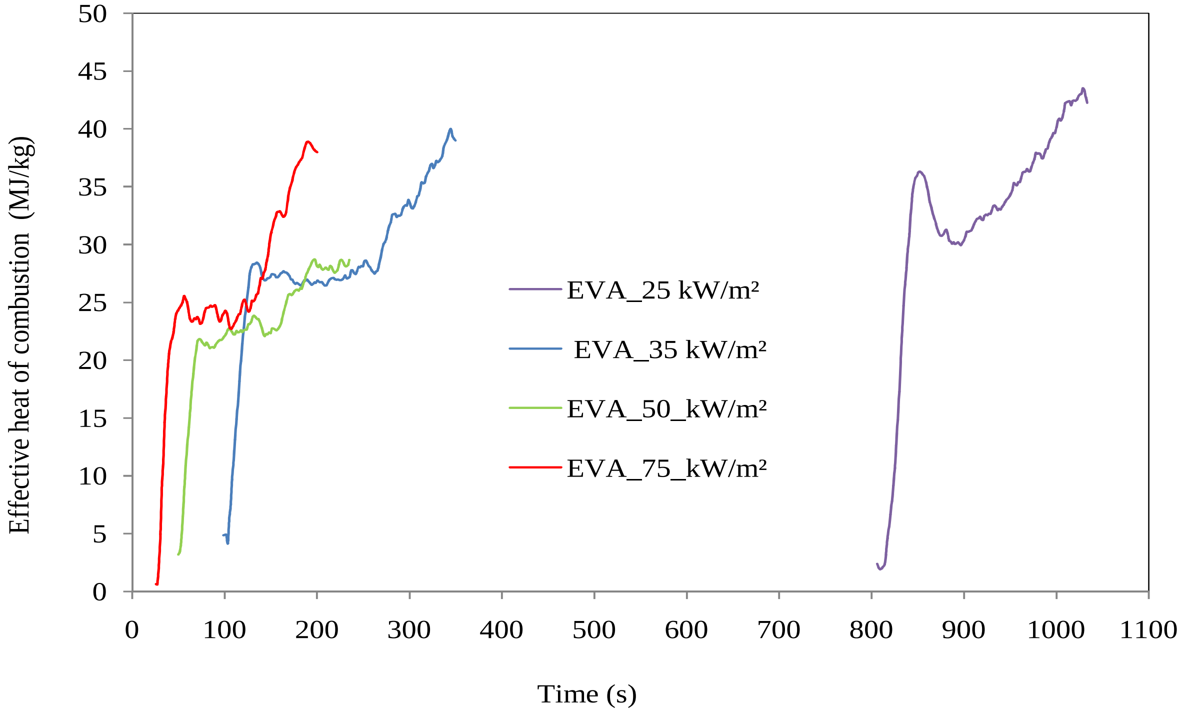

Figure 58. Effective heat of combustion of EVA (MLC - 25, 35, 50, 75 kW/m²)

In the EVA/ATH case, a drop in EHC is again observed at ignition, followed by stabilization during the flaming phase (Fig. 59). The calculated AEHC yields 18, 18, 20 and 19 MJ/kg at 25, 35, 50 and 75 kW/m² respectively, giving an average overall of 19 ± 1 MJ/kg.

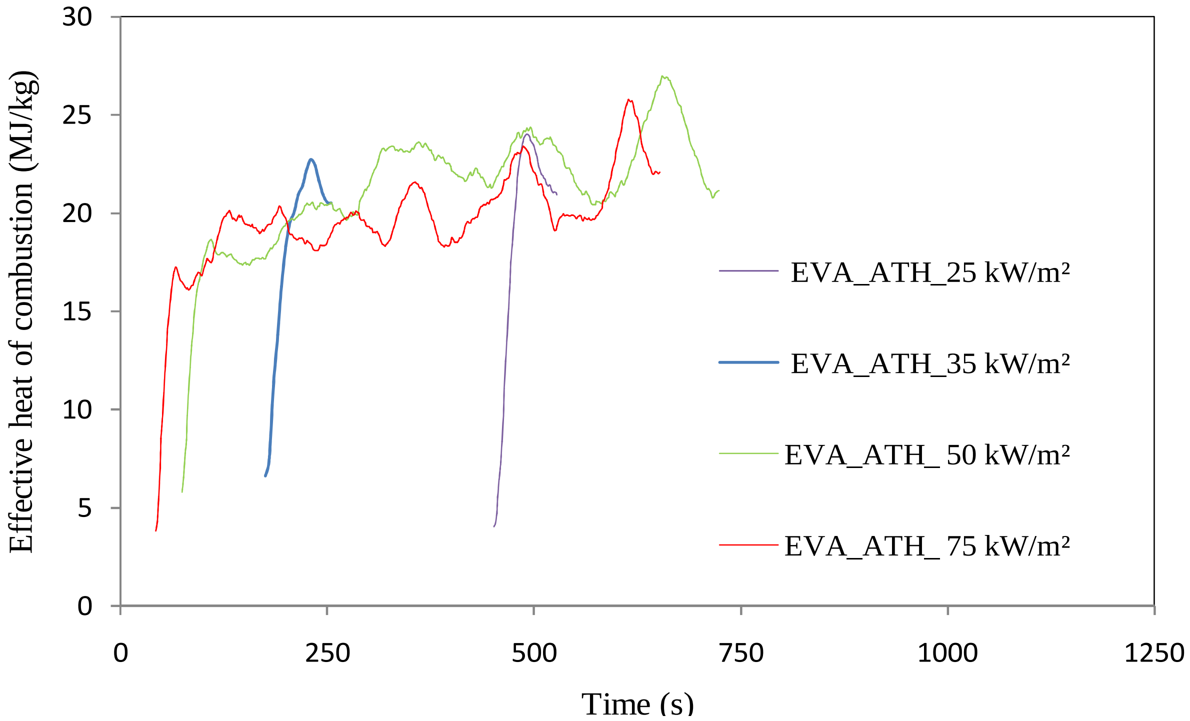

Figure 59. Effective heat of combustion of EVA/ATH (MLC - 25, 35, 50, 75 kW/m²)

The flammability parameters (THR, CHF and AEHC) evaluated at four different heat fluxes lead to the observation that EVA/ATH exhibits lower THR, AEHC and a reduced flame spread in comparison to neat EVA. The EVA and EVA/ATH flammability parameters are brought together in Table 6. These parameters are consistent with a high loading of ATH in the EVA material and a resultant reduction in the amount of hydrocarbons.

Table 6. Flammability parameters of EVA and EVA/ATH.

	THR (MJ/m²)	CHF (kW/m²)	AEHC (MJ/kg)
EVA	75 ± 2	15	27 ± 3
EVA/ATH	8 (25 kW/m²) 17 (35 kW/m²) 53 (50 kW/m²) 58 (75 kW/m²)	20	19 ± 1

2 Heat flux effect on the gas quantitative analyses of EVA and EVA/ATH fires

Quantitative analysis of evolved gases in smoke provides additional data relevant to the investigation of the fire behaviour of materials. It is of interest for understanding the decomposition mechanisms of materials and provides information on eventual toxicity of their gaseous effluents. This section will focus on the effects of heat flux (25, 35, 50, and 75 kW/m²) on the quantification of evolved gases during a fire of EVA and of EVA/ATH cable material. The correlation between the quantitative analysis of the main gases and the measured HRR is also examined. Similarly, the yield per gram of the main gas species in the smoke released as a result of EVA and EVA/ATH degradation is also calculated and discussed in relation to the heat flux variations and the addition of ATH.

2.1 EVA at 25, 35, 50 and 75 kW/m²

Results of the quantitative analysis of evolved gases as well as the HRR measurements obtained during the fires of EVA at 25, 35, 50, and 75 kW/m² are plotted in Fig .60 - 63. The experiments can be divided into three main stages. The first stage (1), covers the period from the start of the test to ignition, the second (2) from ignition to flame out and the third (3) the period following flame out. It is noteworthy that in the case of neat EVA no gases were observed during the third period as EVA leaves no residue. Moreover, the total gas release (CH_3COOH, C_2H_4, CH_4, CO, CO_2 and H_2O) at different stages of the EVA fires at 25, 35, 50 and 75 kW/m² (by integrating gas quantitative curves) are presented in table 7.

During the first stage (1), there is a significant release of CH_3COOH (111856, 2606, 3662 and 3175 ppm at 25, 35, 50 and 75 kW/m²) which represent 98%, 64%, 69% and 70% of the total release at 25, 35, 50 and 75 kW/m² respectively. C_2H_4 (5005, 181, 319 and 299 ppm) and CH_4 (8151, 694, 908 and 967 ppm) at 25, 35, 50 and 75 kW/m² respectively are also present. The measured concentrations of CO_2, CO, H_2O are low compared to those measured during stage 2 (Fig. 60 - 63 and table 7).

Stage 2 is characterized by an increase in HRR, and increased concentrations of CO_2 (2692808, 2980369, 2804253 and 2344824 ppm), CO (82137, 72869, 71030 and 60515 ppm) and H_2O (3064778, 4060639, 4048600 and 3478300 ppm) at 25, 35, 50 and 75 kW/m²; whereas there is a significant reduction of CH_3COOH and C_2H_4 during this combustion stage (Table 7). In the latter case, CH_4 emission decreases locally at ignition and reappears briefly in the smoke at 35, 50 and 75 kW/m², probably because of the pool fire of molten EVA given that a recurrence of CH_4 is not observed at 25 kW/m² (Figures 60 - 63). Note that the highest percentage of CH_3COOH (64 - 98%) and C_2H_4 (92 - 97%) generation from the EVA fires occurs during stage (1) and this for all of the heat flux cases. For CO_2, CO and H_2O, the highest percentage release is during stage 2 (Table 7) representing more than 94%. For CH_4, the percentage release at 25 kW/m² is 93% during stage 1, this being due to the formation of a carbonaceous layer; while at 35, 50 and 75 kW/m², 58 - 60% of CH_4 is released during stage 2, or when the pool fire of molten EVA occurs.

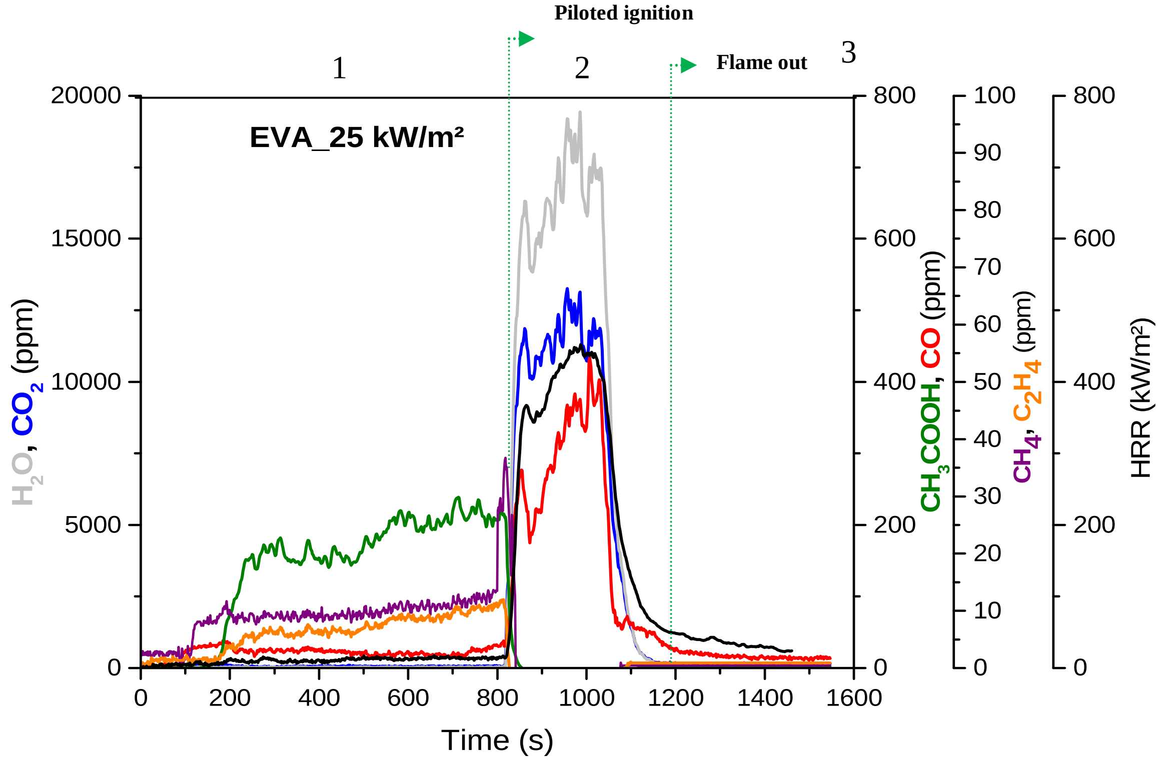

Figure 60. HRR and concentration of gases for EVA (MLC/FTIR - 25 kW/m²)

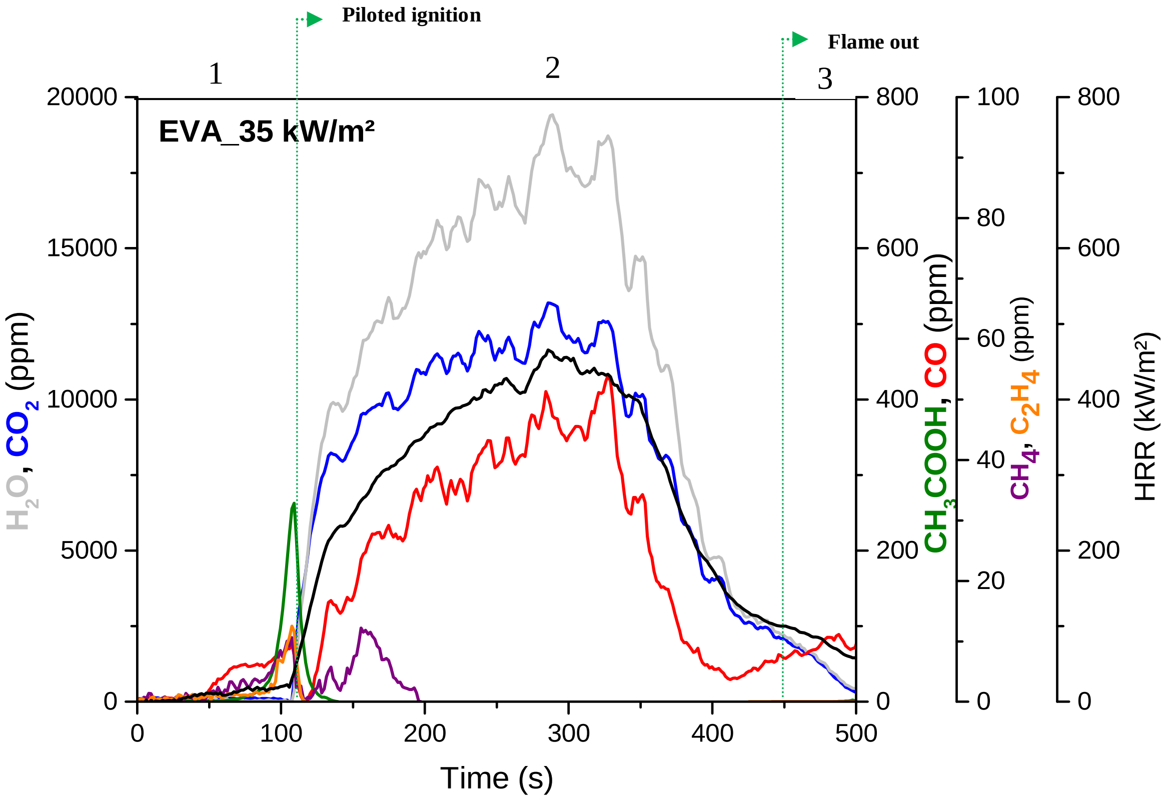

Figure 61. HRR and concentration of gases for EVA (MLC/FTIR - 35 kW/m²)

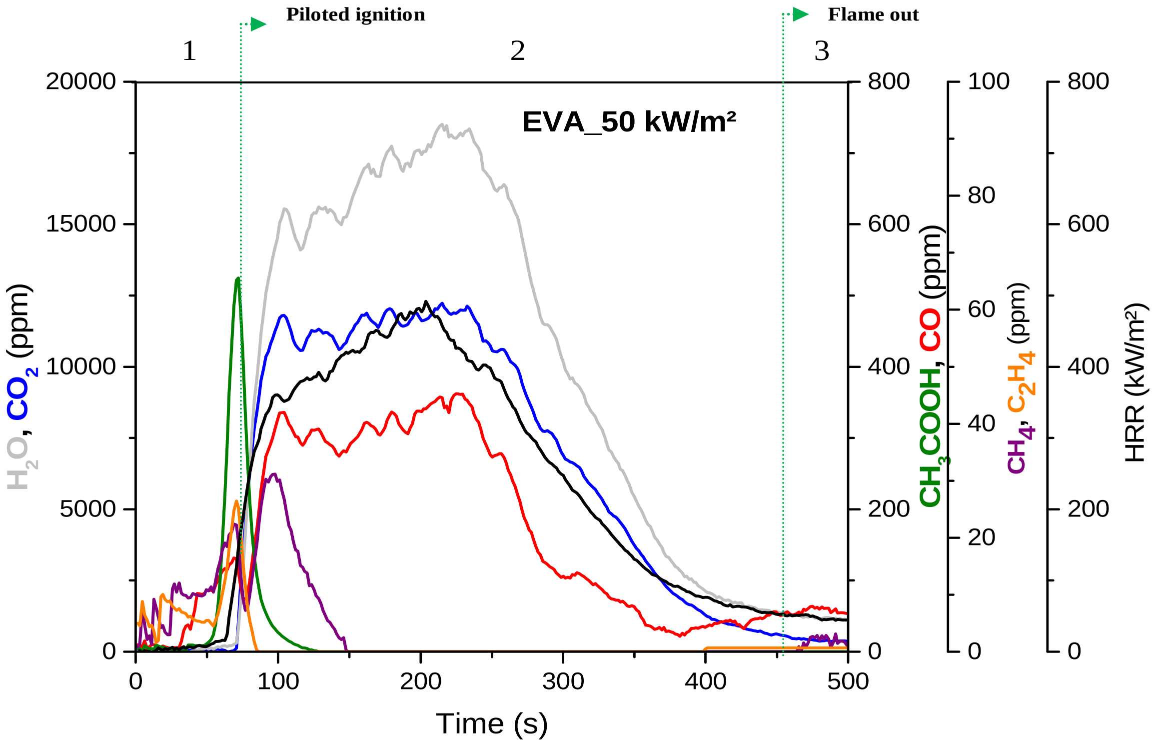

Figure 62. HRR and concentration of gases for EVA (MLC/FTIR - 50 kW/m²)

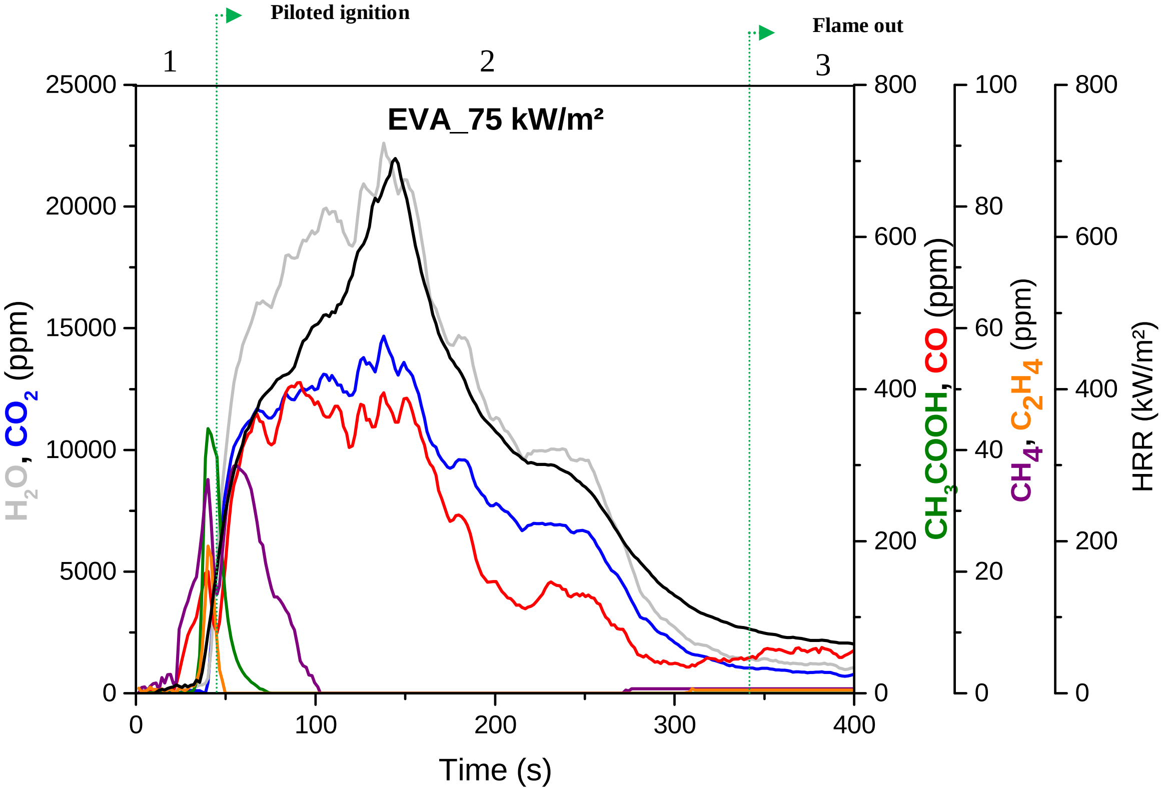

Figure 63. HRR and concentration of gases for EVA (MLC/FTIR - 75 kW/m²)

Table 7. Total gas concentration of EVA fires at 25, 35, 50, 75 kW/m²

Heat fluxes (kW/m²)	**25 kW/m²**	**35 kW/m²**	**50 kW/m²**	**75 kW/m²**
	CH_3COOH (ppm)			
Part 1	111856 (98 %)	2606 (64 %)	3662 (69 %)	3175 (70 %)
Part 2	528 (2 %)	1467 (36 %)	1511 (31 %)	1361 (30 %)
Total	113928	4073	4873	4536
	C_2H_4 (ppm)			
Part 1	5005 (97 %)	181 (94 %)	319 (90 %)	299 (92 %)
Part 2	144 (3 %)	49 (6 %)	36 (10 %)	26 (8 %)
Total	5149	230	355	325
	CH_4 (ppm)			
Part 1	7557 (93 %)	278 (40 %)	390 (43 %)	406 (42 %)
Part 2	594 (7 %)	416 (60 %)	518 (57 %)	561 (58 %)
Total	8151	694	908	967
	CO_2 (ppm)			
Part 1	54934 (2 %)	30105 (1 %)	28326 (1 %)	54785 (1 %)
Part 2	2692808 (98 %)	2980369 (99 %)	2804253 (99 %)	2344824 (99 %)
Total	2746743	3010474	2832579	2399610
	CO (ppm)			
Part 1	9126 (10 %)	3036 (4 %)	3738 (5 %)	2521 (4 %)
Part 2	82137 (90 %)	72869 (96 %)	71030 (95 %)	60515 (96 %)
Total	91263	75905	74768	63036
	H_2O (ppm)			
Part 1	30954 (1%)	41015 (1%)	40892 (1%)	35130 (1%)
Part 2	3064778 (99 %)	4060639 (99 %)	4048600 (99 %)	3478300 (99 %)
Total	3095732	4101654	4089492	3513430

With regard to the quantitative analysis of the gaseous phase for EVA at different heat flux levels (25, 35, 50 and 75 kW/m²), the following facts can be reported:

(i) Upon heating and prior to the ignition of EVA, the main gases detected in the smoke are CH_3COOH, CO, CH_4 and C_2H_4. CH_3COOH, which is produced from the deacetylation of the vinyl acetate group, as the highest concentrations and its peaks (238, 263, 280 and 348 ppm at 25, 35, 50 and 75 kW/m² respectively) increase as a function of the heat flux (Fig. 64). Moreover, the persistence of CH_3COOH in the smoke is noticeably longer as the heat flux is lower corresponding to the time of ignition (Fig. 64), with a conspicuous difference at 25 kW/m² as compared to 35, 50 and 75 kW/m².

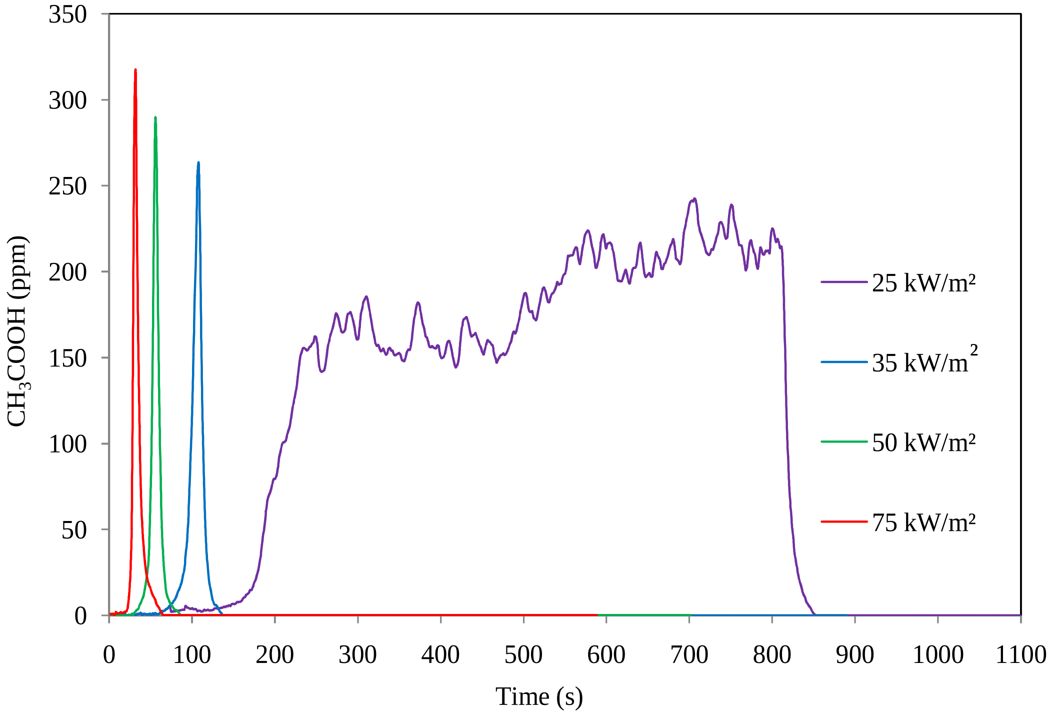

Figure 64. Heat flux effect on the peaks and duration of CH_3COOH release during EVA fire

(ii) During the combustion stage, the more concentrated gases in smoke are H_2O, CO_2 and CO; the maximum concentration levels of these gases are in line with the peaks in the HRR (Fig. 60 - 63). Moreover, no significant difference is observed in either the concentration or duration of CO_2, CO and H_2O release during the burning phase of EVA (Fig 60 - 63), mostly at 35 and 50 kW/m². It appears globally that the emission (duration and concentration) of CO_2, CO and H_2O is governed more by the flaming period than by the heat flux applied for the specific fire scenario. It is nonetheless noteworthy that the onset of the flaming period and the subsequent drop off in CO_2, CO and H_2O release occur sooner when the heat flux is increased. In summary, during the EVA combustion process, the level of heat flux has impact effect on the kinetics leading to the spontaneous increase of CO_2, CO and H_2O, without altering significantly the range of concentration or the release duration of these gases, as is clearly seen in Figures 60 - 63 and table 7.

A time quantification of the gas species during the EVA/ATH fires at 25, 35, 50 and 75 kW/m² was also conducted. The results are presented and discussed in the next section.

2.2 EVA/ATH at 25, 35, 50 and 75 kW/m²

The main gases identified are H_2O, CO_2, CO, CH_3COCH_3, CH_3COOH, CH_4 and C_2H_4. They are quantified in the smoke generated during the fires at 25, 35, 50 and 75 kW/m² (Fig. 65 - 68). As with EVA, the charts at figures 65 - 68 are divided into three main parts. The first part (1) consists of the period from the start of the test to the piloted ignition, the second (2) from ignition to flame out and the third (3) from flame out to 120 s after fire extinction, owing to the continued smoldering of EVA/ATH residue. The total concentrations of the gases released during each of these parts is also calculated for the fires at 25, 35, 50 and 75 kW/m² and all of the results listed in table 8.

During part 1 of the EVA/ATH thermal decomposition, there is significant release of H_2O (392495, 200474, 46630, 37578 ppm) and CO_2 (56158, 66087, 5895, 5732 ppm) at 25, 35, 50 and 75 kW/m² respectively. There is also a significant release, at 25 and 35 kW/m² respectively, of CO (26479, 16278 ppm), whereas the CO release during the fires at 50 and 75 kW/m² is rapid but slight: 4236 and 3613 ppm. In addition, competitive release of CH_3COCH_3 (1191, 631, 205, 110 ppm) against that of CH_3COOH (2700, 373, 224, 151 ppm) is observed at 25, 35, 50 and 75 kW/m² respectively. CH_4 and C_2H_4 are also present in concentration magnitudes of between 100 and 1000 ppm. CO_2 and HRR exhibit low values as compared to those subsequently measured during part (2).

Part 2 is characterized by an increase in HRR and increased concentrations of CO_2 (313553, 311553, 2829129, 2694068 ppm) and H_2O (507935, 588057, 4523139, 3644998 ppm) at 25, 35, 50 and 75 kW/m² respectively; while those of CH_3COOH, CH_4, C_2H_4 and CO drop rapidly at 25 and 35 kW/m². At 50 and 75 kW/m², there is on the contrary a recurrence of CO, CH_4 and C_2H_4 in the smoke (Fig.67 – 68). It is worthy of note moreover that CH_3COOH disappears entirely during all the heat flux tests whereas CH_3COCH_3 continues to be released proportionally to the heat flux increase (1395, 1623, 9415 and 9955 at 25, 35, 50 and 75 kW/m² respectively (cf. Fig. 65 - 68).

During the final stage (part 3), the concentrations of CO, CH_4 and C_2H_4 increase once more in the tests at 25 and 35 kW/m² (Fig 65-66) due to the smoldering of EVA/ATH residue, while at 50 and 75 kW/m², CO, CH_4 and C_2H_4 decrease eventually because of the lack of fuel (Fig 67 - 68).

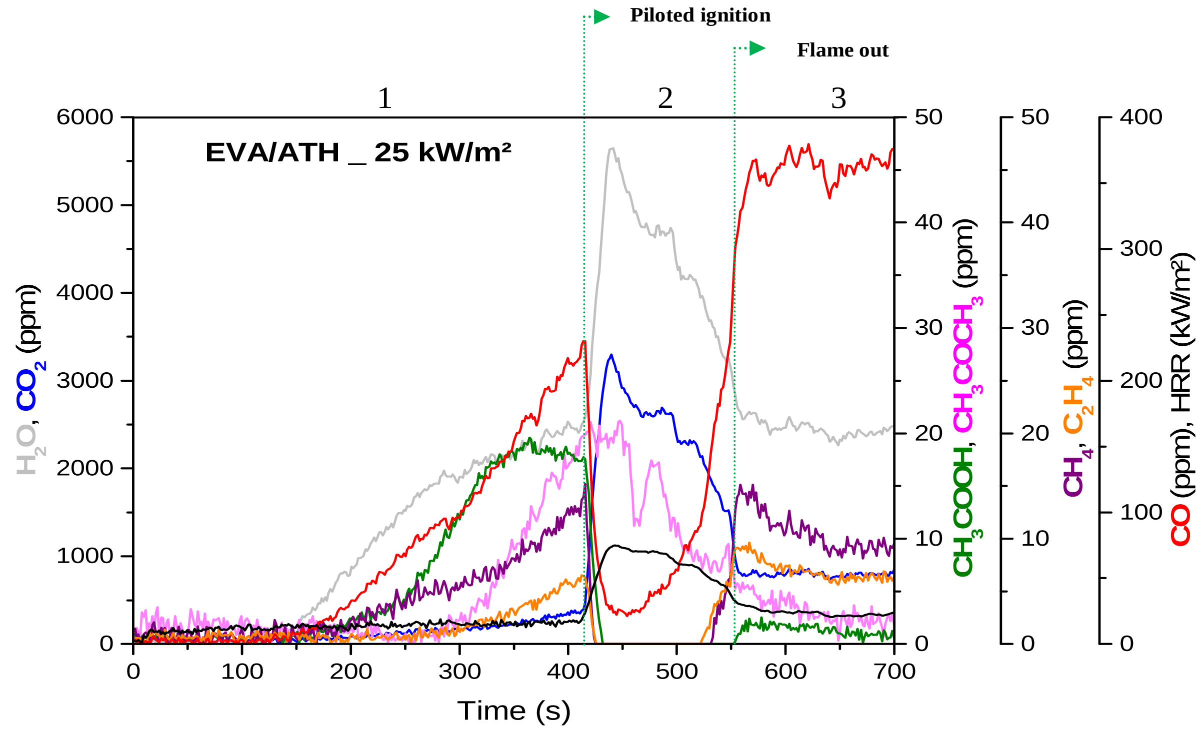

Figure 65. Gas quantitative analysis and HRR of EVA/ATH fire at 25 kW/m²

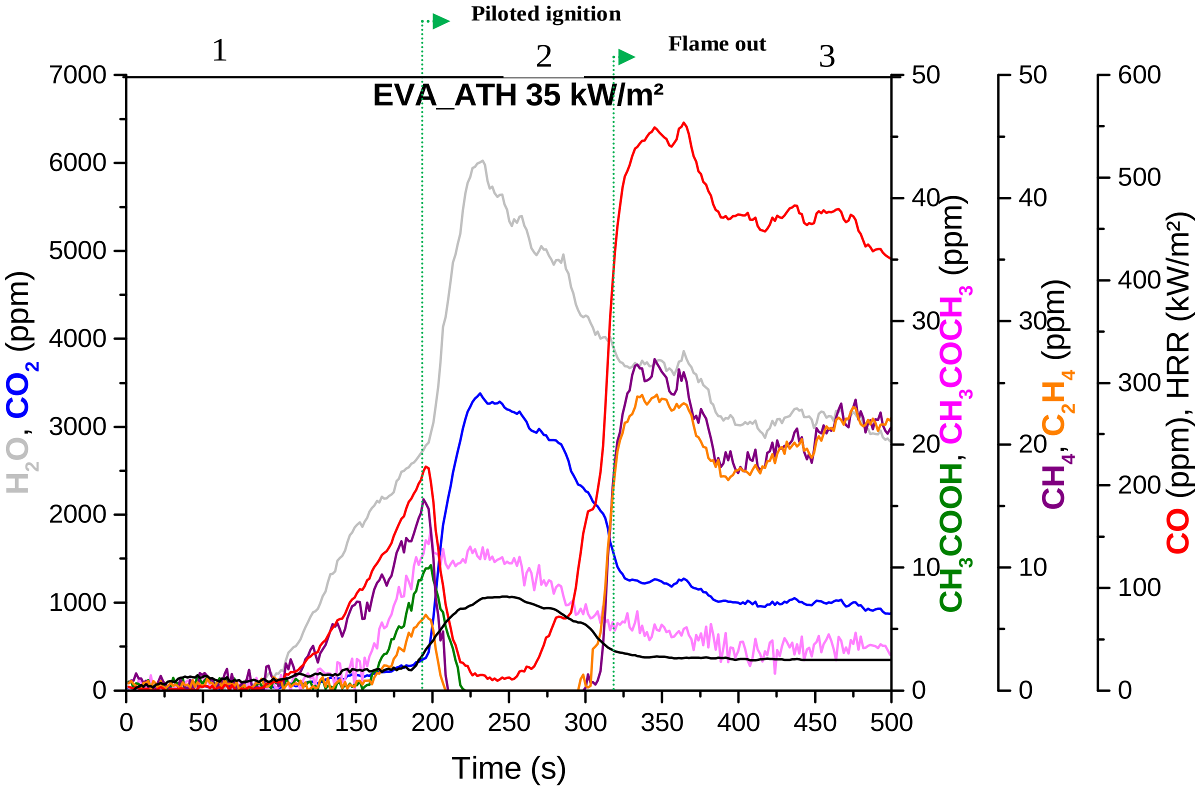

Figure 66. Gas quantitative analysis and HRR of EVA/ATH fire at 35 kW/m²

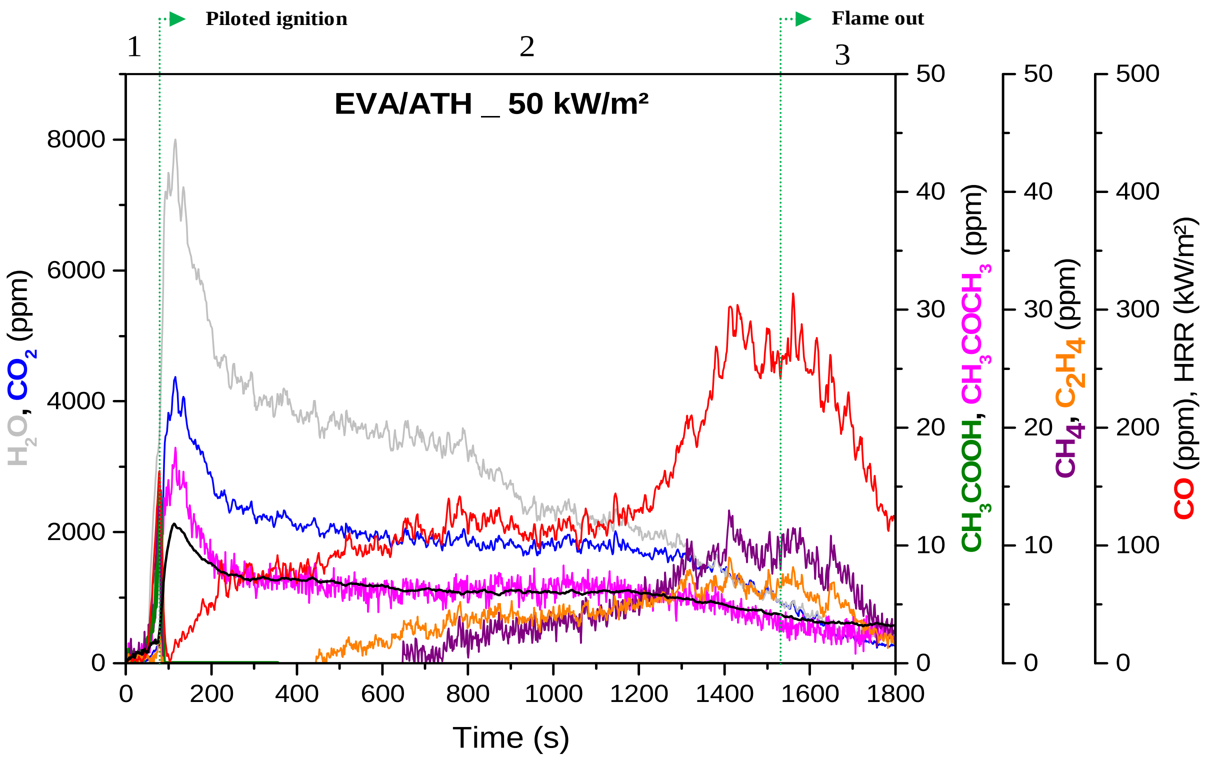

Figure 67. Gas quantitative analysis and HRR of EVA/ATH fire at 50 kW/m² (C_2H_4)

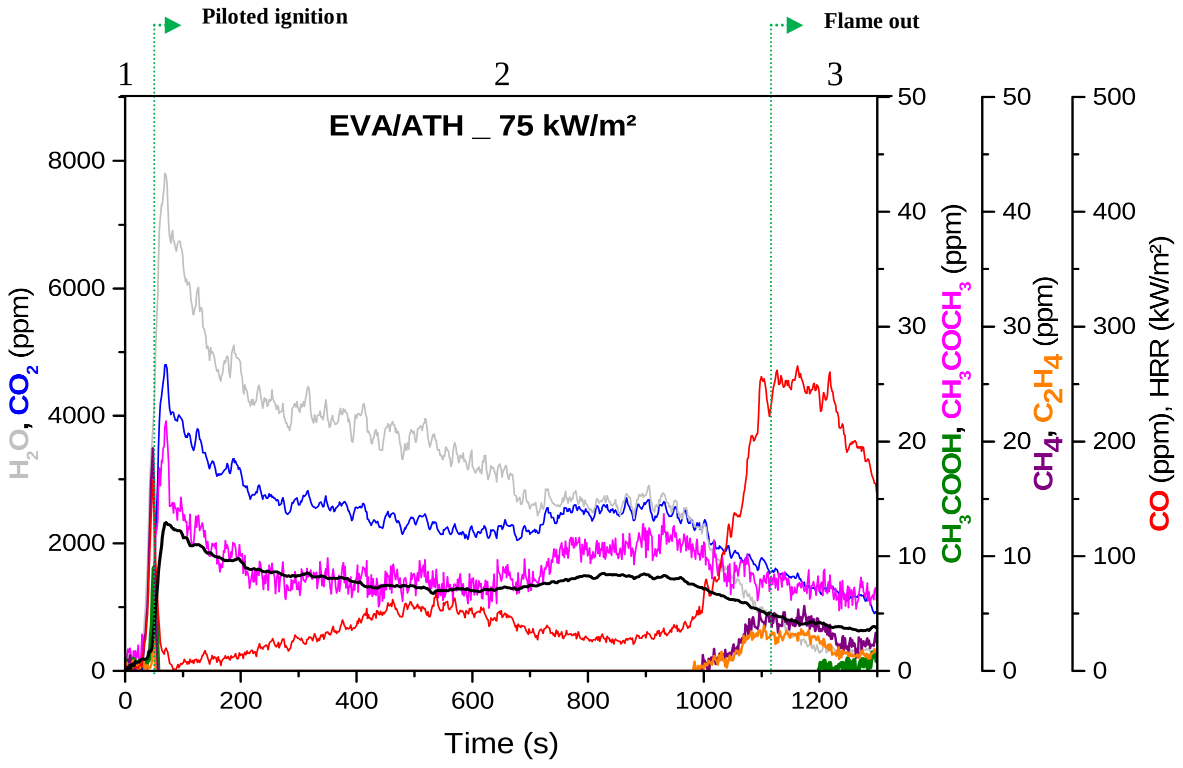

Figure 68. Gas quantitative analysis and HRR of EVA/ATH fire at 75 kW/m²

Table 8. Total gas concentration of EVA/ATH fires at 25, 35, 50, 75 kW/m^2

	25 kW/m^2	**35 kW/m^2**	**50 kW/m^2**	**75 kW/m^2**
	CH_3COOH (ppm)			
Part 1	2700 (90 %)	373 (93 %)	224 (91 %)	151 (94 %)
Part 2	-	-	-	-
Part 3	299 (10 %)	28 (7 %)	22 (9 %)	10 (6 %)
Total	2999	401	246	161
	CH_3COCH_3 (ppm)			
Part 1	1191 (41 %)	631 (21 %)	205 (2 %)	110 (1 %)
Part 2	1395 (48 %)	1623 (54 %)	9415 (92 %)	9955 (91 %)
Part 3	320 (11 %)	751 (25 %)	614 (6 %)	875 (8 %)
Total	2906	3005	10234	10940
	C_2H_4 (ppm)			
Part 1	845 (51 %)	352 (17 %)	212 (4 %)	193 (20 %)
Part 2	116 (7 %)	124 (6 %)	3924 (74 %)	376 (39 %)
Part 3	695 (42 %)	1595 (77 %)	1167 (22 %)	395 (41 %)
Total	1656	2072	5303	964
	CH_4 (ppm)			
Part 1	1672 (54 %)	730 (21 %)	229 (4 %)	190 (19 %)
Part 2	108 (3 %)	139 (4 %)	4341 (76 %)	360 (36 %)
Part 3	1319 (43 %)	2606 (75 %)	1142 (20 %)	450 (45 %)
Total	3099	3475	5712	1000
	CO_2 (ppm)			
Part 1	56158 (12 %)	66087 (14 %)	5895 (0.2 %)	5732 (0.2 %)
Part 2	313553 (67 %)	311553 (66 %)	2829129 (96 %)	2694068 (94 %)
Part 3	98278 (21 %)	94410 (20 %)	11986 (3.8 %)	166229 (5.8 %)
Total	467989	472050	2947010	2866030
	CO (ppm)			
Part 1	26479 (34 %)	16278 (20 %)	4236 (2 %)	3613 (2 %)
Part 2	10125 (13 %)	8953 (11 %)	175796 (83 %)	146314 (81 %)
Part 3	41273 (53 %)	56159 (69 %)	31770 (15 %)	30708 (17 %)
Total	77877	81390	211802	180635
	H_2O (ppm)			
Part 1	392495 (34 %)	200474 (15 %)	46630 (1%)	37578 (1 %)
Part 2	507935 (44 %)	588057 (44 %)	4523139 (97 %)	3644998 (97 %)
Part 3	253967 (22 %)	547962 (41%)	93261 (2 %)	75154 (2 %)
Total	1154397	1336493	4663030	3757730

Drawing on the results of this quantitative analysis of the gaseous phase of the EVA/ATH fires at four externally applied heat fluxes (25, 35, 50 and 75 kW/m^2), the key point to report are that:

(i) During the fire process of EVA/ATH, the highest concentration exhibited in the gas phase is that of H_2O (dehydration of ATH). It is present in the smoke in significant concentrations, not only during the combustion phase but also from the early stages of thermal decomposition for 25 and 35 kW/m^2 heat fluxes, which also concurs with the delayed times to ignition (451 and 179 s at 25 and 35 kW/m^2

against 75 and 43 s at 50 and 75 kW/m² respectively). In regard to the CO quantification at 25 and 35 kW/m², this gas is highly concentrated in the smoke prior to ignition and during the smoldering phase of EVA/ATH; however its concentration drops to a low level during the burning phase (Fig. 65 - 68). For 50 and 75 kW/m² almost all the CO is observed during the flaming process. This is notably to the contrary of the EVA case, where the concentrations of CO were very low before ignition but then more significant during the burning phase (Fig. 60 - 63 and Table 7). Furthermore, the concentrations of H_2O and CO_2 increase as a function of heat flux, with a significant difference between the levels measured during the fires at 25 - 35 kW/m² and at 50 –75 kW/m² (Table 8), the amount of degraded EVA/ATH being proportional to the heat flux. This was not observed in the case of neat EVA where the concentration peaks of CO_2, CO and H_2O were not particularly influenced by the applied heat flux.

(ii) The total disappearance of CH_3COOH and the persistence of CH_3COCH_3 during the flaming phase of EVA/ATH (Fig 65 - 68) are also worth reiterating. This result emphasizes that competitive release between CH_3COOH and CH_3COCH_3 favors the release of CH_3COCH_3 rather than CH_3COOH. It would seem that the increase in temperature promotes the catalytic effect of Al_2O_3 in the transformation of CH_3COOH to CH_3COCH_3. This may be ascribed to the fact that the activation energy (Ea) of CH_3COCH_3 release during thermal decomposition of EVA/ATH ($Ea = 3.45 \times 10^5$ J/mol) is higher than that of CH_3COOH release ($Ea = 1.69 \times 10^5$ J/mol).[151]

3 Gas species yields in the smoke of EVA and EVA/ATH fires at different heat fluxes

The proposed experimental bench test has the advantage of allowing simultaneous monitoring of evolved gas concentrations and mass loss rate during MLC tests. The yields of the different gases emitted in the smoke from the fire of a given material can therefore be calculated.

The yield Y_i of gas i by gram of mass loss of sample (g_i/g_{sample}) in the smoke of a fire of material can be calculated as the ratio of the mass flow rate of the gas species i (m_i) and the mass loss rate (MLR) of the sample subjected to thermal decomposition (Equation 13).

$$Y_i = m_i / MLR \qquad (12)$$

The mass flow rate (m_i) is determined by the product of the concentration of species i (X_i), the volumetric flow rate of the gas phase in the exhaust line (V_e) and the molar mass of the species (M_i); divided by its molar volume (V_i) as written in Equation 14.

$$m_i = X_i V_e M_i / V_m \qquad (13)$$

With

$$V_m = RT / P \qquad (14)$$

Where R is the universal constant of perfect gas (0.08206 L.atm/mol.K), T the temperature in Kelvin (K) and P the pressure of the gas mixture in the analysis system in (atm)

The yields of CH_3COOH, CO_2, CO, and H_2O in the EVA and EVA/ATH smoke during the fire tests at 25, 35, 50 and 75 kW/m² are shown and compared at Fig. 69 - 72. It is noteworthy that the yield of CH_3COOH at 25 kW/m² is 1.9 $g_{CH_3COOH}/g_{EVA,}$ whereas it is only 0.3, 0.2 and 0.1 g_{CH_3COOH}/g_{EVA} at 35, 50 and 75 kW/m² respectively (Fig 69). This result confirms that the quantity of CH_3COOH (detected in the smoke at low heat flux (25 kW/m²)) is significantly reduced as thermal stress increases (35, 50 and 75 kW/m²). It also illustrates that the potential hazardous effect of CH_3COOH (irritation, burns, etc.) as a fire effluent of EVA are higher when the heat flux is low (25 kW/m² vs 35, 50 and 75 kW/m²).

For EVA/ATH, the CH_3COOH yield is very low (around 10^{-2} $g_{CH_3COOH}/g_{EVA/ATH}$), whatever the heat flux (Fig. 69). This is consistent with a low proportion of EVA in the EVA/ATH formulation and the transformation of CH_3COOH to $CH_3COCH_{3,}$ as previously reported.

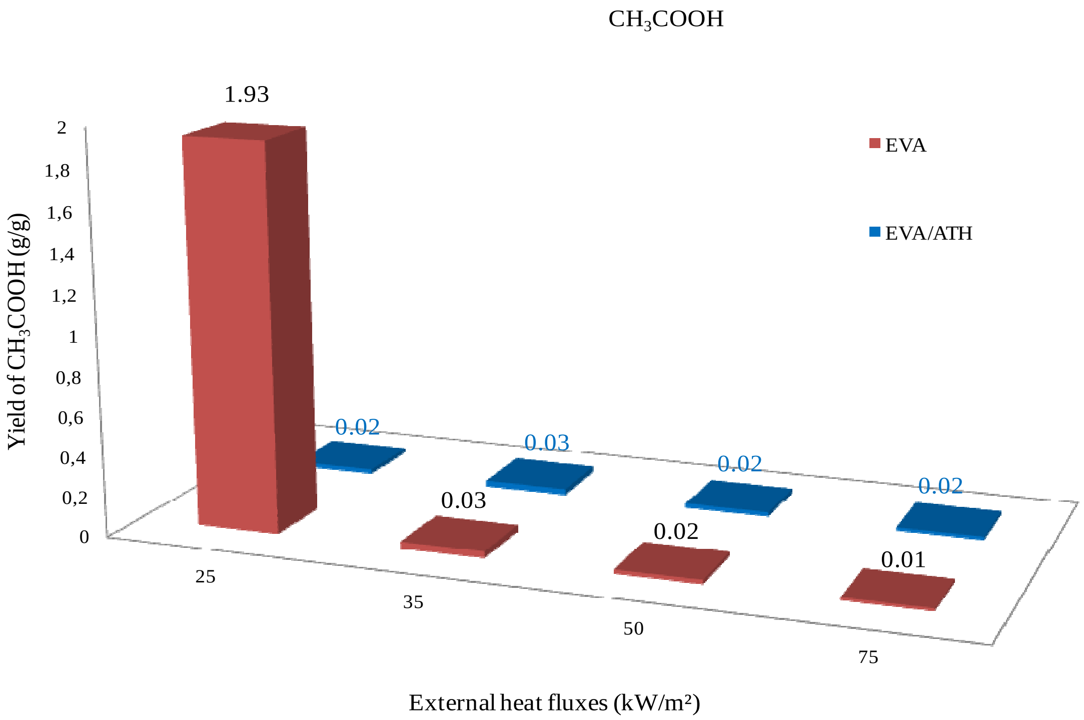

Figure 69. Yields of CH_3COOH in EVA and EVA/ATH smoke

(MLC/FTIR - 25, 35, 50, 75 kW/m²)

The CO_2 yield of EVA is calculated at approximately 2.7 g_{CO_2}/g_{EVA} at 25 kW/m² and around 6.5 g_{CO_2}/g_{EVA} at 35, 50 and 75 kW/m² (Fig. 70). The yield of CO_2 in the smoke per gram of degraded EVA is therefore considerably lower at 25 kW/m² than at 35, 50 and 75 kW/m² where the calculated yields are quite similar. The lowest value of CO_2 yield, at a heat flux of 25 kW/m², can be attributed to the formation of carbonaceous char hindering a complete combustion reaction. On the other hand, at 35, 50 and 75 kW/m², there is no char formation and complete combustion of the molten EVA or a pool fire is observed.

For EVA/ATH, the yield of CO_2 increases with the heat flux (Fig. 70) with values of 2.30, 2.65, 5.13, and 5.55 $g_{CO_2}/g_{EVA/ATH}$ calculated for heat fluxes of 25, 35, 50 and 75 kW/m² respectively. The higher CO_2 yields of EVA for EVA/ATH can be explained by the fact that the proportion of hydrocarbons is lower in the EVA/ATH formulation than in pure EVA.

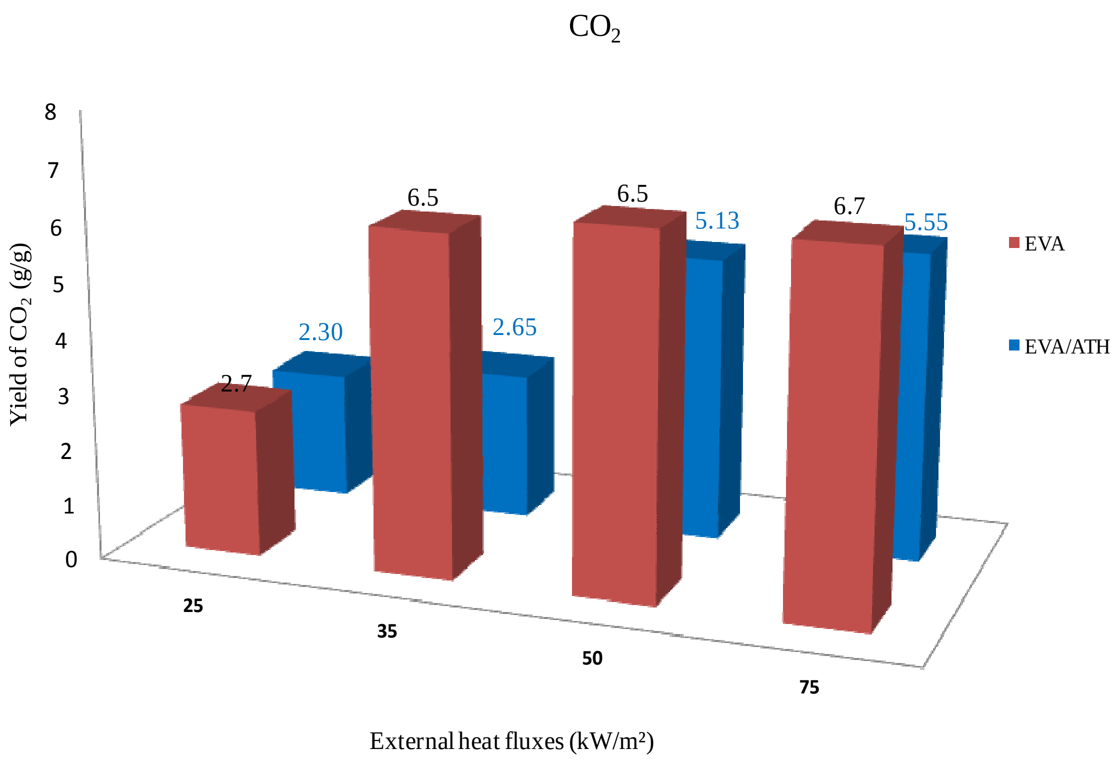

Figure 70. Yields of CO_2 in EVA and EVA/ATH smoke (MLC/FTIR - 25, 35, 50, 75 kW/m²)

Concerning CO yields in EVA and EVA/ATH, the calculated values are in the order of 10^{-1} g_{CO}/g_{sample} (Fig. 71). For EVA they are 0.36, 0.18, 0.15 and 0.14 g_{CO}/g_{EVA}, with yields decreasing as the heat flux increases. In the EVA/ATH case, the yields are 0.12, 0.29 0.65 and 0.72 $g_{CO}/g_{EVA/ATH,}$ the increasing values corresponding to heat flux increases. These results indicate higher CO yields for EVA/ATH than for EVA, with the exception of the fire tests conducted at a heat flux of 25 kW/m². It would therefore appear that both the addition of ATH in EVA and the level of the heat flux play a role in augmenting CO yields during the thermal decomposition of EVA/ATH. This may be ascribed to the fact that the highest concentrations of CO in the EVA/ATH smoke are detected, for the most part, before ignition and during smouldering of the EVA/ATH residue (Fig 65 - 68), when the MLR is low, in which case the ratio of mass flow rate of CO over the MLR naturally leads to relatively high values.

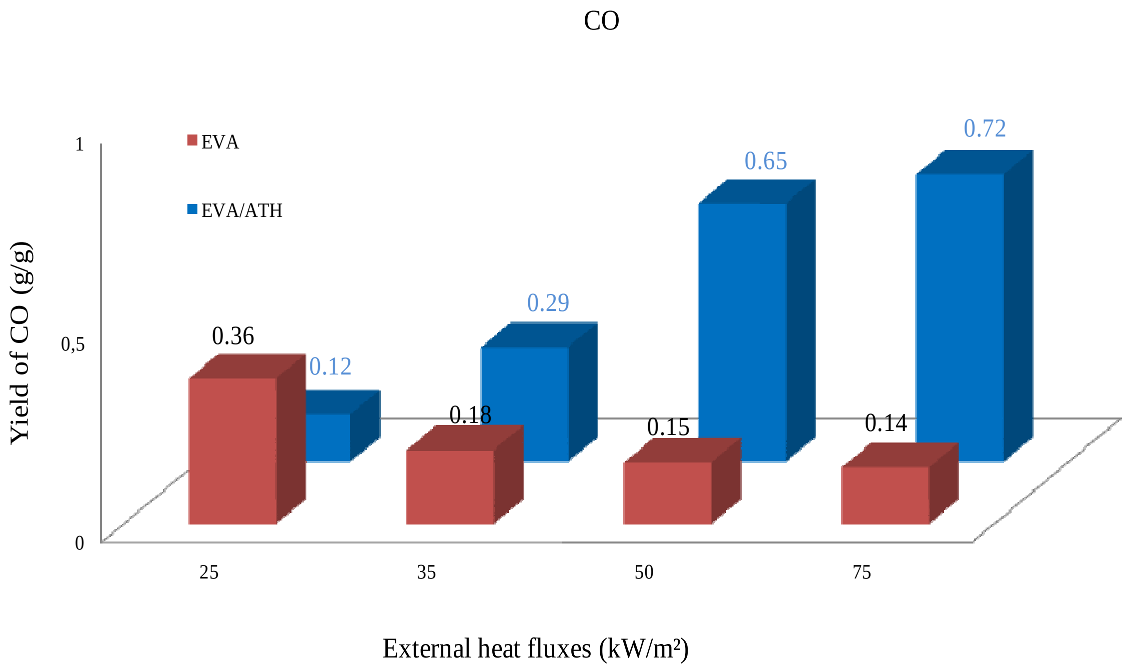

Figure 71. Yields of CO in EVA and EVA/ATH smoke (MLC/FTIR 25, 35, 50 75 kW/m²)

The yields of H_2O resulting from the EVA and EVA/ATH fires at 25, 35, 50 and 75 kW/m² are plotted at Fig. 72. Except for the test at 25 kW/m², i yield of H_2O in the EVA/ATH fire smoke are noticeably higher than those of neat EVA. This can be explained by the endothermic dehydration of ATH in the EVA/ATH material, which releases significant amounts of water.

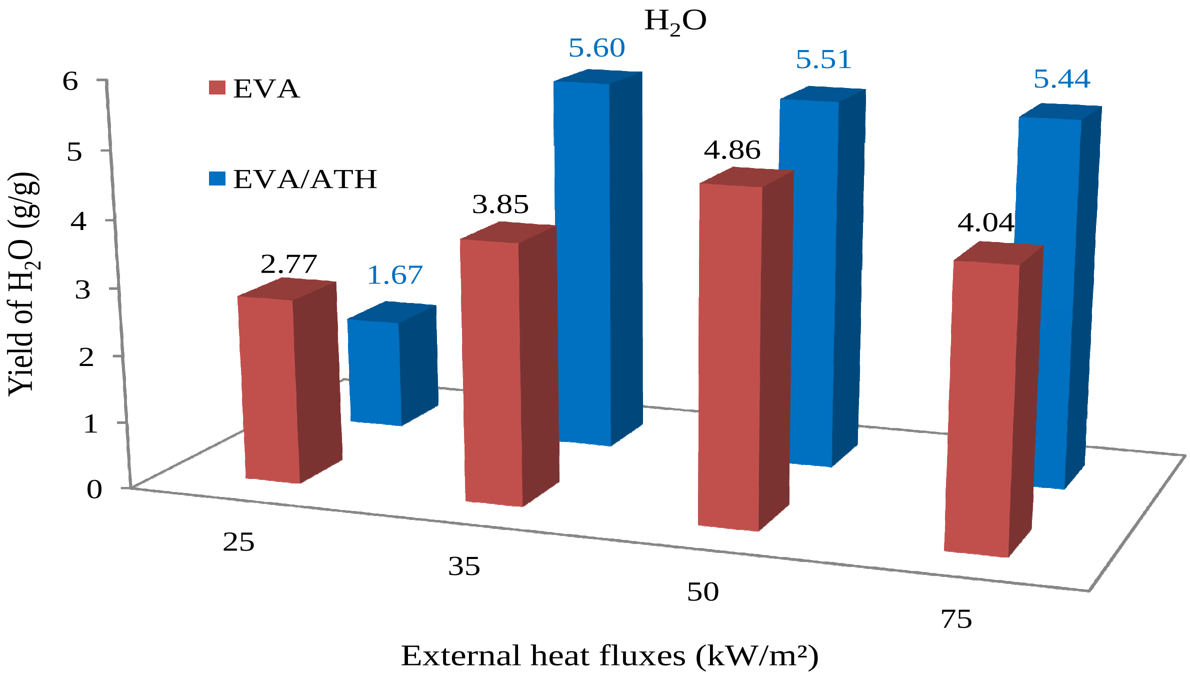

Figure 72. Yields of H_2O in EVA and EVA/ATH smoke (MLC/FTIR - 25, 35, 50, 75 kW/m²)

4 Effect of heat flux on the particles in the smoke from the EVA and EVA/ATH fires

Besides investigation of the gas phase of EVA and EVA/ATH fire, the size distribution and concentration of particles out of the flame were also examined in relation to different heat fluxes to assess whether thermal aggression (heat stress) and/or the addition of ATH have a significant impact on the data obtained from particles analyses.

Comparisons of the size distribution and number of particles per cm^3 in the smoke generated by fires of EVA and EVA/ATH at 25, 35, 50 and 75 kW/m² is provided in Fig.73 - 76. The main observation drawn for both materials (EVA and EVA/ATH) is that the highest concentrations in number per cm^3 are of ultrafine, followed by fine particles, this being the same for all of the heat flux tests. These results confirm that the size range of particles in the fire smoke of these two materials is essentially dominated by particles $\leq$ 1µm. During the dynamic process of fire combustion, particles are oxidized by O_2 and OH• radicals. O_2 can provoke particle oxidation, causing the break-up of particles, while OH• diffusing at the particles’ surface can break-down particle aggregates and hence reduce particle size. Moreover, varying the applied heat flux has no significant effect on the particle size range in the smoke, which remains predominantly comprised of submicron particles during all EVA and EVA/ATH fire tests.

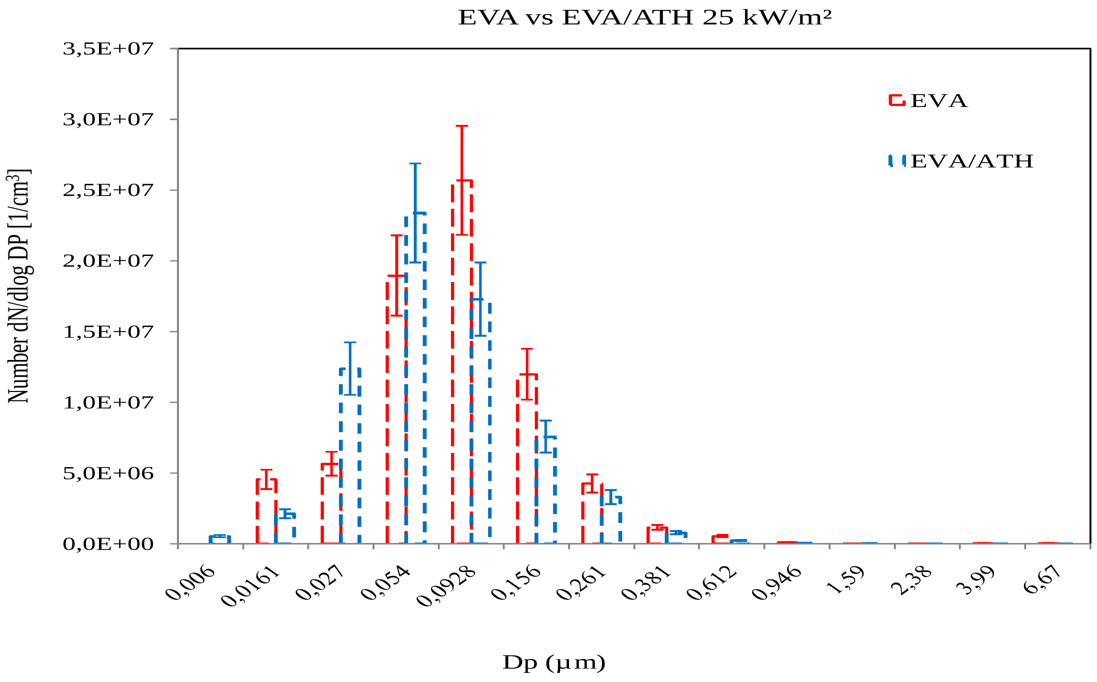

Figure73. Particle size distribution and number for EVA and EVA/ATH (MLC/ELPI - 25 kW/m²)

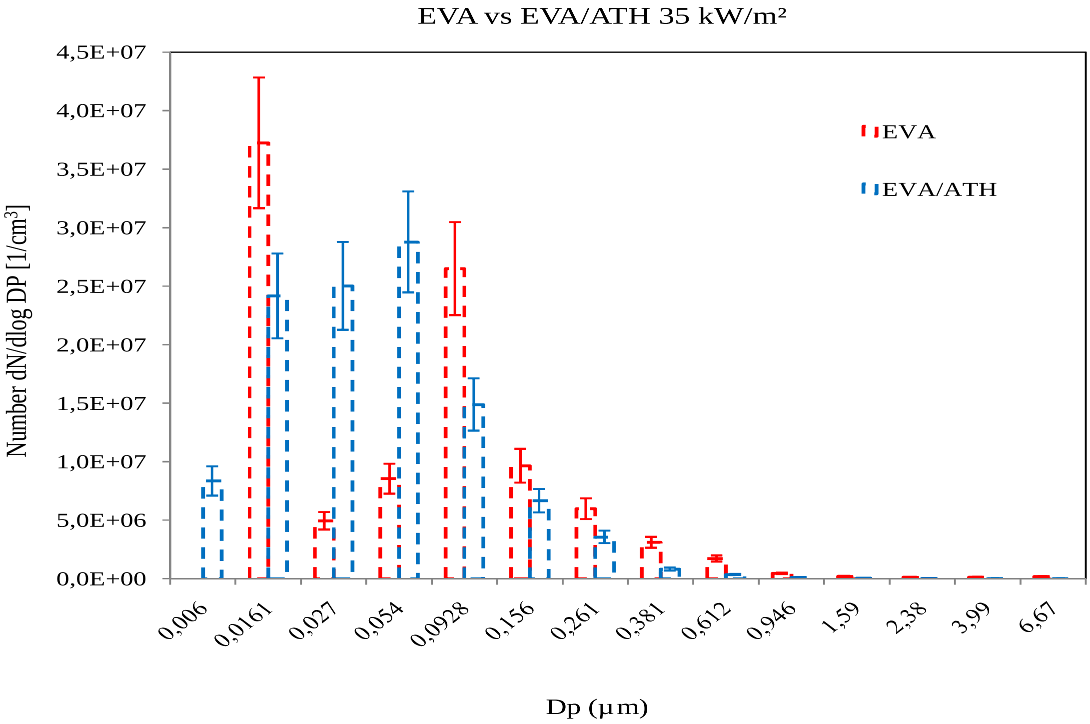

Figure 74. Particle size distribution and number for EVA and EVA/ATH (MLC/ELPI - 35 kW/m²)

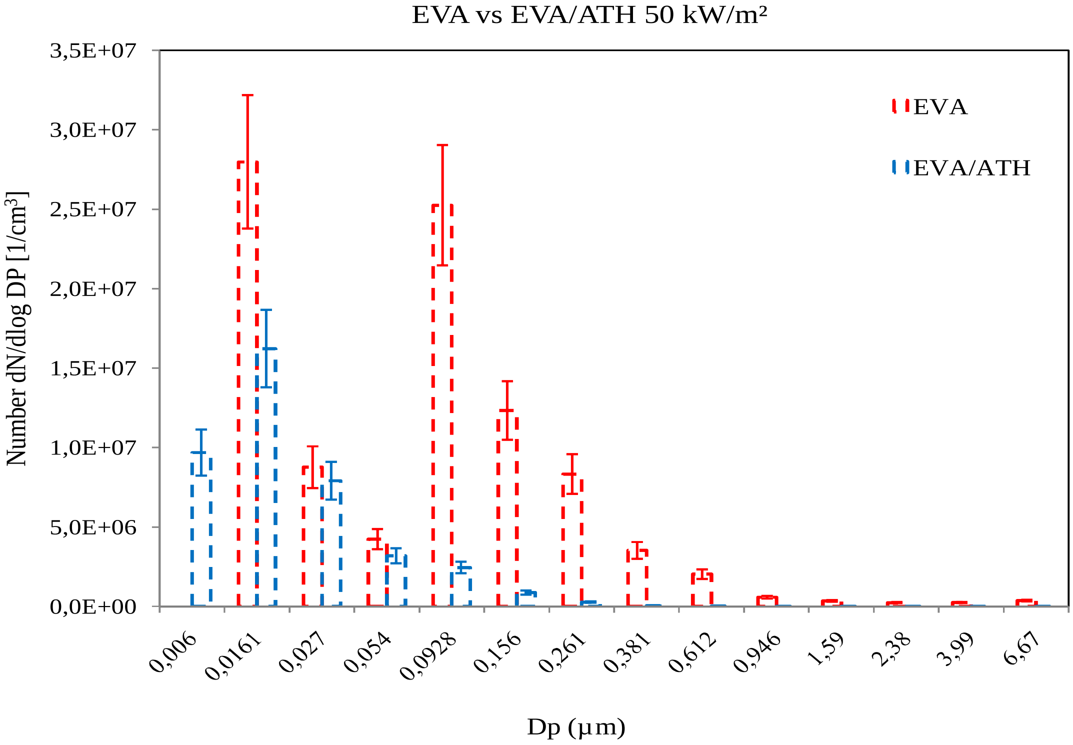

Figure 75. Particle size distribution and number for EVA and EVA/ATH

(MLC/ELPI - 50 kW/m²)

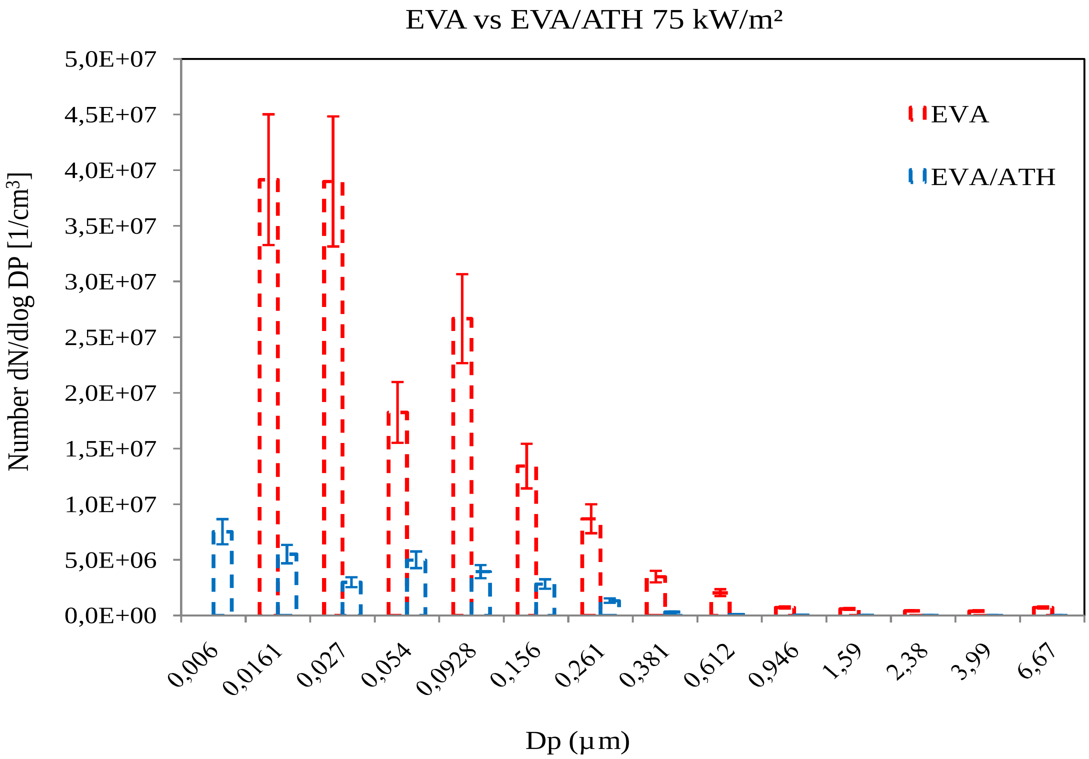

Figure 76. Particle size distribution and number for EVA and EVA/ATH (MLC/ELPI - 75 kW/m²)

Not with standing, analysis of the results on particles ≤ 1 µm at 25 and 35 kW/m² leads to the observation that the concentration of particles ≤ 54 nm is higher in the EVA/ATH smoke than in that of EVA (the exception being for particles of 16 nm). For particles ≥ 93 nm, the concentrations detected in the EVA smoke are higher than those of EVA/ATH (Fig 73 and 74).On the other hand, at 50 and 75 kW/m², the number of particles is observed to be higher in the EVA case than for EVA/ATH for all particles sizes from 16 nm and above (Fig 75 and 76). Finally, a noticeable difference between the two materials is the emission of particles of 6 nm as can be clearly observed in all four heat flux tests (at 25, 35, 50 and 75 kW/m²) these particles are only emitted in the EVA/ATH case and never for EVA. This indicates that ATH is the emission source of these nanometric-size particles results.

5 Conclusion

The focus of this chapter has been on the study into the effects of heat flux on the fire behaviour characterization of EVA and EVA/ATH using the combination of MLC/FTIR/ELPI. The first highlight was the utility of the simultaneous Gram Schmidt and mass loss rate results from the MLC/FTIR bench to investigate the fire behaviour of materials. Empirical evidence of the delay in piloted ignition of neat EVA in comparison to EVA/ATH at 25 kW/m² was provided for the first time. This delay is imputed to the formation of char on the EVA surface, protecting the material and decreasing the MLR. The flammability parameters including THR, CHF and EHC were calculated at different heat fluxes for EVA and EVA/ATH. The emphasis of these results is that the different heat fluxes have no impact on the THR of EVA, which remains constant because the material is totally consumed after the flaming phase of combustion. For the EVA/ATH formulation, THR increases with the heat flux; moreover, the addition of ATH in the EVA formulation leads to lower values of THR, and EHC. The latter is ascribed to the endothermic dehydration of ATH and the formation of a ceramic layer of Al_2O_3 in condensed phase. During the third stage of the study, concerning the effects of heat flux on the quantitative analysis of evolved gases, the persistence of CH_3COOH in the smoke generated by the EVA fire was shown to be more significant at 25 kW/m² than at 35, 50 and 75 kW/m², this being due to the kinetics of the VA deacetylation. However, in respect of the quantification of CO_2, H_2O and CO released during combustion of neat EVA, it was remarkable that the concentration of these gases and the duration over which they were generated were not greatly affected by the variation of the external heat flux. The release of CO_2, H_2O and CO would appear to be essentially governed by the flaming phase. For EVA/ATH, a noteworthy result was that the concentrations of H_2O and CO_2 augment with the applied heat flux, the amount of material degraded being proportional to the external heat flux. In addition, H_2O is present in significant quantity in the smoke, not only during the flaming phase, but also from the early stage of thermal decomposition of EVA/ATH. Quantitative analysis of the gaseous phase has moreover shown a shift from CH_3COOH to CH_3COCH_3 evolution for EVA/ATH, which is attributed to the catalytic effect of Al_2O_3 promoting the formation of acetone.

In relation to the gas species yields, the results from the EVA fire tests have confirmed that the quantity of CH_3COOH in the smoke is greater when EVA is degraded at lower (25 kW/m²) rather than higher heat flux (35, 50 and 75 kW/m²). In the case of CO, the results revealed that EVA/ATH yields higher quantities than neat EVA. Moreover, the highest concentrations of CO released by the EVA/ATH sample were generated before ignition and during the smouldering phase, while for the neat EVA, CO concentrations were, on the contrary, very low before ignition and more significant during the combustion phase. Finally, analysis of the size distribution and concentration of particles in the smoke revealed that particles ≤ 1 µm exhibit the highest concentration in all four applied heat flux test cases for the EVA and EVA/ATH reference materials. Nonetheless, the more ultrafine particles (those of 6 nm) were solely detected in the EVA/ATH smoke.

This investigation highlights the advantages of combining the MLC/FTIR/ELPI techniques to characterize how a material would behave in a thermal stress situation. For EDF R&D, the current objective is to evaluate the fire hazards of electrical cables intended for use in its facilities by extending the knowledge of their flammability parameters, evolved gases and particles emitted in the smoke generated by a fire of cable material. To obtain additional input data, electrical cables should be evaluated with the developed MLC/FTIR/ELPI bench. This will be dealt with in the next chapter.

CHAPTER 5: MLC/FTIR/ELPI APPLIED TO THE CASE OF A HALOGEN FREE FLAME RETARDANT ELECTRICAL CABLE

The MLC/FTIR/ELPI combination is proposed for use in the characterization of electrical cables, since the latter represent almost 80% of potential combustible fuel in EDF NPP localization compartments. A Halogen Free Flame Retardant electrical cable (hereafter referred to as HFFR cable) intended for use in new generation EDF NPPs is therefore tested in the MLC/FTIR/ELPI. Background material and a discussion of the test and the results obtained are presented in this chapter.

1 Halogen Free Flame Retardant electrical cable

HFFR electrical cable is mainly comprised of an outer and internal sheath, three insulators and metallic conductors (Fig 77). Details of the physical and chemical characteristics of each of the HFFR cable component parts are provided in Table 9, bearing in mind that the strict formulation of electrical cable coverings and insulators is kept confidential. The raw materials data reported in Table 9 are taken from the literature.[152]

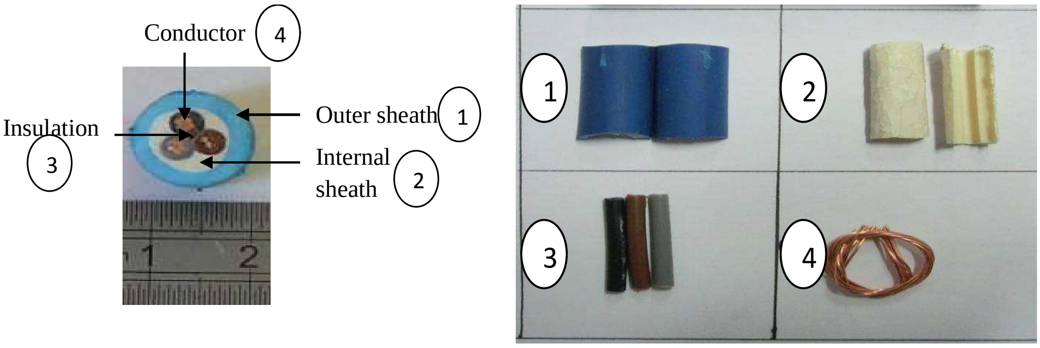

Figure 77. Architecture of the halogen free low voltage electrical cable

Table 9. Characteristics of the halogen free low voltage electrical cable

HFFR cable	% masse	compounds	density (kg/m^3)	thickness (mm)
Outer sheath	42	EVA, ATH, ε	1788	10
Intern sheath	26	EVA, ATH, ε		
insulation	10	EVA and or PE		
conductors	22	Copper		

With ε : cross-linked poly-acrylic acid or anionic acrylic polymer and PE: polyethylene
To obtain more information about the HFFR cable, thermo-gravimetric analyses of the outer and internal sheaths as well as the insulators were performed (TGA 10 °C/min under air). The results reveal that each component of HFFR cable has its own unique formulation, demonstrated by their distinctive TGA profiles all obtained under the same conditions (Fig 78). The internal sheath is slightly more refractory than the outer (respective residues of 45 and 41% at 800 °C), while the insulators exhibit a residue of 5% at identical temperature. Based on the residue, it would appear that the internal sheath contains more ATH or other synergistic components than the outer sheath and that the insulators do not contain flame retardants. The latter is consistent with the fact that HFFR cable insulators should not contain ATH because this mineral filler is a conductor of electricity and could therefore disturb the basic function of the electrical cable. Note that the main objective of the present analysis was to underline the heterogeneity of the HFFR cable, highlighting the importance of analyzing entire sections of this material to obtain a more precise characterization of its parameters in a fire scenario.

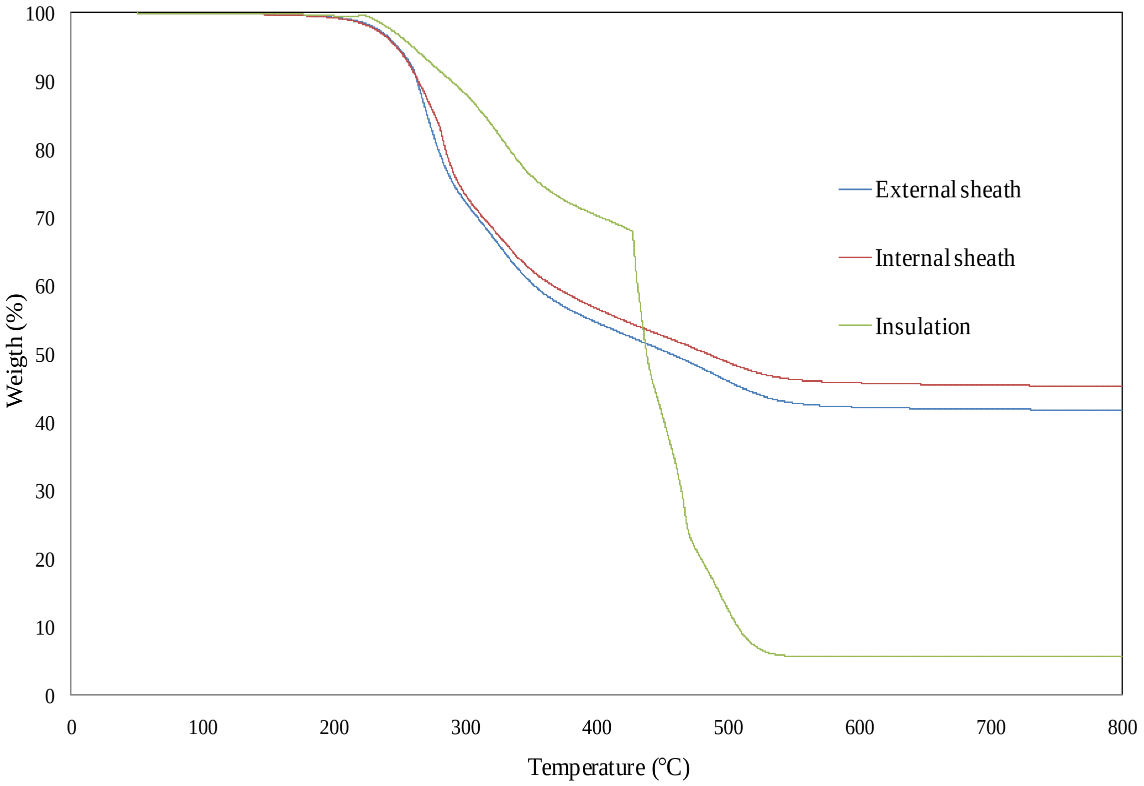

Figure 78. Thermo-gravimetric analysis of HFFR cable layers (10 °C/min under air)

2 Characterization of HFFR cable fire behaviour with MLC/FTIR/ELPI

The fire behavior characterization of HFFR cable using the coupled MLC/FTIR/ELPI technique follow the same three-step approach described in the preceding chapters 3 and 4:

(i) Determination of flammability parameters (HRR, t_{ig}, THR, CHF, EHC)
(ii) Analysis of evolved gases (qualitative and quantitative)
(iii) Analysis of smoke particles (size distribution and concentration).

Eight samples of 9.8 cm long HFFR cable (Fig. 79) with a mass of almost 132 ± 3 g are tested under experimental fire simulation at heat fluxes of 25, 35, 50 and 75 kW/m². The results are discussed in the next few sections.

Figure 79. Sampling of HFFR electrical cable before the MLC/FTIR/ELPI fire test

2.1 Evaluation of the Halogen Free Flame Retardant cable flammability parameters

HRR, t_{ig} and flame out of an HFFR cable during fire tests at 25, 35, 50 and 75 kW/m² are presented at Fig. 80. For each heat flux, there is a shoulder in the HRR close to ignition, followed by stabilization throughout the flaming process and then finally a second peak before the HRR decreases. The t_{ig} increases as a function of the heat flux whereas pHRR is seen to remain within a narrow range, at around 120 ± 10 kW/m², in tests performed at 25, 35, 50 and 75 kW/m². t_{ig} aside, it can be concluded that the pHRR of HFFR cable is not significantly affected by external heat flux; however the duration of the fire phenomenon, from t_{ig} to flame out, decreases as heat flux increases: 46, 40, 34, and 28 min at 25, 35, 50, and 75 kW/m² respectively.

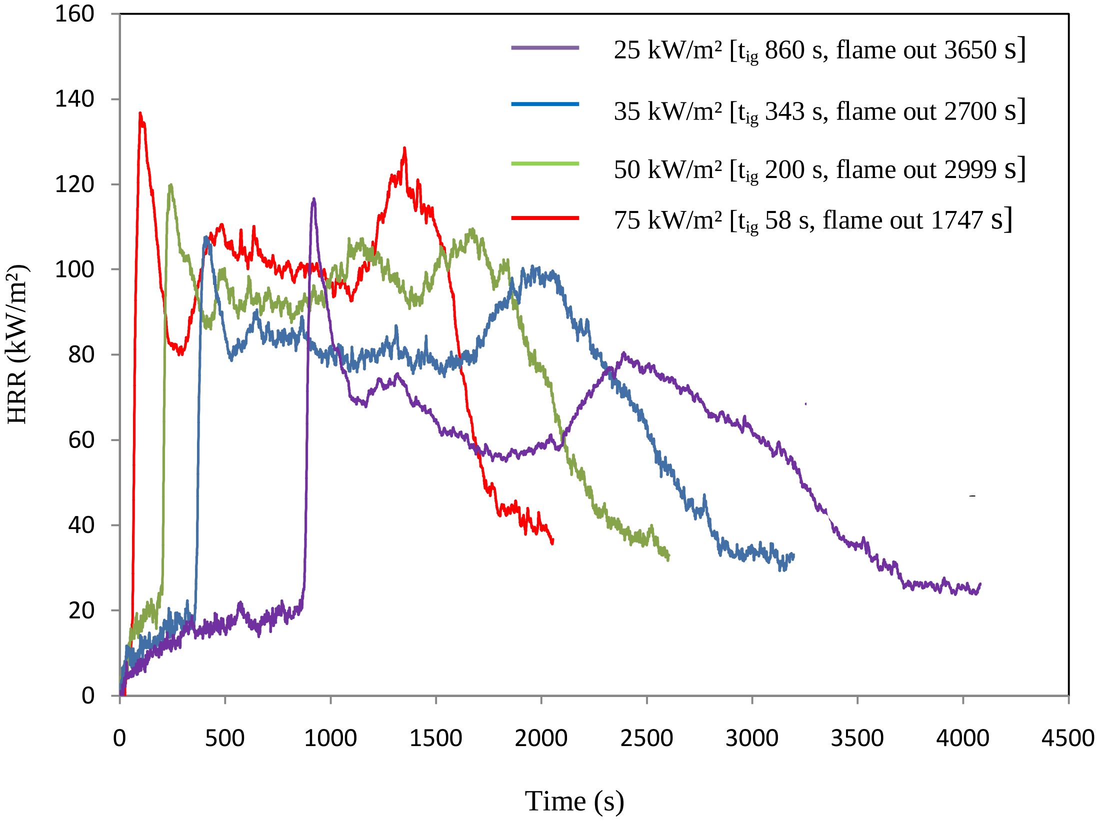

Figure 80. HRRs of HFFR cable (MLC - 25, 35, 50, 75 kW/m²)

The THR values of the HFFR cable at 25, 35, 50 and 75 kW/m² are shown at Fig. 81. It is noteworthy that the THR (126 ± 2 MJ/m²) does not alter as a function of heat flux variation. This is consistent with the fact that the measured total mass loss values of the HFFR cable during tests at 25, 35, 50 and 75 kW/m² are similar (Fig 82). This was notably not the case with EVA/ATH where, on the contrary, both the amount of material degraded and the THR were observed to increase as the heat flux was increased. The HFFR cable residues after tests at 25, 35, 50 and 75 kW/m² are illustrated in Fig. 83. The main difference observed is in the cohesion of the cable residues.

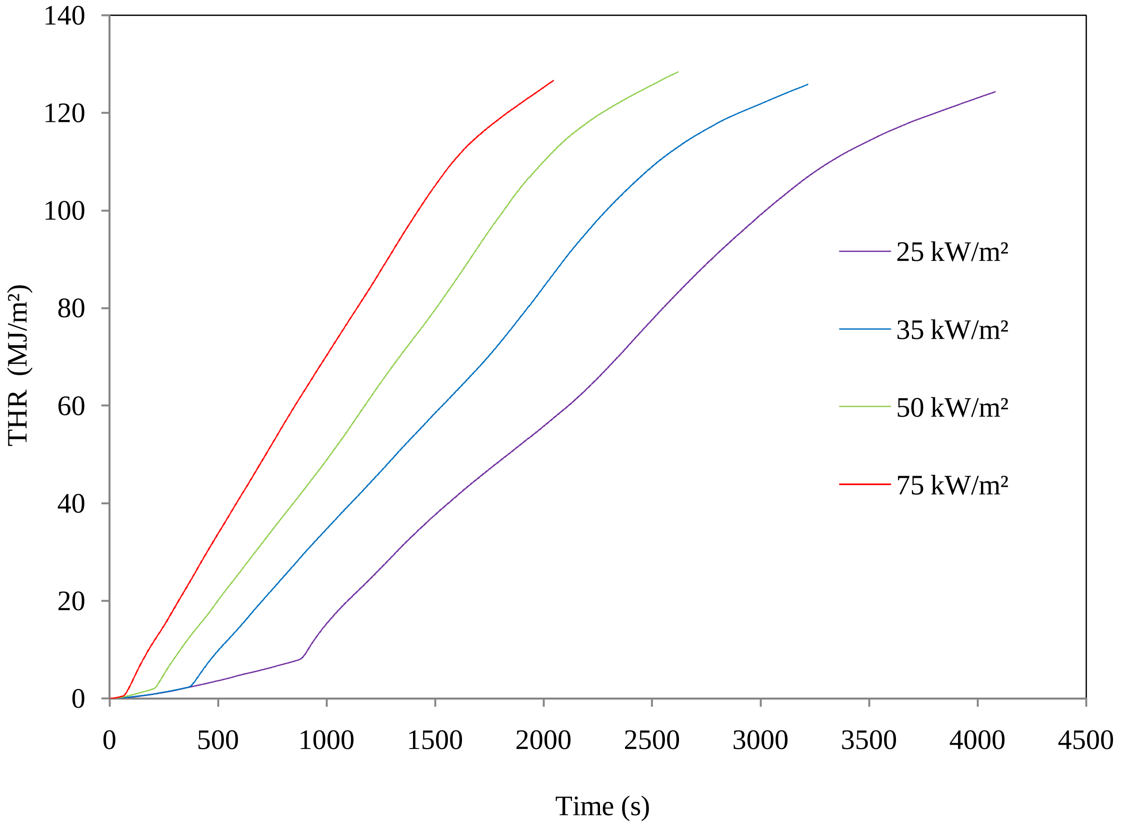

Figure 81. Total heat release of HFFR cable (MLC/FTIR/ELPI - 25, 35, 50, 75 kW/m²)

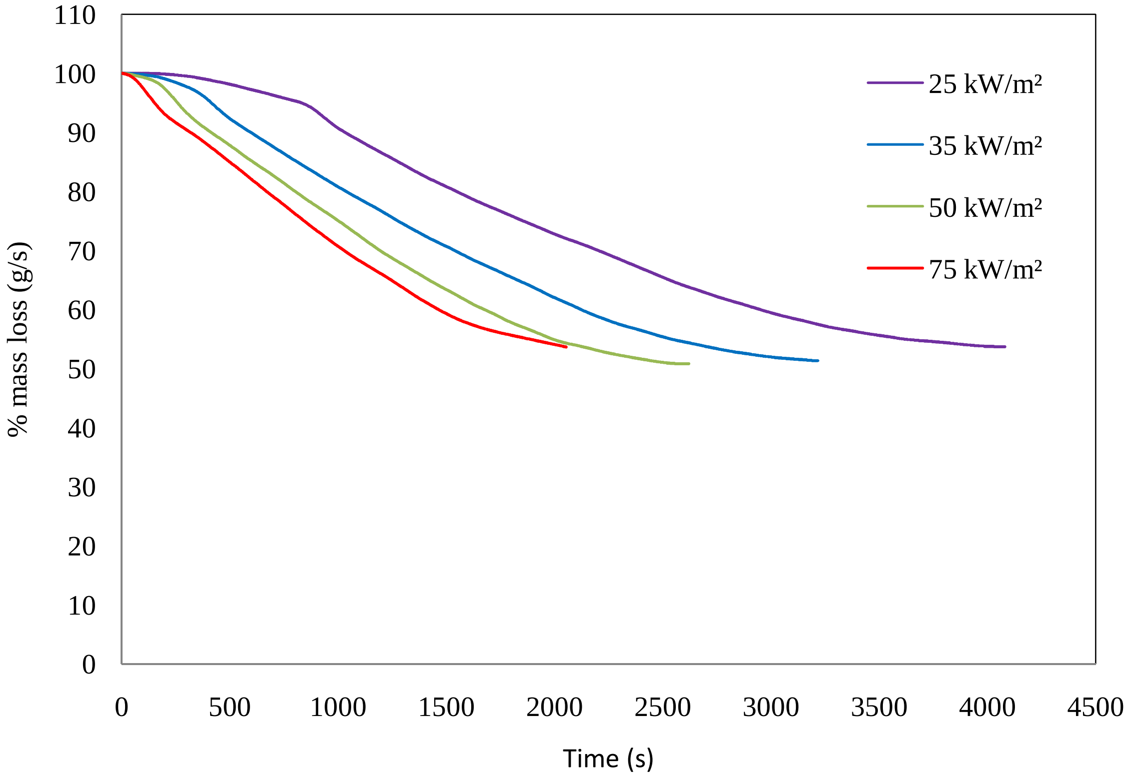

Figure 82. Mass loss of HFFR cable (MLC/FTIR/ELPI - 25, 35, 50, 75 kW/m²)

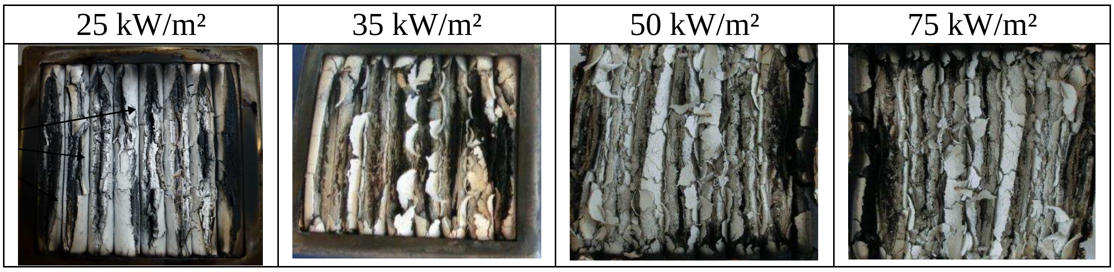
25 kW/m² 35 kW/m² 50 kW/m² 75 kW/m²

Figure 83. Residue of HFFR cable (MLC/FTIR/ELPI - 25, 35, 50, 75 kW/m²)

In addition, the CHF of the HFFR cable was calculated using the thermally thick assumption, since electrical cable is considered to behave as a thermally thick material according to Tewarson.[151] The variation of the inverse of the square root of the HFFR cable t_{ig} has been plotted against the heat flux as shown at Fig. 84. Extrapolation of the linear function gives an x-axis intercept of 10.5 kW/m². Based on the Delichatsios approximation [147], the theoretical CHF of the HFFR cable is estimated at 17 kW/m². Note that no piloted ignition was reported after exposing the HFFR cable to a heat flux 17 kW/m² for a duration of 15 minutes in the MLC fire test configuration.

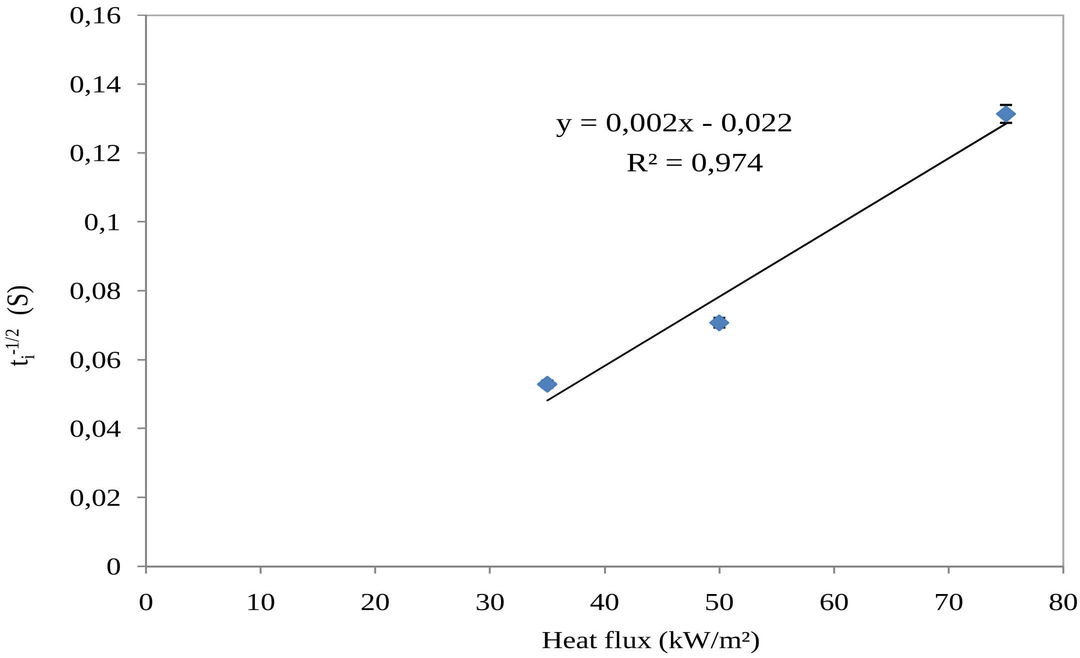

Figure 84. Inverse of square root of piloted ignition versus heat flux for HFFR cable (MLC/FTIR/ELPI - 25, 35, 50, 75 kW/m²)

The EHC of the HFFR cable was also calculated at the different heat fluxes (25, 35, 50, and 75 kW/m²), with results shown at Fig 85. For each heat flux, a drop in EHC can be seen at ignition, followed by stabilization during the flaming phase and then an increase just before extinction. The calculated AEHC for the HFFR cable is 25 ± 4 MJ/ kg.

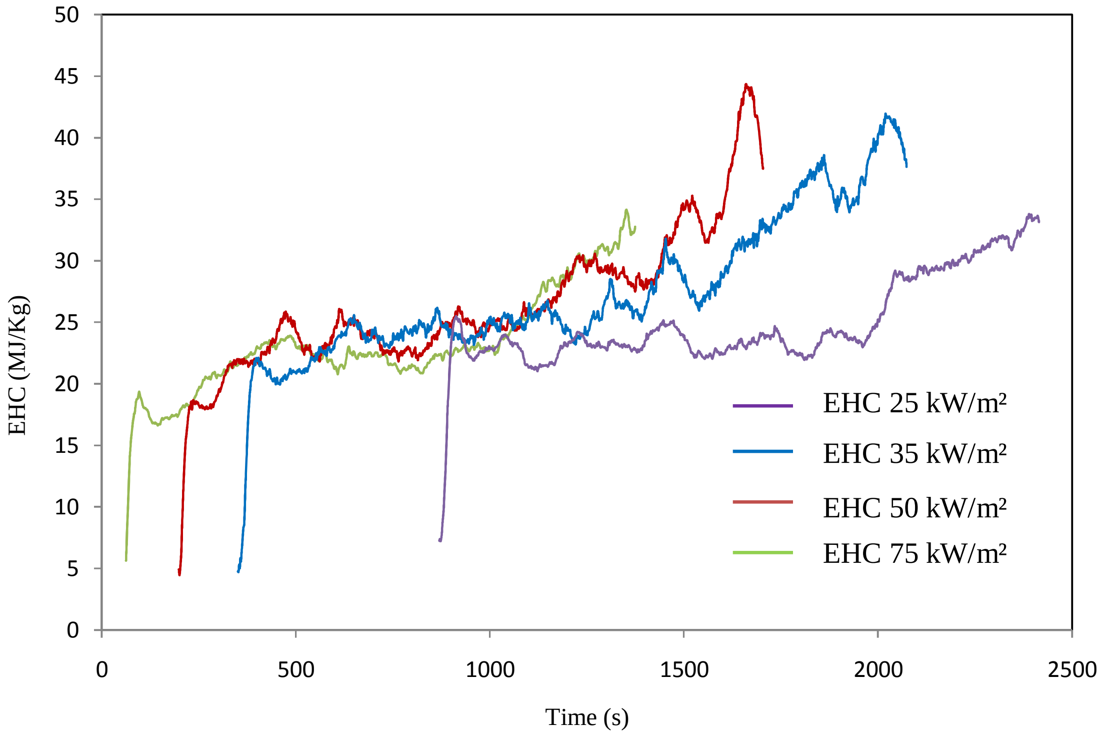

Figure 85. Effective heat of combustion of the HFFR cable at 25, 35, 50, 75kW/m²

Following this analysis, the HFFR cable flammability parameters can be summarised as follows. The HRR behaviour of the HFFR cable can be described as an initial HRR peak (the highest) after ignition, then by stabilization, followed by a second peak close to the flame out and the consequent decrease in the HRR. In addition, both the t_{ig} and the flaming period decrease when the heat flux is increased while the pHRR is nearly identical for all of the heat fluxes tested. It has moreover been calculated that, if exposed to a constant heat flux above 17 kW/m², the HFFR cable should generate piloted ignition with a pHRR of 120 ± 10 kW/m², associated to an average effective heat of combustion of around 25 ± 4 MJ/Kg. These parameters describing the fire performance of the HFFR cable are directly representative of the data obtained during the present study. In consequence, they can be considered either as direct-response or as input data for the purpose of characterizing the flammability of other types of electrical cable that may be of interest.

2.2 Characterization of the gases released from the Halogen Free Flame Retardant cable fire

An FTIR spectrum representing evolved gases in the smoke of the HFFR cable fire at 50 kW/m² (representative of a developed fire in a flashover situation) is shown at Fig 86. The evolved gases spectrum is compared to reference FTIR spectra from the library database. The main gases identified are H_2O (broad bands around 3900 - 3500 cm^{-1} and 1900 - 1250 cm^{-1}), CO_2 (high absorption around 2357 - 2310 cm^{-1}), CO (absorption around 2187 – 2115 cm^{-1}), CH_4 (absorption around 3030 – 2990 cm^{-1}), C_2H_4 (characteristic peak at 2985 cm^{-1}) and an overlapping phenomenon between CH_3COCH_3, CH_3COOH and H_2O around 1750 cm^{-1}.

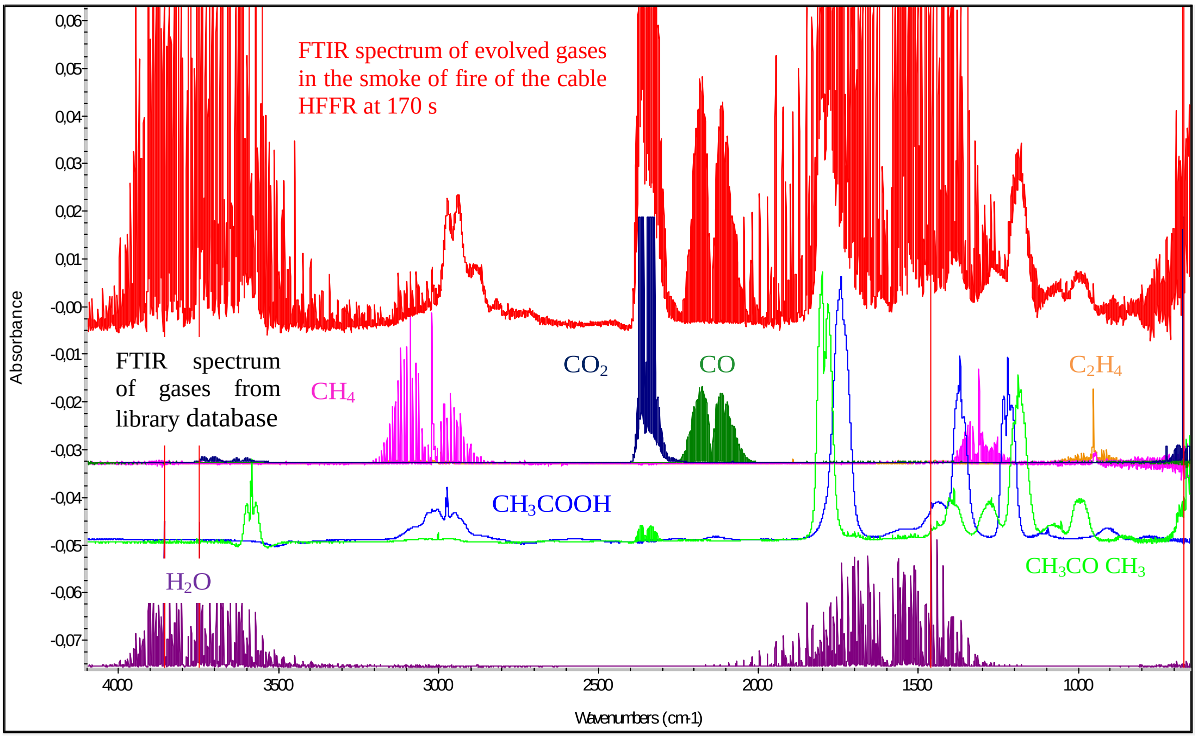

Figure 86. Identification of evolved gases in HFFR cable smoke (MLC/FTIR - 50 kW/m²)

The quantitative analyses of these gases (H_2O, CO_2, CO, CH_3COOH, CH_3COCH_3, CH_4 and C_2H_4) released during the HFFR cable fire at 50 kW/m² are plotted at Fig 87, along with the HRR profile. This chart is divided into three parts: pre-ignition (1), combustion phase (2) and from flame out until 120 s after fire extinction (3). The total concentration of each gas in each of the parts is calculated (cf. table 10).

In part 1, there is the release of 1 % of CO_2 (62658 ppm), 4 % of H_2O (396387 ppm), 5% of CH_3COCH_3 (2836 ppm), 44 % of C_2H_4 (1900 ppm), 41 % of CH_4 (3545 ppm) and 93 % of CH_3COOH (3144 ppm). The highest concentration gas in the smoke during the first part of thermal decomposition of the HFFR cable is H_2O (396387 ppm).

In part 2, the quantities of H_2O, CH_3COCH_3 and CO_2, as well as the measured HRR increase. The former reach their maximums, namely 81% of CH_3COCH_3 (45938 ppm), 93% of H_2O (9215993 ppm) and 97% of CO_2 (6077826 ppm) (cf. Fig. 87 and table 10). On the other hand, CH_3COOH, CO, CH_4 and C_2H_4 decrease to their lowest percentages (Fig. 88 and table 10). The highest concentration gas in the smoke is again H_2O. While CH_3COCH_3 remains present in the smoke during combustion, CH_3COOH notably disappears.

After flame out, there is a recurrence of CO (53%), CH_4 (35%) and C_2H_4 (33%), gas emission due to the smoldering of the residual fuel (i.e. the HFFR cable residue), while that the levels of H_2O (3%), CO_2 (3%), and CH_3COCH_3 (7%) decrease. Subsequently, the generation of CO shuts down due to the lack of combustible fuel (Fig. 88).

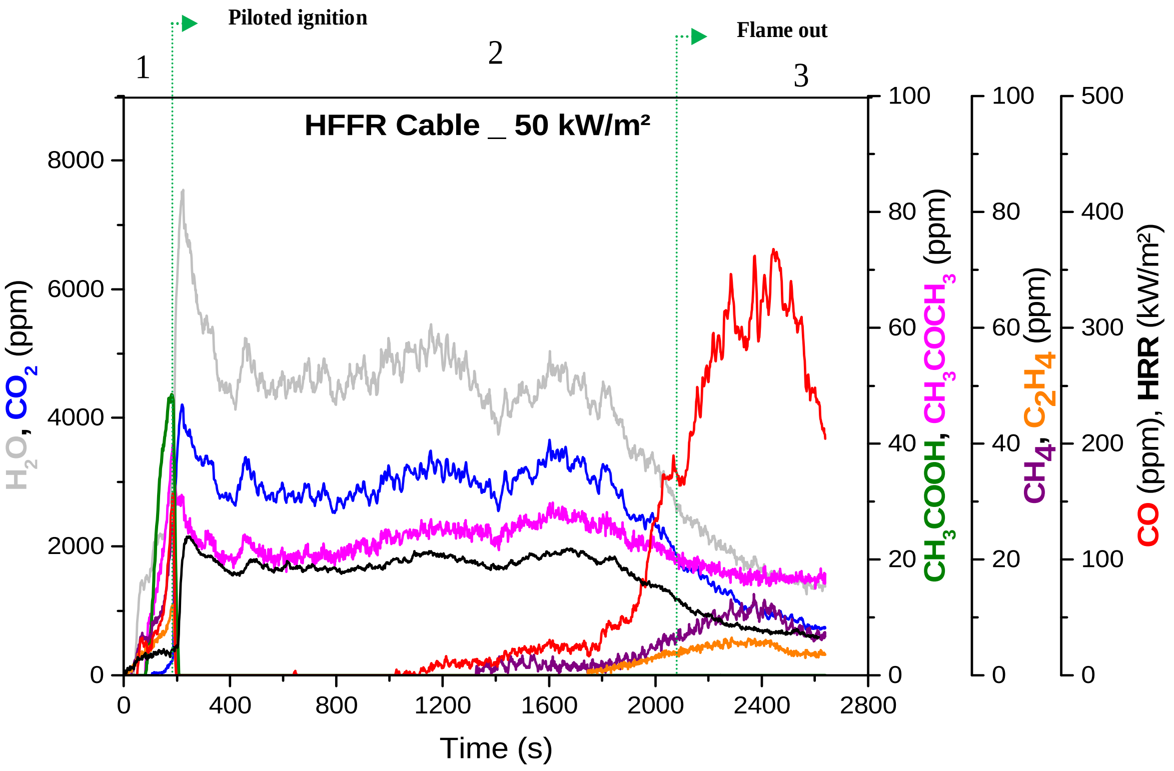

Figure 87. Transient evolution of gas species during HFFR cable fire at 50 kW/m²

Table 10. Total gases HFFR cable fire at 50 kW/m²

	Total gases (ppm)						
	CH_3COOH	**CH_3COCH_3**	**C_2H_4**	**CH_4**	**CO_2**	**CO**	**H_2O**
Part 1	3144 (93 %)	2836 (5 %)	1900 (44 %)	3545 (41 %)	62658 (1 %)	181590 (9 %)	396387 (4 %)
Part 2	237 (7 %)	45938 (81 %)	994 (23 %)	2075 (24 %)	6077826 (97 %)	76671 (38 %)	9215993 (93 %)
Part 3	-	6806 (12 %)	1426 (33 %)	8646 (35 %)	3926024 (3 %)	106936 (53 %)	297290 (3 %)
Total	3381	56714	4320	8646	6265800	201767	9909670

Furthermore, the yields of the main gases evolved during the HFFR cable fire at 50 kW/m² were calculated and the results plotted as shown in Fig. 88. The data plot illustrates that for one gram of combusted HFFR cable, 4.4 g of CO_2, 3.5 g of H_2O and 0.1 g of CO are generated, as well as almost 0.07 g of CH_3COCH_3, 0.01 g of CH_3COOH and 0.01 g of hydrocarbons (CH_4 + C_2H_4).

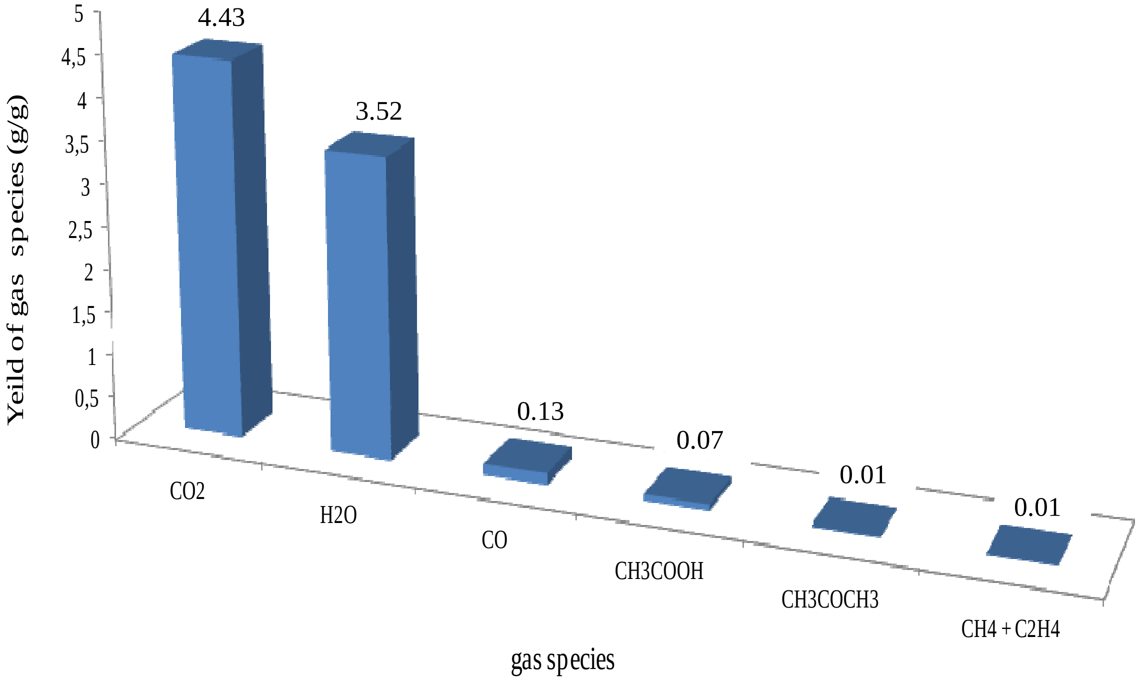

Figure 88. Yield of gas species in the smoke of the HFFR cable fire at 50 kW/m²

This qualitative and quantitative analysis shows that the evolved gases present in the smoke of the HFFR cable fire are consistent with those detected in fire smoke of the EVA/ATH reference material. This is coherent with the raw materials used in the HFFR cable formulation of (mainly EVA and ATH) as reported in the literature.[152]

2.3 Size distribution and concentration of particles in the HFFR cable fire smoke

The particles of soot emitted in the HFFR cable smoke were also examined to extend the characterization of the fire effluents of HFFR cable. Figure 89 shows the results of measurements of the size distribution and number of particles per cm^3 at heat fluxes of 25, 35, 50 and 75 kW/m^2. As expected, the results confirm the predominance of submicron particles; particles of above 1 µm are present but in very insignificant numbers (approximately 90% below those of submicron particles).

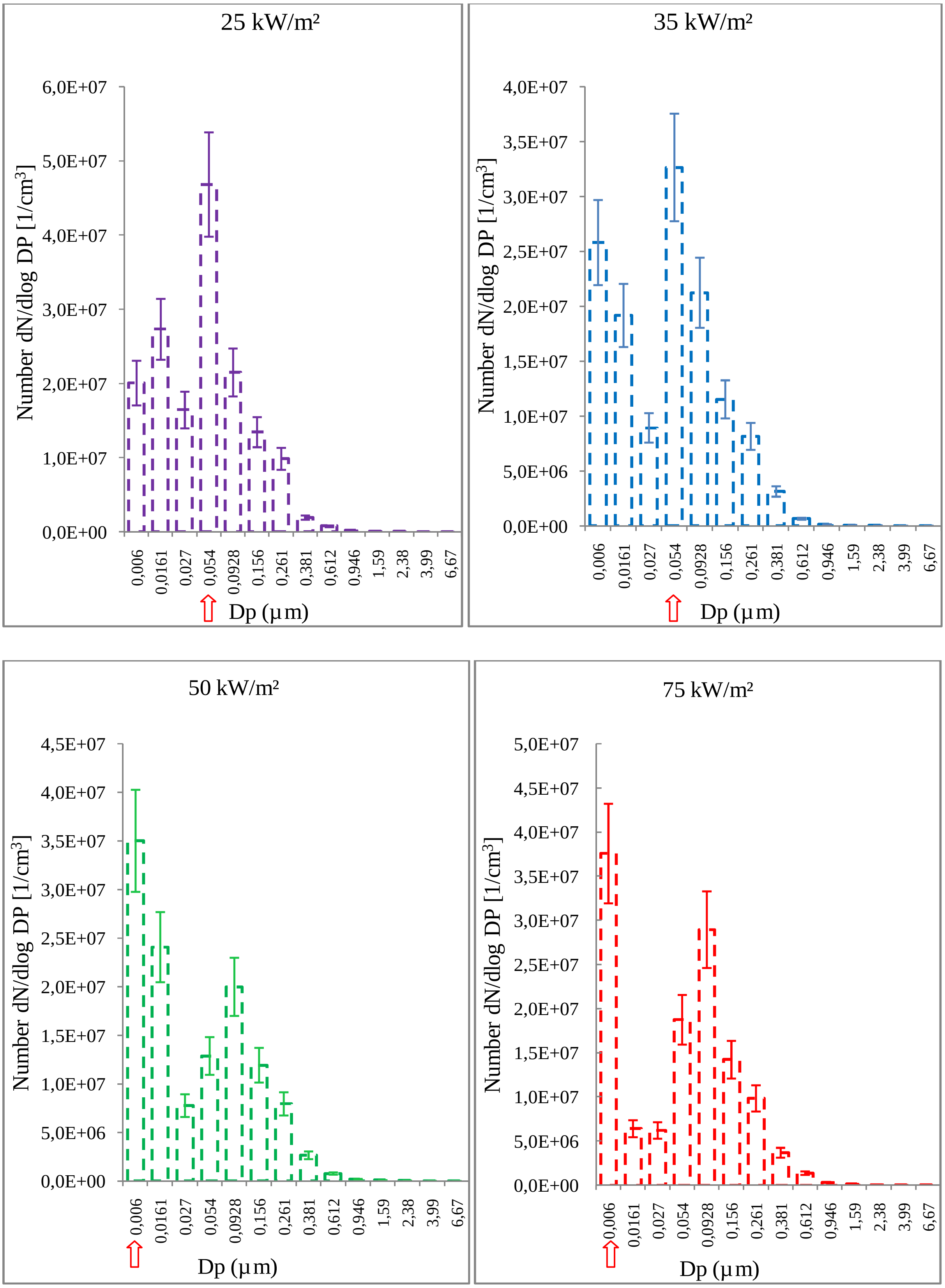

Figure 89. Soot size distribution and number in the smoke of HFFR cable

(MLC/FTIR/ELPI - 25, 35, 50, 75 kW/m²)

On analysis of the submicron particles, a characteristic peak of 54 nm particles was observed at heat fluxes of 25 and 35 kW/m², whereas at 50 and 75 kW/m², the characteristic peaks are representative of particles of 6 nm. Photos of the particles collected at each stage of the ELPI impactor during the HFRR cable fire test at 50 kW/m² are presented at Fig. 90. The collected particles can be used for microscopy observation or elementary analysis, to extend the knowledge of these particles in the context of fire safety assessment.

Figure 90. HFFR cable soot particles collected on aluminium foils

(MLC/ELPI - 50 kW/m²)

3 Conclusion

This chapter has dealt with a real case application of MLC/FTIR/ELPI for the fire behaviour characterization of an HFFR cable. In terms of flammability parameters, this cable was found to exhibit two pHRRs during combustion in a fire simulation test, the first of which was around to the time of ignition and the second before the flame out. Furthermore, exposing the HFFR cable to a constant heat flux above 17 kW/m² may result in piloted ignition and its combustion will generate total energy of around 126 ± 2 MJ/m² with an AEHC of almost 25 ± 4 MJ/kg.

The composition of the gas phase released during combustion of HFFR cable at 50 kW/m² is constituted, in descending order of concentration, of H_2O (5865548 ppm), CO_2 (3723397 ppm), CO (65740 ppm), CH_3COCH_3 (31985 ppm), CH_4 (3220 ppm) CH_3COOH (2106 ppm) and C_2H_4 (1768 ppm). Calculation of the yield of these gases shows that CO_2 exhibits the highest concentration per gram of combusted HFFR cable (4.4 $g_{CO2}/g_{cable\ HFFR}$), followed by H_2O (3.5 $g_{H_2O}/g_{cable\ HFFR}$), CO (0.1 $g_{CO}/g_{cable\ HFFR}$) and CH_3COCH_3 (0.07 $g_{CH_3COCH_3}/g_{cable\ HFFR}$). The particles emitted in the smoke during combustion of cable HFFR are in the submicron size range. These results are similar overall to those obtained from the reference EVA/ATH sample, indicating that the MLC/FTIR/ELPI coupling can be applied with confidence to a manufactured product such as electrical cable. They can be used by EDF R&D as direct-response data describing the characteristic flammability parameters and effluents (gas and particles) of HFFR cable in a fire situation, or as input data for other applications.

GENERAL CONCLUSION AND OUTLOOK

A coupling of a Mass Loss Cone / Fourier Transform Infrared Spectroscopy and Electrical low pressure impactor was proposed in this project for use in the characterization of the fire behaviour of materials, including electrical cables, which are difficult to examine with small bench tests such as TGA/FTIR, Py-GC/MS. The objective was to develop a comprehensive technique that would enable the simultaneous analysis of flammability parameters, gases and particles in the smoke of a fire of materials. After setting up the intermediate bench and establishing methodologies for qualitative and quantitative analysis of evolved gases and particles, validation tests performed with ethylene vinyl acetate/aluminium trihydroxide enabled to demonstrate that the bench test exhibits accurate, meaningful and repeatable results concerning the quality and quantity of gases evolved during MLC tests. Likewise, determination of particle-size distribution in smoke, in the current combination of mass loss cone with an electrical low pressure impactor has yielded accurate, precise and repeatable results. With respect to repeatability, some random deviations were observed in the estimation of the particles concentration in the smoke, this being due to the specific fire dynamics and certain limitations of the ELPI instrument. On the other hand, the combination of MLC/FTIR/ELPI has proven to provide excellent results from a single fire test, extending the scope of data on the fire behaviour characteristics of ethylene vinyl acetate/aluminium trihydroxide. Application to a real case of a halogen free electrical cable has also given consistent results, not only for the flammability parameters but also for fire effluents (gas and particles) in the smoke from the manufactured material. MLC/FTIR/ELPI therefore appears to be a complete analytical bench of utility for research and development, in particular to elucidate the mechanisms of thermal decomposition of materials including flame retarded polymerics. It can also be used to investigate different designs and formulations of materials with results being available almost immediately after testing, which will enable research to proceed quickly. As a consequence, the MLC/FTIR/ELPI bench will be used at Eletricité de France Research & Development to characterize the fire behaviour of various electrical cables intended for use in nuclear power plant accident localization compartments. The resulting data should prove a useful aid in fire impact assessments (such as the effect of smoke on the functioning of electronic devices) and/or for improving fire safety policy in industrial facilities. With this information, the industry will be in a position to make balanced decisions as to the most appropriate cable formulations based on their fire safety, electrical performance and environmental impact. It is planned to improve the experimental bench (specifically, the ELPI side) by implementing a Fine Particles Sampling dilution system (appendix 2), in order to reduce random deviation in the repeatability of the estimation of particles concentration in the MLC test smoke release. As it diminishes the quantity of particles being monitored, sample dilution should limit the abrupt variations in the quantity of particles being impacted on the different ELPI stages, and even prevent saturation of the ELPI analyzer. In addition, for the FTIR side, other gases of interest (benzene, etc.) could be integrated, as required, into the established quantitative method and ideas for modifying the present MLC configuration, to obtain a confinement space could also be discussed, although the latter point lies beyond the scope of this dissertation.

APPENDIX 1: CALIBRATION CURVE RESULTS OBTAINED FOR OTHER GASES DURING DEVELOPMENT OF THE FTIR QUANTITATIVE METHOD

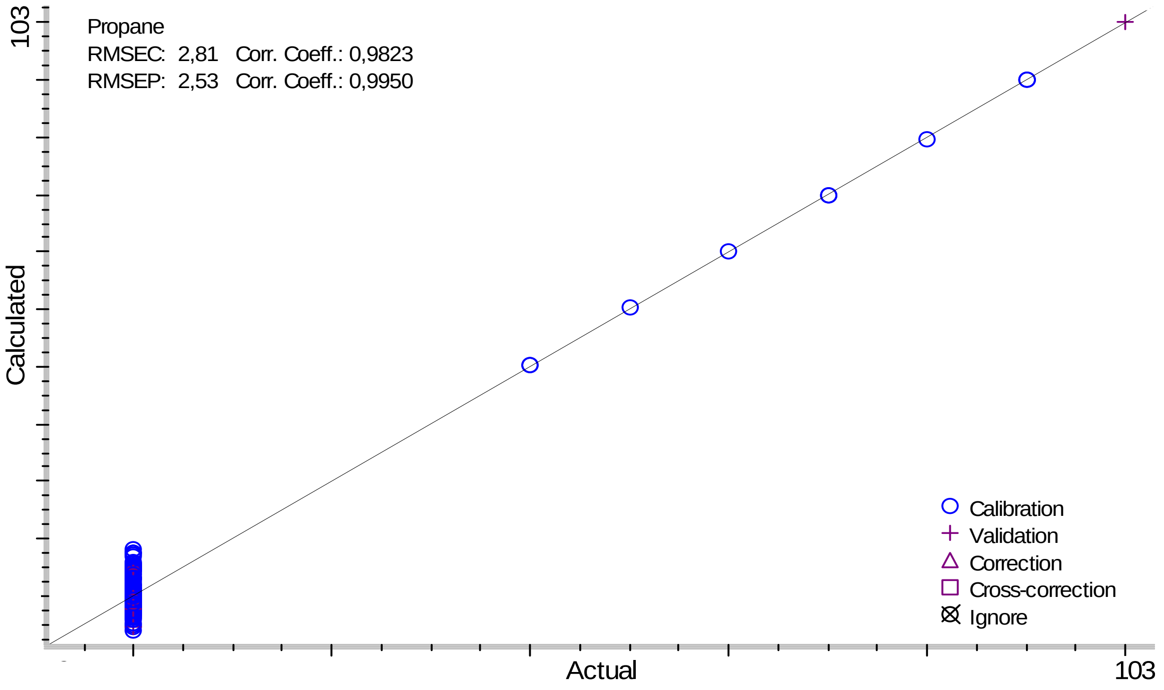

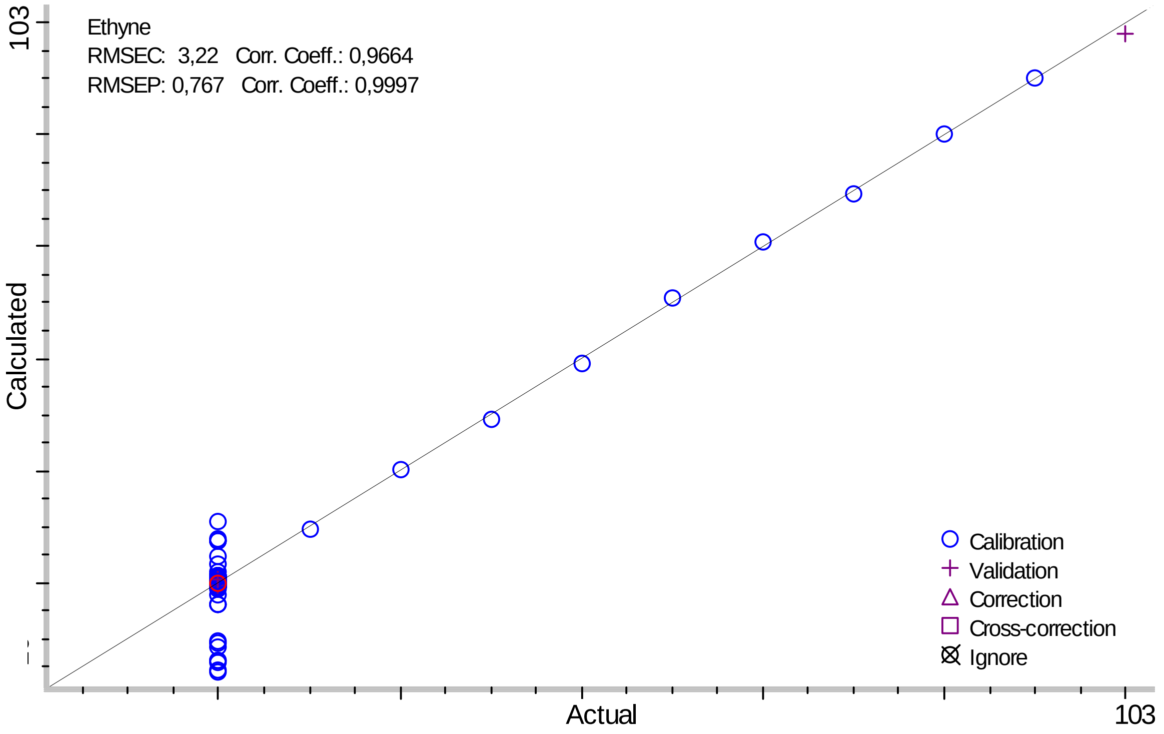

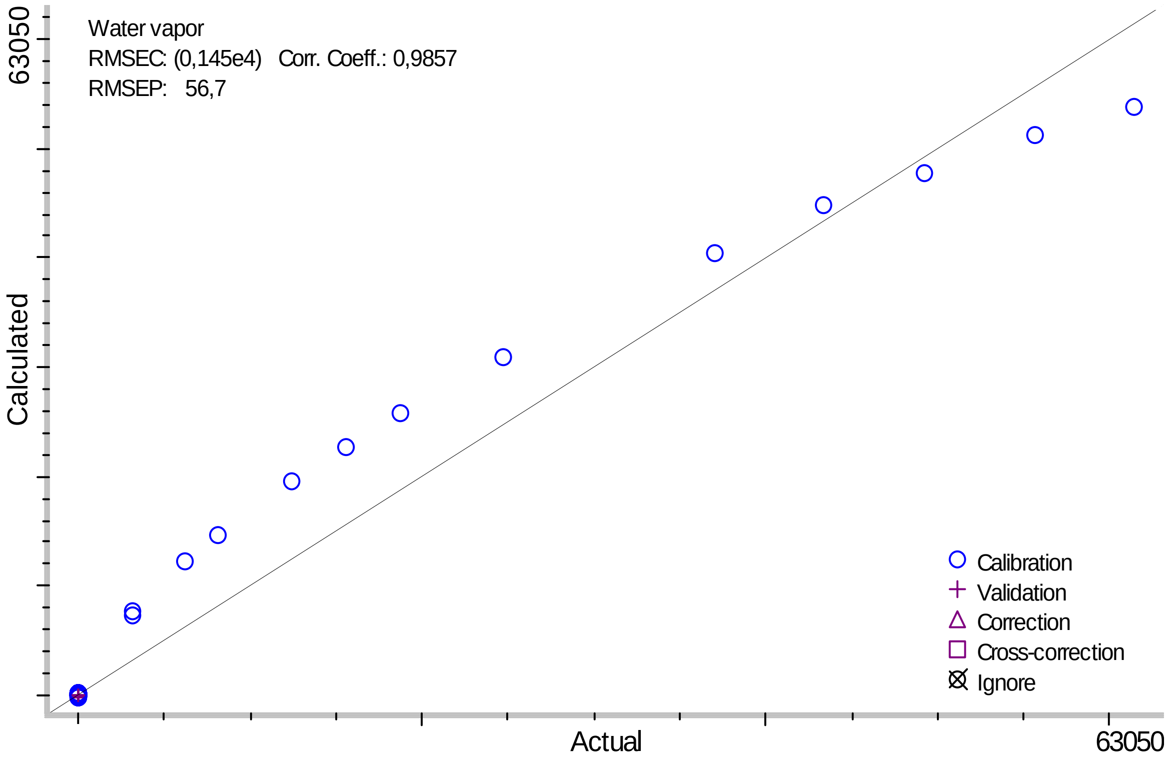
Water vapor
RMSEC: (0,145e4) Corr. Coeff.: 0,9857
RMSEP: 56,7
63050
Calculated
Actual
63050
○ Calibration
+ Validation
△ Correction
□ Cross-correction
⊠ Ignore

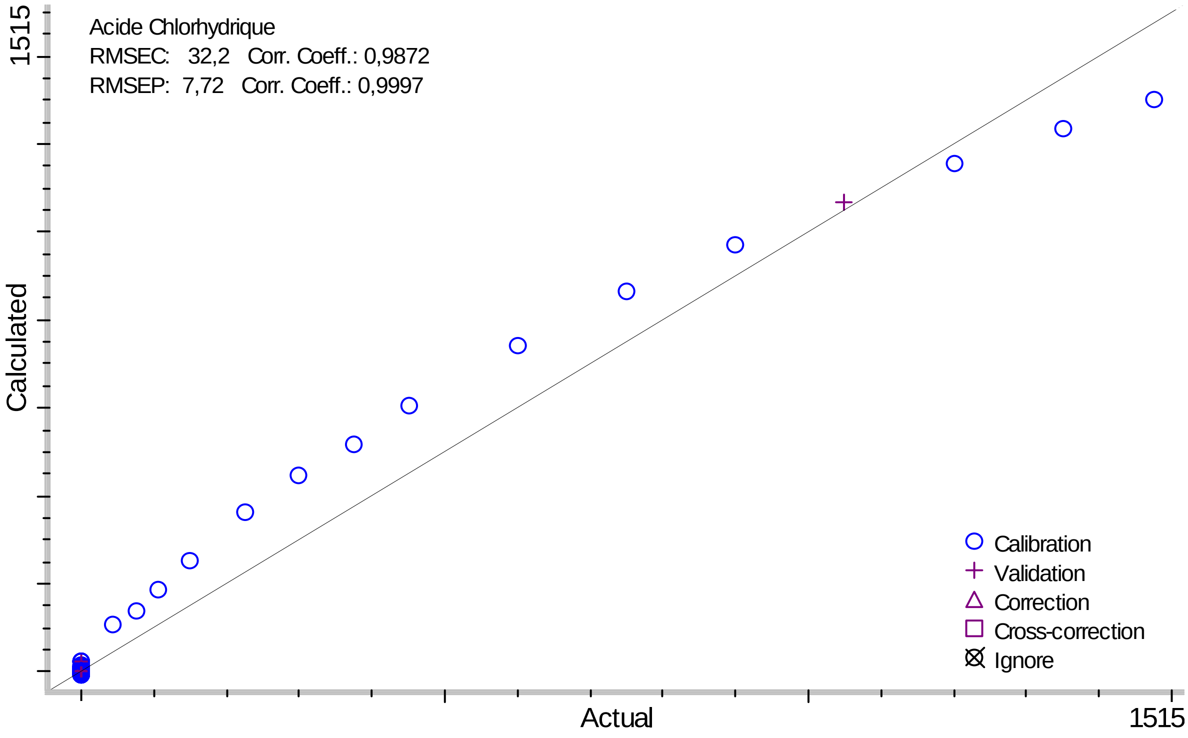
Acide Chlorhydrique
RMSEC: 32,2 Corr. Coeff.: 0,9872
RMSEP: 7,72 Corr. Coeff.: 0,9997
1515
Calculated
Actual
1515
○ Calibration
+ Validation
△ Correction
□ Cross-correction
⊠ Ignore

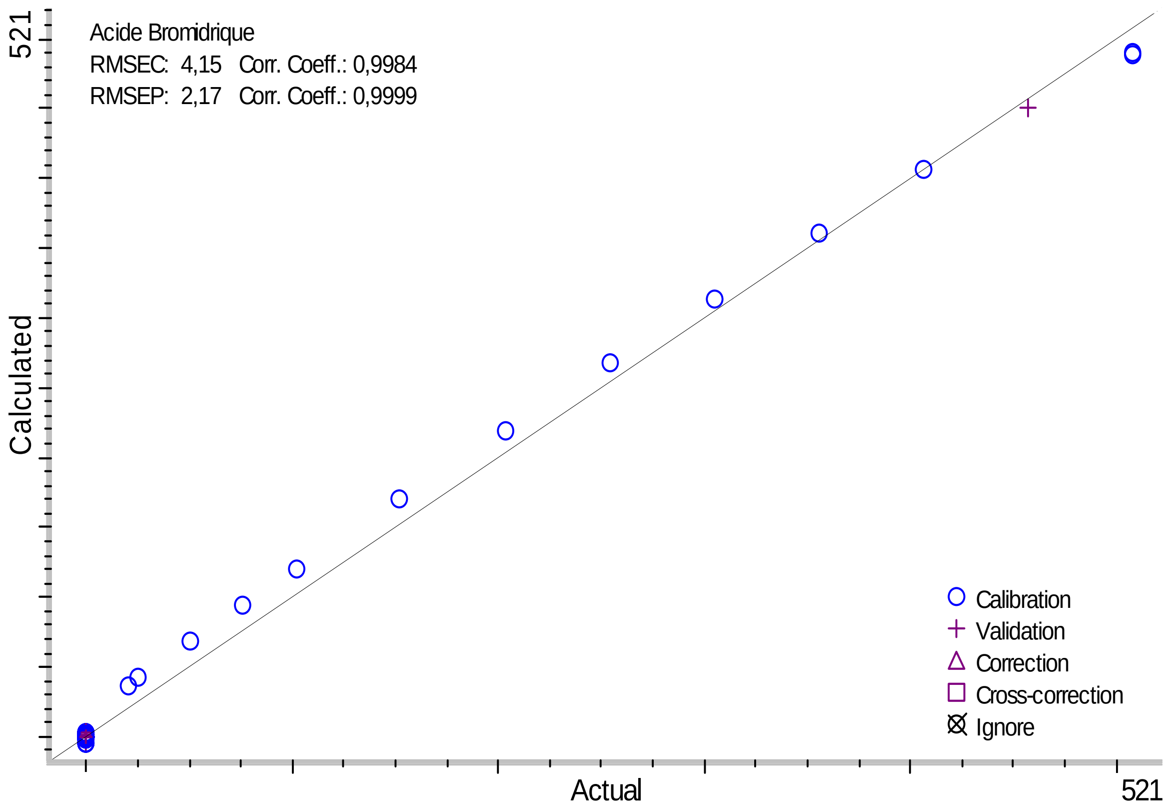
521
Calculated
Acide Bromidrique
RMSEC: 4,15 Corr. Coeff.: 0,9984
RMSEP: 2,17 Corr. Coeff.: 0,9999
○ Calibration
+ Validation
△ Correction
☐ Cross-correction
☒ Ignore
Actual
521

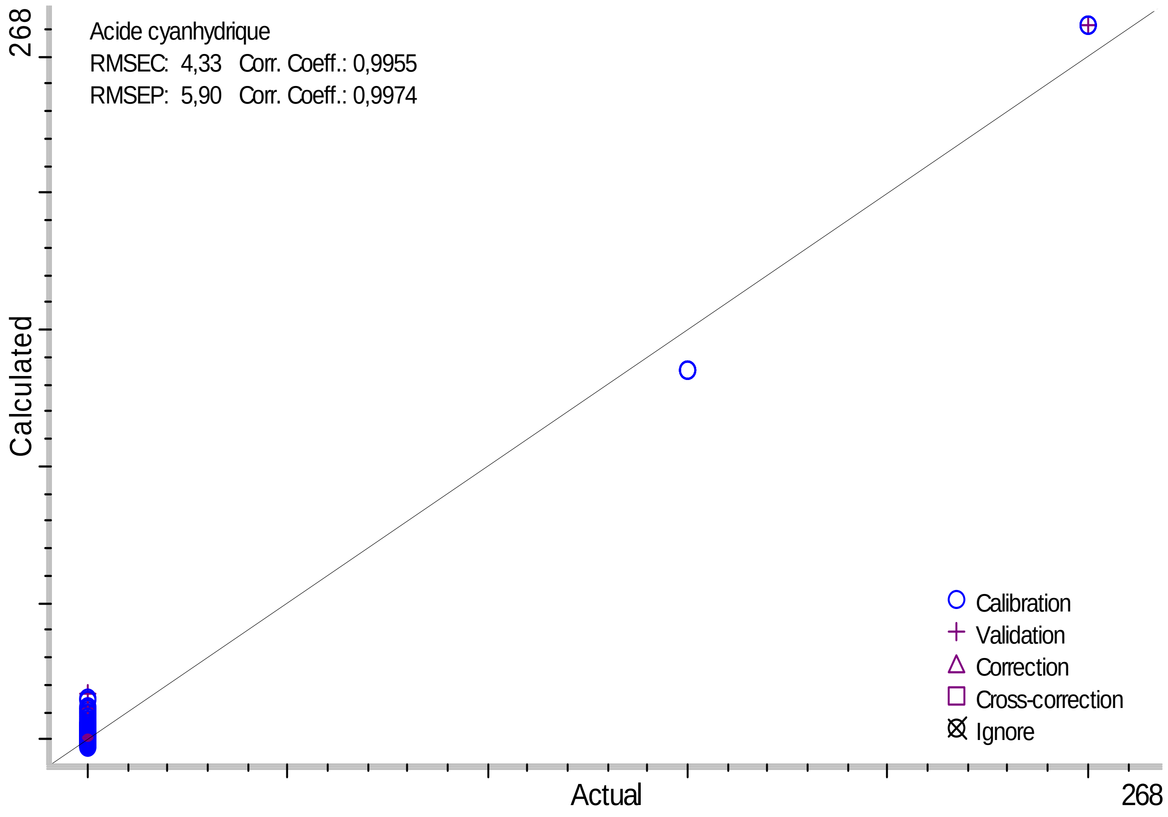
268
Calculated
Acide cyanhydrique
RMSEC: 4,33 Corr. Coeff.: 0,9955
RMSEP: 5,90 Corr. Coeff.: 0,9974
○ Calibration
+ Validation
△ Correction
☐ Cross-correction
☒ Ignore
Actual
268

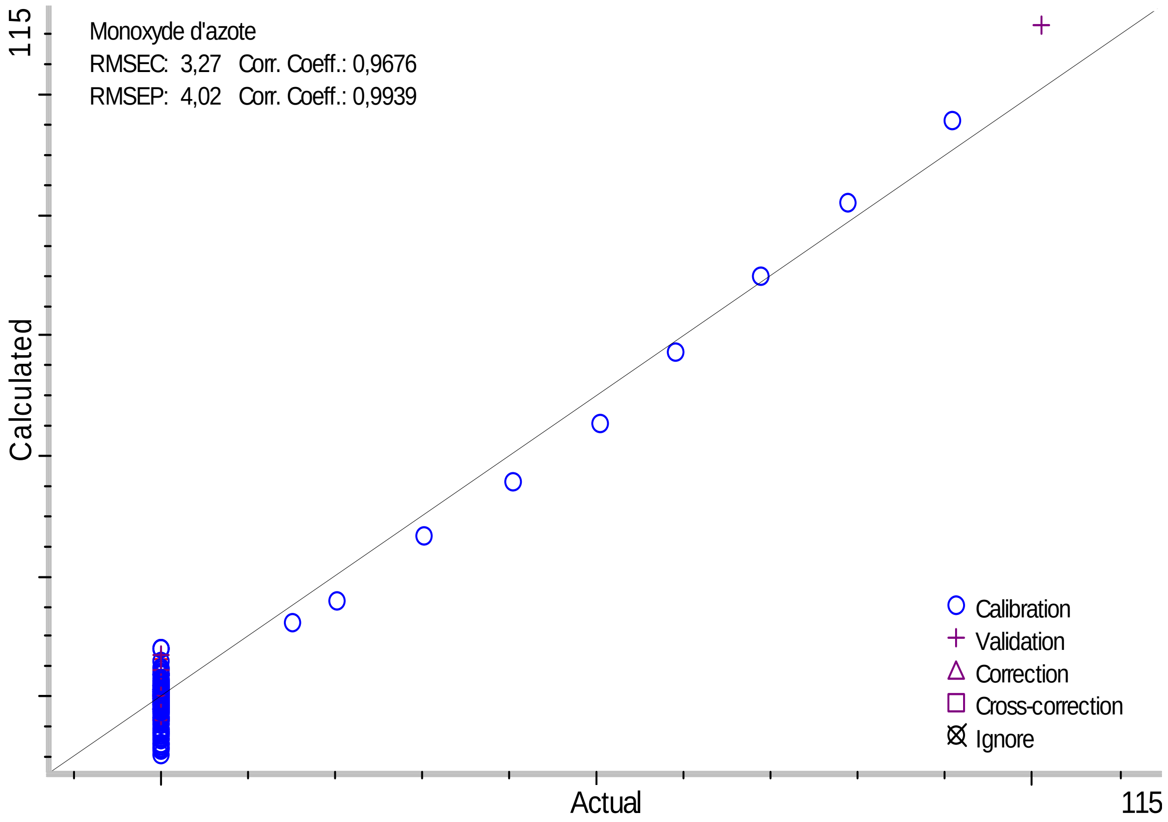
Monoxyde d'azote
RMSEC: 3,27 Corr. Coeff.: 0,9676
RMSEP: 4,02 Corr. Coeff.: 0,9939
115
Calculated
Actual
115
Calibration
Validation
Correction
Cross-correction
Ignore

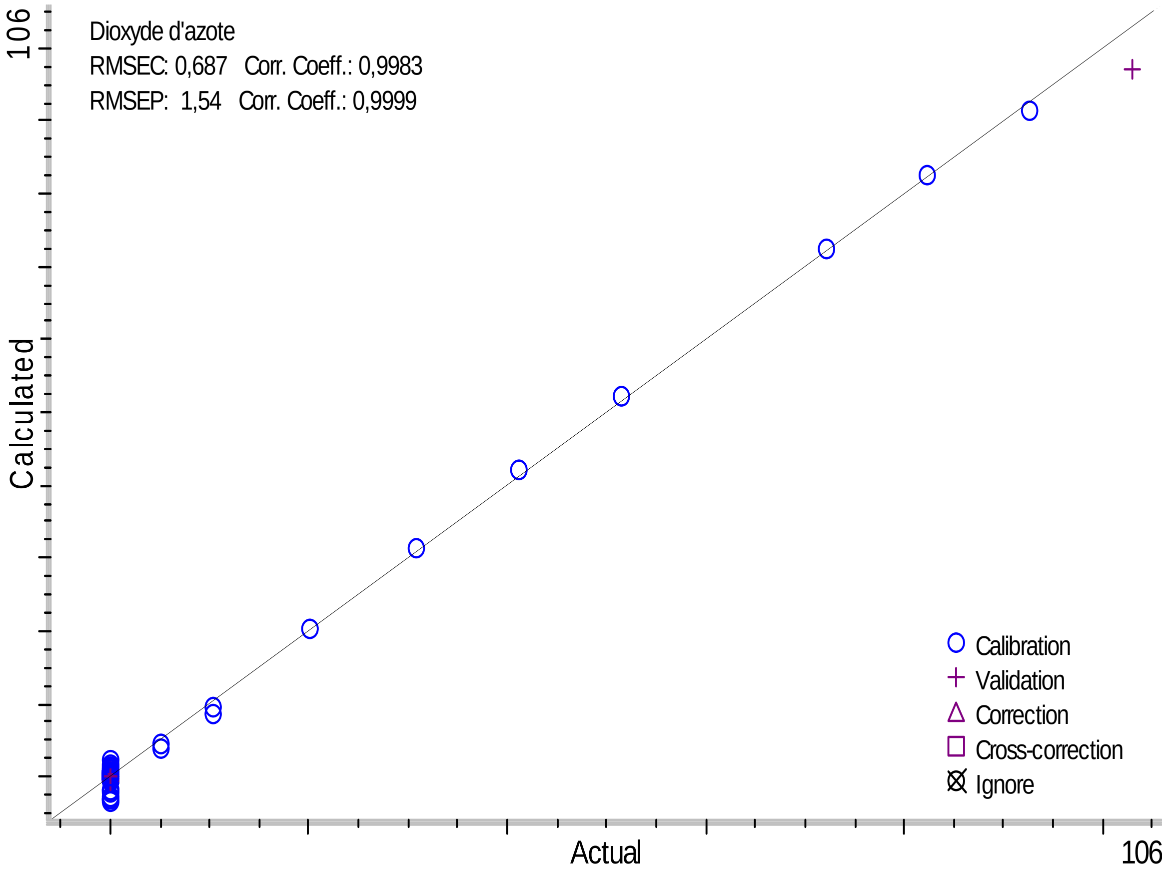
Dioxyde d'azote
RMSEC: 0,687 Corr. Coeff.: 0,9983
RMSEP: 1,54 Corr. Coeff.: 0,9999
106
Calculated
Actual
106
Calibration
Validation
Correction
Cross-correction
Ignore

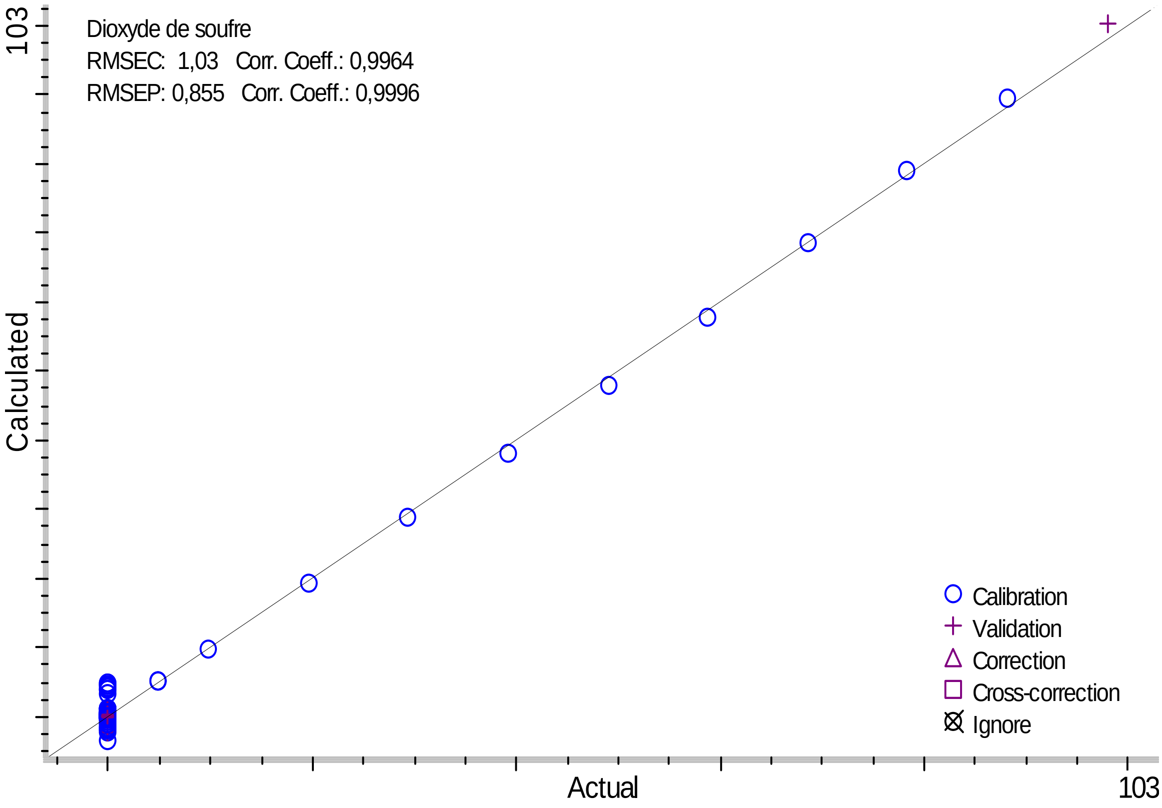
103
Calculated
Dioxyde de soufre
RMSEC: 1,03 Corr. Coeff.: 0,9964
RMSEP: 0,855 Corr. Coeff.: 0,9996
Calibration
Validation
Correction
Cross-correction
Ignore
Actual
103

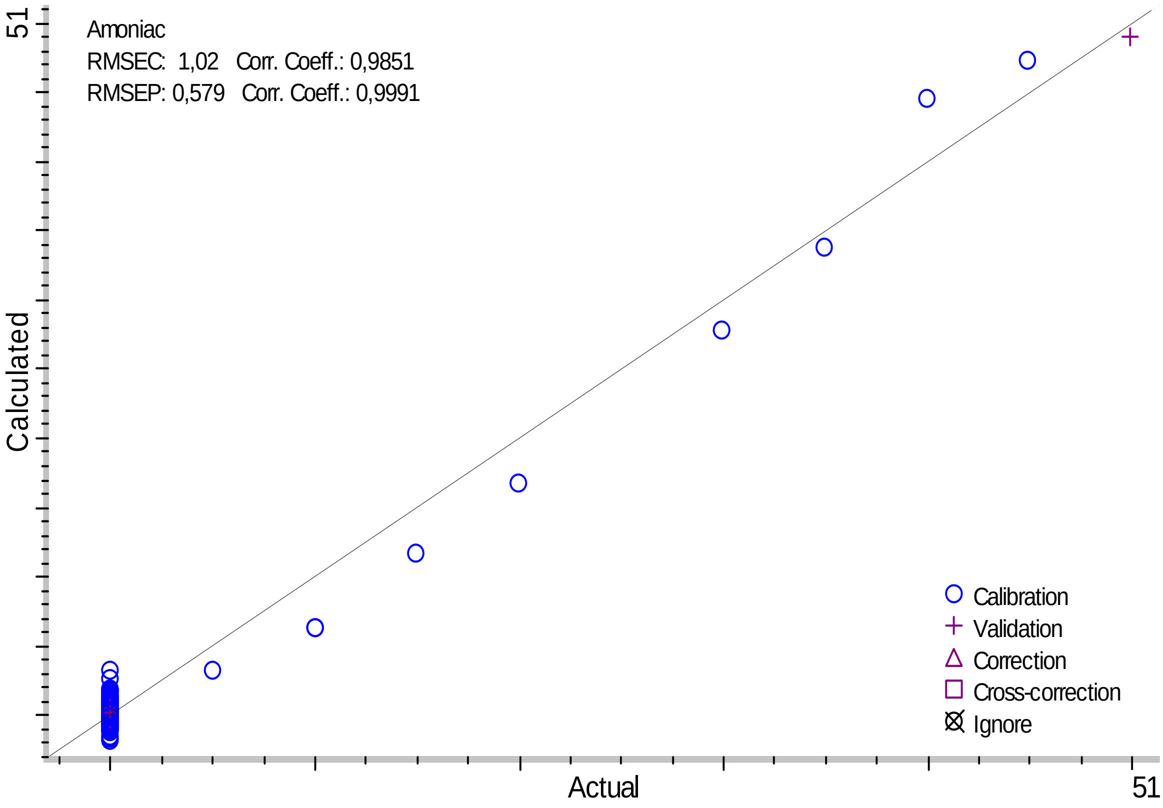
51
Calculated
Amoniac
RMSEC: 1,02 Corr. Coeff.: 0,9851
RMSEP: 0,579 Corr. Coeff.: 0,9991
Calibration
Validation
Correction
Cross-correction
Ignore
Actual
51

APPENDIX 2: FINE PARTICLES SAMPLER

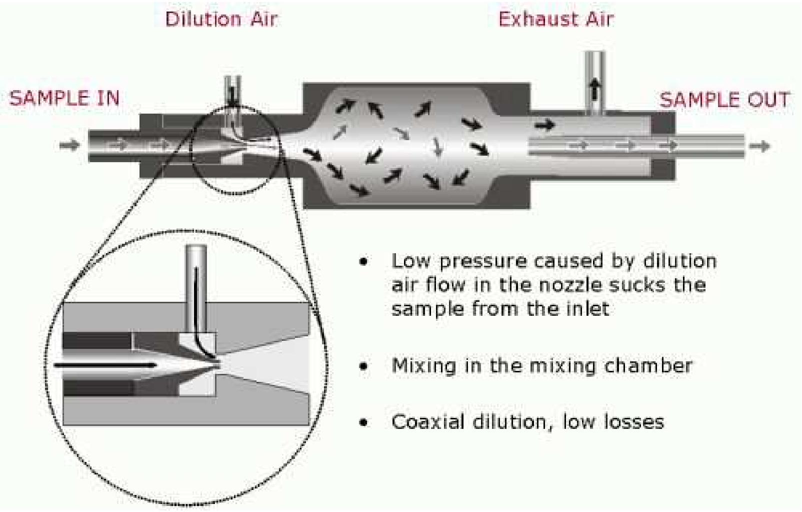

The Dekati diluter is typically applied for combustion dilution in a two stage “double diluter” setup, where the first Dekati diluter is heated and the second operates at ambient temperature. In this way, unwanted condensation and nucleation during dilution can be eliminated and the measured results will be more stable.

APPENDIX 3: PUBLICATION

F.E. Ngohang, G. Fontaine, L. Gay, S. Bourbigot: Revisited investigation of fire behaviour of ethylene vinyl acetate/aluminium trihydroxide using a combination of mass loss cone, Fourier transform infrared spectroscopy and electrical low pressure impactor, *Polymer Degradation and Stability* 106 (**2014**) 26-35

REFERENCES

---

[1] T.R. Hull, A.A. Stec. Part I Introduction to fire toxicity, Fire toxicity, Edited by A.A. Stec and T.R. Hull (**2010**) *Woodhead Publishing Materials* ISBN 978-1-84569-502-6

[2] J.Jacobus. Screening tests of representative nuclear power plant components exposed to secondary environments created by fires, *US Nuclear Regulatory Commission Regulation* (**1986**) Sandia National Laboratories 45 - 96

[3] K. Korsah, T.J. Tanaka, T.L. Wilson. Environmental testing of an experimental digital safety channel, *US Nuclear Regulatory Commission Regulation* (**1996**) Oak Ridge National Laboratory CR-64 - 76

[4] T.J. Tanaka, S.P. Nowlen. Results and Insights on the Impact of Smoke on Digital Instrumentation and Control, *US Nuclear Regulatory Commission Regulation* (**2001)** Sandia National Laboratories 65 - 97

[5] J. Mangs, O. K. Rahkonen. Acute effects of smoke from fires on performance of control electronics in NPPs, *16th International Conference on structural Mechanics in Reactor Technology* 1804 August 12 -17 (**2001**) Washington DC

[6] J.S. Newman, P. Su, G.G Yee, S. Chivukula. Development of smoke corrosion and leakage current damage functions, *Fire Safety Journal* 61 (**2013**) 92-99

[7] C.A. Wilkie. TGA/FTIR: an extremely useful technique for studying polymer degradation, *Polymer Degradation and Stability* 66 (**1999**) 301-306

[8] E.M. Anderson, I. Ericsson. Samples from ng to mg in pyrolysis-gas chromatography, *Journal of Analytical and Applied Pyrolysis* 2 (**1980**) 97-107

[9] Restriction of Hazardous Substance Directive 2002/95/EC

[10] A. Nemmar, J.A. Homes, I. Rosas, P.E. Schwarze, E.A. Moreno. Recent advances in particulate matter and nanoparticles toxicology: A review of in vivo and in vitro studies, *BioMed Research International* (**2013**) 22

[11] M. Roewekamp, H. Liemersdorf. Analysis of Fire Events in Nuclear Power Plants and Conclusions with Respect to Fundamental Requirements Concerning Fire Safety, *Proceedings of 3rd International Seminar on Fire Safety of Nuclear Power Plants* (**1994**) work report 40.070

[12] D.D. Coney. The Fire at Brown's Ferry Nuclear Power Station, *Friends of the Earth* (**1976**) http://www.ccnr.org/browns_ferry.html (2014)

[13] NFPA 921 Guide For Fire and Explosion Investigations, *Elwood Willey* (**2004**) CFI Senior Associate FIREPRO Incorporated

[14] H.W. Emmons. Heat transfer journal in fire, *Journal of Heat Transfer* 95 (**1973**) 45-51

[15] SFPE, Handbook of Fire Protection Engineering, *National Fire Protection Association* (**2002)** 1600

---

[16] P.V. Cang. Les fumées: origine et conséquences, synthèse des travaux de la DER dans le domaine (**1992**) HM65/2873

[17] W. Taylor, K.A.C Scott. Fire performance and testing of plastics, *The Plastics and Rubber Institute* chapter 7 (**1975)** 25-30

[18] H. Bockhom, A. D'Anna, A.F. Sarofim, H. Wang. Combustion Generated Fine Carbonaceous Particles, *Karlsruhe University Press* (**2009**) ISBN: 978-3-86644-441-6

[19] Z.A. Mansurov. Soot Formation in Combustion Processes, *Combustion Explosion and Shock Waves* 41 (**2005**) 727–744

[20] H. Savolainen, N. Kirchner. Toxicological Mechanisms of fire smoke, *The Internet Journal of Rescue and Disaster Medicine* 1 (**1998**)

[21] J. Eleanor, R. Highwood, P. Kinnersley. When smoke gets in our eyes: The multiple impacts of atmospheric black carbon on climate, air quality and health, *Environment Internationa l*32 (**2006**) 560-566

[22] B.S. Haynes, H.G. Wagner. Soot formation, *Progress in Energy and Combustion Science* 7 (**1981**) 229-273

[23] H. Richter and J. B. Howard. Formation of polycyclic aromatic hydrocarbons and their growth to soot a review of chemical reaction pathways, *Progress in Energy and Combust Science* 26 (**2000**) 565-608

[24] J. B. Howard. Carbon addition and oxidation reactions in heterogeneous combustion and soot formation, *Proceedings of the Combustion Institute* 23 (**1990**) 1107-1127

[25] M. Frenklach, Reaction mechanism of soot formation in flames, *Journal of Chemical Physics* 4 (**2002**) 2027-2037

[26] C. Vovelle, J.L. Delfau. Combustion des plastiques, *Techniques de l'ingénieur* (**1997**) AM 3170

[27] C.F. Cullis, M.M. Hirschler. The Combustion of Organic Polymers, *Oxford University Press* (**1981**) Oxford

[28] R.J. Pazur, J. Richard, H. Meisenheimer. EVM copolymer: the forgotten rubber, Rubber World (**2005**)

[29] H. Meisenmeier, A. Zens. Ethylene Vinyl Acetate Elastomers (EVM), *Handbook of Specialty Elastomers* (**2008**) CRC Press 576

[30] M.C. Costache, D.D. Jianga, C.A. Wilkie. Thermal degradation of ethylene vinyl acetate copolymer nanocomposites, *Polymer Degradation and Stability* 46 (**2005**) 6947-6958

[31] B.J. Mc Grattan. Examining the decomposition of Ethylene Vinyl Acetate Copolymers using TG/GC/IR, *Applied Spectroscopy* 48 (**1994)** 1472-1476

[32] N.S. Allen, M. Edge, M. Rodriguez, C. M. Liauw, E. Fontan, Aspects of the thermal oxidation of ethylene vinyl acetate copolymer, *Polymer Degradation and Stability* 68 (**2000**) 363-371

---

[33] T.R. Hull, D. Price, Y. Liu, C.L. Wills, J. Brady. An investigation into the decomposition and burning behaviour of Ethylene vinyl acetate copolymer nanocomposite materials, *Polymer Degradation and Stability* 82 (**2003)** 365-371

[34] A. Marcilla, A. Gomez, S. Menargues. TG/FTIR study of the thermal pyrolysis of EVA copolymers, *Journal of Analytical and Applied Pyrolysis* 74 (**2005)** 224-230

[35] M.C. Costache, D.D. Jiang, C.A. Wilkie. Thermal degradation of ethylene vinyl acetate copolymer nanocomposites, *Polymer Degradation of Stability* 46 (**2005)** 6947-6958

[36] B. Rimez, H. Rahier, G.V. Assche, T. Artoos, M. Bieseman, B. Van Mele. The thermal degradation of poly(vinyl acetate) and poly(ethylene-co-vinyl acetate), Part I: Experimental study of the degradation mechanism, *Polymer Degradation and Stability* 93 (**2008)** 800-810

[37] B. Rimez, H. Rahier, G.V. Assche, T. Artoos, B.V. Mele. The thermal degradation of poly(vinyl acetate) and poly(ethylene-co-vinyl acetate), Part II: Modelling the degradation kinetics, *Polymer Degradation and Stability* 93 (**2008**) 1222-1230

[38] A.Witkowski, A.A. Stec, T.R. Hull. The influence of metal hydroxide fire retardants and nanoclay on the thermal decomposition of EVA, *Polymer Degradation and Stability* 97 (**2012**) 2231-2240

[39] H. Meisenheimer. Ethylene-Vinyl Elastomers (EVM) for Improved Safety in Mass Transit, *Rapra Conference Proceedings* (**2001**) 52

[40] E.D. Weil, S.V. Levchik. Flame retardants for plastics and textiles, *Hanser Publications* (**2009**) ISBN 978-1-56990-454-1

[41] F. Laoutid, L. Bonnaud, M. Alexandre, J.M. Lopez-Cuesta, Ph. Dubois. New prospects in flame retardant polymer materials: From fundamentals to nanocomposite, *Materials Science and Engineering* 63 (**2009**) 100-125

[42] E.D. Weil, S.V. Levchik. Flame Retardants in Commercial Use or Development for Polyolefins, *Journal of Fire Sciences* 26 (**2008**) 243-281

[43] C.P. Yang, W.T. Chan. Effect of brominated flame retardants and crosslinking agent on the flame retardancy of rubbers, *Journal of Applied Polymer Science* 3 (**1998**) 963-978

[44] P.L. Simon, S.K. Scott, S. Kalliadasis, J.H. Merkin. The effect of a radical scavenger on the propagation of flames in an exothermic-endothermic system, *Journal of Mathematical Chemistry* 38 (**2005**) 203-231

[45] F.B. Clarke. Effects of brominated flame retardants on the elements of fire hazard: A re-examination of earlier results, *Fire and Materials* 23 (**1999**) 109-116

[46] E.R. Larsen. Halogenated Flame Retardants, *Krik-Othmer Encyclopedia of Chemical technology* John Willey and Sons (**1980**) 373-395

[47] T. Kashaiwagi. Polymer Combustion and Flammability-Role of the Condensed Phase, *Symposium (International) on Combustion* 25 (**1994**) 1423-1437

[48] J.W Hastie. Mass spectroscopic studies of flame inhibition: Analysis of antinomy trihalides in flames, *Combustion and Flame* 21 (1973) 49-54

---

[49] S. Bourbigot, M. le Bras. S. Duquesne. 9th European Meeting on Fire Retardancy and Protection of materials September 17 -19 (**2003**) Villeneuve d'ascq

[50] B. Schartel, R. Kunze, D. Neubert. Red phosphorus-controlled decomposition for fire retardant PA 66, Journal of applied Polymer Science 83 (**2002**) 2060-2071

[51] A. Horrocks, G. Smart, D. Price, B. Kandola. Zinc Stannates as Alternative Synergists in selected Flame Retardants System, *Journal of Fire Science* 5 (**2009**) 495-521

[52] N. Kaprinidis, R.E King III, P. Shields, J. Zingg, G. Leslie. Recent Advances in Flame Retardant Compositions UV Stable Antinomy Free Retardant Systems for Polypropylene Molding, *Society of Plastics Engineers* (**2002**) Houston

[53] R. F.W Atwell, A. Stallings, J.P Termine, J. Enrico. Flame retardant graft copolymers of ethylene vinyl acetate, *Great Lakes Chemical Corporation* (**1991**) US5036129 A

[54] C. P. Yang, W.T. Chan. Effect of brominated flame retardants and crosslinking agent on the flame retardancy of rubbers, *Journal of Applied Polymer Science* 3 (**1998)** 963-978

[55] D. Santillo, P. Johnston. Playing with fire: The global threat presented by brominated flame retardants justifies urgent substitution, *Environment International* 29 (**2003**) 725-734

[56] F. Rahman, K.H. Langford, M.D. Scrimshaw, J.N. Lester.Polybrominated diphenyl ether (PBDE) flame retardants, *Science of the Total Environment* 275 (**2001**) 1-17

[57] R. Smith, P. Georlette, I. Finberg, G. Reznick. Development of environmentally friendly multifunctional flame retardants for commodity and engineering plastics, *Polymer Degradation and Stability* 54 (**1996**) 167-173

[58] G. Camino, A. Maffezzoli, M. Braglia, M. De Lazzaro, M. Zammarano. Effect of hydroxides and hydroxycarbonate structure on fire retardant effectiveness and mechanical properties in ethylene-vinyl acetate copolymer, *Polymer Degradation and Stability* 74 (**2001**) 457-464

[59] J. Matyjaszewski. Synthesis of magnesium dihydroxide hybrid nanocomposites, *Journal of Inorganic and Organometallic Polymers and Materials* 16 (**2006**) 129-137

[60] X. Zhang, F. Guo, J. Chen, G. Wang, H. Liu. Investigation of interfacial modification for flame retardant ethylene vinyl acetate copolymer/alumina trihydrate nanocomposites, *Polymer Degradation and Stability* 87 (**2005**) 411-418

[61] P.R. Hornsby. The application of magnesium as magnesium hydroxides as fire retardant and smoke suppressing additive for polymers, *Fire Material* 18 (**1994**) 269-276

[62] G. Beyer. Flame retardant properties of EVA nanocomposites and improvement by combination of nanofillers with aluminium trihydrate, *Fire and materials* 25 (2001) 193-197

[63] F. Carpentier, S. Bourbigot, M. Le Bras, R. Delobel, M. Foulon. Charring of fire retarded ethylene vinyl acetate copolymer - magnesium hydroxide/zinc borate formulations, *Polymer Degradation and Stability*69 (**2000**) 83-92

[64] P.A. Cusack, P.R. Hornsby. Recent Advanced in Flame Retardancy of Polymeric Material, *Fire Properties of Polymer Composite Materials* 143 (**2000**) 237-286

---

[65] W. Zhu, E.D. Weil. A paradoxical flame-retardant effect on nitrates in ATH-filled ethylene-vinyl acetate copolymer, *Journal applied polymer science* 56 (**1995**) 925-933

[66] M. Fu, B. Qu. Synergistic flame retardant mechanism of fumed silica in ethylene-vinyl acetate/magnesium hydroxide blends, *Polymer Degradation and Stability* 85 (**2004**) 633-639

[67] K.W. Wagenknecht, U. Burns, M. Wagenknecht, U. Kretzschmar, B. Focke. Effect of hydrated fillers and red phosphorus on the limiting oxygen index of poly(ethylene-co-viny acetate)-poly(vinyl butyral) and low density poly(ethylene-co-vinyle alcohol) blends, *Journal of Vinyl and additives Technology* 14 (**2008)** 113-119

[68] V. Babushok, W. Tsang. Inhibitor rankings for alkane combustion, *Combustion and Flame*123 (**2000**) 488-506

[69] M. Le Bras, S. Bourbigot, C. Delporte, C. Siat, Y. Le Tallec. New intumescent formulations of fire retardant polypropylene - Discussion of the free radical mechanism of theformation of carbonaceous protective material during the thermo-oxidative treatment of theadditives, *Fire and Materials* 20 (**1996**) 191-203

[70] S. Bourbigot, S.Duquesne. Fire retardant polymers: Recent developments and opportunities, *Journal of Materials Chemistry* 17 (**2007)** 2283-2300

[71] P. Ducrocq, S. Duquesne, S. Magnet, S. Bourbigot, R. Delobel. Interactions between chlorinated paraffins and melamine in intumescent paint-investing a way to suppress chlorinated paraffins from the formulations, *Progress in Organic Coatings* 57 (**2006**) 430-438

[72] S.V. Levchik, G.F. Levchik, A.I. Balabanovich, E.D. Weil, M. Klatt. Phosphorus oxynitride: A thermally stable fire retardant additive for polyamide 6 and poly(butylenes terephthalate), *Angewandte Makromolekulare Chemie* 264 (**1999**) 48-55

[73] J. Zilberman, T.R.Hull, D.Price, G.J.Milnes, F. Keen.Flame retardancy of some ethylene-vinyl acetate copolymer-based formulations, *Fire and Materials* 24 (**2000**) 159-164

[74] S.C. Moldoveanu. Analytical pyrolysis of synthetic organic polymers, *Techniques and Instrumentation in Analytical Chemistry* 25 (**2005**) 714

[75] J. Zhang, J. Hereid, M. Hagen, D. Bakirtzis, M.A. Delichatsios, A. Fina, A. Castrovinci, G. Camino, F. Samyn, S. Bourbigot. Effect of nanoclayand fire retardants on fire retardancy of a polymer blend of (EVA) and LDPE, *Fire Safety Journal* 44 (**2009)** 504-513

[76] C. Nyambo, E. Kandare, C. A. Wilkie. Thermal stabilitty and flammability characteristics of ethylene vinyl acetate (EVA) composites blended with a phenyl phosphonate-intercalated layered double hydroxide (LDH), melamine polyphosphate and/or boric acid, *Polymer Degradation and Stability*, 94 (**2009**) 513-520

[77] W. Stark, M. Jaunich. Investigation of Ethylene Vinyl Acetate Copolymer (EVA) by thermal analysis DSC and DMA, *Polymer Testing* 30 (**2011**) 236-242

[78] Hui Liu, P. Song, Z. Fang, L. Shen, M. Peng. Thermal degradation and flammability properties of HDPA/EVA/C60 nanocomposites, *Thermochimica Acta*, 506 (**2010**) 98-101

[79] R.E. Lyon, R.N. Walters, Pyrolysis. Combustion Flow Calorimeter, *Journal of Analytical and Applied Pyrolysis* 71 (**2004**) 27-46

---

[80] ASTM D7309 - 13: Standard Test Method for Determining Flammability of Plastics and Other Solid Materials Using Microscale Combustion Calorimetry

[81] Y. Shi, T. Kashiwagi, R.N. Walters, J.W. Gilman, R.E. Lyon, D.Y. Sogah. Ethylene vinyl acetate/layered silicate nanocomposites prepared by a surfactant-free method: Enhanced flame retardant and mechanical properties, *Polymer Degradation and Stability* 50 (**2009**) 3478-3487

[82] K. MC Grattan. Cable heat release, ignition and spread in tray installation during fire, *nuclear regulatory commission regulation* 1 (2010) CR-7010 Christifire

[83] H. Yang, Q. Fu, X. Cheng, R.K. Yuen, H. Zhang. Investigation of the flammability of different cables using pyrolysis combustion flow calorimeter, *Procedia Engineering* 62 (**2013**) 778-785

[84] Norme ISO 5660-1 (**2002**) Reaction-to-fire tests - heat release, smoke production and mass loss rate

[85] Norme ISO 13927 (**2001**) Plastics-Simple heat release test using a conical radiant heater and a thermopile detector

[86] J. Luche, T. Rogaume, F. Richard, E. Guillaume. Characterization of thermal properties and analysis of combustion behavior of PMMA in a cone calorimeter, *Fire Safety Journal*46 (**2011**) 451-461

[87] B. Schartel, M. Bartholmai, U. Knoll. Some comments on the use of cone calorimeter data, *Polymer Degradation and Stability* 88 (**2005**) 540-547

[88] Norme ISO 13823 (**2010**) Reaction to fire tests for building products – Building products excluding floorings exposed to the thermal attack by a single burning item

[89] ASTM E-84 (**1996**) Steiner Tunnel Test, Underwriters Laboratories 723 NFPA 255, UBC42-1, Version .

[90] IEC 60332-3-10 (**2009**) Tests on electric and optical fibre cables under fire conditions, Part 3-10: Test for vertical flame spread of vertically-mounted bunched wires or cables

[91] S.J. Grayson, P. Van Hess, A.M. Green, H. Breulet, U. Vercelloti. Assessing the fire performance of electric cables (FIPEC), *Fire and materials* 25 (**2001**) 49-60

[92] F. Gyppaz. Flame spread behaviour of electric cables: Round-robin characterization of the IEC/EN 60332-1 tests, *Journal of Fire Science* 30 (**2012**) 404 - 412

[93] Norme ISO 19701 (**2013**) Method for sampling and analysis of fire effluents

[94] A.T. James, A. J. Martin. Gas-liquid partition chromatography: the separation and micro-estimation of volatile fatty acids from formic acid to dodecanoic acid, *Biochemical Journal* 50 (**1952**) 679-680

[95] R.Yang, J. Zhao, Y. Liu. Oxidative degradation products analysis of polymer materials by pyrolysis gas chromatography / mass spectrometry, *Polymer Degradation and Stability* 98 (**2013**) 2466-2472

[96] N. Dadvand, R.S. Lehrle, I.W. Parsons, M. Rollinson, I.M. Horn, A.R. Skinner. Use of pyrolysis-GC-MS to assess the thermal degradation behavior of polymers containing chlorine II. Thermal stability characteristics of neoprene/chlorobutyl rubber composites, before and after artificial ageing. *Polymer Degradation Stability* 67 (**2000**) 407-419

[97] F.R. Quant, R.C. Flagan, K.D. Horton. 13 O 04 Implementation of a Scanning Mobility Particles Sizer (SMPS), *Journal of Aerosol Science* 24 (**1993**) S83-S84

---

[98] E. Gustafsson, M. Strand, M. Sanati. Physical and Chemical Characterization of Aerosol Particles Formed during the Thermochemical Conversion of Wood Pellets using a Bubbling Fluidized Bed Gasifier, *Energy and Fuel* 21 (**2007**) 3660-3667

[99] B. Giechaskiel, M. Maricq, L. Ntziachristos,C. Dardiotis, X. Wang, H. Axmann, A. Bergmann, W. Schindler. Review of motor vehicle particulate emissions sampling and measurement: From smoke and filter mass to particle number, *Journal of Aerosol Science* 67 (**2014**) 48-86

[100] H. Patashnick, E.G. Rupprecht. Continuous PM_{10} measurements using the tapered element oscillating microbalance, *Journal of the Air and Waste Manage Association* 41 (**1991**) 1079-1083

[101] J. Rhodes, C. Smith, A. A.Stec. Characterization of soot particulates from fire retarded and nanocomposite materials and their toxicological impact, *Polymer Degradation and Stability* 96 (**2001**) 277-284

[102] J. Keskinen, K. Pietarinen, M.Lehtimâki. Electrical Low Pressure Impactor, *Journal Aerosol Science*23 (**1992**) 353-360

[103] http://dekati.com/cms/elpi/publications#a (**2014**)

[104] E.E. Smith. Heat release rate, *Fire Technology* 32 (**1996**) 333-347

[105] R. Filipczak, S. Crowley, R.E. Lyon. Heat release rate measurement of thin sample in the OSU apparatus and the cone calorimeter, *Fire Safety Journal* 40 (**2005**) 628-45

[106] B.C. Smith. Fundamentals of Fourier Transform Infrared Spectroscopy, Second Edition-CRC (**2011**) ISBN 0-8493-2461-0

[107] P.R. Griffiths, J.A. Haseth. Fourier Transform Infrared Spectrometry, *Wiley and Sons* (**1986**) New York

[108] M.B. Elser, D.W. Griffiths, S.R. Wilson, L.P. Steele. Precision trace gas analysis by FT-IR spectroscopy: simultaneous analysis of CO_2, CH_4, N_2O and CO in air, *Analytical Chemistry* 72 (**2000**) 206-215

[109] P. Faradell, E. Guillaume. Sampling and measurement of toxic fire effluent. Fire toxicity, Edited by A.A. Stec and R. Hull (**2010**), *Woodhead Publishing Materials* ISBN 978-1-84569-5026.

[110] Dekati ELPI $^{+TM}$ (**2012**) user manual' Electrical Low Pressure Impactor

[111] B. H. Stuart. Infrared Spectroscopy: Fundamentals and Applications (**2004**) *Wiley* and *Sons* ISBN 978-0-470-85428-0

[112] L.H. Kidder, A.S. Haka, E.N. Lewis. Instrumentation for FTIR Imaging, *Handbook of Vibrational Spectroscopy* (**2006**)

[113] B. C. Smith. Quantitative Spectroscopy: Theory and Practice, Academic Press (**2002**) 200

[114] J. K. Kauppinen, D. J. Moffatt, H. H. Mantschand, D. G. Cameron, Fourier self-deconvolution: a method for resolving intrinsically overlapped bands, *Applied Spectroscopy* 35 (**1981**) 271–276

---

[115] T. Hakkarainen, E. Mikkola, J. Laperre, F. Gensous, P. Fardell, Y. Le Tallec, C. Baiocchi, K. Paul, M. Simonson, C. Deleu, E. Metcalfe. Smoke gas analysis by Fourier transform infrared spectroscopy-summary of the SAFIR project, *Technical research center of Finland* 24 (**1999**) 101-112

[116] A. A Stec, P.Fardell, P.Blomqvist, L. Bustamante-Valencia, L.Saragoza, E. Guillaume. Quantification of fire gases by FTIR: Experimental characterisation of calibration systems, *Fire Safety Journal* 46 (**2011**) 225-253

[117] M. Howard, Jr. Workman. Linearity in Calibration: Act II Scene III, *Chemometrics in Spectroscopy* 14 (**1999**) 16-27

[118] L.C Speitel. Real Time Fourier Transform Infrared Analysis of Combustion Gases; Federal Aviation Administration, Airport and Aircraft Safety Research and Development Division (**2001**) Atlantic City International Airport, NJ 08405

[119] D.M.Haaland, R.G.Easterling, D.A.Vopicka. Multivariate Least-Squares Methods Applied to the Quantitative Spectral Analysis of Multicomponent Samples, *Applied Spectroscopy* 39 (**1985**) 73-84

[120] G. Biskos, K. Reavell, N. Collings. Electrostatic characterization of corona-wire aerosol chargers, *Journal of Electrostatics* 63 (**2005**) 69-82

[121] M. Marjamäki, J. Keskinen, D. R. Chen,D. Y. H.Pui, D. Y. H. Performance Evaluation of the Electrical Low-Pressure Impactor (ELPI), *Journal of Aerosol Science* 31 (**2000**) 249-261

[122] N. Ibaseta. Ph.Dthesis, Etude expérimentale et modélisation de l’émission d’aérosols ultrafins lors du déversement de poudres nanostructuréesDecember 13 (**2007**) Mécanique Energétique Génie Chimique et Procédés, Toulouse

[123] A. Järvinen, M. Aitomaa, A. Rostedt, J. Keskinen, J. Yli-Ojanperä.Calibration of the new electrical low pressure impactor (ELPI), *Journal of Aerosol Science* 69 (**2014**) 150-159

[124] A. Reynolds. Raw materials usage in the European cable industry paper given at International Event For The Plastics Cable Industry March 19-21 (**2002**) Düsseldorf

[125] M. Zanetti, T. Kashiwagi, L. Falqui, G. Camino. Cone Calorimeter Combustion and Gasification Studies of Polymer Layered Silicate Nanocomposites, *Chemistry of Materials* 14 (**2002**) 881-887

[126] Y. Soudais, L. Mogaa, J. Blazeka, J.F. Lemortb. Coupled DTA–TGA–FT-IR investigation of pyrolytic decomposition of EVA, PVC and cellulose, *Analytical and Applied Pyrolysis* 78 (**2007**) 46-57

[127] E. M. Barrall, R. S. Porter, J. F. Johnson. Gas Chromatographic Analysis of Poly (ethylene Ethyl Acrylate) and Poly (ethylene Vinyl Acetate) Pyrolyzates, *Analytical Chemistry* 35 (**1963**) 73-76

[128] A. Marcilla, S.A. Gomez, J. R. Labarta. MCM-41 Catalytic Pyrolysis of ethylene vinyl acetate copolymers, *Kinetic model Polymer* 74 (**2001**) 224-230

[129] A. R. Khalek. Characterization of Particle Size Distribution of a Heavy-Duty Diesel Engine During FTP Transient Cycle Using ELPI, *SAE Technical paper series* 1 (**2000**)

[130] V. Hulle, M. Talbaut, M. Weill, A. Coppalle. Inversion method and experiment to determine the soot reactive index: application to turbulent flames, *Measurement Science Technology* 13 (**2002**) 375-382

---

[131] I. J. Jagoda, G. Prado, J. Lahaye. An experimental investigation into soot formation and distribution in polymer diffusion flames, *Combustion and Flames* 37 (**1980**) 261-274

[132] G.P. Forney, D. Madrzykowski, K.B. Mcgrattan, L. Sheppard. Understanding Fire and Smoke Flow Through Modeling and Visualization, *IEEE Computer Graphics and Application* 23 (**2003**) 6-13

[133] A. Virtanen, M. Marjamäki, J. Ristimäki, J. Keskinen. Fine particle losses in electrical low-pressure impactor, *Journal of Aerosol Science* 32 (**2001**) 389-401

[134] L. Delfosse, C. Baillet, A. Brault, D. Brault. Combustion of ethylene vinyl acetate copolymer filled with aluminum and magnesium hydroxides, *Polymer Degradation and Stability* 23 (**1989**) 337-385

[135] S. Bourbigot, M. Le Bras, R. Leewendal, K. K. Shen, D. Schubert. Recent advances in the use of zinc borates in flame retardancy of EVA, *Polymer Degradation and Stability* 64 (**1999**) 419-425

[136] J. Troitzsch. Plastics flammability handbook: Principle regulations, testing and approval 3 rd Ed *Hanser Publishers* (**2004**) 748

[137] L. Karlsson. Polyolefin Flame Retardant Cable Materials: Effect of Additive and Copolymer Structure, *Department of Chemical and Biological Engineering* (**2004**) Chalmers University of Technology Göteborg Sweden

[138] P. Blomqvist, T. Hertzberg, M. Dalene, G. Skarping. Isocyanates, aminoisocyanates and amines from fires a screening of common materials found in building, *Fire and Materials* 27 (**2003**) 275-294

[139] L. Ye, B. Qu. Flammability characteristics and flame retardant mechanism of phosphate-intercalated hydrotalcite in halogen free flame retardant, *Polymer Degradation and Stability* 93 (**2008**) 918-924

[140] F. Carpentier, S. Bourbigot, M. Le bras, R. Delobel, M. Foulon. Charring of retarded ethylene vinyl acetate copolymer-magnesium hydroxide/zinc borate formulation, *Polymer Degradation and Stability* 69 (**2000**) 83-92

[141] V. Babrauskas, R. D. Peacock. Heatrelease rate: The single most important variable in fire hazard, *Fire Safety Journal* 18 (**1992**) 255-272

[142] M. Zanetti, L. Costa. Preparation and combustion behaviour of polymer/layered silicate nanocomposites based upon PE and EVA, *Polymer Degradation and Stability* 45 (**2004**) 4367-4373

[143] E. Mikolla, I. S. Wicham. On the thermal ignition of combustible materials, *Fire and Material* 14 (**1989**) 87-96

[144] R. Kallonen. Test methods for hazards of construction plastics, *Technical Research Center of Finlande* (**1988**) research report 542

[145] M. Janssens. Use of bench-scale piloted ignition data for mathematical fire models *In Proceedings of International Conference on Fire in Buildings* (**1989**) 31-35 Toronto

[146] M. A. Delichatsios, Th. Panagiotou, F. Kiley. The use of time to ignition of data for characterizing the thermal inertia and the minimum critical heat flux for ignition or pyrolysis, *Combustion and Flame*, 84 (**1991**) 323-332.

---

[147] M. A. Delichatsios. Piloted ignition times, critical heat fluxes and mass loss rates at reduced oxygen atmospheres, *Fire Safety Journal* 40 (**2005**) 197-212

[148] M. J. Spearpoint, J.G. Quintiere. Predicting the piloted ignition of wood in the cone calorimeter using an integral model-effect of species, grain orientation and heat flux, *Fire Safety Journal* 36 (**2001**) 391-415

[149] A. Tewarson, M.M. Khan. Parameters for the Assessment of Fire Hazard from Electrical Wires and Cables. *International Wire & Cable Symposium Proceedings* (**1984**)

[150] J. Madrigal, M. Guijarro, C. Hernando, C. Díez, E. Marino. Effective heat of combustion for flaming of Mediterranean forest fuels, *Fire technology* 47 (**2011**) 461-474

[151] A. Witkowski. Ph.D. thesis. The use of numerical methods to interpret polymer decomposition data May (**2012**) University of Central Lancashire

[152] Fascicule de brevet Européen EP.1.818.364.B1 (**2009**) Bulletin 04